INVESTIGATION OF ~~UNSATURATED FLOW~~ UNSATURATED FLOW AND SOLUTE TRANSPORT THROUGH ~~THE~~ CHALK

Gerd F.A. Van den Daele

Thesis submitted in partial fulfilment of the requirements of the University of London for the degree of Doctor of Philosophy

2005

Department of Earth Sciences
University College London
Gower Street
London WC1E 6BT

ProQuest LLC
789 East Eisenhower Parkway
P.O. Box 1346
Ann Arbor, MI 48106-1346

Abstract

The Chalk is a fractured rock with a fine-grained porous matrix, where the matrix provides most of the porosity and storage capacity and the fractures greatly enhance the permeability. For the unsaturated zone, the role of the fractures and the matrix in flow and solute transport is not well understood. Therefore a tracer test was carried out in the unsaturated chalk at the Fleam Dyke research site in Cambridgeshire. The experiment, under natural rainfall conditions, involved distributing deuterium and bromide on a grass-covered lysimeter (a cube of volume 125 m^3) and on an adjacent 4×4 m plot. Up until 15 months after the tracer application, none of the tracer was detected in the lysimeter drainage at 5 m depth. Repeated core profiles on the adjacent plot revealed significant differences in vertical tracer distribution, indicating lateral heterogeneity of transport pathways. The results of the tracer test were modelled with MACRO 5.0, a numerical dual permeability model that was initially developed for macroporous soils. The model suggested that fracture flow is important at the site, but that it is only initiated below a depth of about 1 m. The extent of fracture flow appeared to be highly variable in different layers of the profile, mainly depending on the saturated hydraulic conductivity of the matrix. Regarding exchange of solutes between the fractures and the matrix, the model indicated that advective exchange could be important and might even outweigh diffusive exchange. The results suggested that the Chalk aquifer at the Fleam Dyke site was only moderately vulnerable to pollution, but it was concluded that even for moderate rainfall conditions some bypass flow was possible. When modelling recharge without solute transport, it was shown that a simple water balance model called DFIDGWR could perform similar or better than MACRO 5.0.

Acknowledgements

First, I wish to express my gratitude and appreciation for my supervisors Prof. John Barker and Dr. Luke Connell. Their continued encouragement, patience, and excellent advice have guided me to finish this work. I would also like to thank Prof. Tim Atkinson, who showed his usual ingenuity when providing me field advice and in his mass spectrometry work.

I am very grateful to John Wormald from the Environment Agency, whose technical know-how proved essential to me in the field. I also owe thanks to Cambridge Water Company and the Environment Agency to provide me access to the Fleam Dyke site. I especially would like to thank David Cooper of the Centre of Ecology and Hydrology and George Darling of the British Geological Survey for allowing me to use their invaluable database of the Fleam Dyke site.

The list doesn't stop here. More thankyous go to Nick Jarvis, Mats Larsbo and Fredrik Stenemo of SLU, Uppsala for their support and patience with the MACRO modelling, to Jon Finch of the Centre of Ecology and Hydrology for his generous help with the DFIDGWR model, to Alina Marka of the University of East Anglia for her ^{18}O analyses, to Sudeep Kanungo for his biostratigraphy work, to David Kinniburgh for his geochemical advice, to the UCL and Birkbeck Geography departments for generously lending me their field equipment, and to Tony Osborn and Sarah Houghton for kindly helping me in the Wolfson laboratory.

This work would not have been possible without the British taxpayer who, via an EPSRC project (CFEP, GR/N33119), sponsored my research. I also wish to thank all my colleagues at the Department of Earth Sciences, UCL, for their assistance and friendship throughout the years. Finally, I am very grateful to my parents, whose love and endless support have brought me to where I am now. And thank you Ricardo, for everything.

Table of contents

List of Figures

List of Tables

List of symbols

a	[L]	Characteristic radius or half-width
a_f	[L]	Fracture aperture
b	[-]	Empirical constant (Campbell)
b_f	[L]	Fracture spacing
B	[L T^{-1}]	Bypass flow
c	[M L^{-3}]	Solute concentration
c_a	[-]	Local solute concentration
c_f	[-]	Correction factor for canopy evaporation
c_{im}	[M L^{-3}]	Solute concentration in the immobile zone
c_{ma}	[M L^{-3}]	Solute concentration in the macropores
c^*_{ma}	[M L^{-3}]	Solute concentration entering the macropores
c_{mi}	[M L^{-3}]	Solute concentration in the micropores
c_{mo}	[M L^{-3}]	Solute concentration in the mobile zone
c_p	[J M^{-1} $°C^{-1}$]	Specific heat of moist air
c_r	[M L^{-3}]	Solute concentration in the incoming rainfall
c_x	[M L^{-3}]	Solute concentration in the donor cell
C	[L^{-1}]	Specific capacity
d_S	[L]	Maximum (Stokes) diameter
D	[L^2 T^{-1}]	Water diffusivity
D^*	[-]	Current day number of the year
D_0	[L^2 T^{-1}]	Free-water diffusion coefficient
D_A	[L^2 T^{-1}]	Apparent diffusion coefficient
D_E	[L^2 T^{-1}]	Effective diffusion coefficient
D_{eff}	[L^2 T^{-1}]	Effective dispersion coefficient
D_L	[L^2 T^{-1}]	Longitudinal dispersion coefficient
e_d	[M L^{-1} T^{-2}]	Actual vapour pressure
e_s	[M L^{-1} T^{-2}]	Saturated vapour pressure
$e_{s,Twb}$	[M L^{-1} T^{-2}]	Saturated vapour pressure at T_{wb}
E_r	[L T^{-1}]	Actual root water uptake
E_s	[L T^{-1}]	Actual soil evaporation rate

E_t	[L T^{-1}]	Total actual evapotranspiration rate
E_{wc}	[L T^{-1}]	Actual wet canopy evaporation rate
f	[-]	Proportion of effective rainfall diverted to bypass flow
f_c	[-]	Concentration factor for root water uptake
F	[-]	Formation factor
F_a	[C mol^{-1}]	Faraday constant
g	[L T^{-2}]	Gravimetric constant
G	[J L^{-2} T^{-1}]	Outgoing heat conduction into the soil
$GLAI$	[-]	Green leaf area index
h	[L]	Pressure head
h_b	[L]	Boundary pressure head
h_c	[L]	Mean vegetation height
h_e	[L]	Air-entry pressure
h_{ma}	[L]	Pressure head in the macropores
h_{mi}	[L]	Pressure head in the micropores
H	[L]	Total head
I_c	[L T^{-1}]	Canopy interception rate
I_{ma}	[L T^{-1}]	Infiltration rate into the macropores
I_{max}	[L T^{-1}]	Infiltration capacity of the micropores
I_{mi}	[L T^{-1}]	Infiltration rate into the micropores
J	[M L^{-2} T^{-1}]	Diffusive flux of solutes in free water
J_m	[M L^{-2} T^{-1}]	Diffusive flux of solutes in a porous medium
k	[M L^2 T^{-2} K^{-1}]	Boltzmann constant
K	[L T^{-1}]	Hydraulic conductivity
K_a	[L T^{-1}]	Apparent hydraulic conductivity
K_b	[L T^{-1}]	Boundary hydraulic conductivity
K_{eff}	[L T^{-1}]	Effective hydraulic conductivity
K_{ma}	[L T^{-1}]	Hydraulic conductivity of the macropores
K_{mi}	[L T^{-1}]	Hydraulic conductivity of the micropores
K_s	[L T^{-1}]	Saturated hydraulic conductivity
K_s^*	[L T^{-1}]	Fictitious saturated hydraulic conductivity
L	[L]	Characteristic flow length

LAI	[-]	Total leaf area index
m_s	[-]	Mass of solute sorbed per mass of solid
m	[-]	van Genuchten parameter
n	[-]	van Genuchten parameter
n^*	[-]	Pore size distribution index of the macropores
n_s	[T]	Number of bright sunshine hours a day
N_d	[T]	Total day length
P	[L T^{-1}]	Precipitation rate
P_a	[M L^{-1} T^{-2}]	Atmospheric pressure
P_B	[L T^{-1}]	Threshold of effective rainfall for bypass flow
P_c	[M L^{-1} T^{-2}]	Capillary pressure
Pe	[-]	Peclet number
P_e	[L T^{-1}]	Net precipitation rate
PE_r	[L T^{-1}]	Potential root water uptake rate
PE_s	[L T^{-1}]	Potential soil evaporation rate
PE_t	[L T^{-1}]	Total potential evapotranspiration rate
PE_w	[L T^{-1}]	Potential wet canopy evaporation rate
q	[L T^{-1}]	Water flux
q_{in}	[L T^{-1}]	Vertical water flux entering a layer
q_{max}	[L T^{-1}]	Maximum upward water flux
q_n	[L T^{-1}]	Vertical water flux out of the profile
$q_{out,mi}$	[L T^{-1}]	Vertical water flux leaving a layer
Q	[L T^{-1}]	Recharge
Q_d	[M L^{-2} T^{-1}]	Mass of solute stored in the mixing depth
Q_s	[L T^{-1}]	Soil drainage
r	[L]	Capillary radius
r_a	[T L^{-1}]	Aerodynamic resistance
r_i	[-]	Proportion of the total root length in layer i
r_p	[L]	Radius of diffusing solute
r_s	[T L^{-1}]	Surface resistance
R	[-]	Retardation factor
R_g	[J mol^{-1} K^{-1}]	Gas constant
R_i	[L T^{-1}]	Interflow

R_n	[J L^{-2} T^{-1}]	Net incoming radiation
R_o	[L T^{-1}]	Surface runoff
S	[T^{-1}]	Sink/source of water
S_e	[-]	Effective saturation
$S_{e,ma}$	[-]	Effective saturation of the macropores
$S_{e,mi}$	[-]	Effective saturation of the micropores
S_{ma}	[-]	Degree of saturation in the macropores
S_r	[T^{-1}]	Root water uptake
S_t	[J L^{-2} T^{-1}]	Incoming solar radiation
t	[T]	Time
T	[°C]	Air temperature
T_f	[L^2 T^{-1}]	Transmissivity of a fracture
T_K	[K]	Absolute temperature
T_s	[°C]	Soil temperature
T_w	[°C]	Temperature at the water surface
T_{wb}	[°C]	Wet bulb temperature
u	[L T^{-1}]	Wind speed
U_e	[T^{-1}]	Solute exchange between domains
U_r	[T^{-1}]	Uptake of solutes by the roots
U_s	[T^{-1}]	Solute evaporation from the soil
v	[L T^{-1}]	Effective velocity
V	[L^3 mol^{-1}]	Molar volume
w	[-]	Gravimetric water content
W_c	[L]	Amount of water stored on the canopy
$W_{c,max}$	[L]	Canopy interception capacity
x	[L]	Horizontal distance
x_1	[-]	Factor controlling increase in GLAI
x_2	[-]	Factor controlling decrease in GLAI
x_c	[L]	Location of the centre of mass
z	[L]	Vertical distance, or Elevation head
z_d	[L]	Mixing depth
z_r	[L]	Root depth
Z	[-]	Ionic charge

α	[L^{-1}]	van Genuchten parameter
α^*	[-]	Albedo
α_c	[°]	Contact angle
α_L	[L]	Longitudinal dispersivity
α_s	[T^{-1}]	Solute transfer coefficient
α_w	[L^{-1} T^{-1}]	Water transfer coefficient
β	[-]	Geometry coefficient
δ	[-]	Constrictivity
Δ	[M L^{-1} T^{-2} °C^{-1}]	Slope of the saturation vapour pressure curve
ΔS	[L T^{-1}]	Change in soil water content
Δt	[T]	Time step
Δz	[L]	Layer thickness
ϕ	[-]	Porosity
ϕ_D	[-]	Through-diffusion porosity
ϕ_f	[-]	Rock capacity factor, or fictitious porosity
Φ	[M L^{-1} T^{-2}]	Total potential
Φ_g	[M L^{-1} T^{-2}]	Gravitational potential
Φ_m	[M L^{-1} T^{-2}]	Matrix potential
γ	[M T^{-2}]	Surface tension of water
γ_p	[M L^{-1} T^{-2} °C^{-1}]	Psychrometric constant
γ_w	[-]	Empirical scaling factor
Γ_s	[M L^{-3} T^{-1}]	Mass exchange of solutes
Γ_w	[T^{-1}]	Exchange of water
λ	[-]	Pore size index
λ_w	[M^2 T^{-2}]	Latent heat of evaporation of water
λ_0	[A^2 T^3 kg^{-1} mol^{-1}]	Equivalent ionic conductivity at infinite dilution
μ	[T^{-1}]	First order degradation rate
μ_w	[M L^{-1} T^{-1}]	Dynamic viscosity of water
θ	[-]	(Volumetric) water content
θ_a	[-]	Upper critical water content for root water uptake
θ_b	[-]	Boundary water content

θ_d	[-]	Lower critical water content for root water uptake
θ_e	[-]	Equilibrium water content
θ_f	[-]	Water content at field capacity
θ_{im}	[-]	Water content of the immobile zone
θ_{ma}	[-]	Water content of the macropores
θ_{mi}	[-]	Water content of the micropores
θ_{mo}	[-]	Water content of the mobile zone
θ_r	[-]	Residual water content
θ_s	[-]	Saturated water content
θ_s^*	[-]	Fictitious saturated water content
θ_w	[-]	Wilting point
ρ_a	[M L^{-3}]	Atmospheric density
ρ_b	[M L^{-3}]	Bulk dry density
ρ_s	[M L^{-3}]	Particle density
ρ_w	[M L^{-3}]	Density of water
τ	[-]	Tortuosity
τ_e	[T]	Equilibration time constant
ω	[T^{-1}]	Water transfer coefficient
ω^*	[-]	Water stress index
ω^*_c	[-]	Root adaptability factor
ω_i	[-]	Water stress reduction factor for layer *i*
Ω	[T^{-1}]	Pseudodiffusivity
ψ	[-]	Diffusibility
ζ	[-]	Root distribution factor

1 Introduction

1.1 Background

The research described in this thesis is about flow and solute transport through unsaturated chalk, and the role of the fractures and the matrix in these processes. The driving force behind such effort is the need to estimate recharge to the chalk aquifer and to protect the chalk aquifer from pollution, and more specifically to assess its vulnerability. Before proceeding with the physical aspects of unsaturated chalk, this section gives an overview of the policy and environmental background related to this subject.

In the UK about 30% of the public water supply relies on groundwater (Haigh, 2003). Over the last few decades, this important resource has come under threat of pollution. Sources of groundwater pollution are widespread, including diffuse sources and point sources. The major diffuse pollutants are nitrate and pesticides, derived from agricultural practices. It is predicted that nitrate concentrations for many outcrop areas of major aquifers in the UK may exceed the maximum allowable concentration for drinking water supply (50 mg/l as NO_3) early in the 21st century (Harris, 1998). For pesticides, the maximum allowable concentrations are much lower (0.1 μg/l for individual pesticides). As a consequence, pollution by pesticides is often difficult to detect and small quantities of pesticide can have large impacts. Substances emanating from point sources such as landfills or industrial spills may spread as a well-defined plume and can give rise to widespread contamination.

Faced with these pollution problems there is clearly a need for regulation to allow a sustainable use of the groundwater resources. Both at European and national level several controls have been put forward. An important step at European level was the Groundwater Directive (80/68/EEC) of the Council of European Communities (1980)

on the protection of groundwater against pollution caused by certain dangerous substances. Importantly, it required *all* groundwater to be protected, regardless of any use in present or future. The Water Framework Directive was adopted in the year 2000. It sets out quality objectives for all waters in Europe, including groundwater. The emphasis is on integrated water management based on river basins and on sustainability (Environment Agency, 2002). Specific measures for groundwater have now been drafted in the Groundwater Daughter Directive.

The Water Framework Directive still needs implementation in UK law. Existing water legislation in the UK is contained in the Water Resources Act (1991), which includes control of groundwater pollution. It states that the National Rivers Authority (later integrated into the Environment Agency) has the duty for England and Wales to protect the quality of groundwater and to secure its proper use. In 1992, the National Rivers Authority (NRA) published a document: Policy and Practice for the Protection of Groundwater. It sets out a framework for groundwater decision making in England and Wales and was later updated by the Environment Agency (Environment Agency, 1998). In short the policy provides classification of groundwater vulnerability, definition of source protection zones and statements on groundwater protection policy. An overview of groundwater vulnerability mapping is included underneath.

Foster (1987) defined *aquifer pollution vulnerability* as "the intrinsic characteristics of the strata separating the saturated aquifer from the immediately overlying land surface which determine its sensitivity to being adversely affected by a surface applied (anthropogenic) contaminant load". A distinction can be made between intrinsic vulnerability and specific vulnerability. *Intrinsic vulnerability* considers all kinds of contaminants and refers to the inherent hydrogeological and geological characteristics of the strata overlying the saturated aquifer. *Specific vulnerability* is defined for a given contaminant and requires consideration of the characteristics of the contaminant and of the aquifer relative to the contaminant, in addition to the inherent hydrogeological and geological characteristics.

A guidebook on groundwater vulnerability mapping has been published by Vrba and Zaporozec (1994). Most vulnerability mapping procedures are based on so-called overlay and index methods. They use an empirical approach, based on a classification

of key attributes where each attribute is assigned a numerical index or score. Examples are the GOD scheme (Foster, 1987), the DRASTIC method developed by the US EPA (Aller et al., 1987), and the EPIK method designed specifically for karstic systems (Doerfliger et al., 1999). Although all these indices are useful and easy to use, they are essentially empirical, based on expert judgement. They are qualitative and lack a clear physical basis.

Process-based simulation models form an alternative approach. They start from the accepted physics of solute transport through the unsaturated zone and attempt to predict solute concentrations in both time and space. Sophisticated models exist, but the required input parameters are often not available, which leads to errors and uncertainties. Models are better kept simple for ubiquitous use in vulnerability mapping. The use of a geographic information system (GIS) is a suitable aid in the construction of a vulnerability map (e.g. Hiscock et al., 1995).

The Environment Agency, as part of their Policy and Practice for the Protection of Groundwater, publishes a series of 53 vulnerability maps of 1:100,000 scale, covering the whole area of England and Wales (Environment Agency, 1998). The approach used is a simplified overlay method for inherent vulnerability assessment, where the key attributes are: (1) presence and nature of overlying soil, (2) presence and nature of drift, (3) nature of strata and (4) depth of unsaturated zone. So far the depth to the unsaturated zone has not been included in the maps, due to a lack of good quality data.

The groundwater vulnerability approach applied for England and Wales exhibits the typical shortcomings of overlay methods, being mainly empirical and qualitative. New methods are being developed to be more physically based, e.g. the COST Action 620 programme which proposed an approach suitable for all European carbonate aquifers (Daly et al., 2002). There is a need to integrate process-based models in the groundwater vulnerability methodology, thus giving the vulnerability maps a stronger physical basis (Gogu and Dassargues, 2000; Gogu et al., 2003). To achieve this, the mechanisms of flow and solute transport through the unsaturated zone must be well understood. Notably in the Chalk, the most important aquifer in England and Wales, this understanding is still lacking. Hence to establish a proper assessment of the

vulnerability of the Chalk aquifer, more research is needed on the flow and solute transport processes in the chalk unsaturated zone.

1.2 Objectives

The general aim of this work is to improve the understanding of flow and solute transport through unsaturated chalk. The Chalk is a fractured porous medium consisting of a porous matrix intersected by fractures. The respective role of the matrix and the fractures in unsaturated flow and solute transport is not well understood. Hence the specific objectives of this work are twofold:

1. To assess the importance of fracture flow in unsaturated chalk: its contribution to recharge, as well as the factors that control its occurrence.
2. To clarify the exchange of solutes between the fractures and the matrix: the processes involved and its influence on solute transport.

In turn, the findings of this work should contribute to a better assessment of the vulnerability of the Chalk aquifer.

1.3 Thesis outline

After this introductory chapter, Chapter 2 contains a review of flow and solute transport through unsaturated porous media, and the different modelling approaches that are suitable for specific types of porous media. In Chapter 3, the discussion is concentrated on the Chalk, and a review is given of current research and understanding regarding flow and solute transport through unsaturated chalk. Chapter 4 focuses on the Fleam Dyke research site, and includes an overview of all previously published research at this particular site. Chapter 5 presents the fieldwork undertaken by the author at the Fleam Dyke site. This includes a physical characterisation of the unsaturated profile, and a tracer test on the Fleam Dyke lysimeter covering two recharge seasons. In Chapter 6, a technical description is given of the MACRO 5.0 model that was used in the current research. Chapter 7 describes the flow modelling with MACRO, moving on to solute transport modelling in Chapter 8. Therefore the extensive data set is used that is available for the Fleam Dyke site, including the

historical tritium and deuterium profiles and the current tracer test. In Chapter 9, a simplified water balance method is applied to simulate the recharge from the Fleam Dyke lysimeter. Finally, Chapter 10 discusses conclusions and implications of this work, and makes suggestions for future research.

2 Flow and solute transport through unsaturated porous media

2.1 Introduction

The consideration of the unsaturated zone (also called *vadose zone*) is essential in any assessment of the vulnerability of an aquifer to contaminants released at or near the surface. The travel time through the unsaturated zone represents a delay of contaminants before they reach the water table. Moreover, it is here that the rates of degradation by chemical and biological processes are likely to be highest. It is thus important to have a good understanding of the processes that govern transport of contaminants through the unsaturated zone. In the context of this work, the discussion is limited to soluble contaminants. Because transport is mainly driven by flow, the discussion must involve unsaturated flow together with transport.

In this chapter, the physics of flow and solute transport through unsaturated porous media will be reviewed. The text has been organized according to the structure of the porous medium, making a distinction between single porous media, aggregated porous media and fractured porous media. It will be shown that each of these types of porous media may require a different conceptualization, reflecting specific processes related to their structure. For each type of porous medium, possible modelling approaches for unsaturated flow and transport will be discussed.

2.2 Single porous media

2.2.1 Qualitative description

As a first approach, let us consider an idealized porous medium, consisting of a skeleton of solid material giving rise to a uniform network of interconnected regular pores. The surface of the solid material is assumed to be smooth, while all the pores have identical shape and size. An example of such a porous medium would be a column with uniform spherical glass beads, stacked in a regular manner.

Starting from such an idealized porous medium, deviations can be considered in which the size and shape of the pores are not uniform anymore. This would be the case of a homogeneous soil consisting of a regular packing of particles of variable grain size. Another example would be a massive block of porous rock with a non-uniform pore size distribution. At this stage, however, we still assume that all the pores are well connected and can contribute to the flow of fluids through the porous medium. The porous network lacks any hierarchical structure and can be considered as a single continuum. For the rest of this work, such a medium will be referred to as a *single porous medium* (Figure 2-1).

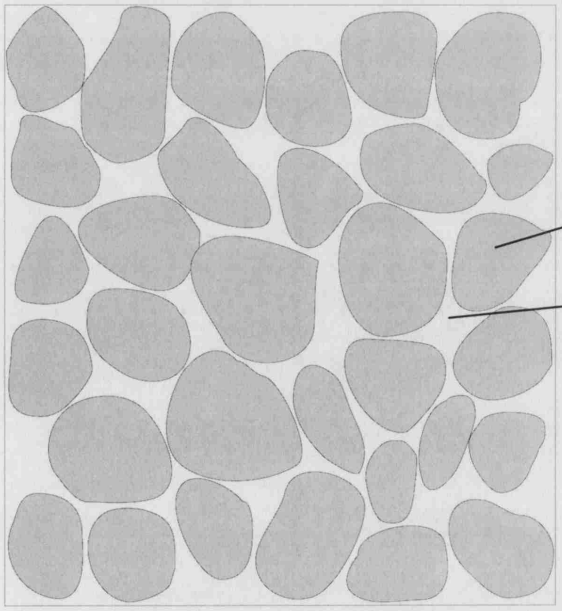

PORES CONTAIN	
Saturated	Unsaturated
Fluid	Gas and/or Fluid and gas

Figure 2-1 Single porous medium

When the pores contain fluids in both liquid and gaseous phase, the medium is said to be unsaturated. An unsaturated porous medium then consists of three phases: the solid phase (the skeleton of the medium, generally consisting of a mineral and an organic fraction), the liquid phase (the liquid fluid) and the gaseous phase (the gaseous fluid). For the scope of this work, the liquid phase is water and the gaseous phase is air. Table 2-1 summarizes some important parameters that characterize unsaturated porous media. These properties relate to the macroscopic scale rather than the microscopic scale. Indeed, when describing water movement, it is more the bulk water flow rather than the flow through individual pores that is important.

In the following two sections, some basic concepts of flow and solute transport through unsaturated single porous media will be described. These concepts stem from the classic theory of soil physics on the one hand (Childs, 1969; Hillel, 1971; Kirkham and Powers, 1972) and hydrogeology on the other hand (Bear, 1979; Bear and Verruijt, 1990; Fetter, 1994; Fetter, 1999; Freeze and Cherry, 1979; Zheng and Bennett, 1995).

Table 2-1 General parameters of unsaturated porous media

Solid mass [M]	M_s
Liquid mass [M]	M_L
Solid volume [L^3]	V_s
Liquid volume [L^3]	V_L
Gaseous volume [L^3]	V_g
Mean particle density [$M\ L^{-3}$]	$\rho_s = M_s / V_s$
Bulk dry density [$M\ L^{-3}$]	$\rho_b = M_s / (V_s + V_L + V_g)$
Porosity [-]	$\phi = (V_L + V_g) / (V_s + V_L + V_g)$
Volumetric water content [-]	$\theta = V_L / (V_s + V_L + V_g)$
Gravimetric water content [-]	$w = M_L / M_s$

2.2.2 Unsaturated flow

2.2.2.1 Richards' equation

The continuity equation for water flow in a porous medium is an expression of the conservation of total water volume in a *representative elementary volume* (REV). An REV is a volume of small size compared to the scale of the problem and in which flow and transport properties are statistically homogeneous. In 3D, the continuity equation is written as:

$$\frac{\partial \theta}{\partial t} = -\nabla . q + S \qquad \textit{Eq. 2-1}$$

where q is the water flux (the volume of water flowing through a unit cross-sectional area per unit time) [L T^{-1}] and S is an optional sink/source term (taken positive for a source and negative for a sink) [T^{-1}] for processes such as plant water uptake or diversion to a drainage system.

The classical equation to describe the water flux q through a porous medium is Darcy's law, which expresses the water flux as a function of the hydraulic head gradient (Darcy, 1856). The total hydraulic head H [L] is the energy per unit weight of water at any point, and will be further discussed in section 2.2.2.2. The factor that links the water flux to the total hydraulic head gradient is the hydraulic conductivity K [L T^{-1}], which is a measure of the ease of water transmission in a porous medium. Although originally developed for saturated media, Darcy's law is valid for unsaturated media as well, provided that the hydraulic conductivity is represented as a function of the pressure head h (further discussed in 2.2.2.2.2). The general form of Darcy's law for unsaturated flow in 3D becomes then:

$$q = -K(h)\nabla H \qquad \textit{Eq. 2-2}$$

or, in 1D:

$$q_z = -K(h)\frac{\partial H}{\partial z} \qquad \textit{Eq. 2-3}$$

where $K(h)$ is the unsaturated hydraulic conductivity as a function of the pressure head [L T^{-1}], H is the total head [L] and z is the vertical distance (positive upward) [L].

Note that the water flux q, also called *Darcy velocity*, is not the same as the actual velocity of the water molecules in the porous medium. This *effective velocity* (also called kinematic velocity) is considerably higher, because the actual flow section is smaller than the total section. The effective velocity v [L T^{-1}] is related to the flux q by the water content θ:

$$v = \frac{q}{\theta} \qquad \textit{Eq. 2-4}$$

Darcy's Law is not universally valid. Although it can be used in most practical situations, it has some limitations:

1) Darcy's law is only valid under laminar flow conditions. This may not be the case for large hydraulic gradients in large pores.
2) At low hydraulic gradients in small pores, the flux may be lower than predicted by Darcy's law.

The continuity equation can now be combined with Darcy's law to obtain a general expression for unsaturated flow. Inserting Eq. 2-2 into Eq. 2-1 gives:

$$\frac{\partial \theta}{\partial t} = \nabla.[K(h)\nabla H] + S \qquad \textit{Eq. 2-5}$$

Writing the total head H as the sum of the pressure head h (negative in the unsaturated zone) and the elevation head z (positive upwards), this becomes:

$$\frac{\partial \theta}{\partial t} = \nabla.[K(h)\nabla h] + \frac{\partial K(h)}{\partial z} + S \qquad \textit{Eq. 2-6}$$

This equation is known as the mixed form of Richards' equation. It is called mixed form because both the water content θ and the pressure head h feature in the equation. Alternative forms are the pressure-based form:

$$C(h)\frac{\partial h}{\partial t} = \nabla.[K(h)\nabla h] + \frac{\partial K(h)}{\partial z} + S \qquad \textit{Eq. 2-7}$$

or the moisture-based form:

$$\frac{\partial \theta}{\partial t} = \nabla.[D(\theta)\nabla \theta] + \frac{\partial K(\theta)}{\partial z} + S \qquad \textit{Eq. 2-8}$$

where $C(h)$ is the specific capacity [L^{-1}]:

$$C(\theta) = \frac{d\theta}{dh} \qquad \textit{Eq. 2-9}$$

and $D(\theta)$ is the diffusivity [$L^2\ T^{-1}$]:

$$D(\theta) = \frac{K(\theta)}{C(\theta)} \qquad \textit{Eq. 2-10}$$

Because unsaturated flow through heterogeneous porous media is generally a vertical problem, the equation can often be reduced to 1D:

$$\frac{\partial \theta}{\partial t} = \frac{\partial}{\partial z}\left[K(h)\frac{\partial h}{\partial z}\right] + \frac{\partial K(h)}{\partial z} + S \qquad \textit{Eq. 2-11}$$

Richards' equation has been derived from the flow continuity equation, and the use of the latter inherently introduces some assumptions:

1) The temperature and the atmospheric air pressure are constant.
2) The solid matrix is non-deformable and the water incompressible.
3) The density of the water is independent of the solute concentration.
4) The air is assumed to be perfectly mobile, so that the whole gaseous phase is at atmospheric pressure.

These assumptions are generally acceptable, provided that extreme temperature fluctuations are damped in the profile, that the solid structure is rigid and that the water does not contain solutes in very high concentrations.

To solve Richards' equation, the moisture retention relationship, $h(\theta)$, and the unsaturated hydraulic conductivity function, $K(h)$ or $K(\theta)$, need to be included. Both are highly non-linear, and will be described in 2.2.2.3. This makes the mathematical

problem difficult to solve. Analytical solutions[1] have been proposed for a limited number of problems, starting from simplifying hypotheses about the boundary conditions or the geometry of the flow problem. Usually it means that the transient water movement needs to be represented by constant parameters. Numerical solutions provide much greater flexibility in geometry, soil properties and boundary conditions.

2.2.2.2 Water potential

The water in a porous medium is subject to several forces. As a result of these forces, the water can be thought of as having energy, defined as the water potential. This total potential generally consists of several components, such as the gravitational potential, the matric potential, the osmotic potential and the kinetic potential. In moderate climates without excessive evapotranspiration, and where salt concentrations are low, the osmotic forces are usually relatively small (except at the interface between plant roots and soil), so that the osmotic potential can often be ignored. Similarly, the kinetic potential (defined as $v^2/2g$) is usually assumed negligible, because of the low fluid velocities in porous media. Hence only the first two potentials are described underneath, with their effect on the dynamics of water in the unsaturated zone.

2.2.2.2.1 Gravitational potential

The water is subject to the earth's gravity, which creates a vertical downward force. The gravitational potential, Φ_g, is then defined as the elevation relative to some arbitrary reference level, referred to as the *datum*. This level is often chosen either at the soil surface or at the water table. Because the level of the water table is not always known, and provided that the soil surface is flat, it is often more convenient to take the soil surface as the datum, and this convention will be used throughout this work. Hence the elevation is chosen negative downwards from the soil surface.

---

[1] *Analytical methods* apply formal mathematical solutions to the governing differential equations, and usually require some simplifying assumptions. *Numerical methods* use a computer code to approximate the differential equations with a set of algebraic equations, and are generally less constrained by restricting assumptions.

2.2.2.2.2 *Matric potential*

In an unsaturated porous medium, the contact angle between the liquid and the solid is defined by the combination of the surface tensions between the solid, liquid and gaseous phases. For a wetting liquid, such as water on argillaceous soil, the contact angle is smaller than 90°, and a concave meniscus is formed in the pores. The curvature of a concave meniscus causes the liquid pressure under the meniscus to be smaller than atmospheric pressure. For a cylindrical tube, this difference in pressure between the water and the atmosphere across the curved liquid-gas interface is called *capillary pressure* and is given by (Hillel, 1971):

$$P_c = \frac{2\gamma \cos \alpha_c}{r} \qquad \textit{Eq. 2-12}$$

where γ is the surface tension of water [M T^{-2}], α_c is the contact angle [-], and r is the radius of the capillary tube [L]. This pressure difference leads to capillary rise: the water rises in the tube, until the hydrostatic pressure of the water column compensates the pressure difference (Figure 2-2). The height of capillary rise h [L] is then given by:

$$h = \frac{P_c}{\rho_w g} = \frac{2\gamma \cos \alpha_c}{\rho_w g r} \qquad \textit{Eq. 2-13}$$

where ρ_w is the density of water [M L^{-3}] and g is the gravimetric constant. In addition to those capillary forces, water is also drawn to the surface of the solid phase by adsorption, which forms hydration envelopes around the particle surfaces. The matric potential Φ_m is then the result of the combination of capillary and adsorptive forces, which together lower the energy of the soil water below that of free water.

The matric potential needs to be defined relative to a reference pressure potential, which is generally taken as the atmospheric pressure. In fact, the matric potential is the unsaturated counterpart of the hydrostatic pressure potential in the saturated zone. A continuous *pressure potential* can then be defined on both sides of the water table, which leads to a quantitative definition of the saturated and unsaturated zones. In the saturated zone, the pressure potential is positive due to hydrostatic pressure, and the water table is defined as the surface where the pressure potential equals zero. The

unsaturated zone is always at a negative pressure potential, due to the capillary and adsorptive forces described above. Incidentally, capillary rise starting from the water table creates a zone where all pores are filled with water. This zone above the water table is called the *capillary fringe*, and its height is inversely proportional to the radius of the pores. Although the pores are practically saturated in the capillary fringe, it still belongs to the unsaturated zone because the pressure potential is negative.

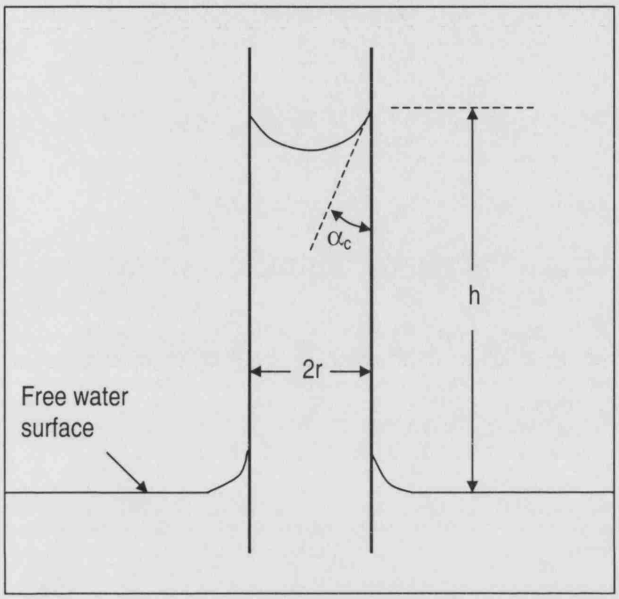

Figure 2-2 Capillary rise (after Hillel, 1971)

2.2.2.2.3 Total potential or total head

The total potential Φ is defined as the sum of the gravitational potential Φ_g and the matric potential Φ_m:

$$\Phi = \Phi_g + \Phi_m \qquad \textit{Eq. 2-14}$$

The potential can be expressed in units of pressure (bars or Pascals), or more conveniently as energy per unit weight. In the latter case, the total potential is called total (hydraulic) head H, in units of cm, and consists of the pressure head h (taken as negative in the unsaturated zone) and the elevation head z (positive upwards):

$$H = h + z \qquad \textit{Eq. 2-15}$$

This terminology is applied in Richards' equation (Eq. 2-6) and will be used throughout this work. An example of a field profile of the total head and its components is shown in Figure 2-3. Differences in total head from point to point in the profile cause water to flow from higher head to lower head. The absolute value of the total head is irrelevant, as it is expressed relative to an arbitrary reference datum. Rather, it is the total head gradient that directs the water movement, as expressed in Darcy's law (Eq. 2-2).

2.2.2.3 Hydraulic properties

2.2.2.3.1 Moisture retention curve

The moisture retention curve expresses the relationship between the water content θ and the pressure head h, and is required to solve Richards' equation (Eq. 2-6). An example for two typical field soils is given in Figure 2-4. When the pressure head is zero, the porous medium is saturated and the water content equals the porosity. When the pressure head decreases, or suction is exerted on the medium, some pores start to drain and the water content decreases. The critical suction when the pores start to drain is also called the *air-entry pressure* or *bubbling pressure*. The largest pores will drain first, and when the pressure head decreases further (i.e. the suction increases), then successively smaller and smaller pores will drain. The relation between the pressure head and the radius of the pores that are emptied is obtained from the capillary equation (Eq. 2-13).

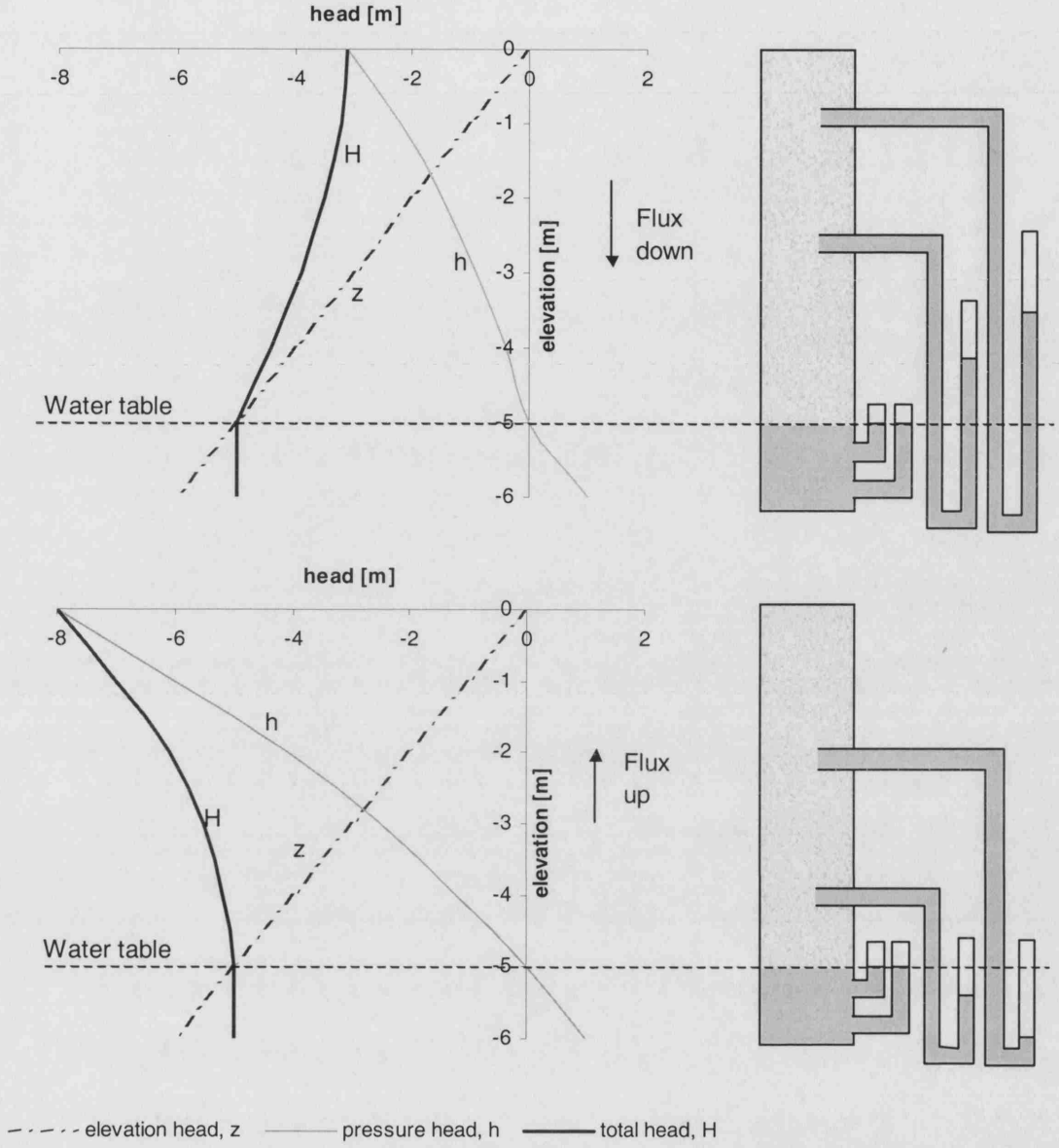

Figure 2-3 Typical profiles of elevation head, pressure head and total head during winter (top) and summer (bottom) for a shallow water table, and with the reference elevation head taken at the surface. Also shown is a set of tensiometers, used for measuring the total head.

Several authors have proposed empirical relationships describing the moisture retention curve. By far the most popular is the model of van Genuchten (1980). It gives the relationship between the effective saturation S_e and the pressure head h, using the empirical parameters α, n and m:

$$S_e(h) = \left[\frac{1}{1+(\alpha h)^n} \right]^m \qquad \textit{Eq. 2-16}$$

with

$$S_e = \frac{\theta - \theta_r}{\theta_s - \theta_r} \qquad \textit{Eq. 2-17}$$

where θ_r is the residual water content and θ_s is the saturated water content. The parameter α is related to the inverse of the air entry pressure. Usually a relationship is defined between the parameters n and m, notably m = 1-1/n. Another popular empirical function is the one proposed by Brooks and Corey (1964):

$$S_e(h) = \left(\frac{h_e}{h}\right)^{\lambda} \qquad \text{if } h \le h_e$$

$$S_e(h) = 1 \qquad \text{if } h > h_e \qquad \textit{Eq. 2-18}$$

where h_e is the air entry pressure and λ is the pore size index.

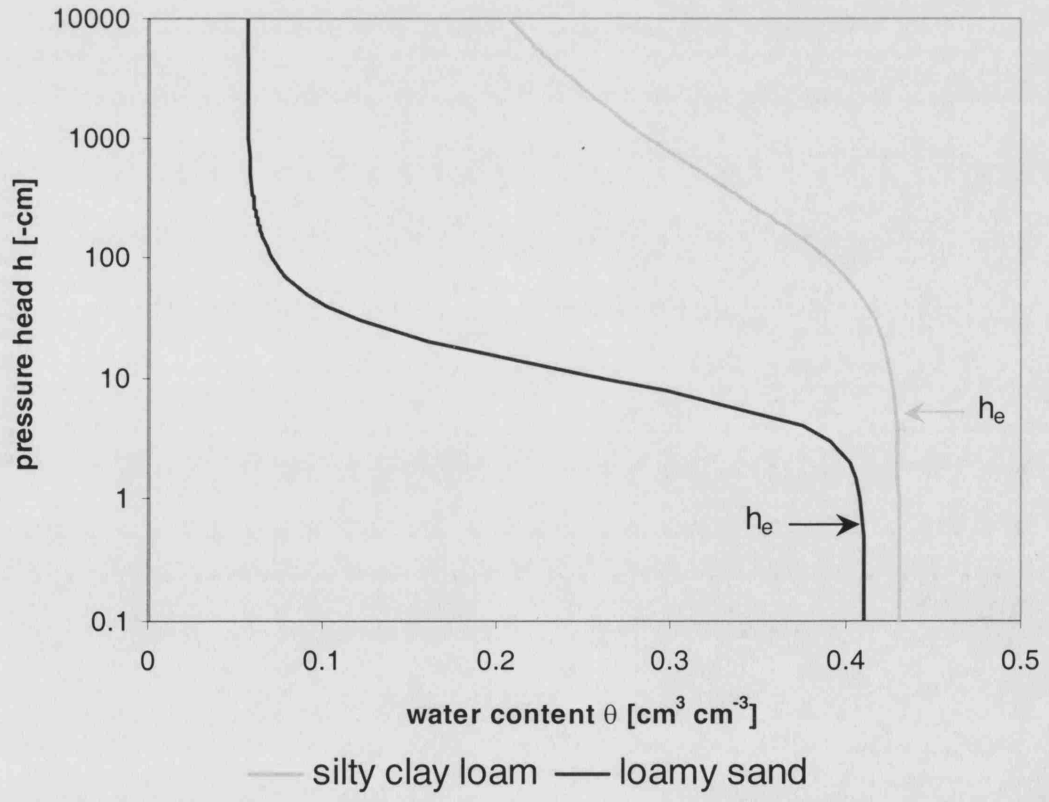

Figure 2-4 Examples of moisture retention curves for two typical field soils, with indication of the bubbling pressure h_e.

The relationship $h(\theta)$ is not unique for a given porous medium, but is dependent on the moisture history of the porous medium. Depending on whether the curve is obtained by wetting or drying, the moisture retention curve follows a different course. This phenomenon is called *hysteresis* and is illustrated in Figure 2-5. In addition to the main branches of wetting and drying, the figure also shows some *scanning curves* which occur when the wetting or drying cycles are reversed. Hence the $h(\theta)$ relationship depends on the wetting-drying history of the porous medium. Two main causes, among others, may be indicated to explain the hysteresis phenomena (Bear, 1979; Hillel, 1971):

1) The *inkbottle effect*. Consider a pore consisting of a large void of radius R, connected by narrow channels of radius r. Starting from saturation, the pore will drain when the pressure head decreases to the air entry value for radius r. To saturate the pore, however, a pressure head is needed corresponding to the air entry value for radius R.
2) The *raindrop effect*. An advancing meniscus exhibits a greater contact angle than a receding meniscus. Hence the corresponding pressure heads are different as well.

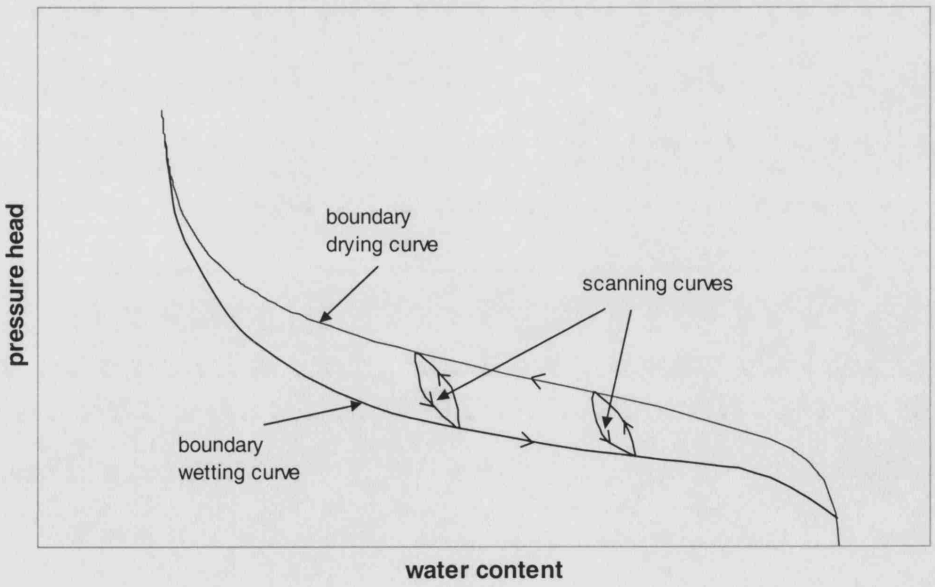

Figure 2-5 Hysteresis of the water retention function, showing the boundary wetting and drying curves and some scanning curves.

To account for hysteretic effects in the moisture retention curve, adaptations to the empirical formula have been proposed (Kool and Parker, 1987; Pickens and Gillham, 1980), but often the effects are simply neglected.

2.2.2.3.2 Unsaturated hydraulic conductivity

The hydraulic conductivity of a porous medium expresses its ability to conduct water, and features in Darcy's Law (Eq. 2-2). The hydraulic conductivity is at its maximum value K_s when the medium is saturated and all pores conduct water. When the medium becomes unsaturated, the conductive portion of the pores decreases. Moreover, the connectivity of the remaining water decreases as it forms isolated pockets of water surrounded by air. Thus the hydraulic conductivity will decrease when the water content decreases. As the hydraulic conductivity varies with the water content, it also varies with the pressure head. An example of the unsaturated hydraulic conductivity function *K(h)* for two field soils is shown in Figure 2-6.

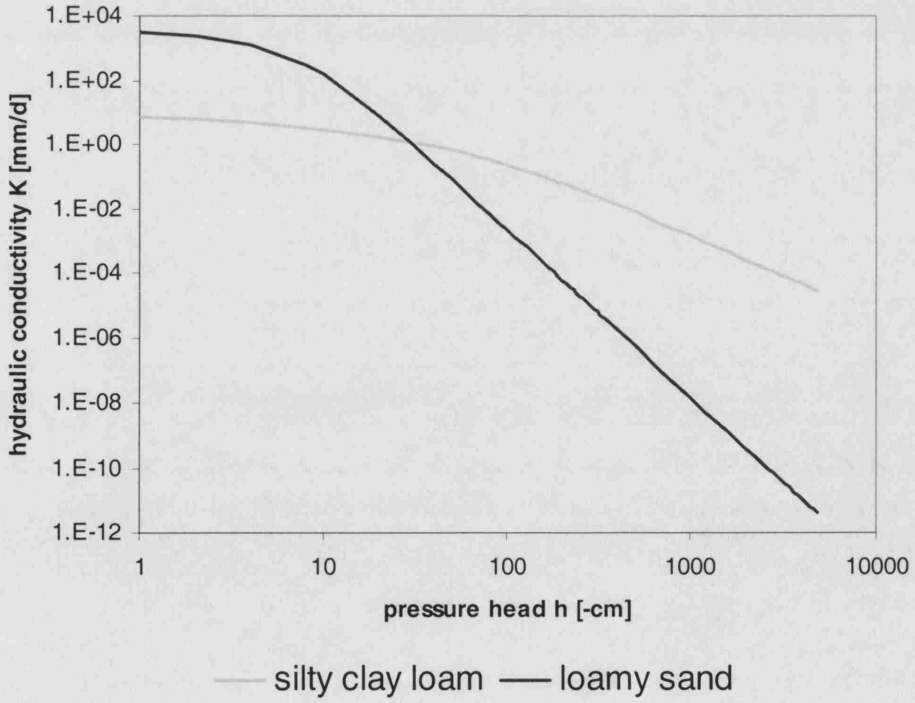

Figure 2-6 Examples of unsaturated hydraulic conductivity functions K(h) for two typical field soils (based on Eq 2-19 with parameter values taken from Clapp and Hornberger (1978)).

Similar to the moisture retention curve, empirical formula have been developed for the unsaturated hydraulic conductivity function *K(h)*. Van Genuchten (1980) used the same parameters as for his moisture retention formula to propose the following model, based on the original model by Mualem (1976):

$$K(h) = K_s \frac{\left\{1-(\alpha h)^{n-1}\left[1+(\alpha h)^n\right]^{-m}\right\}^2}{\left[1+(\alpha h)^n\right]^{m/2}} \qquad \text{Eq. 2-19}$$

or, directly as a function of the effective saturation S_e (and thus related to θ):

$$K(S_e) = K_s S_e^{1/2}\left[1-\left(1-S_e^{1/m}\right)^m\right]^2 \qquad \text{Eq. 2-20}$$

with $m = 1\text{-}1/n$. Likewise, the Brooks and Corey model (1964) gives:

$$K(S_e) = K_s (S_e)^{3+2/\lambda} \qquad \text{Eq. 2-21}$$

Like the moisture retention curve, the *K(h)* function also exhibits hysteresis, but the *K(θ)* function is less prone to hysteresis (Childs, 1969; Poulovassilis, 1969).

The parameters of the empirical hydraulic functions can be obtained by fitting the functions to experimental water retention and conductivity data. Because these data are often hard to gather, empirical methods have been developed for soils to obtain the parameters indirectly from readily available soil data. These so-called pedo-transfer functions (PTFs) derive the hydraulic parameters from data such as grain size distribution, porosity and organic carbon content (e.g. Saxton et al., 1986; Wagner et al., 2001; Zhuang et al., 2001).

2.2.3 Unsaturated solute transport

Earlier it was stated that, for the scope of this work, the liquid phase of the porous medium is water. This generally is not pure water but rather a watery solution, containing various amounts of positive and negative ions, organic molecules, gases etc. A *solute* is here defined as any substance present in the aqueous phase at a

concentration below its solubility limit. It is further assumed that the solute concentration is sufficiently low, so that it has no influence on the viscosity and the density of the water.

In addition to solutes, the water can also contain material in particulate form. Examples are micro-organisms (bacteria, viruses, prions, spores) or colloidal material. By virtue of their size, they may behave differently from solutes, and are often excluded from the smallest pores. However, the study of particulate transport falls beyond the scope of this work and the focus will be on solute transport.

The solutes in the water are susceptible to a variety of physical and chemical processes, leading to migration of the solutes through the porous medium or rather to their immobilization. A short overview of these processes is given in this chapter, together with a mathematical approach to describe the behaviour of solutes in an unsaturated single porous medium.

2.2.3.1 Transport processes

2.2.3.1.1 Advection

Advection is simply the movement of solutes together with the water flow. The solutes move at the same mean effective velocity v as the water molecules.

2.2.3.1.2 Hydrodynamic dispersion

Hydrodynamic dispersion results from variations of the solute velocity and causes the solutes to spread around their average advective position. It is a combination of molecular diffusion and mechanical dispersion.

Molecular diffusion is driven by a concentration gradient, and has its origin in the Brownian motion of solute molecules in the solvent. When a soluble substance is introduced in a solvent, it has a tendency to spread until the solute concentration is

uniform throughout the solvent volume. The same process acts in the fluid phase of a porous medium, but there the diffusion will be slowed down because of the presence of the solid structure. Hence the effective diffusion coefficient D_E will be considerably smaller than the free-water diffusion coefficient D_0. An overview of the different types of diffusion coefficients and their interrelation, together with some values for typical solutes is given in Appendix I.

Mechanical dispersion is due to effects such as differences in length of flow path through the porous network and differences in velocities in the centre of a pore compared to the edges of a pore. The mechanical dispersion of a porous medium is characterized by the longitudinal dispersivity α_L.

The longitudinal dispersion coefficient[2] [$L^2\ T^{-1}$] becomes then:

$$D_L = \alpha_L v + D_E \qquad \textit{Eq. 2-22}$$

where α_L is the longitudinal dispersivity [L], v is the effective velocity [$L\ T^{-1}$] and D_E is the effective diffusion coefficient [$L^2\ T^{-1}$].

The *Peclet number* is a dimensionless number that relates the time to diffuse over distance L to the time to advect over distance L:

$$Pe = \frac{v L}{D_o} \qquad \textit{Eq. 2-23}$$

where L is the characteristic flow length [L]. The dominance in solute transport of either dispersion or diffusion can be illustrated by plotting D_L/D_0 versus the Peclet number (Figure 2-7). The plot shows that for low flow velocities diffusion is predominant, whereas for high flow velocities mechanical dispersion becomes dominant.

[2] In addition to the longitudinal dispersion coefficient, a *transverse dispersion coefficient* can be defined as $D_T = \alpha_T v + D_E$, where α_T is the transverse dispersivity. For 1D problems, however, D_T is often ignored.

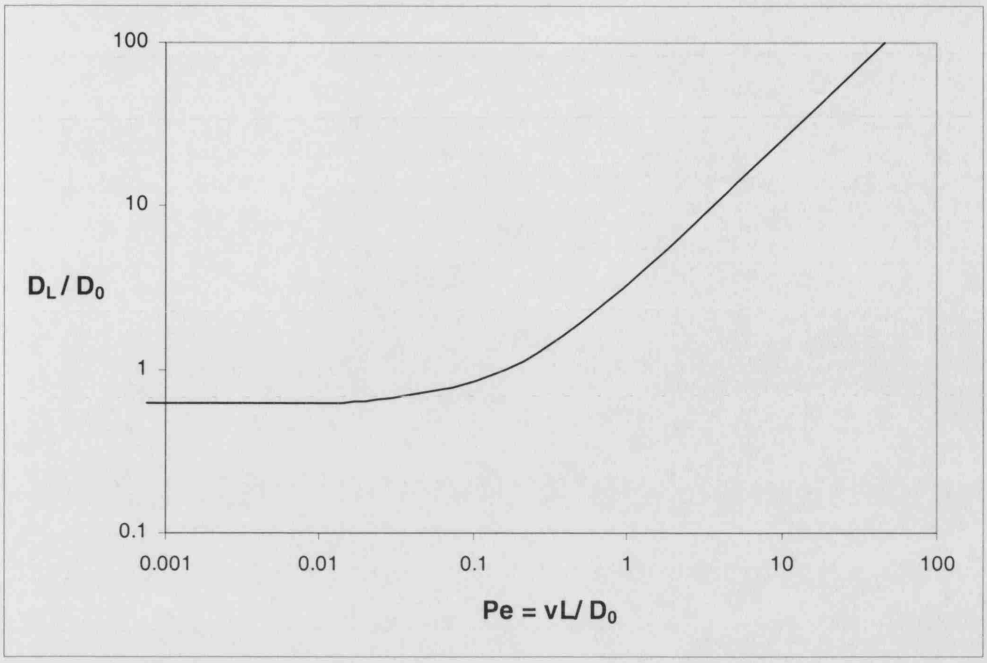

Figure 2-7 D_L/D_0 versus the Peclet number, based on experiments in sand columns (after Perkins and Johnson, 1963). Note that the intercept is less than unity, because at low flow velocities D_L/D_0 tends towards D_E/D_0. The slope of the curve is the dispersivity α.

2.2.3.1.3 Sorption

Sorption is a chemical interaction between the solutes and the solid matrix, and is a term that comprises a variety of processes (Fetter, 1999):

1) adsorption on the solid matrix: fixation of the solute to the surface of the solid;
2) ion exchange: cations attached to the negatively charged solid matrix are replaced by other cations with a higher affinity for the solid;
3) chemisorption: the solute is chemically incorporated into the solid matrix;
4) absorption: diffusion of a solute into the micropores of the solid material and sorption onto interior surfaces.

The net effect of the sorption mechanism is a retardation of the solutes relative to the water flow. If equilibrium is reached in the partitioning of the solute between the liquid and solid phase, then an equilibrium sorption isotherm can be assumed. Practically, this can be used if the sorption reaction is fast compared to the flow velocity. Examples of equilibrium sorption isotherms are the linear sorption isotherm,

the Freundlich isotherm and the Langmuir isotherm. If the sorption reaction is slow compared to the flow velocity, then a kinetic sorption model needs to be used. In the case of nonlinear sorption isotherms or kinetic sorption models, an asymmetrical breakthrough curve can be the result (Brusseau, 1999).

2.2.3.1.4 Transformation reactions

Depending on its nature, the solute can be subject to a range of *transformation reactions*, like biodegradation, radioactive decay, precipitation and volatilization. The general effect of these decay reactions is to decrease the solute concentration. Alternatively, production reactions can lead to an increase in concentration. Usually the production and decay reactions are modelled by zero or first order kinetics.

2.2.3.2 The Advection Dispersion Equation

The classical expression that describes solute transport and that accounts for all previously described processes is the *Advection Dispersion Equation* (ADE). It expresses conservation of solute mass in the porous medium. For 1D vertical unsaturated transport, including equilibrium sorption and first order decay, the ADE is written as:

$$\frac{\partial(c\theta)}{\partial t}+\rho_b\frac{\partial m_s}{\partial t}=\frac{\partial}{\partial z}\left[\theta D_L\frac{\partial c}{\partial z}\right]-\frac{\partial(qc)}{\partial z}+\mu\theta c+cS \qquad \textit{Eq. 2-24}$$

where c is the solute concentration [M L^{-3}], ρ_b is the bulk dry density [M L^{-3}], m_s is the mass of solute sorbed per mass of solid [-], S is a sink/source of water [T^{-1}] and μ is the first order degradation rate [T^{-1}]. The water flux q forms the link between the transport equation and the flow equation (Eq. 2-2). For an unsaturated transient flow regime, the flux and water content are normally calculated by the Richards' equation.

Not all solutes are equally subject to sorption and transformation reactions. A *conservative solute* is a solute where sorption and transformation are assumed to be non-existent. It is thus chemically inert and shows no interaction with the solid matrix. Although it is recognized that sorption and transformations reactions can

greatly influence solute transport in the majority of field situations, they do not form the subject of this work. For a conservative solute in 1D, the ADE is reduced to:

$$\frac{\partial(c\theta)}{\partial t} = \frac{\partial}{\partial z}\left[\theta D_L \frac{\partial c}{\partial z}\right] - \frac{\partial(q c)}{\partial z} + cS \qquad \textit{Eq. 2-25}$$

A range of analytical solutions have been obtained, e.g. the classical solution given by Ogata and Banks (1961) for longitudinal transport through a homogeneous semi-infinite medium. Van Genuchten and Alves (1982) published a compendium of analytical solutions for various initial and boundary conditions. To account for vertical non-homogeneity, other authors have proposed analytical or semi-analytical solutions for layered media. Connell and Van den Daele (2003) developed a two-layer approach for solute transport through unsaturated soils, consisting of a root zone and a sub-root zone. They used a transformation of the ADE that simplifies the way in which water movement is described. The model assumes quasi-steady-state conditions for the flow behaviour, using a time-averaged water content profile and cumulatives of infiltration and evapotranspiration. The equations are analytically solved in Laplace space and then numerically inverted. The same approach was later used by Connell and Van den Daele (in review) in a combined model for unsaturated and saturated solute transport. They used a 1D ADE for vertical transport in the unsaturated zone, coupled to a 3D ADE for lateral transport in the saturated zone. In addition to the two-layer approach, they included a one-layer solution and a formulation with a lumped root zone (Connell, 2002). In general, however, numerical solutions to the ADE are more widely used because they are more flexible.

2.2.3.3 Alternative approach: the transfer function

Other approaches than the deterministic Advection Dispersion Equation have been proposed. Jury (1982) used a transfer function formulation in a stochastic framework to model solute transport, producing average and extreme solute concentrations as a function of depth and time. The model transforms an input function into an output function, without necessarily describing the actual physical processes involved. The transfer function gives the distribution of travel times and is fitted to a probability distribution by calibration with field data. Often a log-normal distribution is used. The model is based on the concept of solutes moving at different velocities in isolated

stream tubes without lateral mixing (Jury and Roth, 1990). A similar approach has been proposed by Williams et al. (2003) in their Multiple Analytical Pathways (MAP) model. Their model simulates flow and transport along a series of stream tubes from the ground surface to an output feature such as a well. It is thus a combined model for unsaturated and saturated flow and transport, using a series of transfer functions to describe each section.

The transfer function formulation has advantages over the deterministic approach, because there is no need to know the hydraulic parameters of the porous medium, and therefore it is particularly useful to deal with lateral and vertical variability in hydraulic parameters. However, the model depends on the assumptions of quasi-steady flow and of a linear system response. In reality, unsaturated flow may be highly transient and non-linear. The approach has proven efficient to fit to a given breakthrough curve or concentration profile, but the model performance often breaks down when predictions are made for a different depth or time (Schoen et al., 1999b). Finally, because it is essentially a 'black box' model, its parameters do not necessarily have a physical basis. Therefore the transfer function approach is not suitable for gaining insight into the specific processes involved in solute transport, and the method will not be addressed further in this work.

2.3 Aggregated porous media

2.3.1 Qualitative description

So far this chapter has dealt exclusively with single porous media. They were regarded as continuous porous networks, where all the pores could almost equally contribute to the flow. While this is a valid assumption for artificial porous media like laboratory columns filled with glass beads, or for some idealized soils, this assumption is often not valid in field situations. Even a well-sorted sandy soil often has an aggregated structure, where the sand grains are attached together in aggregates, which are bound by organic matter. As a result the pore size distribution can be represented by a bi-modal distribution, i.e. the pore size distribution has two maxima: one for the inter-aggregate pores and one for the intra-aggregate pores. The fluid velocities in the former are usually much higher than in the latter, so that the conditions of a single porous medium are not met. For the rest of this work, such a medium will be referred to as an *aggregated porous medium* (Figure 2-8). Important here is the notion of hierarchy in the pore structure. A porous network is formed on a small scale by the intra-aggregate pores, and a second porous network is formed on a larger scale by the inter-aggregate pores. Besides the differences in scale, both networks bear a clear resemblance in structure. This discriminates them from fractured porous media, where the structure of the fracture network has no resemblance with the structure of the porous matrix. Fractured porous media will be the subject of section 2.4.

In a broader sense, an aggregated porous medium is thus a porous medium where the pore structure can be represented as a hierarchical system of two or more, structurally similar, porous domains. In what follows, different approaches are discussed to model unsaturated flow and transport in aggregated porous media. Because flow and transport models are usually closely linked, they will be treated together.

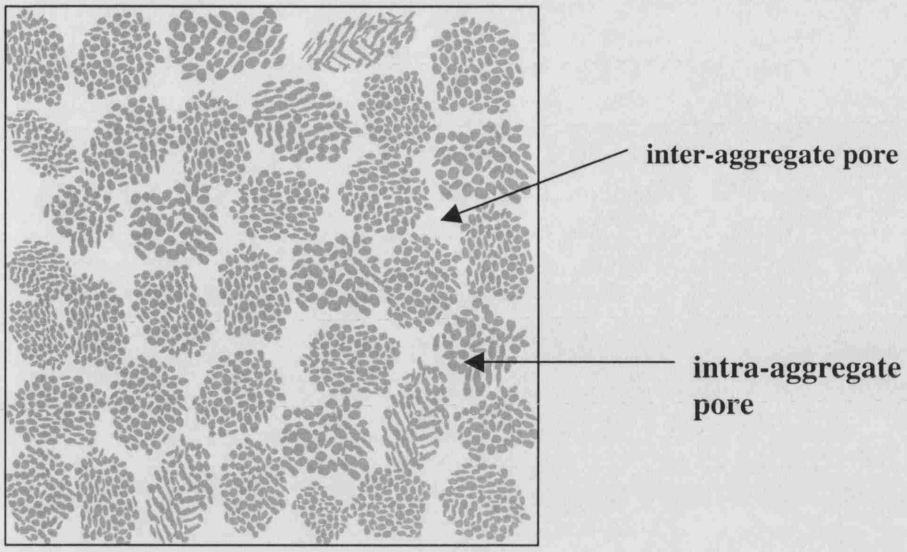

Figure 2-8 Aggregated porous medium

2.3.2 Continuum models

Continuum models are based on the concept of an REV. In a continuum approach, a porous medium consisting of a number of porous domains can be replaced by a model where each of the domains is assumed to be present at every point within the entire medium (Berkowitz, 1994). Hence a continuum method is a method of volume averaging, using a number of separate overlapping continua, corresponding to the porous domains. Depending on the number of continua, a distinction can be made between single continuum models and double continuum models. In principle, multiple continuum models are also possible, containing more than two continua, but they are normally reserved for fractured porous media and will be discussed later.

2.3.2.1 Single continuum models

In a single continuum model, the porous domains of an aggregated porous medium are represented by one continuum. Different approaches can be used, depending on whether local equilibrium is assumed between the porous domains.

2.3.2.1.1 Equilibrium models

If the advective exchange of water and the diffusive exchange of solutes between the porous domains are rapid compared to the flow, then local (almost instantaneous) equilibrium can be assumed. The mathematical description is then analogous to that for a single porous medium, and the resulting model is called an *equivalent porous medium* model.

For unsaturated flow conditions, Richards' equation is used as for a single porous medium, but some adaptations are usually needed for the moisture retention curve and the unsaturated hydraulic conductivity function. Let us consider an aggregated porous medium consisting of two flow domains, indicated as micropores and macropores (corresponding to respectively the intra-aggregate and the inter-aggregate pores of Figure 2-8). Typically the micropores have a much lower hydraulic conductivity than the macropores. If the medium is saturated, then both micropores and macropores are filled with water and the hydraulic conductivity is high. If the medium is unsaturated, then capillary forces dictate that the remaining water preferably resides in the smallest pores. Thus when the diameter of the macropores is relatively large, only a weak suction is needed to desaturate them completely, while the micropores need much stronger suctions to be desaturated. Desaturation of the macropores then leads to a sudden drop in the hydraulic conductivity. As a result, the moisture retention curve (Figure 2-9) and the unsaturated hydraulic conductivity functions cannot be represented by a simple empirical function like the van Genuchten model (1980). Several authors have proposed composite functions instead, using linear superposition of two or more single empirical functions (Durner, 1994; Ross and Smettem, 1993).

For the description of unsaturated transport, the equivalent porous medium model uses the ADE as for a single porous medium. The effects of diffusion between domains with different flow velocities are then lumped together in a modified dispersion coefficient (Brusseau, 1993; Passioura, 1971; van Genuchten and Dalton, 1986). The model still assumes that diffusion between the domains is instantaneous. This condition is often not met in field situations, so that the use of an equivalent porous medium model for transport of aggregated porous media is rarely applicable.

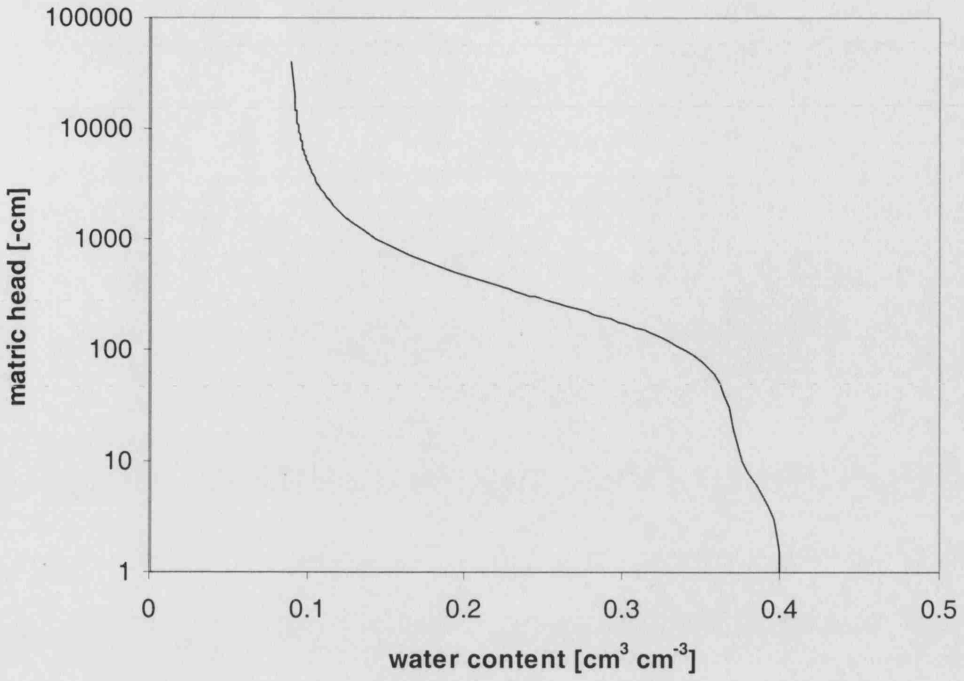

Figure 2-9 Water retention curve for an aggregated porous medium consisting of micropores and macropores.

2.3.2.1.2 Non-equilibrium models

Ross and Smetten (2000) proposed a simple and elegant method to account for physical non-equilibrium between flow domains, while still using a single continuum. They started from the observation that aggregated porous media often exhibit a water content that deviates from the moisture retention curve. Therefore they suggested using Richards' equation with a kinetic description for the water content towards equilibration. They expressed this as:

$$\frac{\partial \theta}{\partial t} = \frac{1}{\tau_e}(\theta_e - \theta) \qquad \text{Eq. 2-26}$$

where θ is the actual water content [-], θ_e is the equilibrium water content [-] and τ_e is an equilibration time constant [T]. The model requires only one extra parameter, τ_e, in addition to the moisture retention and hydraulic conductivity functions, and can be easily implemented into classical numerical models. Ross and Smetten (2000) showed that the equilibration time constant had a major effect on the wetting profile,

producing wetting fronts that travel faster and to greater depth. The model only accounts for non-equilibrium flow; to include non-equilibrium transport (e.g. rate-limited diffusion), another formulation is needed.

2.3.2.2 Double continuum models

The single continuum approach is often not applicable, especially in situations of preferential flow phenomena and bypass of solutes. In an aggregated porous medium, preferential flow may occur in the macropores, such that the solutes bypass the micropores. Hence it may be more desirable to represent both flow domains explicitly. The *double continuum model* was first introduced by Barenblatt et al. (1960), and uses two separate but overlapping continua, with different hydraulic properties for each continuum. The link between both continua is made by including a mass exchange term for water and/or solutes. A distinction is made between *dual porosity models*, where one continuum is considered immobile, and *dual permeability models*, where both continua can conduct flow.

2.3.2.2.1 Dual porosity models

In an aggregated soil consisting of micropores and macropores, it may be acceptable to assume that the water in the micropores is stagnant and that only the macropores conduct flow. This is a common approach for saturated aggregated porous media, where both domains are filled with water. The fluid velocity in the macropores is usually much higher than in the micropores, so that the attribution of the micropores to the total flow can easily be neglected. This is not necessarily the case in the unsaturated zone, where the macropores are often empty, so that the low flow velocities in the micropores may be the only contribution to the total flow. Still the approach is used in the unsaturated zone for certain situations. For example, in the case of a wet argillaceous soil, where the macropores are fully or partially active for most of the time, and where the hydraulic conductivity of the micropores is very low, the approximation of stagnant water in the micropores may be legitimate.

In a *dual porosity model* then, the aggregated porous medium has a mobile domain and an immobile domain (which overlap). Correspondingly, the total water content θ is divided into the mobile water content θ_{mo} and the immobile water content θ_{im}:

$$\theta = \theta_{mo} + \theta_{im} \qquad \textit{Eq. 2-27}$$

where θ_{mo} and θ_{im} are expressed relative to the total bulk volume. Full flow and transport equations are written for the mobile zone, whereas the immobile zone only acts as a storage reservoir for solutes. Diffusion of solutes between the mobile and immobile zones causes retardation of the solutes as they travel through the mobile zone. For unsaturated flow, Richards' equation is used for the mobile zone. For unsaturated transport, the dual porosity model is based on the ADE for the mobile zone, combined with an exchange term Γ_s to describe the change in solute mass in the immobile zone. In its most elemental form, for a conservative solute, this can be written as (van Genuchten and Wierenga, 1976):

$$\frac{\partial (c_{mo}\theta_{mo})}{\partial t} = \frac{\partial}{\partial z}\left[\theta_{mo} D_{L,mo} \frac{\partial c_{mo}}{\partial z}\right] - \frac{\partial (q\, c_{mo})}{\partial z} - \Gamma_s \qquad \textit{Eq. 2-28}$$

$$\frac{\partial (c_{im}\theta_{im})}{\partial t} = \Gamma_s \qquad \textit{Eq. 2-29}$$

where c_{mo} and c_{im} are the mobile and immobile concentrations [M L^{-3}] and $D_{L,mo}$ is the longitudinal dispersion coefficient for the mobile phase [L^2 T^{-1}]. The exchange term Γ_s [M L^{-3} T^{-1}] is taken positive for solutes moving from the mobile domain into the immobile domain. The effect of the dual porosity formulation is to create a breakthrough curve characterized by an early rise in concentration, followed by a long tail (Bajracharya and Barry, 1997; Gaudet et al., 1977).

The exchange term Γ_s describes diffusion of solutes across the boundary between the mobile and immobile domains, and into the immobile domain. The effect of the diffusion into the immobile domain is to reduce the effective solute velocity in the mobile domain (Grisak and Pickens, 1980). For the formulation of Γ_s, two different approaches are common: if the geometry of the aggregates can be specified explicitly, then a diffusive model can be used; alternatively, a quasi-steady-state approximation

is used in the form of a semi-empirical first-order rate expression. Both approaches are detailed in the following sections.

a) Diffusive model

For aggregates of well-defined geometry, Fick's second law can be applied for diffusion through the aggregates. For instance, for rectangular aggregates van Genuchten and Dalton (1986) proposed following expressions:

$$\frac{\partial c_a}{\partial t} = D_A \frac{\partial^2 c_a}{\partial x^2} \qquad \textit{Eq. 2-30}$$

$$c_{im}(z,t) = \frac{1}{a}\int_0^a c_a(z,x,t)dx \qquad \textit{Eq. 2-31}$$

where c_a is the local solute concentration in the immobile domain [M L^{-3}], D_A is the apparent diffusion coefficient in the immobile domain [L^2 T^{-1}], x is the direction in the immobile domain [L], c_{im} is the average solute concentration in the immobile domain [M L^{-3}] and a is the half-width of the rectangular slabs [L]. At the boundary between the domains, the concentrations c_{mo} and c_{im} are assumed equal. For aggregates of arbitrary geometry, van Genuchten & Dalton (1986) proposed the introduction of a geometry-dependent shape factor, to convert the geometry into an equivalent sphere for which solutions are available. This approach is similar to the block-geometry functions defined earlier by Barker (1985a).

b) Quasi-steady-state model

An approximation can be made by assuming that the concentration in the immobile zone can be represented by a single average value. For such a *quasi-steady-state* assumption, the exchange between the mobile and immobile zones can be written as a first-order rate expression, analogous to Fick's first law (Coats and Smith, 1964):

$$\frac{\partial(c_{im}\theta_{im})}{\partial t} = \Gamma_s = \alpha_s \theta_{im}(c_{mo} - c_{im}) \qquad \textit{Eq. 2-32}$$

where α_s is the solute transfer coefficient [T^{-1}]. The quasi-steady-state assumption is valid as long as the time to approach diffusive equilibrium across the immobile zone is small compared to the time for a significant change in concentration in the mobile zone (Barker, 1991). For aggregated porous media, this means that the inter-aggregate flow velocity must be low, and that the aggregates must be small. Barker (1985b) argued that the quasi-steady-state assumption is a good approximation to the diffusive type model at large times, but not at small times. A semi-empirical expression for α_s has been obtained by comparing the first-order formulation with solutions of the diffusive type approach for well-defined geometries (Gerke and van Genuchten, 1993b; van Genuchten and Dalton, 1986):

$$\alpha_s = \frac{\beta}{a^2} D_e \qquad \textit{Eq. 2-33}$$

where β is a geometry coefficient [-], a is the characteristic radius or half-width of the immobile domain [L] and D_e is the effective diffusion coefficient at the interface of the porous domains [$L^2\,T^{-1}$]. The geometry coefficient β has been determined to be 3 for rectangular aggregates (Gerke and van Genuchten, 1993b; van Genuchten and Dalton, 1986) and π^2 for spherical aggregates (Dykhuizen, 1987). In many cases, however, α_S is considered to be a fitting parameter. Note that the double-porosity formulation reduces to an equivalent of the classical ADE when the water content of the immobile zone θ_{im} is zero, or when the mass exchange is zero ($\alpha_S = 0$) or instantaneous ($\alpha_S \rightarrow \infty$).

The dual porosity concept has found wide application in aggregated porous media, where it can improve the modelling performance as compared to the single porous medium concept. Moreover, it has been observed that the dual porosity formulation can be beneficial for modelling of unsaturated transport though porous media without any aggregated structure (e.g. De Smedt et al., 1986; Poletika et al., 1995). The reason is that, even in a fairly homogenous soil, unsaturated flow tends to generate immobile regions: the water-filled pores are often not well connected, leading to stagnant fluid films on larger pores and to capillary traps due to the presence of air (De Smedt and Wierenga, 1979; Gaudet et al., 1977; van der Zee and van Riemsdijk, 1994). These small pockets of immobile water act in a similar way as the micropores in aggregated porous media, and as a result the same model may be suitable for both

media. When applied to these immobile regions in the unsaturated zone, the dual porosity model is usually called *mobile-immobile model* (MIM). Bajracharya and Barry (1997) extended this reasoning, by stating that the dual porosity model can even be applied to heterogeneous media where immobile water regions are absent. They suggested using the model for media with randomly distributed hydraulic conductivities, where the high-conductivity layers represent the mobile zone and the low-conductivity layers the immobile zone.

2.3.2.2.2 Dual permeability models

In the dual porosity formulation outlined above for aggregated porous media, it is assumed that the water in the micropores is immobile. As stated before, this is not always valid, especially in the unsaturated zone. Moreover, the dual porosity formulation inherently assumes that the distributions of pressure heads in both domains are equal and that there is no pressure gradient between the domains. In practice, in cases where preferential flow is quick, local non-equilibrium conditions may occur in the transient pressure head distributions, leading to pressure-driven advective flow between the porous domains. To account for these phenomena, *dual permeability models* have been developed (see Figure 2-10). They include full flow and transport equations for both porous domains, and exchange terms for water and solutes. Hence there are two active flow domains with different hydraulic properties, and the total porosity θ can be written as:

$$\theta = \theta_{ma} + \theta_{mi} \qquad \textit{Eq. 2-34}$$

where θ_{ma} and θ_{mi} are the volumetric water contents of the macropores and the micropores, both expressed relative to the total bulk porous volume[3]. Using this terminology, the coupled unsaturated flow equations can be written as (Dykhuizen, 1987):

[3] Note that many authors, like Gerke and van Genuchten (1993a), express the water content in each porous domain relative to the volume of the local porous domain. For the sake of conformity with the dual porosity model, it was chosen in this work to express the water contents relative to the total bulk volume, as used in Dykhuizen (1987).

$$C_{ma}\frac{\partial h_{ma}}{\partial t}=\frac{\partial}{\partial z}\left[K_{ma}(h_{ma})\frac{\partial h_{ma}}{\partial z}\right]+\frac{\partial K_{ma}(h_{ma})}{\partial z}-\Gamma_w \qquad \textit{Eq. 2-35}$$

$$C_{mi}\frac{\partial h_{mi}}{\partial t}=\frac{\partial}{\partial z}\left[K_{mi}(h_{mi})\frac{\partial h_{mi}}{\partial z}\right]+\frac{\partial K_{mi}(h_{mi})}{\partial z}+\Gamma_w \qquad \textit{Eq. 2-36}$$

where Γ_w is an exchange term for advective transfer of water between the flow domains [T^{-1}] (taken positive if flowing from macropores into micropores). The use of a double set of Richards' equations requires characterization of the water retention curve and the unsaturated hydraulic conductivity function for both domains, which significantly complicates the flow problem. Alternative formulations have been proposed, where a simplified approach is used for one of the flow domains. For instance, Jarvis and Larsson (1998) used a kinematic wave approach in the MACRO model to describe gravity flow through macropores. This will be covered in more detail in Chapter 6.

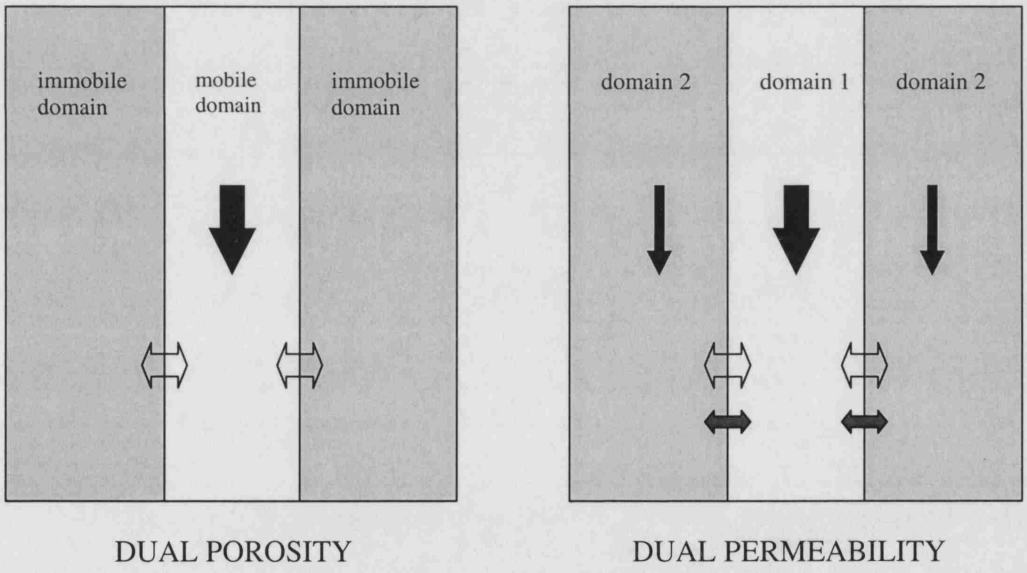

Figure 2-10 Schematic representation of the difference between dual porosity and dual permeability formulation, where a black arrow represents advective flow and a white arrow represents diffusion of solutes.

The water exchange term Γ_w is usually taken to be proportional to the difference in average pressure head between the porous domains:

$$\Gamma_w = \alpha_w (h_{ma} - h_{mi}) \qquad \textit{Eq. 2-37}$$

where α_w is a first-order water transfer coefficient [L^{-1} T^{-1}]. For well-defined geometries, Gerke and van Genuchten (1993b) derived a semi-empirical expression for α_w, based on comparison with the solution for a horizontal flow equation:

$$\alpha_w = \frac{\beta}{a^2} K_a \gamma_w \qquad \textit{Eq. 2-38}$$

where β is a geometry coefficient [-], a is the characteristic radius or half-width of the micropore domain [L], K_a is the apparent hydraulic conductivity at the interface of the porous domains [L T^{-1}] and γ_w is an empirical scaling factor [-]. For a rectangular slab geometry, the geometry coefficient β was found to be 3.

For solute transport, the dual permeability model defines two ADEs, one for each domain, coupled by a solute transfer term Γ_s (Dykhuizen, 1987):

$$\frac{\partial (c_{ma}\theta_{ma})}{\partial t} = \frac{\partial}{\partial z}\left[\theta_{ma} D_{L,ma} \frac{\partial c_{ma}}{\partial z}\right] - \frac{\partial (q_{ma} c_{ma})}{\partial z} - \Gamma_s \qquad \textit{Eq. 2-39}$$

$$\frac{\partial (c_{mi}\theta_{mi})}{\partial t} = \frac{\partial}{\partial z}\left[\theta_{mi} D_{L,mi} \frac{\partial c_{mi}}{\partial z}\right] - \frac{\partial (q_{mi} c_{mi})}{\partial z} + \Gamma_s \qquad \textit{Eq. 2-40}$$

For the solute transfer term in dual permeability models, the full diffusive approach is rarely used, so generally the quasi-steady-state formulation is used. The total solute transfer rate Γ_s [M L^{-3} T^{-1}] is then the sum of an advective term and a diffusive term (Gerke and van Genuchten, 1993a; Vogel et al., 2000):

$$\Gamma_s = \Gamma_w c_x + \alpha_s \theta_{mi} (c_{ma} - c_{mi}) \qquad \textit{Eq. 2-41}$$

where α_s is the solute transfer coefficient [T^{-1}] (defined according to Eq. 2-33). The concentration c_x is defined according to the donor cell concept (Dykhuizen, 1987): if the advective exchange Γ_w flows from macropores into micropores then $c_x = c_{ma}$, and if Γ_w flows from micropores into macropores then $c_x = -c_{mi}$.

The result of the dual permeability formulation is the progression of two distinct moisture fronts (Simunek et al., 2003) and the possible generation of a breakthrough curve with a double peak (Ma and Selim, 1995). For an aggregated porous medium consisting of micropores and macropores, the effect of the water exchange term Γ_w is to reduce the importance of preferential flow in the macropores by imbibition into the micropores (Tseng et al., 1995). A possible drawback of the dual permeability approach is that the delineation of the porous domains into micropores and macropores is often arbitrary (Ma and Selim, 1995).

2.4 Fractured porous media

2.4.1 Qualitative description

The previous section was dealing with aggregated porous media, where the pore structure could be regarded as a hierarchical system of two or more porous domains. In these systems, the porous domains are structurally similar, i.e. the difference in pores between the individual domains is merely a difference in size, but not so much in shape. In contrast with these aggregated porous media, let us now consider *fractured porous media* (Figure 2-11). A classical example would be a fractured rock like the Chalk or the Permo-Triassic Sandstone in the UK. The two porous domains here are the fractures and the porous matrix. They not only have widely varying pore sizes, but also the pore structure of the fractures and the matrix is completely different. The fracture system may consist of intersecting, more or less continuous planar voids, whereas the matrix may consist of a network of sphere-like pores connected by narrow pore necks.

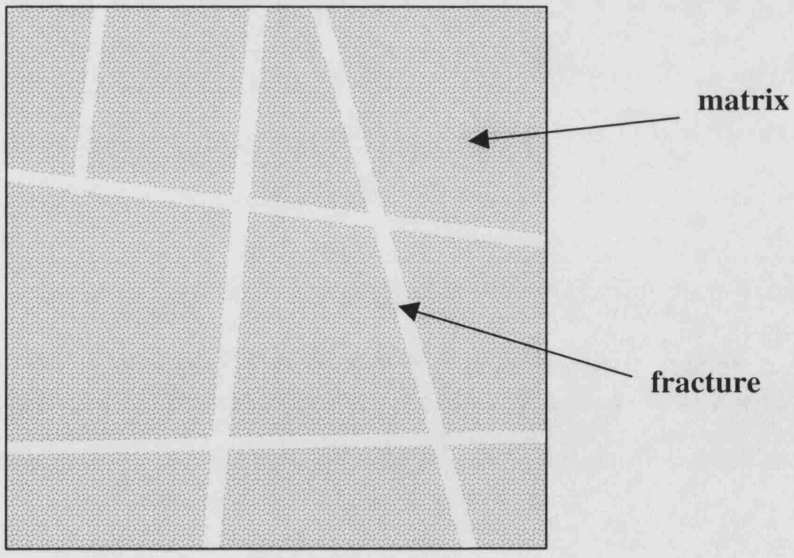

Figure 2-11 Fractured porous medium

In the saturated zone, fractures provide pathways of high permeability and can dramatically enhance the hydraulic conductivity of a porous medium. In the unsaturated zone, however, the fractures are not necessarily filled with water, and therefore can act alternatively as flow conductors and as flow barriers. According to the capillary theory (Eq. 2-12), small pores will saturate prior to large pores. At low pressure potentials the fractures are therefore likely to be empty, and flow from one matrix block to the next is restricted to the regions around fracture contact areas (Wang and Narasimhan, 1985). When the pressure potential increases to near-zero values, the fractures may become active, thereby greatly increasing the hydraulic conductivity and the transport velocity. If the matrix is not completely saturated, then capillary imbibition can occur from the fractures into the matrix pores. This may be slow compared to the fracture flow, so heavy infiltration conditions may lead to fast preferential flow phenomena through the fractures.

Often the fractures are only partially filled, showing thin films of water on rough fracture surfaces. Such film flows along fracture walls may develop a higher flow and transport velocity than that expected when the whole fracture space is saturated (Tokunaga and Wan, 1997). Moreover, because of variability of apertures in the fracture plane, fracture flow is often restricted to localized preferential flow paths (a phenomenon referred to as *channelling*). Pruess (1998) showed that these preferential flow paths can easily enhance the flow and transport velocities by factors of 5-10 in comparison with uniform flow through homogeneous fractures. Finally, it has been reported that the flow paths through unsaturated fracture networks can be highly dynamic. Glass et al. (2002) conducted laboratory experiments on an artificial fracture–matrix system composed of porous bricks. They showed that, even under steady-state infiltration, the flow pathways varied in both time and space.

The above observations illustrate the complexity of flow and transport in unsaturated fractured porous media. At present there is a high level of uncertainty in this area, with the need for both more field observations and up-to-date modelling tools (Berkowitz, 2002; Pruess et al., 1999; Simunek et al., 2003). In what follows, the modelling approaches currently available to simulate flow and transport through an unsaturated fractured porous medium will be described. As in the previous section, flow and transport will be covered together, because they are usually closely linked.

It will be shown that most of the continuum models formulated for aggregated porous media may be used for fractured porous media as well, although with certain limitations. In addition to that, a second category of models can be used, called discrete models, where the geometry of the fracture system is explicitly defined.

This section deals primarily with fractured porous rock, characterised by a non-negligible matrix porosity intersected by fractures. This excludes fractured rock like granite, where the matrix is effectively impermeable to both water and solutes. On the other hand, some porous media that are not fractured rock may still be classified as fractured porous media. Examples are field soils containing earthworm channels or decayed root channels, and clay soils that are fragmented by drying cracks. They are different from the aggregated porous media presented in the previous section, because they consist of two porous domains that are structurally dissimilar.

2.4.2 Continuum models

Continuum models have already been presented for aggregated porous media (2.3), and much of the discussion from that section is valid for fractured porous media as well. However, the continuum approach relies on the assumption that a REV can be defined, and this assumption may be more difficult to justify in a fractured porous medium where the fractures often show complex multiscale or fractal organizations, so the concept of a REV may be questionable (Bodin et al., 2003). Nevertheless, the use of the continuum approach for fractured porous media is widespread, and may be justified if the medium is densely fractured or if the scale of interest is large. In what follows, the use of the previously defined categories of continuum models for unsaturated fractured porous media is briefly discussed. Additionally, some continuum models developed specifically for fractured porous media will be introduced.

2.4.2.1 Single continuum models

To facilitate the modelling effort, fracture networks have often been described as a porous continuum. As a most drastic approximation, some authors have used the

equivalent porous medium (EPM) approach, representing the fractures and matrix together as a single continuum (e.g. Peters and Klavetter, 1988; Pruess et al., 1990). This method assumes local capillary and diffusive equilibrium between fractures and matrix, and falls short in representing heterogeneity and anisotropy caused by factures.

To differentiate the fractures from the matrix, while still using a single continuum, Tsang et al. (1996) proposed the *stochastic continuum model.* They distinguished fractured areas from the matrix by assigning the fractured areas high hydraulic conductivity values with a long-range correlation. Selroos et al. (2002) confirmed that the method compared favourably with other more complex models, but so far its use has been limited to the saturated zone.

2.4.2.2 Double continuum models

Dual porosity and dual permeability models were discussed in the previous section for aggregated porous media. They have been used for unsaturated fractured rock as well. Barker and Foster (1981) applied a diffusive type dual porosity model to simulate transport of tritium through the English Chalk, assuming the fractures to be saturated. Dykhuizen (1987) used a dual permeability model for unsaturated flow and solute transport through fractured media, including cross-flow of water and solutes between the fractures and the matrix. Liu et al. (1998) proposed an active fracture model for the unsaturated zone of Yucca Mountain, based on a dual permeability approach. They started from the observation that only a portion of the connected fracture network conducts flow, and they introduced a parameter describing the fraction of active fractures.

On the surface of the fracture walls, *fracture skins* may develop. They are zones of alteration, formed by a variety of biological, chemical and physical processes, and may reduce the hydraulic connection between the fractures and the surrounding matrix (Zimmerman et al., 2002). Barker (1985b) proposed a fracture skin model in a dual porosity approach to explicitly take account for the flux through the fracture skin.

A new type of dual porosity model, called DP-Pulse, was introduced by Barker et al. (2000). The model simulates the saturated movement of water in discrete pulses between a set of cells. Each pulse involves the same volumetric movement of water, moving the fracture water from one cell to its neighbour. Solute diffuses continuously between the fracture and the matrix according to Fick's first law, and within the matrix according to Fick's second law. Hence the model discretizes the flow velocity and the fracture space, but keeps the time and the matrix space as continuous variables. The equations are solved semi-analytically and are defined by only three parameters: a characteristic block diffusion time, a characteristic fracture diffusion time, and the ratio of matrix to fracture porosity. The geometry of the fracture-matrix system is described by a Block Geometry Function (BGF) (Barker, 1985a). The model has been extended to simulate desaturation and resaturation of the fractures around a fluctuating water table, based on a "weak solution" (Fretwell, 1999).

2.4.2.3 Multiple continuum models

Following the dual continuum models, some authors have proposed *multiple continuum models*, with additional overlapping porous domains (e.g. Bai et al., 1993). They may be of use for embedded fracture networks with different properties or scales, allowing more flexibility. In most cases however, the models are better reduced to dual continuum models, as the parameter requirements may be hard to overcome.

2.4.3 Discrete models

In the continuous approaches described above, the details of the fracture network geometry are overlooked, and only the average properties of the fracture network and the porous matrix are considered. This may not be appropriate when the scale of interest is small or when the fractures are sparsely distributed. In those cases, *discrete models* may be a better approach. Discrete models require that the geometry and the hydraulic properties of each fracture be specified explicitly. They are therefore more flexible and can account for specific effects of individual fractures. Common drawbacks for discrete models, however, are the parameterization and the

computational effort. There is often no useful way to obtain accurate geometrical data on in situ natural fracture networks, and modelling of large-scale flow and transport can pose computational limitations.

In the discussion of discrete models a distinction is made between *discrete fracture models*, where a parallel-plate fracture is taken as the basic unit, and *channel models*, where tortuous channels form the basic unit.

2.4.3.1 Discrete fracture models

In discrete fracture models, single fractures are usually represented as parallel plates with smooth fracture walls. They are given a uniform aperture, or alternatively the fracture plane can be discretized to account for variable apertures. For a perfect planar fracture with smooth surfaces of uniform aperture a_f [L], and assuming laminar flow, the transmissivity T_f [$L^2 T^{-1}$] of a single fracture is given as:

$$T_f = \frac{\rho_w g}{\mu_w} \frac{a_f^3}{12} \qquad \textit{Eq. 2-42}$$

where ρ_w is the density of the water [$M L^{-3}$] and μ_w is the dynamic viscosity of the water [$M L^{-1} T^{-1}$]. This relationship is known as the *cubic law*, and stresses how sensitive the flux is to the aperture. Based on this conceptualization, fracture networks can be generated, either in a deterministic or stochastic framework. Usually the stochastic framework is preferable, for instance by considering Monte Carlo analyses based on multiple realizations of a fracture network.

The discrete fracture approach has developed steadily over the last 25 years. Tang et al. (1981) developed an analytical solution for solute transport through a single saturated fracture, combined with 1D diffusion in the surrounding matrix. Later, Barker (1982) developed a semi-analytical solution for solute transport through a set of saturated parallel fractures, including 1D diffusion into the matrix. As all the fractures were assumed identical and equally spaced, this is essentially equivalent to a dual porosity model. Rowe et al. (1989) extended Barker's model to two or three sets of orthogonal fractures, and to 3D diffusion into the matrix. All these models are uniquely valid in the saturated zone. A discrete fracture model for flow through

unsaturated fractures was proposed by Wang and Narasimhan (1985), driven by the desire to simulate flow through the unsaturated fractured tuff at Yucca Mountain, a potential repository site for high-level nuclear waste. They represented fractures as structures of variable aperture, and adapted the cubic law to unsaturated conditions by averaging the aperture up to a saturation cutoff aperture, according to the capillary theory. They also introduced a phase-separation constriction factor to represent resistance to flow caused by entrapped air. The model allowed for flow through the matrix and advective exchange between fractures and matrix. Alternative formulations for flow through unsaturated fractures were later proposed by Nitao and Buscheck (1991) and by Roels et al. (2003). Therrien and Sudicky (1996) included transport in their unsaturated discrete fracture model, representing the fractures as 2D planes and using a 3D representation for the matrix.

2.4.3.2 Channel models

Because of the existence of contact regions between fracture walls, flow through a fracture plane is often limited to a number of preferential paths or channels. This channelling behaviour is important because it can significantly reduce the effective porosity and hence increase the flow velocity. Moreover, it reduces the contact area for exchange between fracture and matrix.

A channel model abandons the parallel-plate fracture as basic unit, and instead explicitly simulates a network of channels. Tsang and Tsang (1987) developed a channel model based on a limited number of tortuous and intersecting channels, characterized by an aperture density distribution and a spatial correlation length. Later, Moreno and Neretnieks (1992) proposed a channel network with stochastic hydraulic conductivity values arranged on a rectangular grid, conceptually representing channels as discrete, 1D flow paths intersecting in 3D space.

2.5 Conclusion

This chapter has dealt with three general types of porous media. Single porous media lack any hierarchical pore structure, and all the pores can almost equally contribute to flow and transport through the medium. Aggregated porous media have an organized pore structure, where one porous network is superimposed on the next. The porous networks are different in scale, yet have a similar structure. Fractured porous media exhibit the hierarchical pore structure of aggregated porous media, but now the different porous networks have a non-similar structure. The distinction of these three types is not always strict. Indeed, one could envisage a fourth category of single porous media with immobile zones. In this case the pore structure is not hierarchical, but the porous network consists of isolated pockets that do not take part in the flow. Hence their characteristics are somewhere in between of single porous media and aggregated porous media.

Throughout this chapter, a range of modelling approaches has been discussed to simulate flow and solute transport through unsaturated porous media. An overview of these approaches is presented in Table 2-2, together with their suitability for the types of porous media considered above. It shows that one type of porous medium may have several modelling approaches that might be suitable. The approach that is finally preferable for a given situation will depend on additional factors relating to the time-scale of the problem considered or to secondary structural properties of the medium. For instance, for fractured porous media the choice has to be made between a continuum model and a discrete model. When the scale of interest is large or the medium is densely fractured, then continuum models may be more suitable, whereas a discrete models may be preferable when the scale of interest is small or when the fractures are sparsely distributed.

Table 2-2 Suitability matrix, featuring a set of modelling approaches for unsaturated flow and transport, and showing their suitability as a function of the structure of the porous medium. Dark grey areas show high suitability, light grey areas show moderate suitability and white areas mean unsuitable.

		Single porous medium	Single porous medium with immobile zones	Aggregated porous medium	Fractured porous medium
CONTINUUM MODELS	**Equivalent porous medium**				
	Double porosity model				
	Double permeability model				
	Multiple permeability model				
DISCRETE MODELS	**Discrete fracture model**				
	Channel model				

3 The hydrogeology of unsaturated chalk

3.1 The Chalk as a fractured porous medium

3.1.1 Geology and stratigraphy

The Chalk is a soft, fine-grained, pure, white limestone, with a biogenic $CaCO_3$ content of around 98% (Hancock, 1975). It was formed during a marine transgression in the late Cretaceous, which caused the pelagic sedimentation of the skeletal remains of planktonic algae. In this period, most of north-west Europe was covered by the sea, and a non-seasonal climate restricted the erosion of the limited land that was left, hence the purity of the Chalk. The original deposition led to the formation of a chalk ooze with an initial porosity of 70 to 80%, and was followed by cementation and diagenesis. This gave way to the current Chalk with an average porosity between ca. 25 and 40% (Bell et al., 1999) and a pore size varying between 0.1 and 1 μm (Price, 1976). The high porosity of the Chalk leads to its softness and friability.

The chalk material mainly consists of Haptophyta coccoliths and its debris (Hancock, 1993), as shown in Figure 3-1. Occasionally some flint bands or argillaceous marl bands can be present (Allen et al., 1997). The average dry density of the Chalk in England has been given at 1790 kg/m^3 (Bloomfield et al., 1995).

Figure 3-2 shows the outcrop of the Chalk in England and shows its predominance in south-east England, with additional presence in East Yorkshire. In the Hampshire and London basins, the Chalk is overlain by Tertiary deposits. The overall thickness of the Chalk varies between 200 and 400 metres (Lloyd, 1993). In Britain, the major divisions, in depositional order, are traditionally known as Lower, Middle and Upper Chalk. There is a trend for an increase in matrix porosity from Lower to Middle to Upper Chalk, reflecting decreasing compression from overburden. A similar increase

in porosity can be noted from the Northern England region to the Southern England region, to the Thames and Chilterns region, to East Anglia (Bloomfield et al., 1995). The division into Lower, Middle and Upper Chalk is now generally abandoned, because the fossil zones are often poorly defined and correlation between provinces proves problematic. Instead, separate lithostratigraphical subdivisions have been proposed for the northern province and the southern province (Rawson, 1992). East-Anglia represents an intermediate between both provinces. The Chalk is also present in other regions of north-west Europe, notably in northern France, Denmark, and parts of Germany, Belgium and the Netherlands.

The Chalk is the most important aquifer in the UK and has high economical value. It supplies about 60% of the total groundwater used in England and Wales, and in total delivers about 20% of all water supplies in England and Wales (UK Groundwater Forum, 1998). In addition, the Chalk is important ecologically, as it provides baseflow to freshwater ecosystems.

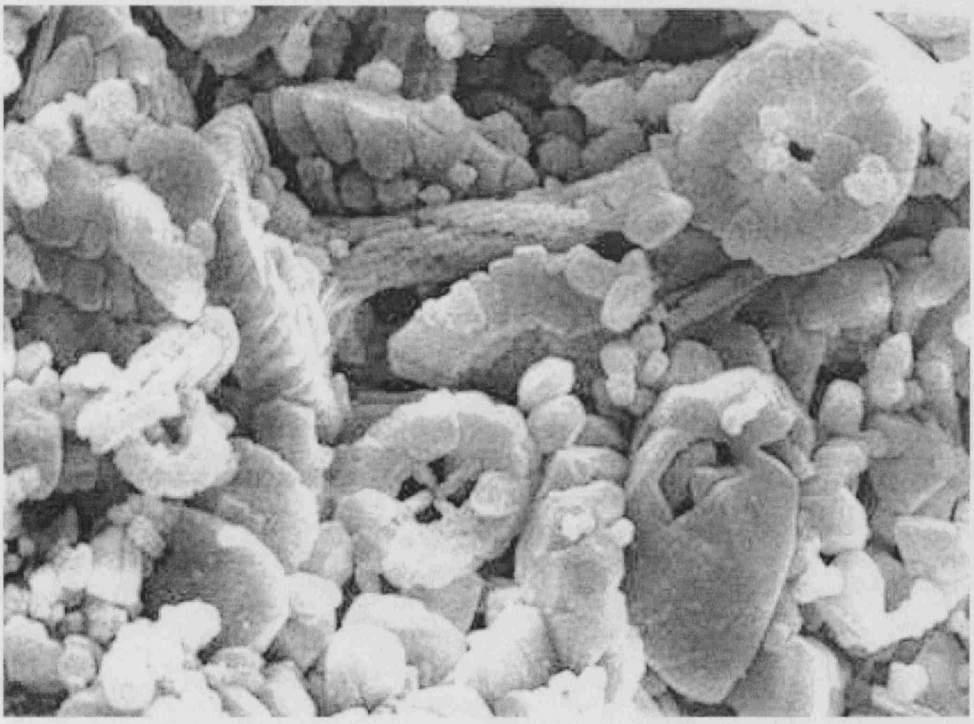

Figure 3-1 Picture taken by Scanning Electron Microscope, showing the chalk matrix consisting of coccoliths and its debris; width of image around 30 μm (image taken from http://www.gl.rhbnc.ac.uk/schools/cabinet01/drawer08.htm).

Figure 3-2 The outcrop of the English Chalk (from Lloyd, 1993).

3.1.2 Hydraulic properties

The pore size of the chalk matrix is small, so the hydraulic conductivity of the matrix is relatively low, with values between 10^{-9} and 10^{-7} m/s (Price, 1987). The chalk matrix is generally assumed to be isotropic (Lloyd, 1993), and has a specific retention[4] that approaches the porosity. Due to the small pore sizes, the water is retained in the pores by capillary forces and the total specific yield[5] is normally smaller than 1% (Price, 1990).

Superimposed upon the matrix is the fracture system, which provides a secondary source of porosity and permeability. Indeed, the Chalk is intersected by a large number of discontinuities, ranging from microscopic fissures to major faults and solution-enlarged channels. The discontinuities can be identified as faults, bedding planes and joints (Bloomfield, 1996), but within the scope of the present work they will all be grouped under the term "fractures". They were formed mainly under tectonic stress, and additionally by burial and subsequent uplift and by release of fluid stresses following diagenesis (Downing et al., 1993).

Typically, three more or less orthogonal sets of fractures are present, with one set parallel to the bedding plane (Figure 3-3). This basic structure can be further developed by weathering in shallow layers or by dissolution of $CaCO_3$, and eventually genuine karstic features, such as swallow holes and dolines, may develop (Allen et al., 1997; Banks et al., 1995). Considering the wide range of fracture sizes encountered, several authors have suggested a classification of the fractures. Reeves (1979) divided the fractures into microfissures, macrofissures and enlarged macrofissures. Price (1987) made the distinction between the primary-fissure component and the secondary-fissure component. For the present work, the author remains with the general term "fractures" for the sake of simplicity, while fully acknowledging that this comprises a whole range of non-uniform discontinuities.

---

[4] The *specific retention* is defined as "the ratio of the volume of water a rock can retain against gravity drainage to the total volume of the rock" (Fetter, 1994)

[5] The *specific yield* is the "ratio of the volume of water that drains from a saturated rock owing to the attraction of gravity to the total volume of the rock" (Fetter, 1994). The porosity is the sum of the specific yield and the specific retention.

Figure 3-3 Typical fracture pattern for the English Chalk (image by J. West).

Table 3-1 shows a comparison between the fracture and matrix components. Although the fractures only contribute less than 1% to the porosity, they can greatly enhance the permeability. This is illustrated in Figure 3-4, which shows the effective saturated hydraulic conductivity of a fracture system that becomes water-filled at a certain pressure head. The relation between the fracture aperture and the air entry pressure is calculated by a modified version of the capillary equation for a planar fracture:

$$a_f = \frac{2\gamma \cos \alpha_e}{\rho g |h_e|} \qquad \textit{Eq. 3-1}$$

where a_f is the aperture [L], γ is the surface tension of water [M T^{-2}], α_c is the contact angle [-], ρ_w is the density of water [M L^{-3}], g is the gravimetric constant and h_e is the air-entry pressure [L]. From the fracture aperture a_f and the fracture spacing b_f [L], the effective hydraulic conductivity K_{eff} [L T^{-1}] of the fracture system can be calculated by the cubic law:

$$K_{eff} = \frac{g \rho_w a_f^{\,3}}{12 b_f \mu_w} \qquad \textit{Eq. 3-2}$$

where μ_w is the dynamic viscosity of the water [M L^{-1} T^{-1}]. Figure 3-4 shows for instance that fractures of 100 μm aperture would become water-filled at a pressure head of around –15 cm H_2O. If fractures of 100 μm aperture are present with a spacing of 1 metre, then this would already yield an effective permeability that is 1 or 2 orders of magnitude times larger than the intergranular permeability.

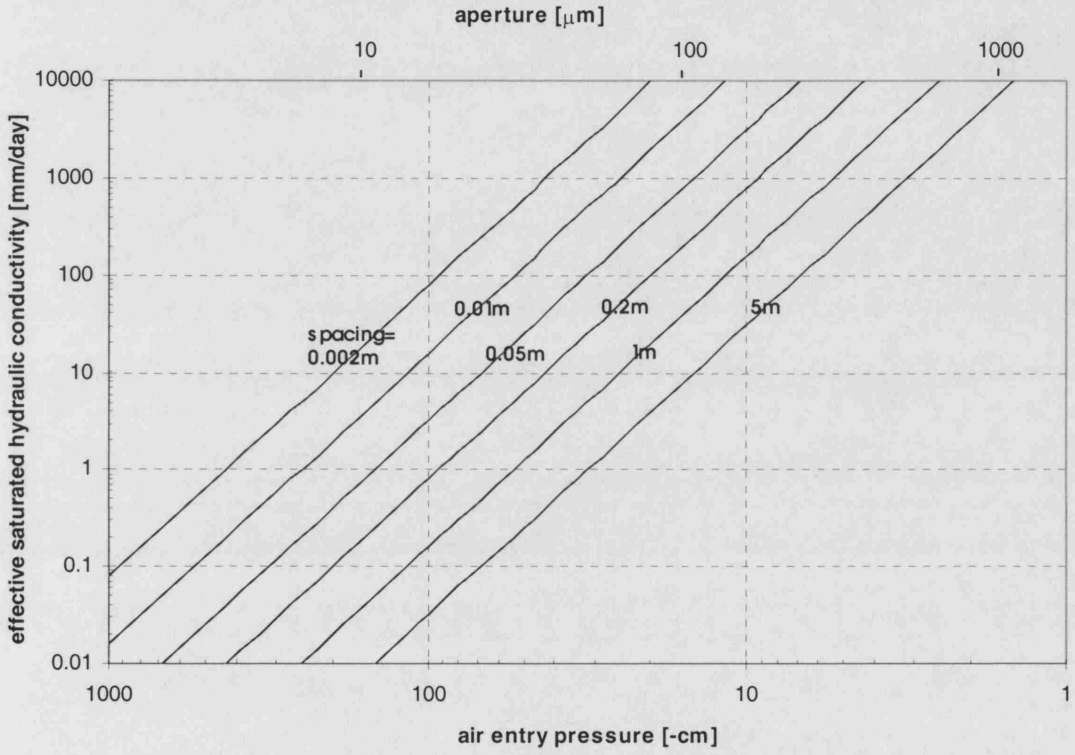

Figure 3-4 Relationship between air-entry pressure, fracture aperture, fracture spacing and effective hydraulic conductivity for plane parallel fractures filled with water at 10°C.

The overall permeability in the saturated zone is often related to the topography: very permeable regions are usually associated with the alignment of valleys and are flanked by less permeable regions beneath the interfluves (Lloyd et al., 1981). The fractures are often more developed around the zone of water table fluctuation and get closed with depth due to the burden of the higher layers. Permeability, fracture density and fracture aperture decrease with depth, so the effective aquifer depth is

usually only between 30 and 60 metres (Lloyd, 1993). The average overall transmissivity has been estimated at 540 m^2/d, with marked differences between regions (MacDonald and Allen, 2001).

Table 3-1 Comparison of typical physical properties of the matrix and the fractures for the Chalk in England.

Matrix	Fractures
Contribution to total porosity = 25 - 40% [1]	Contribution to total porosity < 1% [5]
Hydraulic conductivity = 10^{-1} – 10^{1} mm/d [2]	Hydraulic conductivity = 10^{1}- 10^{4} mm/d [6]
Pore size = 0.1 - 1.0 μm [2]	Aperture = 5 - 5000 μm [7]
Unsaturated transport velocity ≤ 3 mm/d [3]	Unsaturated transport velocity = 1000-50000 mm/d [8]
Air-entry pressure < -3000 cm [4]	Air-entry pressure > -50 cm [3]

[1] Bell et al. (1999); [2] Price (1976); [3] Gardner et al. (1990) [4] Price (1987); [5] Downing et al. (1993); [6] Foster (1993); [7] Reeves (1979);[8] Downing et al. (1978).

3.2 Review of flow and solute transport through unsaturated chalk

In the saturated zone, the Chalk is often regarded as a dual porosity medium: it is assumed that the matrix water is immobile and that all flow occurs through the fractures (e.g. Barker, 1993; MacDonald et al., 1998). In the unsaturated zone, where capillary forces influence the flow pattern, the situation is more complex. Unsaturated flow and transport through the chalk may be the result of interaction between the matrix and the fractures, but the mechanism is not fully understood. In order to assess the vulnerability of the Chalk aquifer to pollution, a good understanding is however essential, as the difference between rapid bypass flow through fractures and slow matrix flow is crucial. Over the last 35 years, considerable research effort has gone into resolving these issues, with mixed success. A review of this combined research is presented in this section.

3.2.1 The tritium anomaly

Evidence for rapid flow through unsaturated chalk is longstanding. Sometimes after heavy rainfall a quick rise in the water table can be observed (Headworth, 1972). Moreover, living specimens of the bacterium *E. coli* have been found in deep groundwater, although they are too large to travel through the matrix pores and they have limited survival time (Maclean, 1969). Finally, runoff is hardly ever observed on chalk outcrop, even under intense rain. Until 1970 it was therefore generally assumed that most of the unsaturated flow occurred through the fracture network. This vision was questioned when observing profiles of thermonuclear tritium in the Upper Chalk at Berkshire (Smith et al., 1970). Tritium is a radio-isotope with a half-life of 12.4 years, and has shown a characteristic temporal distribution in the atmosphere over the last 50 years. Atmospheric testing of nuclear weapons led to a distinct atmospheric fallout of tritium during 1963-1965. The tritium-enriched rainfall infiltrated into the unsaturated zone and the downward movement of this tritium peak can be followed throughout the years. This provides an interesting environmental tracer, as tritium is incorporated in the water molecules as H^3HO, and therefore the water molecules themselves are marked. The profiles in the Chalk (Figure 3-5) showed that this peak was well preserved in the unsaturated zone, indicating slow, relatively uniform infiltration rates not exceeding 1m/year (3 mm/d). Little tritium was recovered in the saturated zone. Smith et al. (1970) concluded that intergranular seepage as piston-displacement through the matrix was the predominant flow mechanism. Still, their analysis could not explain the bacterial contamination of groundwater or the absence of runoff, and the debate continued.

Foster (1975) proposed a new explanation to reconcile these observations, by making a distinction between flow and transport velocities. He argued that most of the flow goes through the fractures, but that there is lateral diffusion of tritium between the mobile fracture-water and the static matrix pore-water, driven by a concentration gradient. If the time for diffusive equilibrium between fractures and matrix is short compared to the residence time in the fractures, then the solute concentrations in the fractures and in the matrix at any given level will be nearly identical. The resulting mechanism is an analogue of piston displacement through the matrix pores, showing little dispersion. A mathematical model for this mechanism was later developed by

Barker and Foster (1981). They proposed a diffusive-type dual porosity model, where the fractures are assumed to be saturated. The model confirmed the effectiveness of the diffusive mechanism proposed by Foster (1975), even though simulation of the measured tritium profiles proved too complex.

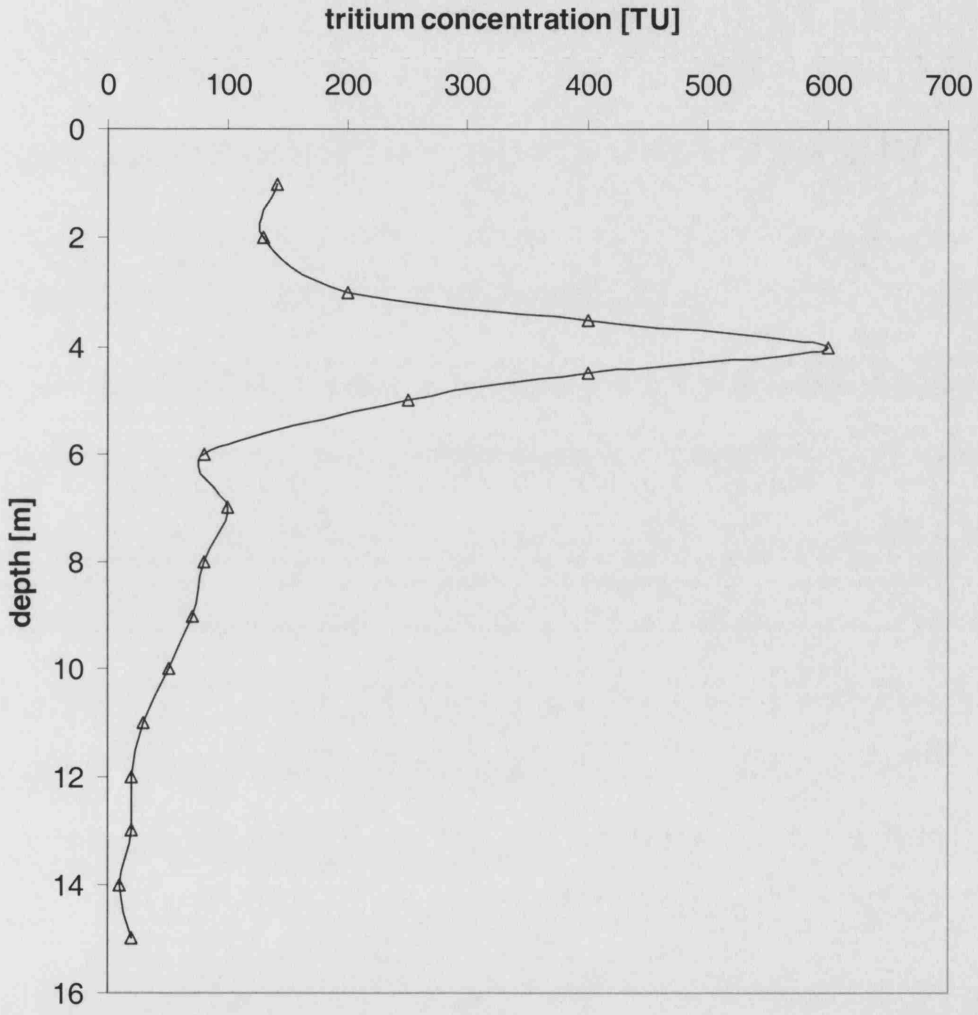

Figure 3-5 Tritium concentrations measured from core profiles in the unsaturated chalk at Berkshire in October 1968 (after Smith et al., 1970). For explanation on Tritium Units, see Appendix III.

Following these new insights, more tritium profiles were measured on different locations in the English Chalk. Foster and Smith-Carington (1980) reported tritium profiles measured at Gussage, Dorset, and at several sites in West Norfolk. Hall et al. (1976) published profiles for Bridget's Farm, Hampshire, while Young (1981)

reported data for Spratling Court, Kent. Geake and Foster (1989) published additional profiles for Fleam Dyke, Cambridgeshire (which will be discussed in Chapter 4). Overseas, similar profiles were recorded in the Chalk of the Champagne region in France (Ballif, 1998). These data generally confirmed the dual porosity mechanism, with a varying degree of dispersion involved. The average travel velocity of the tritium peaks varied between 0.3 and 1.0 m/year (between 1 and 3 mm/d). Similar velocities were obtained from profiles of nitrate and chloride (Geake and Foster, 1989; Hall et al., 1976; Wellings and Bell, 1980).

Downing et al. (1978) published some other interesting work with tritium in Chalk. Instead of measuring core profiles, they monitored tritium concentrations in several wells near Brighton. The concentrations showed seasonal fluctuations correlated with rainfall events, indicating that there is rapid infiltration through fractures in the unsaturated zone after heavy rainfall. They concluded that generally the double porosity mechanism of Foster (1975) was still valid, but that during heavy rainfall events the flow through larger fractures was too fast to allow diffusive equilibrium with the matrix. In those cases, only part of the tritium diffused into the matrix, and some tritium quickly reached the water table as bypass flow. Their results stressed the importance of the infiltration flux on the occurrence of bypass flow, and showed that, at least in some cases, diffusive equilibrium between fractures and matrix may not be achieved.

3.2.2 Soil physics research

Further advances have been made by using soil physics methods to define hydraulic characteristics for unsaturated chalk. Simultaneous measurements of water content and pressure head allow construction of the water retention curve, as shown in Figure 3-6. This was first done in the field by Wellings and Bell (1980) at Bridget's Farm, Hampshire, and later by Gardner et al. (1990) at West Ilsley, Berkshire. Laboratory measurements on small blocks of chalk have been reported by Hollis et al. (1990) for the Upper Chalk in southern England and by Brouyère (2002) for the Belgian Chalk at Bovenistier. A water retention curve can also be calculated from the measurements of pore-size distribution by Price (1976). Figure 3-6 shows that for pressure heads larger

than -1000 cm H_2O, the specific capacity is very small, i.e. there is very little variation in water content. This is a reflection of the narrow pore throats of the chalk matrix, and it implies that the matrix pore space will almost always be saturated, because the air-entry pressure to drain the matrix pores is too low. As a result, the capillary fringe in the Chalk is usually very large, and may extend over 30 metres upwards from the water table (Price, 1987). Note that in the definition of capillary fringe used here, the matrix pores are saturated but the fractures may be empty.

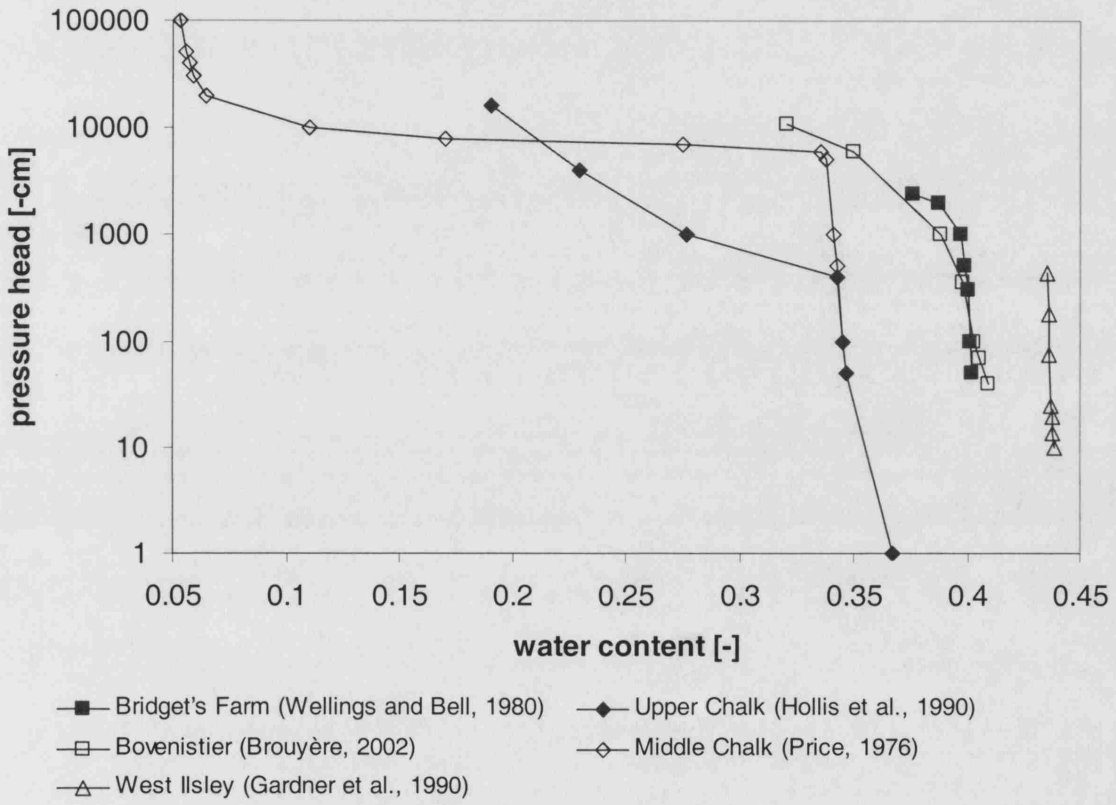

Figure 3-6 Water retention curves for the Chalk.

Field measurements of the unsaturated hydraulic conductivity function have also been reported. Wellings and Cooper (1983) published data for various sites in South-East England, including West Ilsley, Berkshire and Fleam Dyke, Cambridgeshire (the latter site will be discussed further in Chapter 4). Results for Bridget's Farm, Hampshire were given by Wellings (1984a). All curves show high values of hydraulic conductivity at high pressure heads, but these values drop sharply at pressure heads between –25 and –50 cm H_2O (see Figure 3-7). However, the

conductivity remains more or less constant for pressure heads smaller than –50 cm H_2O. It is assumed that this horizontal section corresponds to the chalk matrix, which does not drain until very low pressure heads are reached (as already shown in the water retention curves of Figure 3-6). The steep section in the curve between –25 and –50 cm H_2O is attributed to the conductivity of the fractures. Based on these data, it has been suggested that fracture flow is likely to be initiated once the pressure head rises to a value of -50 cm H_2O (Gardner et al., 1990). From Figure 3-4 it can be seen that this corresponds to the air-entry pressure of a planar fracture with an aperture of 30 μm. Figure 3-4 further shows that a spacing of 1 m between 30 μm fractures would already be sufficient to yield an extra hydraulic conductivity of over 1 mm/d. In reality, a range of fractures will be present with different apertures, and successively larger fractures become water-filled while the pressure head increases, thus increasing the total hydraulic conductivity.

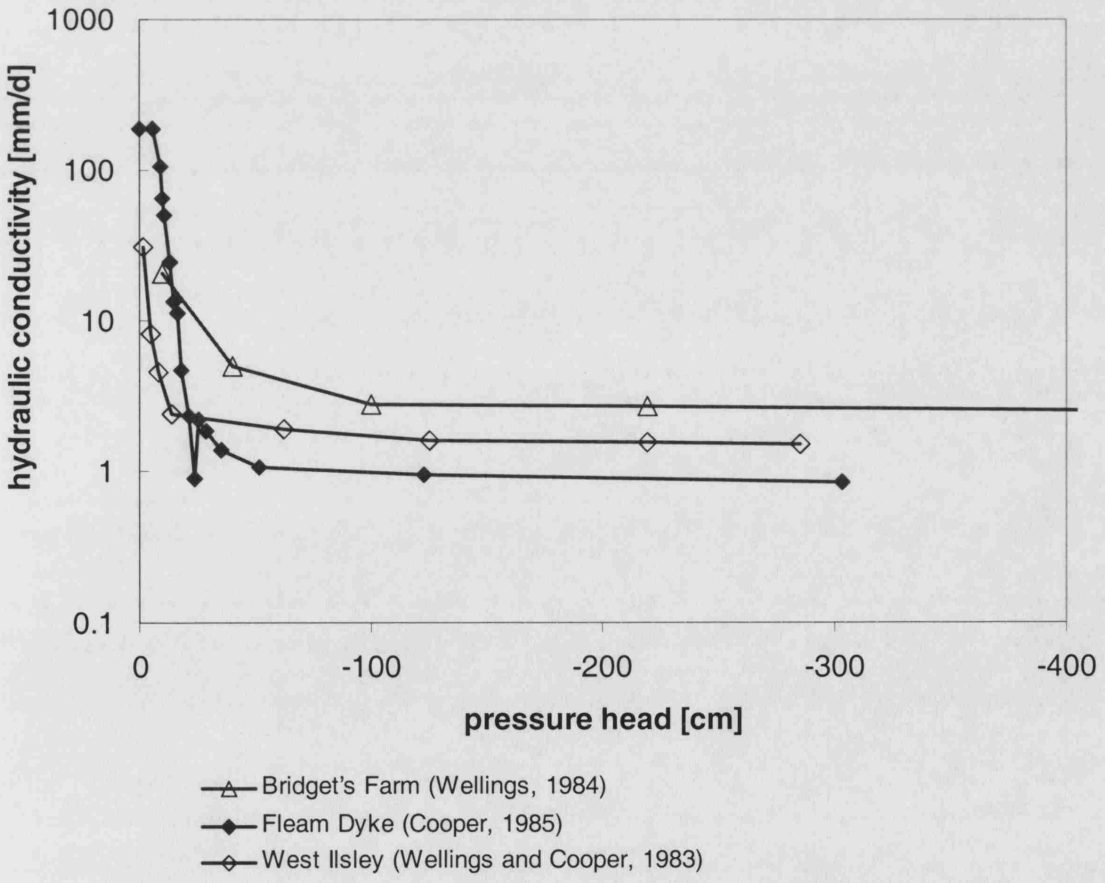

Figure 3-7 Unsaturated hydraulic conductivity functions measured on the Chalk at various field sites.

If the threshold of –50 cm H_2O is reliable, then this is a powerful tool to assess the importance of fracture flow at individual chalk sites. By measuring the pressure head at several depths in the profile, the occurrence of fracture flow would be marked by pressure heads exceeding -50 cm H_2O. Based on this criterion, large differences have been observed between chalk sites. For the Middle Chalk at Fleam Dyke, pressure heads stayed around –20 cm H_2O for much of the time during winter, suggesting that fracture flow is a common phenomenon (Wellings and Cooper, 1983). For the Upper Chalk at West Ilsley, the pressure head only occasionally rose above –50 cm H_2O, so for this site fracture flow may be less important (Gardner et al., 1990). For the Upper Chalk at Bridget's Farm, Wellings (1984a) stated that fracture flow was even very unlikely. Weekly measurements showed that the pressure head at Bridget's Farm during the winter recharge period generally stayed in the range of –200 to –400 cm H_2O. This implies that all the fractures would be empty, and that matrix flow is the dominant mechanism there. This view was later disputed by Mahmood-ul-Hassan and Gregory (2002), who argued that weekly measurements of pressure potential are not frequent enough to measure short-term maximum fluxes after rainfall events. Instead they performed hourly measurements of the pressure head at Bridget's Farm, which showed a rapid response of the upper profile to rainfall events, indicating fast intermittent fracture flow. Their measurements were limited to the upper metre of the profile, and it is uncertain how the chalk below behaved, as there is a possibility that these short-term fluxes were quickly dissipated with depth.

To conclude, the measurements of pressure head at different chalk sites emphasized the importance of two factors for the occurrence of fracture flow. First, the saturated hydraulic conductivity of the matrix plays a significant role, as the fractures are only active when the infiltration capacity of the matrix is exceeded (Price et al., 1993). Second, the presence of additional strata on top of the chalk can have a buffering effect on heavy rainfall events. When the chalk is covered by soil, weathered chalk, or drift, these strata can soak up the water and release it gradually at a slower rate (Gardner et al., 1991).

3.2.3 Tracer tests

The use of artificial tracers made a further contribution to the understanding of unsaturated flow and transport through the Chalk. A variety of tracer tests have been undertaken, with widely varying conclusions. The differences in results may be partly due to differences in setup of the experiments, especially the infiltration rate. Clearly, fracture flow becomes more likely under a forced gradient (high irrigation rate) than under a natural gradient (natural rainfall conditions). Another reason may be the regional variability of the Chalk aquifer, as results from one site cannot easily be extrapolated to other sites. An overview of the main field tracer experiments published for unsaturated chalk is given below.

Black and Kipp (1983) performed a tracer test with ^{82}Br as a radioactive tracer on the Lower Chalk at Harwell, Oxfordshire. A constant irrigation rate was maintained and breakthrough curves were recorded at several depths with gamma-probes. The curves typically showed a minor fast-moving front with a slower-moving remainder (tailing), suggesting by-pass flow through fractures with non-equilibrium diffusion into the matrix. The results were fitted to an analytical solution of a quasi-steady-state dual porosity model, assuming that the matrix is immobile. The model fitted the breakthrough curves reasonably well, but this still leaves doubt as to whether the assumption of an immobile matrix is realistic. The breakthrough curves were only measured for one week, so any tracer possibly moving as piston flow through the matrix could not be recovered.

Another tracer test was accomplished by Wellings (1984b), on an arable field in the Upper Chalk at Bridget's Farm, Hampshire. Deuterium enriched water was spread over the field and core profiles were taken several times a year. The deuterium peak remained discrete and moved down with a velocity of about 0.85 m/year (2.3 mm/d). Moreover the seasonal variations of environmental deuterium input were initially retained as well, after which they became dispersed deeper in the profile. In addition, the leaching of nitrate and chloride was measured by taking core profiles. Again the peaks were retained and moved down with about the same velocity as deuterium. The results seemed to confirm the soil physics research at Bridget's Farm (Wellings, 1984a), that showed that the pressure heads stayed low throughout the year. It was

concluded that here piston flow displacement through the matrix is the prominent mechanism. At this site the matrix hydraulic conductivity is high enough to conduct all infiltration, leaving the fractures empty.

Other tracer tests in the Upper Chalk at West Ilsley, Berkshire, were reported by Barraclough et al. (1994). Deuterium, chloride and $^{15}NO_3$ were applied at the surface, and recovery of chloride after 4 years was still 100% in the 6-metre profile. The seasonal periodicity of the background deuterium was however not well preserved. It was concluded that most of the unsaturated flow went through the matrix, with additional flow through small fractures. By comparing the displacement velocity of the tracer peaks (about 0.8 m/year, or 2.9 mm/d) with the estimated recharge, it was concluded that only about 50% of the water-filled matrix was active in conducting flow, corresponding roughly to those pores with an equivalent diameter[6] greater than 0.7-0.8 μm.

The use of several types of tracers on the same profile can provide a way to distinguish between different transport pathways. Ward et al. (1997; 2001) used a combination of LiBr, bacteriophage, and microspheres up to 10 μm in diameter, under a high irrigation rate. The microspheres were marked with a fluorescent dye and can be dissolved for easy analysis after recovery. While LiBr as a conservative solute can readily diffuse into the matrix pores, the particles can only be transported through larger pathways. The results showed that particles up to 6 μm in diameter could migrate rapidly through the chalk unsaturated zone to the water table, suggesting fracture flow. Core profiles showed a non-uniform vertical distribution, with the presence of microspheres in discrete horizons. These horizons seemed to indicate the existence of horizontal flow paths, associated with bedding planes or flint bands. The profile of LiBr showed an exponentially decreasing concentration with depth, suggesting diffusion into the matrix.

Zaidman et al. (1999) applied a saline tracer on a site in East Yorkshire and monitored its downward movement using cross-borehole electrical resistivity imaging. A high saline concentration close to the surface illustrated the presence of the salt in the chalk

[6] For non-cylindrical pores, an *equivalent diameter* can be defined, such that the flow through the pores is the same as for a cylindrical pore with the same diameter.

matrix. Additionally the results showed distinct horizons of high salinity deeper in the profile, indicating rapid by-pass flow of the tracer through fractures and possible lateral movement into marl layers.

Field studies have been done on the Chalk to investigate the leaching of contaminants beneath storage sites for agricultural waste. It appeared that the presence of the waste itself could have a strong influence on the flow behaviour through the unsaturated chalk underneath, by either enhancing or reducing fracture flow. Gooddy et al. (1998) and Withers et al. (1998) studied leaching from an unlined, earth-banked slurry lagoon excavated in the Upper Chalk at Bridget's Farm, Hampshire. The lagoon was used to store liquid cow manure, and contamination was observed both at the water table and in chalk pore water obtained from unsaturated cores. The results indicated transport of pollutants through the fractures, and it was recognized that this must have been facilitated by the extra hydraulic head caused by the liquid slurry. In contrast, Gooddy (2002) examined core profiles beneath a field heap of turkey litter. Chemical analysis revealed little movement beneath the store, and no preferential flow paths could be identified. In this case the solid turkey litter appeared to be relatively impermeable, thereby reducing the recharge.

Brouyère (2002) performed several tracer tests with a variety of tracers on the Belgian Chalk at Bovenistier. The experiments were run both under natural gradient and forced gradient, and it was shown that this caused a difference in peak travel time of several orders of magnitude. Under natural gradient conditions the solute transport was slow, suggesting matrix flow, whereas under forced gradient conditions solute transport was much faster, indicating the activation of fracture pathways.

An important body of work has been published on the Chalk from the Negev Desert in Israel. Evidence of bypass flow through fractures in the unsaturated zone, even under such arid conditions, has been given by Nativ et al. (1995). Dahan et al. (1999) measured flow through a vertical fracture by sampling in a horizontal borehole divided into segments. Flow trajectories within the fracture were identified using a combination of tracers. They showed that, even under relatively constant boundary conditions, the flow showed high spatial and temporal variability. Clear evidence of channelling was observed, with most of the flow confined to small sections of the

fracture. Moreover the flow channels seemed to be highly unstable. It is not clear, however, what the relevance is of those results for the Chalk in England.

3.2.4 Recent advances

Recently the understanding of unsaturated flow through the Chalk has been given a new impulse by the publication by Price et al. (2000). The aim of their work was to find the source of additional water released from drainage, as described by Lewis et al. (1993). It had been noticed that the drainage from catchments was often significantly higher than could be accounted for by the change in position of the water table. Therefore Price et al. (2000) conducted laboratory experiments on chalk samples, using a combination of air-water capillary drainage, mercury-intrusion porosimetry, acoustic measurements and resin impregnation. No evidence of microfissures was found, and macropores did not contribute significantly to drainage or permeability. The experiments revealed however that considerable storage and drainage was associated with irregularities on the fracture surfaces. This storage component could help to explain the often-observed delay in water table response after recharge events.

The discovery of drainage water on fracture surfaces may have great implications on the debate about the generation of fracture flow. During infiltration, when the saturated hydraulic conductivity of the matrix is exceeded, at first small depressions on the fracture surfaces would be filled. Later small sections of narrow fractures would fill, followed by larger sections of larger fractures. In general, the generation of fracture flow is governed by the pressure head. And since pressure heads tend to be higher near the water table, Price et al. (2000) argued that fracture flow may be more likely to be generated deep in the profile rather than near the ground surface. Instead of the traditional view of continuous fracture flow providing a short-cut between the soil and the water table, this mechanism considers fracture flow derived from the matrix, and which might return to the matrix wherever the pressure head drops again. For solute transport, this implies that on top of the diffusive exchange between fractures and matrix, advective exchange is possible as well. And when fracture flow is generated, it is not necessarily coming from young surface-applied

water, but might rather be derived from older water that has passed previously through higher parts of the profile as matrix flow. This form of bypass flow would remove solutes from within the profile and possibly re-introduce them lower down, but by advection, not diffusion. Bypass flow directly from the surface to the water table, exclusively through fractures, would then only happen during exceptional rainfall events when the fractures become saturated over their full length.

Based on the hypothesis of Price et al. (2000) that initiation of fracture flow is more likely close to the water table, one could argue that complete bypass of the matrix would be more probable at sites with a shallow water table than at sites with a deep water table. Johnson et al. (2001a) performed a tracer experiment with pesticides on a hillslope in the Upper Chalk in Hampshire. After a storm event, they observed increased pesticide concentrations in a borehole with a shallow water table, but no change for a borehole where the water table was deep. They showed that for the site with the deep water table, the pressure heads never rose high enough for fracture flow to be initiated. Conversely, pressure heads around –20 cm H_2O were measured throughout the profile at the site with the shallow water table, indicating that fracture flow is more likely. Haria et al. (2003) assigned this contrasting behaviour to differences in water storage capacity. For a shallow water table, the capillary fringe may extend to the surface, reducing the storage capacity. They envisaged the existence of intermediate storage sites, associated with irregularities on fracture surfaces and with wetting around contact points of horizontal fractures. For a shallow water table, these intermediate storage sites would be mainly saturated through capillary rise from the water table, so that incoming drainage is quickly diverted to fractures. For a deep water table, these intermediate storage sites may often remain empty, so the infiltration flux is delayed and attenuated while these sites are filled.

3.3 Conclusion and research needs

The review presented above shows that research has provided both answers and questions relating to the mechanism of flow and solute transport through unsaturated chalk. Clearly, there is no single mechanism that can explain all the observations for all Chalk sites in England. For instance, the occurrence of fracture flow seems to be

highly variable between individual sites. Wellings (1984a) showed that at some sites on the Chalk in Southern England, the saturated hydraulic conductivity of the matrix is high enough to accept all infiltration, except for some exceptional storm events. At other sites (e.g. Fleam Dyke, Wellings and Cooper, 1983), fracture flow seems relatively common. A first conclusion to be drawn is that the chalk matrix in the unsaturated zone cannot simply be regarded as an immobile zone with respect to water flow and solute transport. For some sites the fractures may rarely become active, so matrix flow, however slow, may be the main mechanism contributing to recharge. Therefore, whereas the saturated zone is commonly regarded as a dual porosity medium, the unsaturated zone would generally be better conceptualized as a dual permeability medium. Occasionally, for sites where the fractures are expected to remain empty, the unsaturated zone of the chalk may be conceptualized as a single porous medium.

One may conclude that the occurrence of fracture flow seems to be mainly dependent on the following factors:

- the rainfall intensity: fracture flow is only observed during high recharge periods;
- the soil moisture deficit (SMD)[7]: the water content in the unsaturated zone needs to reach field capacity before any recharge flow occurs; therefore, during periods of high evapotranspiration (ET) when a SMD exists, no fracture flow is observed; fracture flow normally only occurs in winter and early spring when ET is low and a SMD is absent;
- the thickness of the soil cover and the weathered chalk: they have a buffering effect on the incoming flux;
- the saturated hydraulic conductivity of the matrix: assuming that the hydraulic gradient approaches unity, fracture flow only occurs when the infiltration flux exceeds the matrix saturated hydraulic conductivity;
- the pressure head: fracture flow is likely to be initiated once the pressure head exceeds -50 cm H_2O;

[7] The *soil moisture deficit* is defined as the difference between the field capacity and the actual water content, multiplied by the thickness of the profile. The *field capacity* is defined as the water content of the soil after it has been saturated and allowed to drain by gravity for 24 hours.

- the depth to the water table: high pressure heads, and thus fracture flow, may be more likely close to the water table, because the capillary fringe effect reduces the water storage capacity.

The role of the soil on top of the Chalk deserves more attention. Wellings and Cooper (1983) observed that the importance of fracture flow through the unsaturated chalk appeared to be negatively correlated with the thickness of the soil cover and the depth of disturbance of the Chalk. The soil can dissipate incoming high infiltration events, reducing the maximum fluxes that reach the top of the Chalk.

In general, the typical flow progress over a recharge season in the unsaturated chalk may be understood as follows. At the end of summer, pressure heads are very low and the fractures will normally be empty, but the matrix may still be largely saturated. When recharge starts again in early winter, the infiltration gradually wets up the profile and initially drains through the matrix. At the same time the pressure head increases. As long as the infiltration flux is lower than the matrix saturated hydraulic conductivity, the fractures remain empty. When the infiltration flux exceeds the matrix saturated hydraulic conductivity, some irregularities on the fracture surfaces become water-filled. Possibly, film flow along the fracture surfaces may take place, but whether this actually occurs in the Chalk is uncertain. When the infiltration flux increases further, the pressure head in the fractures becomes higher than the air-entry value and the fractures become fully conductive.

Solute transport is largely defined by the flow behaviour. If the fractures are empty and the matrix conducts all the flow, then of course also the solutes will be transported through the matrix. This situation is depicted in Figure 3-8: the solutes slowly migrate through the matrix, and it may take several years or decades before they reach the water table.

The solute transport behaviour becomes more complex when the fractures are active. In this case there are two flow domains with contrasting velocities. On the one hand, there is piston flow through the matrix, with a velocity of around 1 mm/d. On the other hand, there is rapid bypass flow through fractures, with a typical velocity around 5000 mm/d. Exchange of solutes may occur between the flow domains, by diffusion

or possibly by advection. Based on the solute exchange mechanism, four conceptual models can be distinguished to describe solute transport through unsaturated chalk:

a) *Diffusive equilibrium* (Figure 3-9a). In this case the solutes diffuse quickly between the fractures and the matrix, so at any given level the solute concentrations in the fracture and in its surrounding matrix are equal. This situation has also been called the "chromatographic approximation". The resulting transport is slow, and the solute profile looks very similar to the case where the fractures are empty (Figure 3-8). It is not certain that complete diffusive equilibrium would ever be approached for the Chalk, but in general it is more likely for low-velocity flow through thin fractures surrounded by small matrix blocks with high porosity, and for solutes with large diffusion coefficients.

b) *Complete bypass* (Figure 3-9b). This is the opposite extreme from diffusive equilibrium. When diffusion is very slow compared to fracture flow, the solutes effectively by-pass the matrix and can travel quickly towards the water table without any considerable attenuation. This situation is more likely for high-velocity flow through large fractures, and for solutes with small diffusion coefficients. It may also occur when a fracture skin is present that forms a barrier for the solutes.

c) *Gradual attenuation* (Figure 3-9c). The actual field situation for any given site is likely to be somewhere in between of the two extremes presented above. While solutes travel through the fractures, there is some diffusion into the matrix but it does not reach equilibrium. This means that some solute bypasses the matrix, but that the solute load of the fracture water is gradually attenuated along its transport through the fracture because of progressive loss of solute to the matrix.

d) *Advective exchange* (Figure 3-9d). In the previous conceptual models the fracture walls have been represented by parallel plates, but in reality the fractures may be highly irregular. Fractures preferably get water-filled in their narrowest parts, wherever the pressure head exceeds the air-entry pressure. This means that they do not necessarily become active at the surface. Hence solutes may initially travel through the matrix at a very slow rate, and only later get sucked into the fractures. This is solute exchange by advection (caused by a pressure gradient), and not by diffusion (caused by a concentration gradient). The same mechanism could theoretically arise for plane parallel fractures as well, when the saturated hydraulic conductivity of the matrix decreases with depth or when the pressure potential increases with depth.

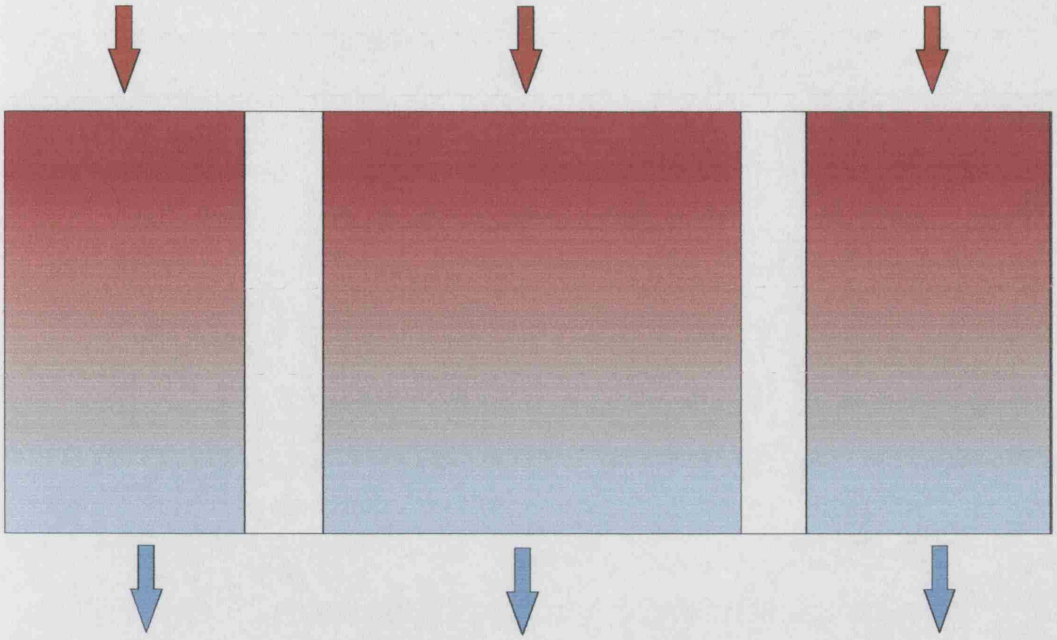

Figure 3-8 Conceptual model of solute transport through unsaturated chalk when the fractures are empty. The drawing shows a cross-section of chalk intersected by two vertical fractures. Clean water is represented in blue, and solutes are represented in red.

The four conceptual models presented above might all be operating at the same site. There might be vertical variation of transport mechanisms between layers with contrasting physical properties. In addition, the transport pattern is likely to vary with time throughout the recharge season. During times of peak rainfall when the profile is wet, the solutes will move rapidly, but the solutes could slow down and not bypass completely as the infiltration event dissipates.

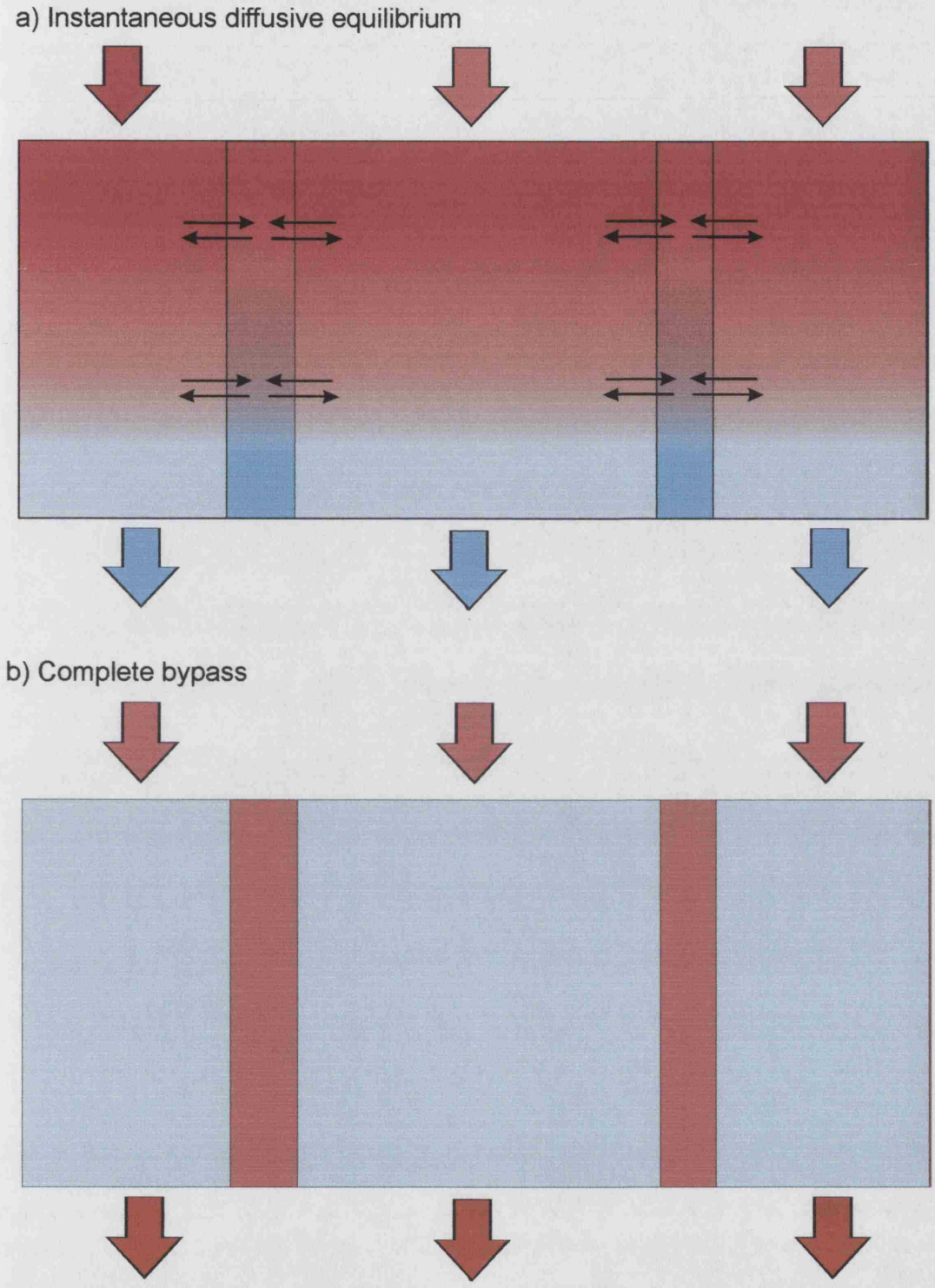

Figure 3-9 Conceptual models of solute transport through unsaturated chalk when the fractures are active, for a) diffusive equilibrium, and b) complete bypass. The drawing shows a cross-section of chalk intersected by two vertical fractures. Clean water is represented in blue, and solutes are represented in red.

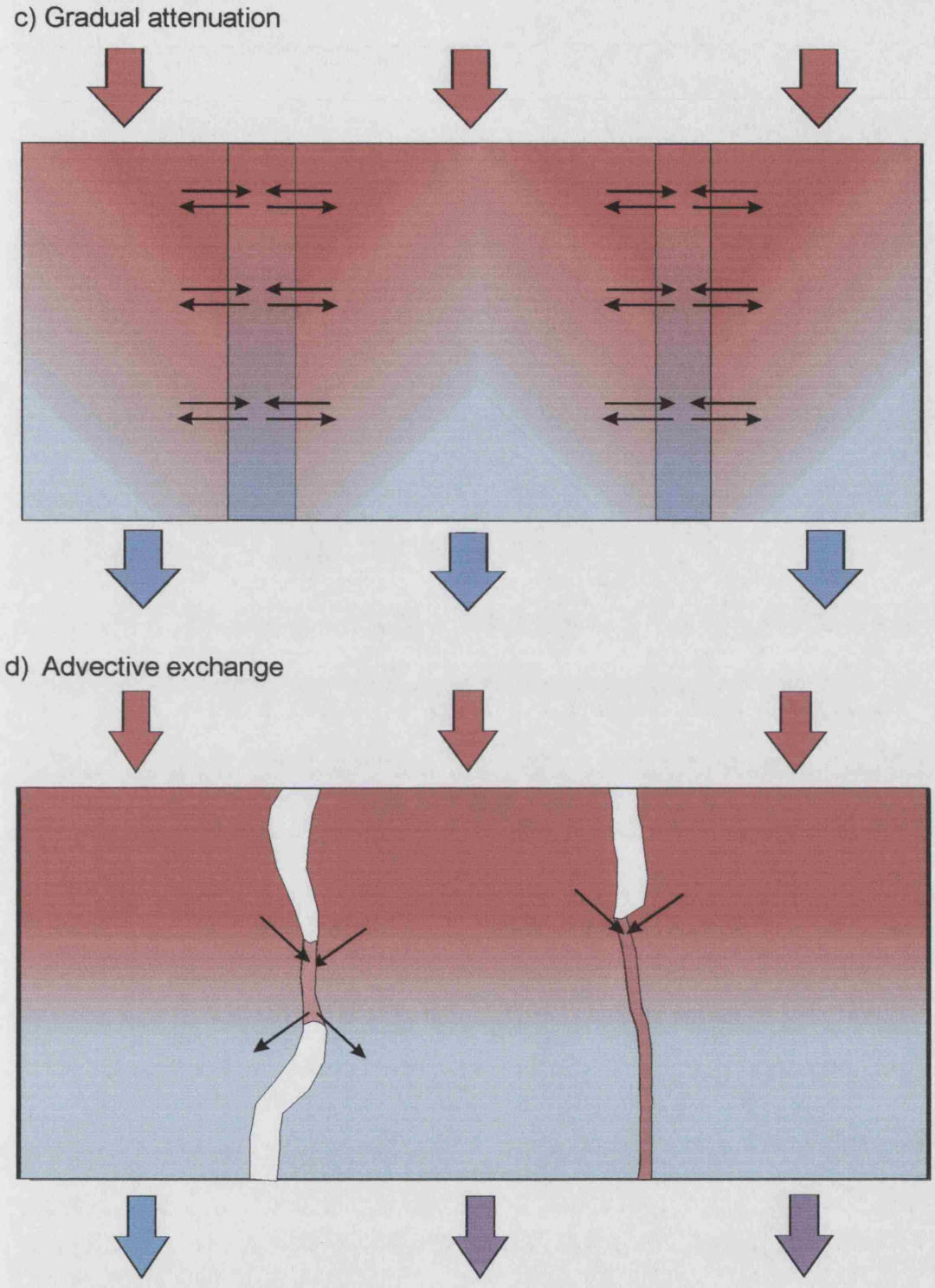

Figure 3-9 (continued) Conceptual models of solute transport through unsaturated chalk when the fractures are active, for c) gradual attenuation, and d) advective exchange. The drawing shows a cross-section of chalk intersected by two vertical fractures. Clean water is represented in blue, and solutes are represented in red.

A limitation of the conceptual models above, is that the presence of horizontal fractures has been ignored. Horizontal bedding plane fractures are often encountered however, and they can influence the flow pattern. If recharge occurs through the matrix only, then horizontal fractures may form a barrier to flow. The hydraulic connection between matrix blocks is then restricted to contact points between the fracture walls, and the effect of the horizontal fracture is to reduce the hydraulic conductivity of the system. If flow occurs mainly through vertical fractures, then intersection by horizontal fractures may cause the solutes to spread laterally, before they continue their way in other vertical fractures. The effect of the horizontal fractures is then to delay and disperse the solute flux.

Despite of all the research reviewed above, the uncertainty about unsaturated flow and solute transport through the Chalk remains large. It is still not possible to give a reliable figure for the contribution of fracture flow to the recharge of the Chalk. The figure seems to be greatly variable according to the strata and the geographical location. A better understanding of the recharge process could lead to a method to assess the importance of fracture flow for a specific location, based on a set of key parameters. This in turn would lead to a better assessment of the vulnerability of the Chalk aquifer. Another critical point is the extent of diffusive exchange of solutes between the fractures and the matrix. Furthermore, the possibility of advective exchange has been suggested. Again, a better understanding of these processes would enable more reliable estimates of travel times of pollutants to the water table. Therefore there is a need for more field experiments, particularly experiments under natural rainfall conditions. Several of the tracer tests described above were run under artificially high irrigation rates, which might reduce the validity of their results. The field research should be combined with modelling work to gain more insight into the physical processes. Indeed, comprehensive modelling of flow and transport through unsaturated chalk has not been attempted so far.

4 The Fleam Dyke research site, Cambridgeshire

4.1 Introduction

The previous chapter has highlighted the current uncertainties about unsaturated flow and transport processes through the Chalk. Several different conceptual models were proposed for the role of the fractures in conducting recharge and for the exchange of solutes between the fractures and the matrix. Field data of solute transport through the unsaturated chalk are limited, so more experiments are needed to help increase understanding. Therefore a tracer test was performed as part of this work, to further investigate the nature of the chalk unsaturated flow and transport process and to provide a comprehensive data set that can be used for modelling purposes. The Fleam Dyke research site is situated on the Chalk in Cambridgeshire and has been the subject of considerable research work. A large-scale lysimeter is present here, and it will be shown in this chapter how this can provide a particularly useful facility for tracer tests. Moreover, the site is well characterized and a long-standing database of daily recharge is available.

The present chapter provides a description of the Fleam Dyke research site, followed by an overview of previous research at the site. In a chapter to follow, a detailed account will be given of the experiments conducted by the author at Fleam Dyke between 2001 and 2003.

4.2 Site description

4.2.1 Location

The Fleam Dyke research site is located in Fulbourn, Cambridgeshire, at 10 km east-southeast from Cambridge (Figure 4-1). It is situated on the grounds of Cambridge Water Company, and a pumping station is located about 100 m to the south. The facilities include a large-scale lysimeter, a control hut, and a weather station with rain gauge (Figure 4-2). The site lies at about 30 m AOD.

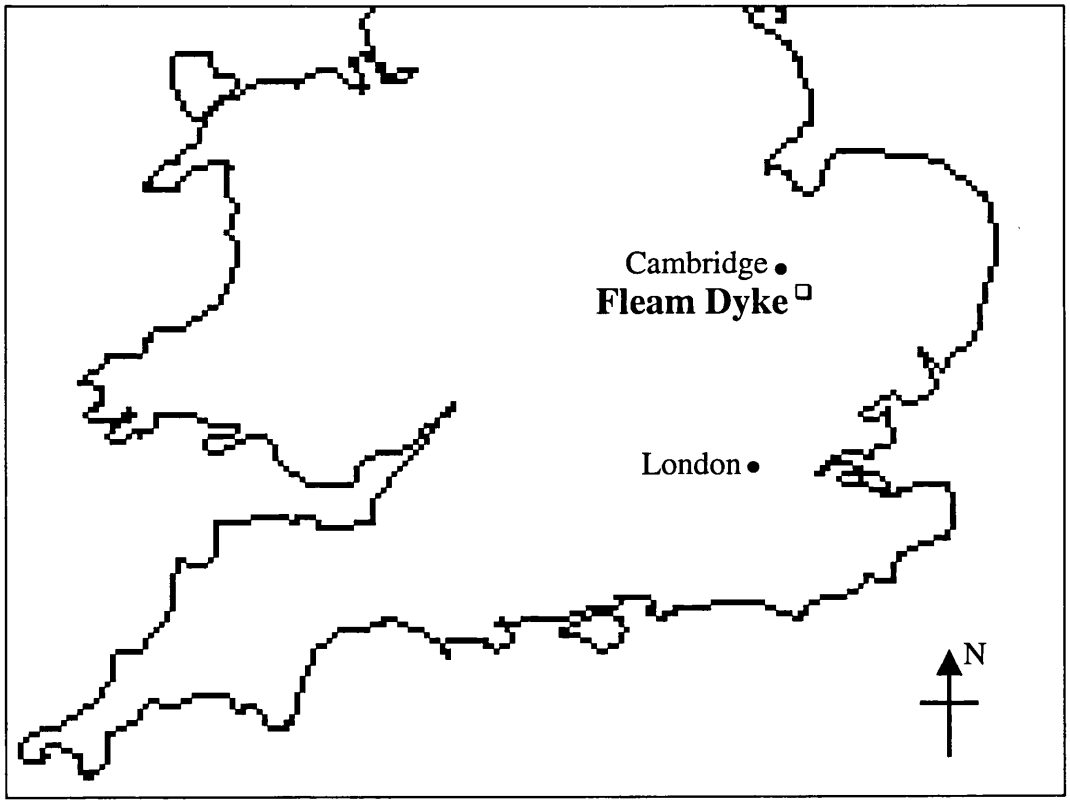

Figure 4-1 Geographical location of the Fleam Dyke research site.

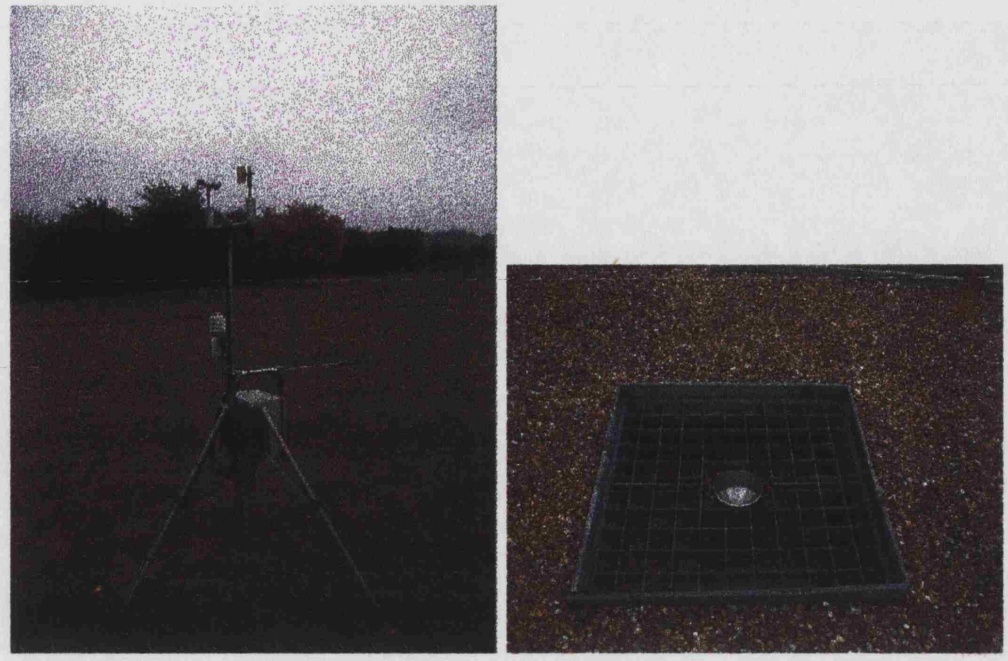

Figure 4-2 Weather station and rain gauge at the Fleam Dyke site

4.2.2 Geology

The geology of the area around the Fleam Dyke site has been described by Osborne-White (1932) and by Worssam and Taylor (1969), and is shown on the *Saffron Walden Sheet (205)* of the British Geological Survey geological maps (Figure 4-3). The geological map locates the Fleam Dyke lysimeter on the outcrop of the lower beds of the Middle Chalk[8]. The general appearance of the Middle Chalk in the larger area is that of nodular and lumpy marl-seamed chalk, in which flints are thinly scattered. The total thickness of the Chalk at the Fleam Dyke site is 65 metres, and the beds show a prevailing low dip to the South East. On top of the Chalk at Fleam Dyke lies a thin soil, labelled as *Swaffham Prior* on the drift Ordnance Survey map of Great Britain (sheet 205). It is a well-drained, calcareous, loamy soil, grading into chalk rubble underneath.

[8] Biostratigraphy of samples taken by the author suggested that the Chalk at the Fleam Dyke site belongs to Lower Chalk, not Middle Chalk. This is further discussed in Appendix II.

Figure 4-3 Geological map of the Fleam Dyke area (British Geological Survey geological maps).

The annual mean rest water table under the lysimeter lies about 18 m below ground level, but the pumped water level drops to about 32 m at a pumping rate of 63 m^3/h. Regional groundwater levels show a low gradient to the North-West.

4.2.3 The Fleam Dyke lysimeter

The Fleam Dyke lysimeter consists of a cube of volume 125 m^3 of undisturbed Chalk overlain by grassed soil, and contained such that drainage water can be collected at the base (Kitching and Shearer, 1982). In this section, the construction and operation of the lysimeter will be described in detail, but first a short review of lysimetry is included.

4.2.3.1 Review of lysimetry

Recharge, defined as the portion of the infiltration that reaches the water table, is an important parameter for the assessment of groundwater resources, as it sets an upper limit to the amount of groundwater that is available for long-term abstraction. However, estimation of recharge is difficult. Usually a water balance is made, calculating the difference between rainfall and estimated evaporation, but this method is subject to significant errors. Therefore lysimeters offer an attractive alternative, as they allow direct measurement of the natural recharge.

A lysimeter is essentially an enclosed block of soil and/or rock, through which water infiltrates to allow measurement of the quantity and/or quality of the percolation. It should be representative of natural moisture conditions, so any disturbance of the material inside the lysimeter or any artefacts due to its construction should be minimized. Therefore, filled lysimeters that are constructed from excavated and repacked material might have limited validity. The use of undisturbed lysimeters is preferable, and in addition the surface area should be large enough to enclose a representative elementary volume (REV) and to reduce edge effects. Ideally, a lysimeter should extend into the saturated zone and a water table should be maintained inside at the same level as outside (Kitching and Shearer, 1982). Lysimeters are traditionally used to measure recharge and evapotranspiration, but they can also be very useful to measure unsaturated transport of solutes in a tracer test (e.g. Poletika et al., 1995; Schoen et al., 1999a).

A whole range of lysimeters has been designed and been in operation in England, on a variety of aquifers. Often sites were chosen with a shallow water table underlain by naturally occurring impermeable strata. The sidewalls then penetrate the impermeable layer, so a complete seal is formed. An example of this is the undisturbed lysimeter on the Bunter Sandstone at Syrrup, Nottinghamshire, with a surface area of 100 m^2 (Shearer, 1979). Here the water level in the lysimeter is kept at the same level as outside by pumping the water out into a measuring tank. Other large-scale undisturbed lysimeters are located on the Lower Chalk in Reach, Cambridgeshire (Shearer, 1979) and on the Lower Greensand in Oxfordshire (Black et al., 1979). At Bridget's Farm in Hampshire, a series of 10 small-scale lysimeters was constructed from undisturbed shallow soil overlying Chalk (Belford, 1979). These monoliths were brought to the laboratory, where experiments were executed on crop uptake and leaching losses of fertilizer nitrogen (Dowdell et al., 1984).

On the Chalk at the Fleam Dyke research site in Cambridgeshire, two small-scale repacked field lysimeters have been present since 1936 (Forbes, 1979). They are a pair of concrete boxes 2 m square by 0.9 m deep, backfilled with material excavated for the construction. Percolation was measured manually on a daily basis from a tank with tap, installed under the perforated boxes. One of the lysimeters was kept turfed with short grass, and the other fallow. They were operated by Cambridge Water Company until at least 1984, and were later abandoned. The mean annual percolation was 186 mm for the turfed soil, and 251 mm for the fallow soil, the difference being due to the transpiration of the grass. However, it is expected that those values are an overestimation of the actual recharge, because of the limited depth of the concrete boxes. Therefore a larger, undisturbed lysimeter was designed to be built at the same site, which is now discussed.

4.2.3.2 Construction

The Fleam Dyke lysimeter was constructed in 1977, and care was taken in every stage of the construction to minimize disturbance to the chalk monolith (Kitching and Shearer, 1982; Shearer, 1984).

First, vertical steel piling in the shape of a square of 5 m side was driven down to 5 m depth. Before driving, the joints of the piles were sealed by coating them with liquid bitumen. The piling caused drawdown of the soil adjacent to the piles, but this was limited to 2-3 cm to a distance about 30 cm from the piles, and the drawdown did not extend into the chalk underneath. After installation, the piles were cut off at a height of 1-2 cm above the ground surface.

In a second stage, a trench of 6 m deep and 6 m wide was excavated around the walls of the lysimeter, to provide access to the bottom edge of the piles (Figure 4-4). The base of the lysimeter was then formed by driving two steel panels from opposite sides towards the centre at an angle of 10° below the horizontal. The joints between the base and the side pilings were sealed with a concrete fillet that was coated with a waterproof compound.

Figure 4-4 Fleam Dyke lysimeter during excavation in 1977 (photograph courtesy of British Geological Survey).

In the final stage, a tunnel 1.4 m high and 1 m wide was dug under the centre of the lysimeter, and a sloping trough was mounted under the outlet to collect the drainage and divert it to the measuring system. Sub-horizontal PVC pipes of 75 mm i.d. were installed in bores parallel to and just above the base panels, to ensure that any drainage reaching the base is quickly discharged into the collecting trough. At the bottom a reinforced concrete access passage, 1.5 m wide by 2 m high, was constructed leading around the base of the lysimeter, and made accessible through a vertical shaft with ladder. Finally the excavation around the lysimeter was backfilled and the original grass cover restored (Figure 4-5).

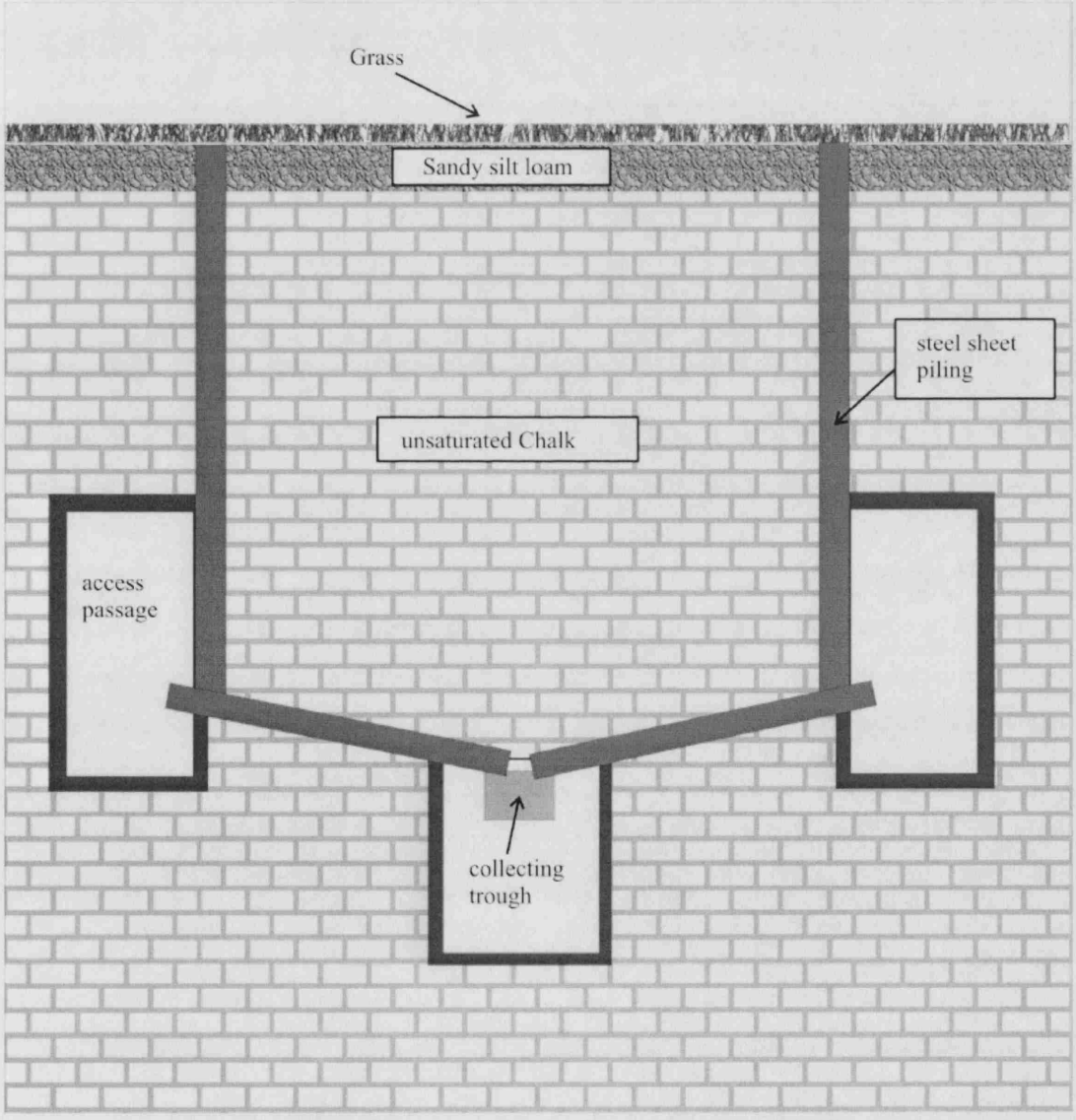

Figure 4-5 Cross-section of Fleam Dyke lysimeter.

4.2.3.3 Operation

From the collecting trough at the bottom of the lysimeter, the drainage is diverted into a tank with a surface area of 0.5 m^2. Recharge is recorded by monitoring the water level in the tank, and measurements are automatically data-logged on an hourly basis. A second independent measuring system has been installed in the form of a tipping-bucket gauge of 0.5 litre capacity, mounted between the collecting trough and the measuring tank (Figure 4-6). Both measuring systems have a resolution of 0.02 mm of recharge. The recordings are processed through an automatic data logging system and stored by the Environment Agency. When the water in the tank reaches a maximum level, the tank is emptied by the opening of a valve and the water drains into the underlying Chalk.

Figure 4-6 Tipping bucket measuring drainage from Fleam Dyke lysimeter.

The Fleam Dyke lysimeter was operated continuously between 1977 and 1986 by the British Geological Survey. At the end of 1995, the lysimeter measurements were started again by the National Rivers Authority (now Environment Agency), and up to date records are held and collected by the Brampton office of the Environment Agency.

4.2.3.4 Potential disturbance of the moisture regime

Ideally, a lysimeter measures recharge as it occurs under natural conditions. However, the lysimeter itself inevitably causes some disturbance to the natural moisture regime, such that there might be differences in the hydrodynamic behaviour inside and outside the lysimeter. What follows is a brief discussion of potential causes of disturbance at Fleam Dyke lysimeter, based on a report by Cooper et al. (1986).

4.2.3.4.1 Area of the lysimeter

The monolith should be representative of the heterogeneities encountered in the porous medium that it is constructed in. The Fleam Dyke lysimeter has a relatively large surface area of 25 m^2, and is therefore likely to be representative of variations smaller than this scale, but not of variations beyond this scale. In the Chalk, fractures occur at a range of apertures and spacings. It is expected that a large proportion of these fracture types are sampled by the Fleam Dyke lysimeter, except for instance for some major faults that are sparsely distributed. Therefore the overall permeability of the lysimeter may be an underestimation of the average regional permeability of the unsaturated zone.

Another effect of the limited size of the lysimeter might be on the natural processes occurring in the soil. The vegetation inside and outside the lysimeter walls should be the same, and the volume of soil should be sufficient to support a stable soil fauna population. Both requirements are likely to be met at Fleam Dyke, and no visual difference in plant composition was noticed on the grassland.

4.2.3.4.2 Construction of the lysimeter

There is a risk that gaps exist between the monolith and the lysimeter walls. This would lead to preferential flow along the walls during heavy storms, thus increasing the total drainage. Such gaps are typically encountered for shrinking clay soils, but are less likely for the chalk found at Fleam Dyke.

The hammering of the piling walls may have caused the artificial production or enlargement of cracks in the chalk next to the lysimeter walls, thereby increasing its permeability and increasing the total drainage. This is probably limited to a small zone around the walls, and its effect would be mitigated by the large area of the lysimeter.

4.2.3.4.3 Truncation of the profile

The bottom of the lysimeter artificially cuts off the moisture profile within the lysimeter from the profile below. This modifies the moisture conditions near the bottom of the lysimeter, with possible effects on drainage. In winter, drainage out of the lysimeter can only occur when the pressure head at the bottom is either zero or slightly positive. This implies that a zone of saturation must exist at the bottom in order for drainage to occur. This does not apply outside the lysimeter, and the water needed to create this saturated layer may therefore delay the onset of the drainage from the lysimeter in early winter. When drainage slows down later in the season, pressure heads at the depth of the lysimeter base will drop outside the lysimeter, but inside the lysimeter the saturated layer will persist as long as drainage continues. This can create significant differences in pressure head close to the base in early summer. This was indeed observed from the tensiometers below 1.50 m, installed inside and outside the lysimeter in the early eighties (see section 4.3.2.1).

It was stated earlier that a lysimeter should ideally extend down into the saturated zone. The rest water table at the Fleam Dyke site is around 18 m below ground level,

so clearly for Fleam Dyke lysimeter, with a depth of 5 m, this condition is not met. Nevertheless the total amount of drainage should be a good estimate of the recharge, because there is no upward water movement expected at the level of the lysimeter base. This is illustrated by the observation that a zero flux plane generally never reaches that deep in the Chalk in southern England. An important difference however is the timing of the recharge, as there will be a significant delay between the drainage at 5 m depth and the arrival of the drainage at the water table several metres below.

4.2.3.4.4 Conclusion

Several possible disturbances to the natural moisture regime at Fleam Dyke lysimeter have been identified. Some of them, like the induction of artificial cracks from the hammering of the piling, might increase the drainage, whereas others, like the exclusion of large regional faults, might decrease the drainage. The net effect is not clear, but it is expected that the overall disturbance would be mitigated due to the relatively large surface area and depth of the lysimeter.

Effects to take into account are a possible delay in the onset of drainage in early winter, and a general delay between the drainage from the lysimeter and the actual arrival of the recharge at the water table. From the tensiometer readings in the early eighties, it was noticed that the pressure head below 1.50 m during the summer was generally higher inside the lysimeter than outside. On a positive note, however, the neutron probe profiles inside and outside the lysimeter looked roughly the same (see section 4.3.2.1). The differences in water contents inside and outside were of the same magnitude as the differences in water contents between two different profiles outside the lysimeter. This may be an indication that the moisture regime inside the lysimeter is overall a good representation of the natural moisture regime in the area.

4.3 Previous work

The Fleam Dyke site in Cambridgeshire has been a subject of intense research, especially in the period 1978-1984 by the British Geological Survey and the Institute of Hydrology, Wallingford. Apart from research on the lysimeter facility, some additional experiments have been conducted on small-scale plots on the surrounding grassland and arable field. The methods included solute profiling and soil physics research, and both aspects will be addressed in this chapter. Finally some conclusions will be drawn on the flow and transport behaviour at Fleam Dyke, and on the likelihood of fracture flow on this site.

4.3.1 Solute profiling

4.3.1.1 Agricultural solutes

To monitor the infiltration of fertilizer-derived agricultural solutes, Foster and Bath (1983) conducted a profiling experiment of the unsaturated chalk at the Fleam Dyke site. On an arable field close to the lysimeter, cores were drilled down to 15 metres on several occasions over the period 1979-1981. The pore-water from the core samples was analyzed for nitrate, chloride and sulphate, with the assumption that the resulting solute profiles should reflect the infiltration of inorganic fertilizers used on the field. A detailed description of the profiles has been published by Coleby et al. (1998). All profiles revealed peaks around 4 m depth, but the depth and magnitude of the peaks could not be accounted for by a simple model of unsaturated zone transport. Although sequential profiling was used, no clear indication was found of downward movement because of lateral heterogeneity of the profiles. The results seem to indicate strongly dispersive solute movement in the upper few metres, corresponding to the soil and the weathered chalk.

4.3.1.2 Environmental isotopes

The same chalk cores that were used for examination of agricultural solutes were analyzed for deuterium and tritium as well (Darling and Bath, 1988; Foster and Bath, 1983; Geake and Foster, 1989).

Deuterium is a useful stable environmental isotope, as it shows a marked seasonal fluctuation in rainfall. Summer rainfall is usually enriched in deuterium relative to winter rainfall, and this cyclic pattern can be preserved with depth in the unsaturated zone. Darling and Bath (1988) reported the results of the deuterium profiling in the unsaturated zone at Fleam Dyke (Figure 4-7). They showed that the seasonal pattern was not well preserved, again suggesting dispersive flow behaviour in the upper few metres. In addition they reported the monitoring of the deuterium concentration of rainfall, lysimeter drainage and groundwater on the same site. The average isotopic composition of the lysimeter drainage was -48‰ VSMOW, whereas the isotopic composition of the core profiles at the same depth (5 m) was between -40 and -45‰ VSMOW (for information on isotope units, see Appendix III). Water extracted from chalk cores of limited size is essentially matrix pore water, whereas the drainage water from a lysimeter is more likely to represent the whole range of pore and fracture sizes that contribute to unsaturated flow. And, since it was observed at Fleam Dyke that water extracted from cores and drainage water at the same depth have a different isotopic composition, it follows that the water in the fractures and the matrix must be isotopically different as well. The difference suggests that the fractures and the matrix are not in diffusive equilibrium, hinting at the occurrence of rapid fracture flow. However, the isotopic composition of the lysimeter drainage was very constant throughout the year at approximately -48‰ VSMOW and did not respond to changes in isotopic rainfall composition, implying that complete bypass from the ground surface to the lysimeter base did not occur. Finally, the groundwater composition measured from a pumped well at the Fleam Dyke site was -49‰ VSMOW, which is fairly similar to the average rainfall composition (at -51‰ VSMOW). This seems to indicate that rainfall from all months of the year contributed to the recharge, which implies strong dispersive mixing over the whole root zone.

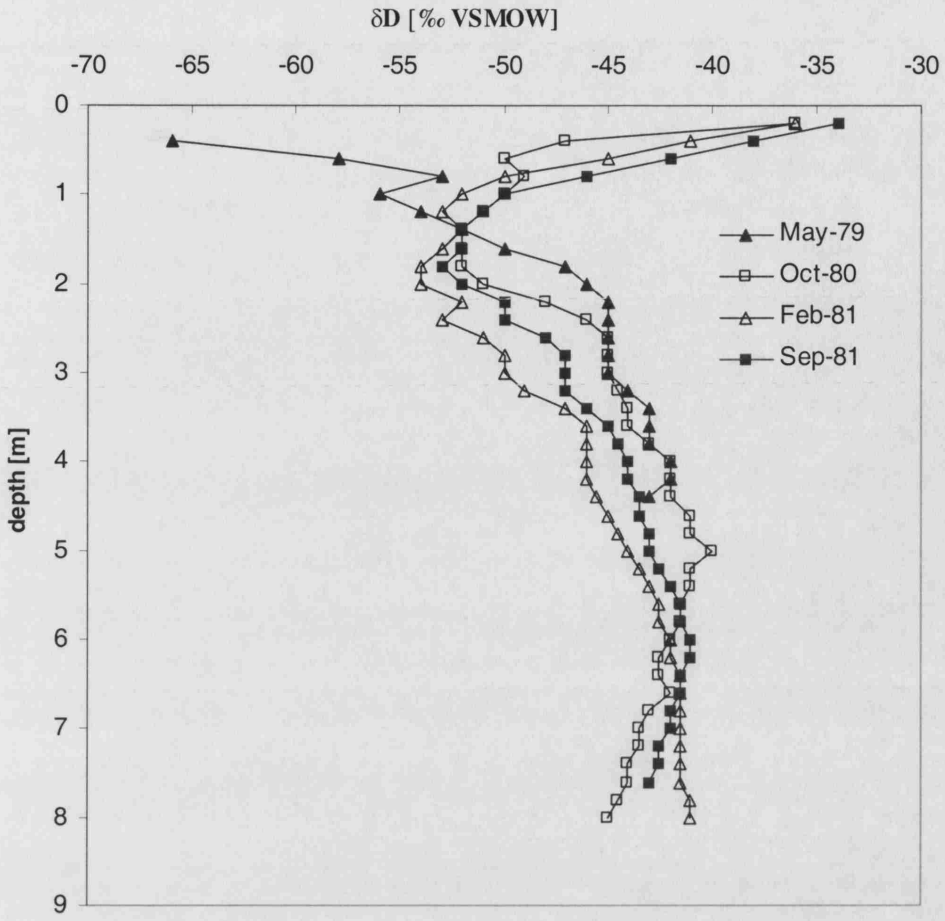

Figure 4-7 Deuterium profiles in the unsaturated zone of the Chalk at the Fleam Dyke site (after Darling and Bath, 1988). For explanation on the δ-notation for deuterium, see Appendix III.

Geake and Foster (1989) reported sequential tritium profiles at Fleam Dyke, again measured from the same cores (Figure 4-8). The tritium peak was less defined than at other Chalk sites, and the profiles showed significant forward tailing and peak retardation. As with the profiles of agricultural solutes, downward movement of tritium was not clear because of lateral heterogeneity between the profiles. A problem of interpretation arose for the high tritium concentrations measured at shallow depth, as they were higher than concentrations in post-1975 winter rainfall. This phenomenon could be partly explained by assuming that summer rainfall, which is usually enriched in tritium, penetrated down to at least a 2-metre depth and equilibrated with the surrounding soil moisture.

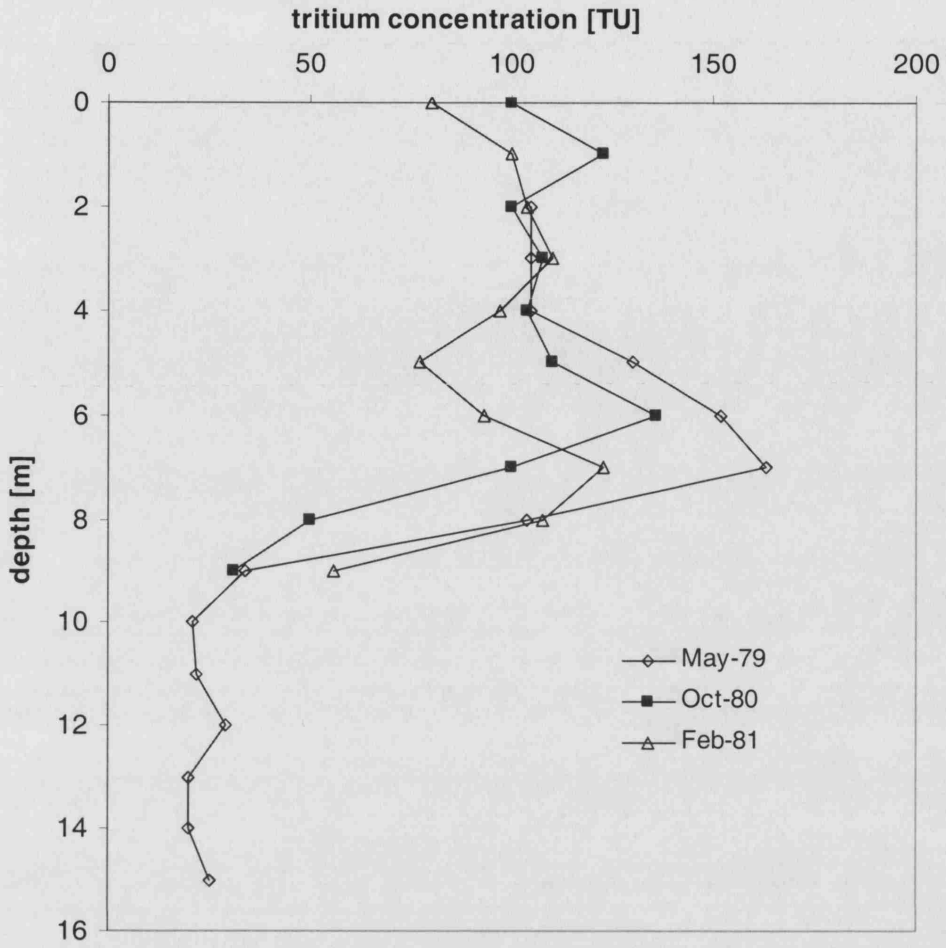

Figure 4-8 Tritium profiles in the unsaturated zone of the Chalk at the Fleam Dyke site (after Geake and Foster, 1989). For explanation on Tritium Units, see Appendix III.

4.3.2 Soil physics research

4.3.2.1 Water content and pressure head

Between 1980 and 1981, the Fleam Dyke lysimeter was equipped with five mercury manometer tensiometers, installed at depths of 0.6 m, 1.2 m, 2.1 m, 3.3 m and 4.5 m (Cooper, 1985). Figure 4-9 shows the evolution of the total head during a wetting phase in early winter and a drying phase in early summer. Large changes were observed over the year, and high pressure heads (> -50 cm H_2O) occur in winter over the whole profile, indicating that the fractures are likely to become active. Note that

at the end of summer the mercury manometer tensiometers go off scale. Gypsum resistance blocks were later installed on site, and total heads down to –6500 cm H_2O were observed (Wellings and Cooper, 1983).

During the same period of 1980-1981, neutron-probe readings were carried out in three neutron probe access tubes that were installed in the lysimeter. Large changes in water content over the year were observed in the soil and the weathered chalk underneath, but below about 1.5 m in the unweathered chalk, changes were minimal (Cooper, 1985).

Figure 4-10 shows water retention curves for five depths in the lysimeter, constructed from simultaneous readings of water contents and pressure heads. A similar pattern is obtained as for the other chalk sites shown in Figure 3-6. The curves are particularly steep for the chalk below 1.5 m depth, with hardly any change in water content over the whole range of pressure heads observed.

A similar arrangement of tensiometers and neutron-probe access tubes was established at two grassland plots about 50 m south of the Fleam Dyke lysimeter. Comparison of simultaneous measurements within plots and between plots shows significant differences. There is marked variability of water contents and pressure heads at a scale of tens of metres, but even at a scale of a few metres, differences in water content of up to 5% were recorded. This suggests spatial heterogeneity of physical properties, but the variability may also be due to measurement errors.

(a) wetting phase

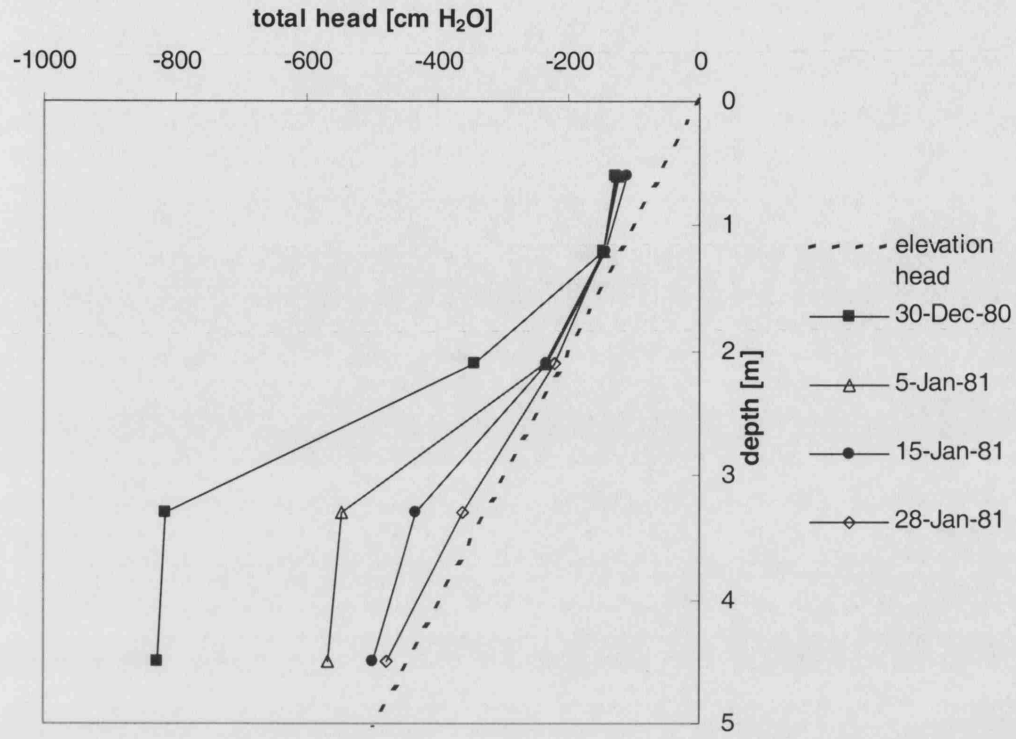

(b) drying phase

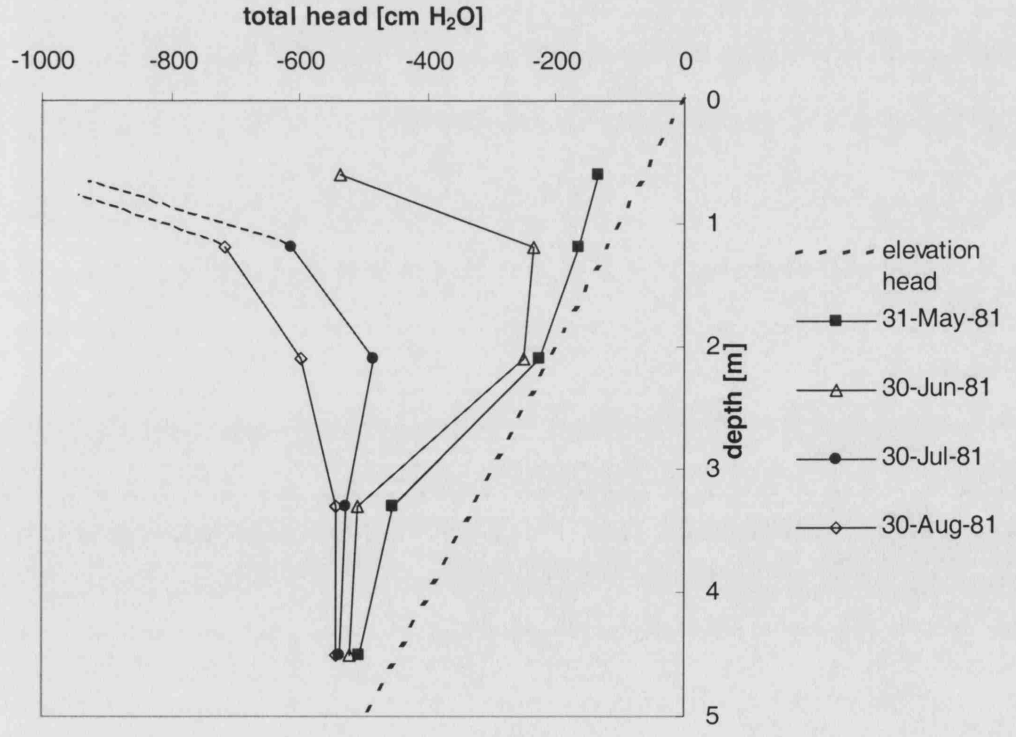

Figure 4-9 Variation of total head with depth recorded at the Fleam Dyke lysimeter: (a) during wetting phase, (b) during drying phase (Data courtesy of Centre of Ecology and Hydrology, Wallingford).

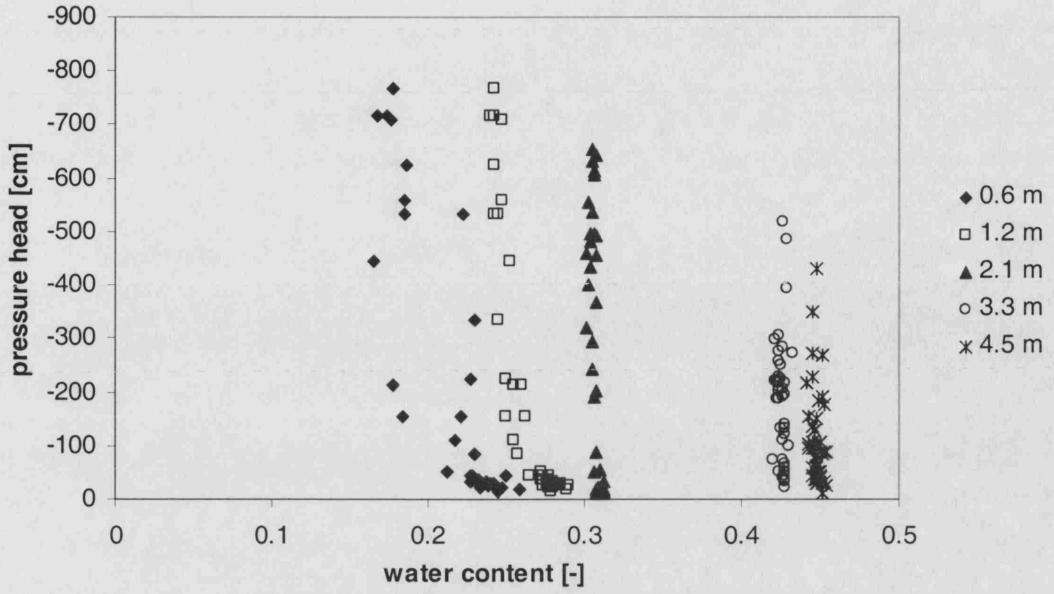

Figure 4-10 Water retention curves constructed from simultaneous measurements of water content and pressure head on the Fleam Dyke lysimeter over the period 1980-1981 (data courtesy of Centre of Ecology and Hydrology, Wallingford).

Cooper (1985) applied the data of water content and total head from the two grassland plots to calculate estimates of evaporation and recharge, using the zero flux plane (ZFP) technique (Cooper et al., 1990; Gardner et al., 1991). A (divergent) zero flux plane is a plane of maximum total head. Water flow across the ZFP is not possible; as a consequence all the changes in water content occurring above the ZFP can be ascribed to rainfall and evapotranspiration. Similarly, all the changes in water content occurring below the ZFP are due to drainage out of the base of the profile. This enables estimation of evaporation and recharge as long as a ZFP is present, and in the absence of a ZFP (in winter) a simple water balance can be calculated, assuming that the actual evapotranspiration equals the potential evapotranspiration, as calculated from meteorological data. Cooper (1985) observed a ZFP at Fleam Dyke for 60% of the time, with a high degree of variability between years. The estimated recharge was about 10% lower than the drainage measured from the lysimeter. The difference may be due to a variety of causes, such as effects inherent to the lysimeter (see 4.2.3.4), errors in soil physics measurements, errors in the calculation of evapotranspiration during non-ZFP periods, or genuine differences in physical properties between the grassland plots and the lysimeter.

4.3.2.2 Unsaturated hydraulic conductivity

Wellings and Cooper (1983) reported measurements of the unsaturated hydraulic conductivity, executed on one of the grassland plots 50 m south of Fleam Dyke lysimeter. A method similar to that of Poulovassilis et al. (1974) was used, which is a combination of steady state infiltration for high pressure heads and the instantaneous profile technique (Watson, 1966) for low pressure heads. A portable greenhouse was erected over the site to prevent rainfall infiltration and evapotranspiration losses. Uniform irrigation was applied at a series of constant rates varying between 1 and 500 mm/d, with each rate being maintained for about 4 days to reach a steady state. After water had been applied at the lowest irrigation rate, the profile was allowed to drain naturally. Neutron probes and tensiometers were read during the experiment, and the unsaturated hydraulic conductivity at specific depths was calculated by dividing the water flux by the total head gradient at that depth.

Figure 4-11 shows curves of the resulting unsaturated hydraulic conductivity as a function of the pressure head. The saturated hydraulic conductivity varies with depth between 70 and 800 mm/d, but drops sharply for all depths at pressure heads between –25 and –50 cm H_2O. For depths below 2.4 m, the curves show the typical shape that has been reported for other chalk sites (Figure 3-7). Below –50 cm H_2O, the hydraulic conductivity remains more or less constant, as the matrix pores stay saturated. From Figure 4-11 it can be inferred that the unweathered chalk at the Fleam Dyke site at 3 m depth has a matrix saturated hydraulic conductivity of about 1 mm/d. This is in accordance with laboratory measurements on samples of the Upper and Middle Chalk (Allen et al., 1997).

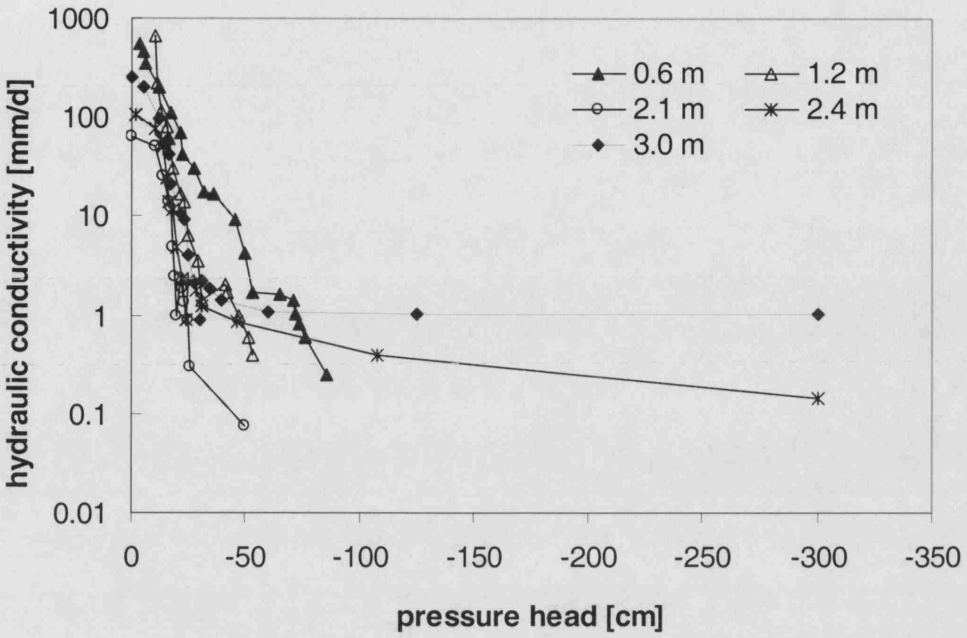

Figure 4-11 Unsaturated hydraulic conductivity as a function of pressure head, measured at different depths on a grassland plot next to the Fleam Dyke lysimeter (data courtesy of Centre of Ecology and Hydrology, Wallingford).

4.3.2.3 Lysimeter drainage

Jones & Cooper (1998) examined drainage records of Fleam Dyke lysimeter from the early eighties. They focussed on periods when a soil moisture deficit was non-existent, as indicated by MORECS[9] data. Figure 4-12 shows three selected periods of rainfall and lysimeter drainage. To smooth out day-to-day variations in the rainfall, the three-day moving average of rainfall is used. Also indicated are the days when the pressure head throughout the profile exceeds –50 cm H_2O, the value that was derived from the unsaturated hydraulic conductivity curves as an indicator of fracture flow initiation (see Figure 4-11). It can be seen from Figure 4-12 that there is a general coincidence between periods when the pressure head exceeds –50 cm H_2O and periods when the drainage exceeds 1 mm/d. The latter was the value obtained for the

[9] MORECS is an acronym for Meteorological Office Rainfall and Evaporation Calculation System. It provides weekly estimates of evapotranspiration, soil moisture deficit (SMD) and hydrologically effective precipitation for each square of a 40 X 40 km grid of Great Britain, based on daily meteorological data (Hough et al., 1995). The SMD is calculated through a two-reservoir model to simulate the extraction of water.

matrix saturated hydraulic conductivity in Figure 4-11. If it is assumed that the hydraulic gradient approaches unity during the recharge season (an assumption which was met for instance at 28 January 1981, Figure 4-9), then the maximum infiltration rate approaches the matrix saturated hydraulic conductivity (Price et al., 1993) and any infiltration exceeding 1 mm/d should be diverted into the fractures. Starting from these observations, Jones & Cooper (1998) assumed that any drainage in excess of 1 mm/d is fracture flow, and all the drainage below is matrix flow. Based on this division, over 30% of the total drainage for the period 1981-1986 could be attributed to fracture flow. Fracture flow was observed most frequently between November and June, and seemed to be possible, but less likely, in October and July (Jones, 1992).

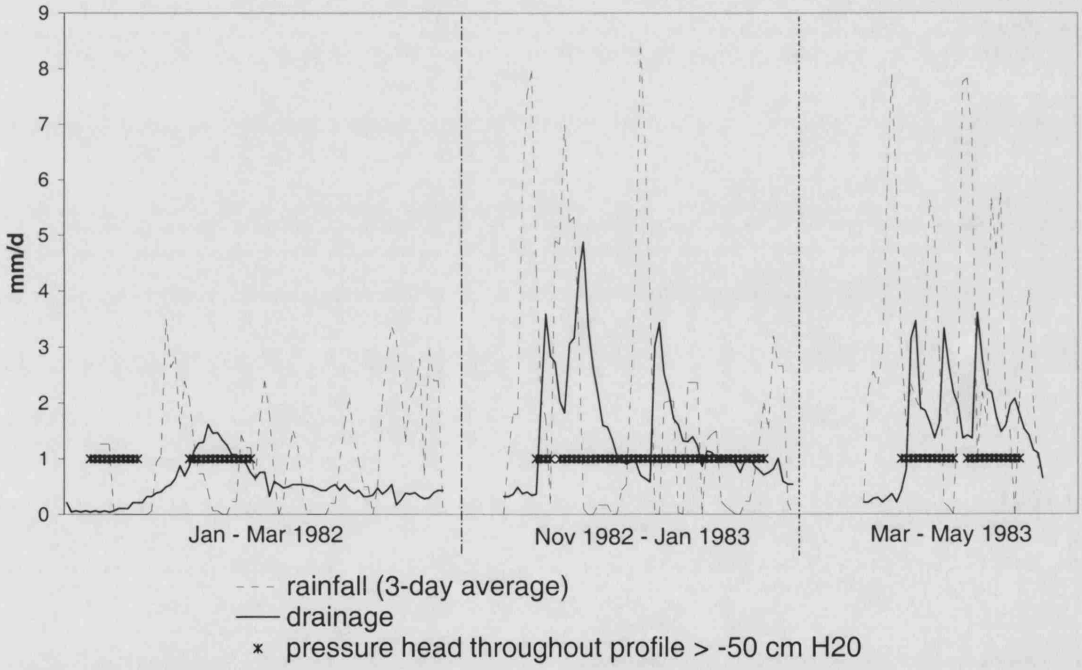

Figure 4-12 Three-day average rainfall and drainage from the Fleam Dyke lysimeter, for periods when MORECS indicated no soil moisture deficit; indicated are the days when the pressure head throughout the profile exceeds –50 cm H_2O (after Jones and Cooper, 1998).

Jones & Cooper (1998) correlated the records of lysimeter drainage statistically with various parameters of rainfall and pressure head, again limited to the times when

MORECS indicated no SMD. They concluded that the drainage was most closely correlated with the three-day moving average rainfall with a time lag of four days, and with the pressure head with a time lag of 4 days.

4.3.3 Conclusion

The previous work into the unsaturated chalk at Fleam Dyke presented in this chapter has highlighted two characteristics of the Chalk discussed in Chapter 3. First of all, the matrix in the unweathered zone stays virtually saturated throughout the year, which demonstrates the steepness of the moisture retention curve. Furthermore, the unsaturated hydraulic conductivity relationship exhibits two characteristic sections, with a sharp transition around –50 cm H_2O, marking the point where fractures become active.

Other conclusions may be more specific to the Chalk at Fleam Dyke in Cambridgeshire, and are related with mixing in the upper few metres and with the likelihood of fracture flow.

Strong mixing in the upper 1.5 or 2 metres, corresponding with the soil and the weathered chalk, was derived from various observations:

- The profiles of agricultural solutes were not clearly defined;
- The seasonal pattern in the deuterium profiles was not well preserved;
- The average deuterium composition of the groundwater was very similar to the annual average rainfall composition, indicating that rainfall over the whole year contributed to the recharge;
- High tritium concentrations at shallow depths suggest mixing of summer rainfall through the soil and the weathered chalk.

This mixing behaviour is expected to have a dampening effect on incoming rainfall fluxes. Nevertheless fracture flow seems to be a common phenomenon at Fleam Dyke, as judged from the following observations:

- Pressure heads throughout the upper 5 metres frequently exceeded –50 cm H_2O;

- The chalk matrix has a saturated hydraulic conductivity of only 1 mm/d, whereas drainage rates in winter are often much higher; assuming that all drainage in excess of 1 mm/d is directed into the fractures, then fracture flow was estimated to contribute over 30% of the total drainage;
- The isotopic composition of the lysimeter drainage did not correspond to that of pore waters from the matrix at the same depth, indicating two different flow paths that are not in isotopic equilibrium; this suggests the occurrence of fracture flow which doesn't reach diffusive equilibrium with the matrix, so there is a possibility that solutes can bypass the matrix.

The observations at Fleam Dyke emphasize that flow and solute transport through the Chalk unsaturated zone is the result of the combination of climatic conditions coupled with the Chalk flow properties. There is evidence from the Fleam Dyke observations of fractures becoming active during winter as the soil profile wets up; however there is also evidence that this fracture flow does not lead to rapid bypass of solute to the groundwater table. Of the four conceptual models proposed in section 3.3, this leaves two possibilities open. First, fracture flow in the unsaturated zone may extend over the whole depth of the unweathered chalk, but there is gradual attenuation of the tracer by diffusion from the fractures into the matrix (Figure 3-9 c). Second, the fractures may only be water-filled over limited depth, with advective exchange of tracer between the fractures and the matrix (Figure 3-9 d). Advective exchange will be further addressed in the modelling part of this work.

5 Tracer experiment at the Fleam Dyke Research Site

5.1 Objectives

The work reviewed in the previous sections has demonstrated the potential for tracers to provide direct information on solute transport behaviour. The motivation for the tracer experiment conducted at Fleam Dyke was to provide a comprehensive dataset that could help to clarify some of the uncertainties regarding flow and solute transport through unsaturated chalk. More specifically, the tracer data should provide an answer to two questions. First, what is the importance of fracture flow on this site? Second, is there significant exchange of solutes between the fractures and the matrix, and does this exchange happen through diffusion or rather through advection? The tracer observations along with the existing data presented in Chapter 4 are modelled in Chapters 7 and 8. This model forms the basis for developing a set of more general conclusions about the nature of Chalk unsaturated flow and transport.

The Fleam Dyke research site was considered a nearly ideal location for the tracer experiments. First of all, the lysimeter presents a convenient tool to collect unsaturated drainage. The tipping bucket underneath the lysimeter integrates the drainage from a 5 × 5 m square of chalk and thus provides an average of spatially heterogeneous flow and transport pathways. The lysimeter makes it easy to collect drainage on a regular basis, and the resulting tracer breakthrough curve is more likely to be representative of the average local conditions than would be achieved with suction cups. As the lysimeter collects all drainage from the 5 × 5 m square, it provides a more reliable basis to calculate a mass balance. A second reason to choose the Fleam Dyke research site was that it is a well-documented site, with considerable research done in the period 1978-1986 (see section 4.3.2). A long-term record of

lysimeter drainage is available since 1977, and drainage data from the small repacked lysimeters (see section 4.2.3.1) go back as far as 1936.

From section 4.3.3 it was concluded that fracture flow is likely to occur at Fleam Dyke. This was another argument to choose this site, as this would provide valuable observations on the potential for bypass flow, an important process in terms of contaminant migration to the water table. If no tracer would appear, that would make a conservative case for the protective capabilities of the chalk unsaturated zone. Furthermore, the tracer test was designed to be executed under natural rainfall conditions, i.e. without artificial irrigation. This was considered essential, as a large part of the tracer tests on unsaturated chalk described in literature (see section 3.2.3) were performed under high irrigation rates. These high irrigation rates are often not representative for natural conditions, and may limit the validity of the results of these tracer tests. The transport behaviour, particularly the potential for solutes to bypass the unsaturated chalk via fracture flow, is determined by the climatic conditions. Therefore at Fleam Dyke the tracer was applied with a minimum of irrigation and afterwards the site was left to the governing climatic conditions. This also ensured that the ongoing recharge measurements on the Fleam Dyke lysimeter were not disturbed.

5.2 Tracer selection

To meet the scientific objectives and to conform to health and safety restrictions, the choice of tracers was limited. The tracers ideally had to be fully conservative, i.e. non-sorbing and non-degrading. To be able to detect the tracers in small concentrations, both the detection limit and the natural background had to be low. An additional constraint in this project was the cost, both for the purchase of the tracers as for their analysis. The first requirement however was the safety of the experiment. There could be absolutely no risk of tracer reaching the pumping station of Cambridge Water Company at a concentration that might jeopardize the use of the water for public water supply. This had to be ensured by choosing tracers with very low and well-documented toxicity characteristics and by applying them in amounts that would not raise concentrations at the pumping station above their natural

background levels. Similarly, the tracers were not to pose a health hazard during handling and were not to disturb the ecosystem.

The diffusion coefficient of a solute tracer diminishes with increasing molecular size (see Appendix I). The use of solute tracers with contrasting sizes, and thus contrasting diffusion coefficients, can be very instructive for the diffusion exchange mechanism. Indeed, it has been shown in the analysis of tracer breakthrough curves that the use of at least two tracers with contrasting diffusion coefficients is essential to distinguish diffusion from other mechanisms such as dispersion and sorption (e.g. Becker and Shapiro, 2000; Hu and Brusseau, 1995; Maloszewski et al., 1999). Such a tracer test is also called a *comparative tracer test.* This was the approach chosen for the Fleam Dyke tracer test.

The tracers selected for the experiment were deuterium and bromide. Their properties are summarized in Table 5-1. Both tracers have been used in numerous groundwater studies and are known for their conservative behaviour (Becker and Coplen, 2001; Levy and Chambers, 1987). The Drinking Water Inspectorate does not give any guidelines for concentrations in drinking water, but both tracers have very low toxicity characteristics and are harmless at low concentrations. Deuterium is a stable isotope of hydrogen and is relatively abundant in nature, comprising about 0.015% of all hydrogen on earth. As it is incorporated in the water molecules themselves, it constitutes a nearly ideal tracer to study the transport of water-soluble contaminants. Deuterated water is taken up by plants at the same rate as normal water, and through evapotranspiration some fractionation may occur. Bromide is expected to be taken up easily by plants as well (Kung, 1990) but cannot evaporate, so evapotranspiration of soil water would lead to concentration of bromide in the plant material and in the soil.

Table 5-1. Properties of selected tracers

Property	Deuterium	Bromide
Formula	^{2}HHO	KBr
Free-water diffusion coefficient at 10°C	1.48 x 10^{-9} m^2/s [(1)]	1.31 x 10^{-9} m^2/s [(2)]
Toxicity guideline	700 mg/l [(3)]	1 mg/l [(4)]
Cost	£250 per litre ^2H_2O [(5)]	£4 per 100 g KBr
Detection Method	Mass spectrometry	Ion chromatography
Detection Limit	1 ‰	1 µg/l
Background concentration	-50 to -30 ‰ [(6)]	35 to 40 µg/l [(7)]

[(1)] Mills (1973), value at 25°C corrected to 10°C by the Stokes-Einstein equation.

[(2)] value for bromide at 10°C, Parker et al (1994).

[(3)] based on a maximum allowable intake of 70 g and on a consumption of 100 litres of water (Koletzko et al., 1998).

[(4)] groundwater quality criterion (Flury and Papritz, 1993).

[(5)] CK Gas Products Ltd.

[(6)] δ ^{2}H values measured in Fleam Dyke porewaters in the early eighties (Darling and Bath, 1988) and in the lysimeter drainage during the period 2001-2002.

[(7)] concentrations measured in the lysimeter drainage during the period 2001-2002.

5.3 Tracer input

The tracer solution was prepared in a 50-litre barrel in the laboratory, one day prior to application, and contained 12% ^2H_2O and 3 g/l bromide (as KBr). The ^2H_2O is expected to mix with H_2O molecules to form ^{2}HHO. The bromide concentration was chosen such that the grass would not be affected, as Bowman et al. (1997) observed no adverse effects on plant growth for a mass input of 3 g/m^2.

For the tracer irrigation, a time was chosen during the winter recharge with a period of high rainfall on the preceding days, to ensure that the profile was close to saturation. Tracer irrigation occurred on 11 February 2002, when 25 litres of the tracer solution were applied on the lysimeter surface (5 × 5 m), and 16 litres on an adjacent 4 × 4 m plot (Figure 5-1). This second plot was chosen to allow drilling of core profiles to construct a vertical profile of tracer concentrations, as such destructive experiments could not be performed in the lysimeter itself. A uniform tracer distribution was obtained by dividing the area into 1-metre squares and by distributing one litre of

tracer solution over each square with a watering can. This corresponds to an irrigation event of 1 mm. No additional irrigation was applied after that, and the site was exposed to natural precipitation and evapotranspiration.

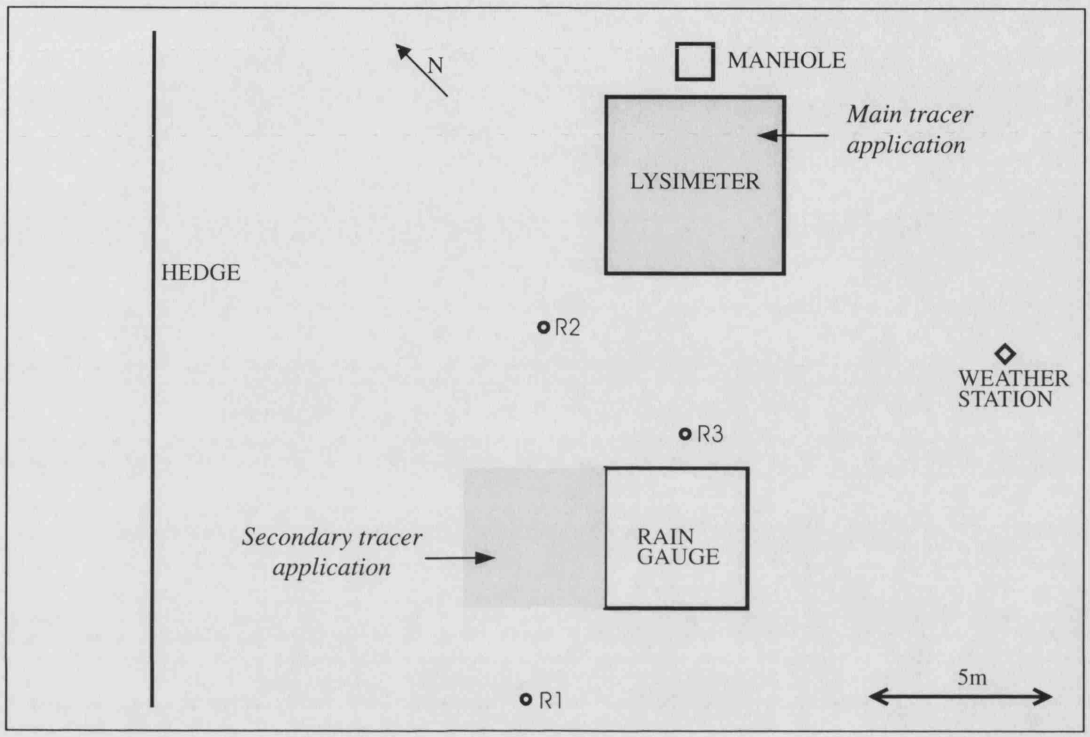

Figure 5-1 Map of the Fleam Dyke research site, showing in grey the area where the tracer was applied on 11th February 2002, and indicating the locations where reference cores were drilled (R1, R2, R3).

5.4 Sampling

5.4.1 Soil and chalk samples for physical characterization

Undisturbed soil samples were needed to measure the bulk density and water content of the upper soil layer. To access a vertical profile, a pit of 55 cm depth was dug in February 2002, several metres away from the tracer-irrigated area. The profile revealed 20 cm of dark soil with an abrupt transition to the weathered chalk underneath. The weathered chalk was well compacted, consisting of chalk fragments becoming larger downwards (varying roughly between 1 and 10 cm), with some putty

chalk in between. Undisturbed soil samples were taken at several depths by hammering hollow PVC cylinders (47.5 mm internal diameter and 114 mm length) horizontally into the profile and subsequently digging them out. After collection, the cylinders were sealed in zip lock polythene bags and stored at 4°C to prevent evaporation. Some larger chalk fragments were also collected from the bottom of the pit for later measurement of bulk dry density and porosity.

5.4.2 Lysimeter drainage

For sampling of the lysimeter drainage, a 0.7-litre sampling vessel was installed between the tipping bucket and the drainage measuring tank (Figure 5-2). Continuous flow and low residence time in the sampling vessel were required to ensure that the samples always corresponded to freshly drained water. At the same time the continuous recording of recharge by the tipping bucket and the measuring tank could not be disturbed. Therefore the drainage from the tipping bucket was directed to the bottom of the sampling vessel, which itself overflows into the drainage tank. The samples were taken by a portable automatic water sampler (Hobo Sampler, Warren Jones Engineering Ltd.), which pumps up a 150 ml sample from the bottom of the sampling vessel by a vacuum pump. Any loss of drainage in the measuring tank was accounted for by measuring the collected volume of samples. The automatic sampler contains a tray with 24 plastic bottles of 500 ml, and the timing of the pumping can be programmed, so a time range of samples can be collected without the need to manually change the sample bottles.

Following the tracer irrigation, samples were taken every hour. As the experiment went on the sampling frequency was gradually reduced to once a day. Samples were taken continuously between February 2002 and May 2003, except for the dry season between July 2002 and November 2002 when the drainage ceased.

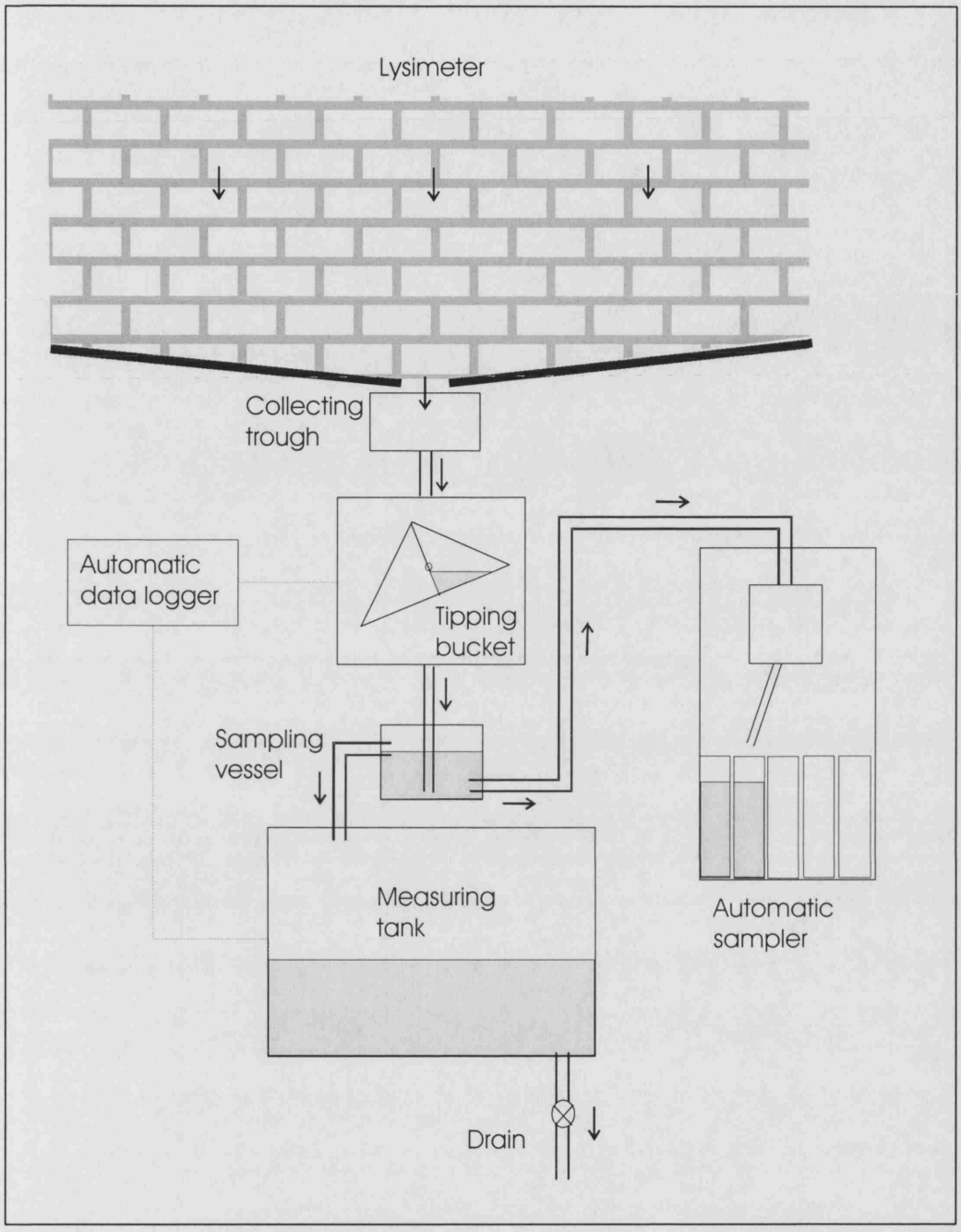

Figure 5-2 Schematic overview of the equipment used in the Fleam Dyke lysimeter pit.

The Fleam Dyke lysimeter has been classified as a category 2 confined space and is subject to specific health and safety requirements. Therefore a detailed risk assessment was formulated for this field work and a series of measures was taken to reduce the associated risks (Appendix IV).

5.4.3 Core profiles

Cores of soil and chalk were taken on the 4 × 4 m plot adjacent to the lysimeter to determine the vertical tracer distribution. Concurrently cores were taken on the same site away from the tracer-irrigated area to determine the tracer background concentrations on the site. No cores were taken from the lysimeter, as this monolith was to remain undisturbed to maintain the recharge measurements.

A first coring event to shallow depth took place on 10 May 2002. A manual soil-coring instrument was used, which drives a steel sleeve (86 mm internal diameter, 75 mm length) into the ground by means of a drop weight. Two cores were taken on the 4 × 4 m plot to a depth of maximum 40 cm (profiles IP1 and IP2, Figure 5-3) and one reference core was taken for background concentrations (profile R1, Figure 5-1). After collection the samples were kept inside their steel sleeves and were stored in zip-lock polythene bags at 4°C. Upon analysis each core was divided into two sub-samples in the laboratory. Because the steel sleeve provides an undisturbed sample of known volume, this procedure allows the analysis of the bulk dry density. A similar shallow coring event took place on 23 October 2002 (profiles IP6 and IP7, Figure 5-3).

Deeper cores, down to a maximum depth of 3.4 metres, were drilled during coring sessions on 2-4 July 2002 (profiles IP3, IP4 and IP5, Figure 5-3, and two reference profiles R2 and R3, Figure 5-1), 13 December 2002 (profile IP8, Figure 5-3) and 21-22 May 2003 (profiles IP9, IP10 and IP11, Figure 5-3). A gasoline-powered percussion gouge was used. This consists of a percussion hammer that drives a gouge auger (also called window sampler) with a hardened cutting head into the ground (COBRA drill, Eijkelkamp Agrisearch Equipment). The augers used were 1 metre long and ranged in diameter from 7 cm for the upper core to 3 cm for the deepest core. After drilling, the augers were extracted manually by levering with a mechanical rod puller; if manual extraction was not possible, then a system with two 2-tonne hydraulic car jacks was used. After extraction the core was inspected visually for texture, colour and stratification. Finally the core was cut up in sections of between 5 and 10 cm length and each sub-sample was sealed in a zip-lock polythene bag and stored at 4°C prior to analysis.

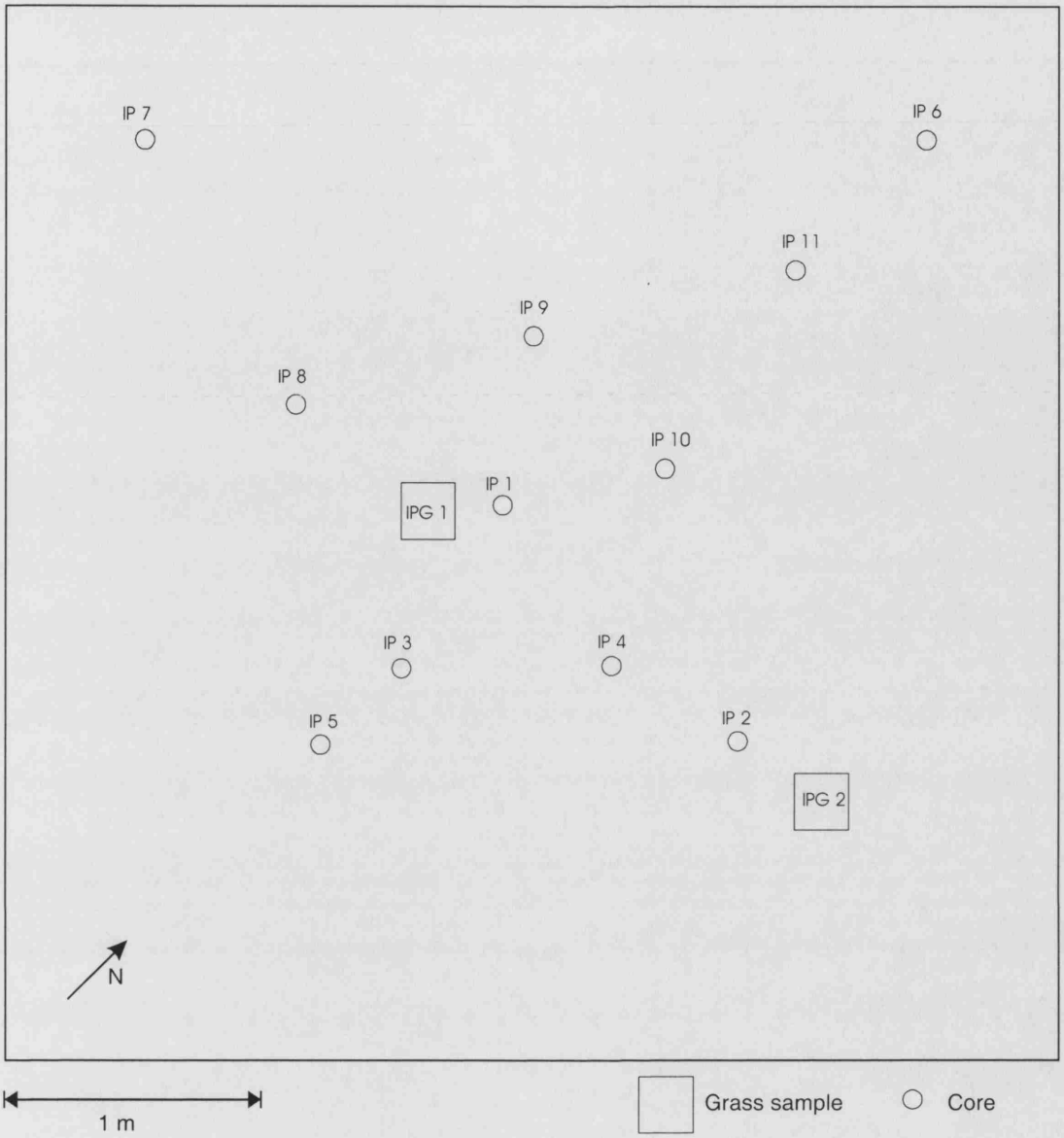

Figure 5-3 Location of sampling points on the 4 × 4 m plot at the Fleam Dyke site.

The maximum depth that could be reached with the percussion gouge varied between 2 and 3.4 metres. Hard bands in the chalk profile prevented the augers from penetrating any deeper, and made mechanical extraction of the augers very difficult. Other coring methods are available that are more suitable. Notably, dry percussion drilling and air-flush or water-flush rotary drilling are commonly used in the Chalk. Both methods are however considerably more expensive; hence budgetary restrictions limited the choice to the percussion gouge used in this project. Because of the slow nature of the unsaturated solute transport, the shallow depths that were reached were considered satisfactory.

5.4.4 Grass

Together with soil and chalk coring, samples were taken of the grass to determine the plant tracer uptake. For each grass sample, an area of 20 × 20 cm was marked out and all aboveground plant material was cut off, sealed in a zip-lock polythene bag and stored at 4°C prior to analysis. Additionally the root system was collected from the upper 20 cm soil layer. The whole root system was packed in a polythene bag after roughly shaking off the soil in the field, and further separation of the roots was done in the laboratory prior to analysis. Grass samples were only taken on 10 May 2002 (samples IPG1 and IPG2, Figure 5-3 and 2 reference samples for background). On 13 May 2002, the grass on the whole Fleam Dyke site, including the lysimeter, was mown by Cambridge Water Company. The plant height is an important parameter driving evapotranspiration, and mowing of the grass was considered favourable as it keeps the grass length constant. The mown grass was disposed off-site, and this inevitably removed some tracer out of the system. Leaving the mown grass in situ would allow re-mobilization of tracer from decayed plant material, which complicates the tracer input function. Rather, disposal of the mown grass assured that all of the tracer taken up by the grass remained unavailable in the unsaturated zone.

5.5 Physical profile characterization

5.5.1 Stratification

The core profiles taken with the percussion gouge allowed a qualitative description of the stratification in the upper metres. The profiles generally showed a thin topsoil with a sharp transition to weathered chalk, grading into harder, unweathered chalk underneath (Figure 5-4). The depth of the topsoil varied between 20 and 28 cm. The weathered chalk consisted of rubbly, soft chalk material, with a mixed appearance. Some of the weathered chalk was white to off-white, whereas other sections had a deep-brown, earthy colour. Biostratigraphy of the chalk samples suggested that they were belonging to the Plenus Marls (see Appendix II). This lithostratigraphical unit consists of alternations of more argillaceous and less argillaceous chalks, which weather differently and might have caused the coloured bands in the profiles.

Alternatively, the brown colour may be caused by leaching of soil material, or by staining related to iron or manganese oxides. When wet, the weathered chalk took on a paste-like consistency. The unweathered chalk underneath was more hard and robust, with a white appearance. Because the coring technique provided partly crushed core samples, identification of fractures was generally not possible.

Figure 5-4 Core profile (100 cm length, 7 cm i.d.) taken with a percussion gouge at the Fleam Dyke research site.

Comparison of profiles shows little consistency in the extent and stratification of the weathered chalk (Figure 5-5). Combining Figure 5-3 and Figure 5-5 reveals that even at the metre-scale the stratification exhibits high variations. This may be an indication of the presence of a fault, causing considerable heterogeneity even at such small scale. The irregularity of the stratification may also be associated with glacial weathering. When glacial activity causes cracks in the chalk to be filled up with ice, later disappearance of the ice can create irregular wedge-shaped patterns of weathered

chalk, as sometimes observed in chalk quarries (P.F. Rawson, personal communication).

The total thickness of the weathered chalk varied between 0 and 150 cm. This corresponds to the work of Foster and Bath (1983), who published data of the acid-insoluble residue, which is considered to be an indication of the amount of quartz and clay minerals. They reported values around 10% for layers above 150 cm depth, and values smaller than 5% for layers below 150 cm depth.

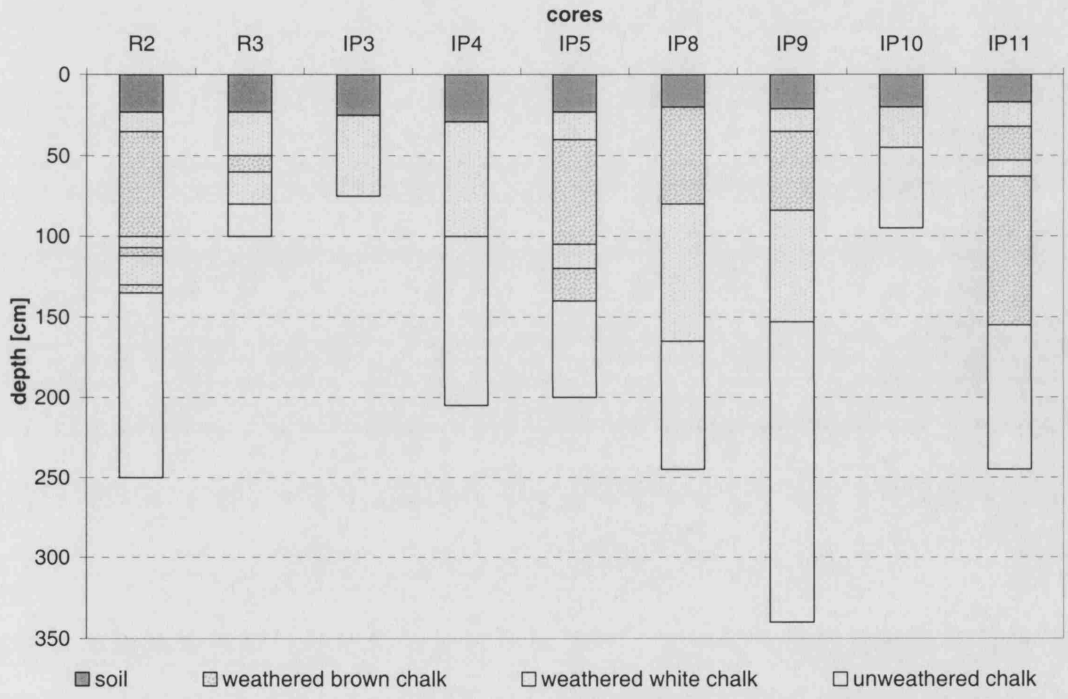

Figure 5-5 Basic stratification of cores taken at the Fleam Dyke research site (two reference cores and seven cores taken from the 4 × 4 m plot).

5.5.2 Bulk dry density, water content, porosity and total organic carbon

Methodology

The undisturbed wet soil samples from the observation pit (section 5.4.1) were dried in the oven at 105°C for 12 hours. Their mass was weighed before and after drying.

Combining these figures with the volume of the cylinders resulted in an estimate of bulk dry density, gravimetric water content and volumetric water content. The same procedure was followed for the undisturbed soil samples from cores IP1 and IP2.

The chalk samples collected from the coring events (section 5.4.3) were dried equally in the oven at 105°C for 12 hours, and from their wet and dry weight the gravimetric water content was calculated. In addition, a measurement was made of the bulk dry density and of the porosity using the liquid saturation method. This involved cutting a small cylinder (37.5 mm diameter and 35 mm length) out of a lump of chalk collected from the observation pit (section 5.4.1), and thoroughly drying it at 70°C for 24 hours. After recording its dry weight, the sample was submerged in water under vacuum for 24 hours, allowing the sample to approach saturation. Subsequently the wet sample was quickly patted with tissue paper to remove excess water and weighed. Combining these figures with the volume of the cylinder resulted in the calculation of bulk dry density and porosity. The porosity measured is an effective or interconnected porosity and not a total porosity.

The total organic carbon content was measured for selected dried samples, using a carbon/sulfur determinator (LECO SC125). Dried samples were first treated with 10% HCl to remove the inorganic carbon fraction (carbonates). The treated samples were dried again at 40°C, and a sub-sample of 750 mg was then heated in a ceramic cup to 1000°C in an atmosphere of pure oxygen, to convert all organic matter to CO_2 and occasional CO. Any CO produced was then further oxidized to CO_2 by catalytic conversion with platinum. Finally the CO_2 gas was measured by infrared detection.

Results

The bulk dry density results of the soil show a gradual increase with depth of around 1 g/cm^3 near the surface to around 1.25 g/cm^3 at the bottom of the soil profile (Table 5-2). This difference may be partly explained by the decreasing presence of grass roots with depth, as reflected by the total organic carbon content (Table 5-3). Table 5-2 also shows results of bulk dry density analyses carried out on chalk samples from Fleam Dyke by the British Geological Survey in the 1980s. They show a band of

denser chalk (2.00 g/cm^3) between 1 m and 1.60 m, underlain by lighter chalk (1.55 g/cm^3). The matrix of the weathered chalk (i.e. an individual block of chalk embedded in the weathered chalk) had an intermediate bulk dry density of 1.62 g/cm^3. The weathered chalk showed a low total organic carbon content of 0.25%, whereas the total organic carbon content of the unweathered chalk underneath was only 0.14%. Such low organic carbon contents offer limited sorption capacity, leading to little retardation in the Chalk for solutes that are normally prone to sorption.

Table 5-2 Bulk dry density of selected layers at the Fleam Dyke research site

Medium	Depth [cm]	Bulk dry density [g/cm^3]
Soil	0 - 6	0.98 [(1)]
Soil	6 - 12	1.17 [(1)]
Soil	12 - 18	1.21 [(1)]
Soil	18 - 24	1.24 [(1)]
Weathered chalk matrix	50	1.62 [(2)]
Unweathered chalk matrix	100 - 160	2.00 [(3)]
Unweathered chalk matrix	180 - 300	1.55 [(3)]

[(1)] measured by drying of undisturbed samples; values shown are averages of samples taken from the observation pit and from profiles IP1 and IP2

[(2)] measured by drying a cylinder cut from a sample collected from the observation pit

[(3)] data courtesy of the British Geological Survey

Table 5-3 Total organic carbon content of selected samples taken from core profile IP5; values shown are averages of triplicate measurements.

Medium	Depth [cm]	Total organic carbon [%]
Soil	10	3.00
Soil	17	2.48
Weathered chalk	80	0.25
Unweathered Chalk	190	0.14

The evolution of the water content at the Fleam Dyke site is shown in Figure 5-6. Values shown in the figure are averages of two or three profiles, except for December 2002 when only one core profile was drilled. The results are expressed as gravimetric water content and can be converted to volumetric water content by multiplying by the bulk dry density of the medium. However, because the vertical variation of bulk dry density in the chalk is not known with great resolution, the original gravimetric values are shown in the figure. On each sampling occasion the top 10 cm of soil was wetter than the underlying profile. As can be expected, the overall profile was wettest in winter (December 2002) and driest in late spring and summer (July 2002 and May 2003). Yearly variations of up to 0.15 gravimetric water content were observed in the topsoil, with moderate variations in the weathered chalk and variations of only around 0.02 gravimetric water content for the deeper chalk. This seems to support the hypothesis that the chalk matrix remains largely saturated throughout the year, even in the unsaturated zone.

Application of the liquid saturation technique on a cylinder of chalk recovered from the weathered chalk at 50 cm depth revealed a matrix porosity of 36.5%. Porosity values for deeper layers at the Fleam Dyke site had been published earlier by Foster and Bath (1983). They reported porosities between 31 and 36% for the chalk between 100 and 250 cm depth, increasing to around 42% for the chalk below 300 cm depth.

5.5.3 Particle size analysis

The particle size distribution was determined mechanically for two samples of the upper soil layer, collected from the observation pit (section 5.4.1). Wet and dry sieving was used for particles down to 45 μm, whereas for smaller particles Andreasen's apparatus was used, which is a sedimentation method (Bowles, 1992; Gee and Bauder, 1986). The methodology is described in detail in Appendix V.

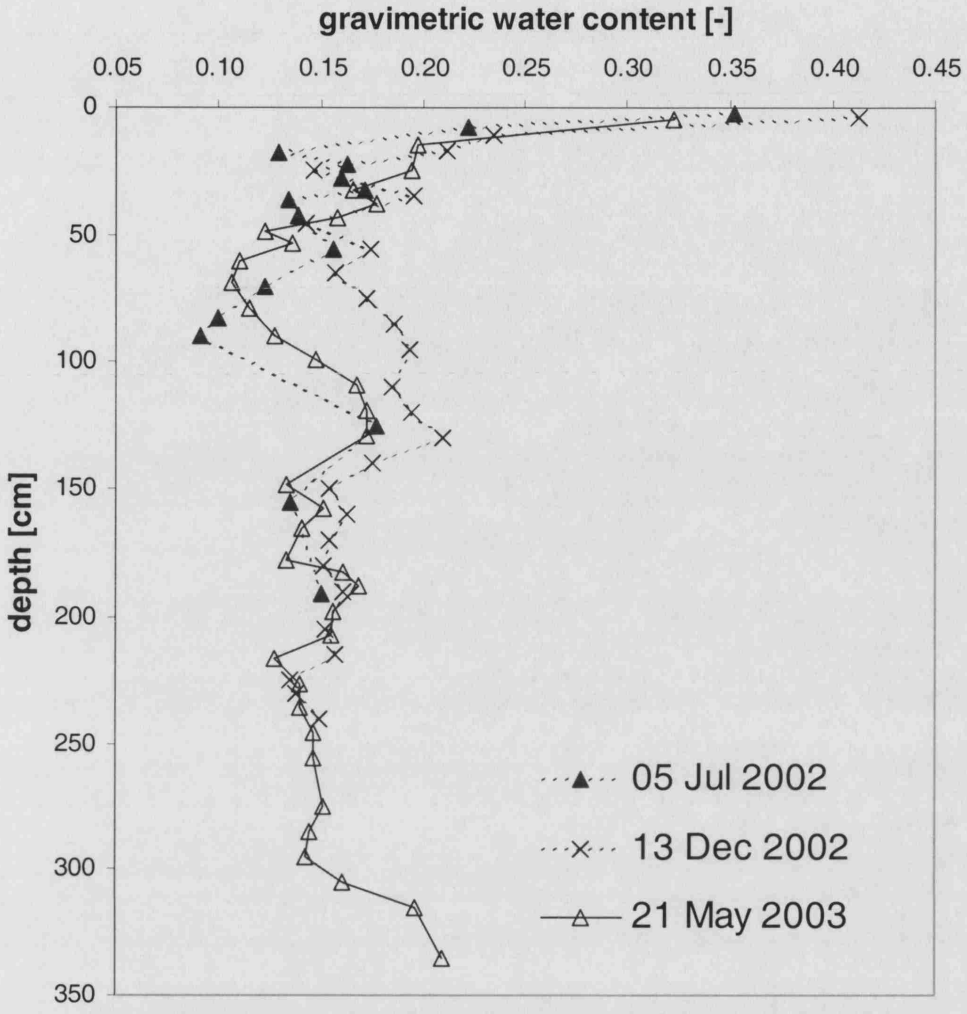

Figure 5-6 Gravimetric water contents measured from samples collected from the 4×4 m plot at the Fleam Dyke research site.

The resulting cumulative particle size distributions for two soil samples from the Fleam Dyke site are shown in Figure 5-7. The distribution curves indicate a well-graded soil, with a d_{50} of 43 μm for the soil between 0 and 7 cm depth, and a d_{50} of 28 μm between 7 and 14 cm depth. According to the texture classification scheme for England and Wales, based on the percentages of sand, silt and clay, the soil is a medium sandy silt loam. On the soil map of the Soil Survey of England and Wales (1983), the topsoil at the Fleam Dyke site has been classified as belonging to the Swaffham Prior association, indicating a loamy calcareous soil.

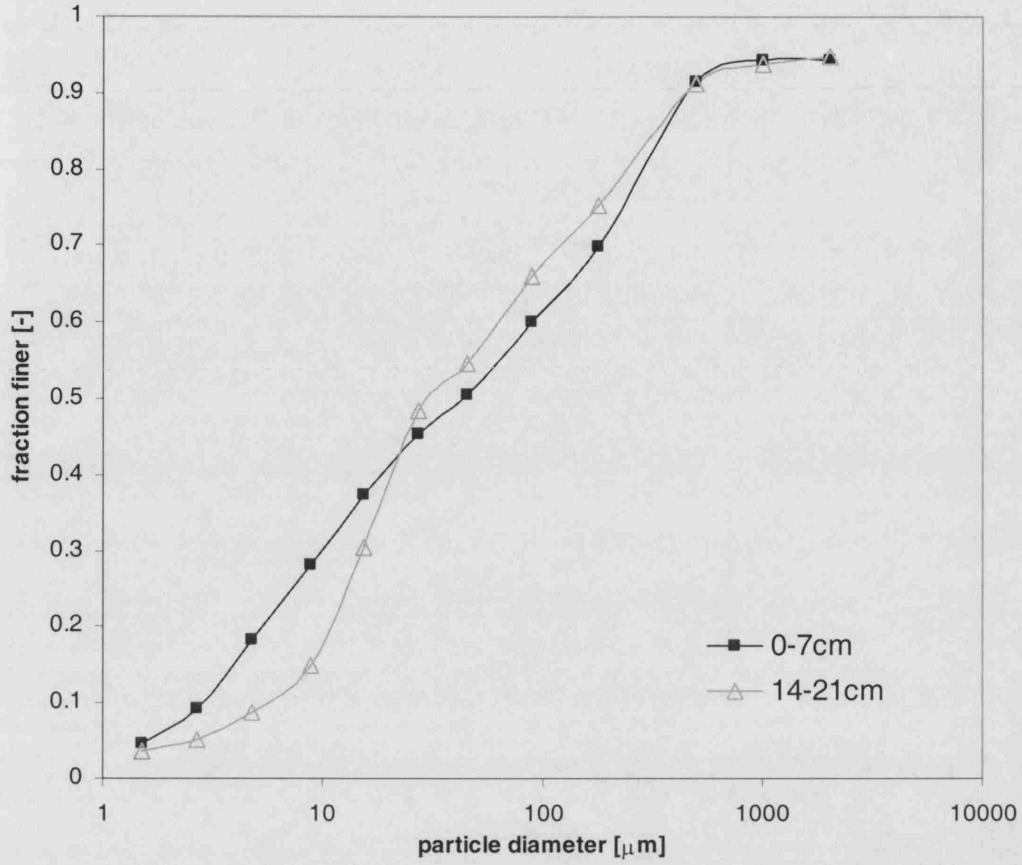

Figure 5-7 Cumulative particle size distribution for two soil samples from the Fleam Dyke research site.

5.5.4 Field-saturated hydraulic conductivity

Methodology

The field-saturated hydraulic conductivity of the soil and the weathered chalk was measured in-situ with a Guelph permeameter (Figure 5-8). This is a constant head permeameter that operates in accordance with the principle of the Mariotte bottle (Soilmoisture Equipment Corp., 1986). The method involves the maintenance of a constant head of water in a cylindrical well, and the measurement of the steady-state rate of water flow from the well into the locally saturated soil around.

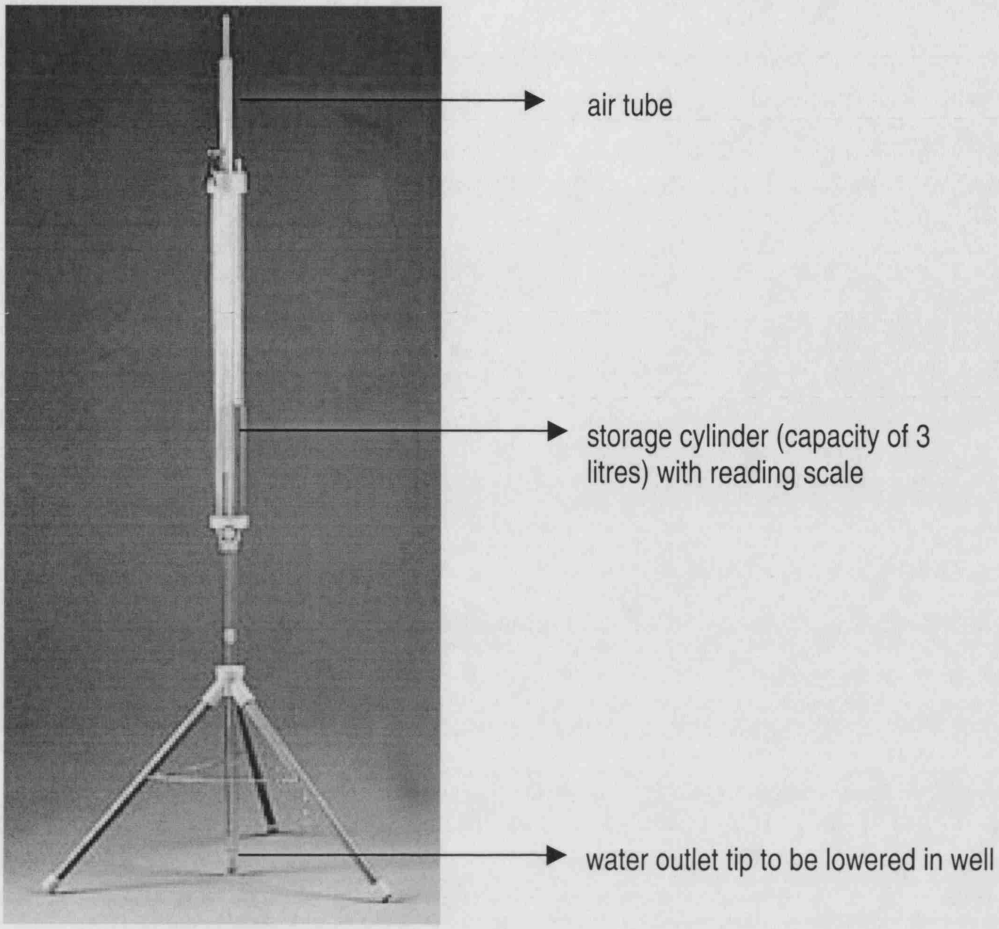

Figure 5-8 Guelph permeameter for the measurement of the field-saturated hydraulic conductivity (image taken from http://www.qcqa.com/category_b.asp?subPID=67).

At the Fleam Dyke research site, six permeameter measurements were carried out (three of the soil and three of the weathered chalk; Figure 5-9). For the soil measurements, a well was bored with a hand auger, reaching a depth of 12.5 cm and a diameter of 6 cm. The same procedure was used for the weathered chalk, but this time with a well depth of 55 cm. The well hole was brushed with a stiff cylindrical brush to remove any smearing of the hole walls caused by the auger. The water outlet tip of the permeameter was lowered into the well and a constant well head height of either 5 or 10 cm was established. Water from the permeameter slowly flowed into the well hole and penetrated into the soil. After a while, a saturated bubble was formed around the well and the outflow of water from the well reached a constant rate. The rate of discharge of water from the storage cylinder into the well hole was read at regular time intervals, until at least three consecutive readings gave the same

rate of discharge (this usually took between 15 to 30 minutes). These data together with the diameter of the well hole and the level of the water in the well were used to determine the field-saturated hydraulic conductivity of the soil. This field-saturated hydraulic conductivity refers to soil containing entrapped air, and can be slightly lower than the truly saturated hydraulic conductivity. However, the field-saturated hydraulic conductivity is generally seen as a more appropriate value for unsaturated zone investigations, as positive pressure heads do not persist in unsaturated conditions long enough for entrapped air to dissolve.

Results

Table 5-4 shows the results of the permeameter measurements on the soil and the weathered chalk. For the soil, the results were very consistent, showing an average field-saturated hydraulic conductivity of 266 mm/d. This is in accordance with values found in literature for loamy soils. For the weathered chalk, the field-saturated hydraulic conductivity was one order of magnitude lower, at an average of 26 mm/d. Also, the results for the weathered chalk showed more variability, indicating considerable spatial heterogeneity in hydraulic properties. This heterogeneity was already apparent in Figure 5-5, which showed the variability in stratification of the weathered chalk within a horizontal scale of a few metres. The field-saturated hydraulic conductivity values measured on the weathered chalk with the permeameter were much lower than the maximum values reported by Wellings and Cooper (1983). They measured values up to 600 mm/d, by using the instantaneous profile technique for the weathered chalk at 60 cm depth (Figure 4-11). The reason for this difference may be the scale of the measuring method. The permeameter creates a saturated bubble of limited size around the well hole, whereas the instantaneous profile technique applies irrigation over an area of at least 10 m^2. Hence the instantaneous profile technique is more likely to include fast-flow pathways through the weathered chalk, such as "macropores" separating the chalk pebbles, fractures or zones of increased permeability. This could explain why a higher hydraulic conductivity is measured by the instantaneous profile technique than by the permeameter.

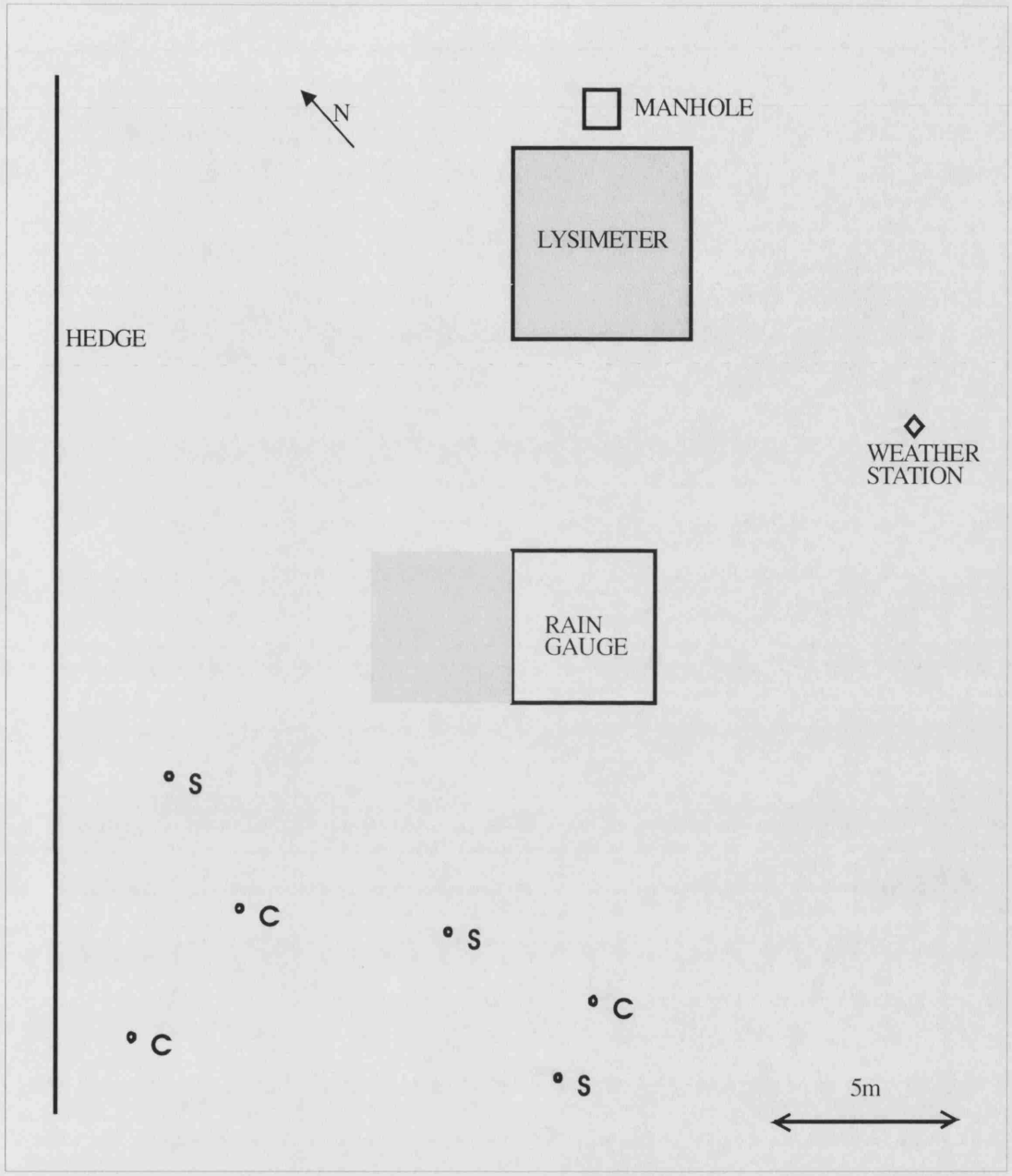

Figure 5-9 Location of permeameter measurements on the Fleam Dyke research site (C stands for measurement on weathered chalk and S stands for measurement on the soil).

Table 5-4 Results of measurements of the field-saturated hydraulic conductivity with a permeameter at the Fleam Dyke research site.

Medium	K_s [mm/d]
Soil	288
Soil	223
soil	286
Weathered chalk	51.6
Weathered chalk	4.56
Weathered chalk	22.6

5.6 Tracer analysis

5.6.1 Bromide

5.6.1.1 Bromide extraction

Careful consideration was given to how to extract the bromide from the samples of soil, chalk and plant material. Several methods have been put forward in literature. Edmunds & Bath (1976) described a squeezing method, where the interstitial water is extracted using hydraulic or gas operated squeezers. However this seems mainly suitable for unconsolidated sediments, and may not be effective for chalk samples. An alternative is extraction by centrifugation, using special liner assemblies to support the rock samples by removable perforated plates. At practically applied centrifugation speeds, the pore water recovery is not complete, and it was demonstrated on samples of English chalk that the centrifugation process may result in fractionation of ion concentrations (Edmunds and Bath, 1976). Still, the method has found reasonable application and has been used in unsaturated tracer studies on Chalk by Barraclough et al. (1994) and by Ward et al. (2001). The most common method of ion extraction, however, is simply by equilibration in water as the extracting agent (= elutriation). This has been successfully applied to soil samples (e.g. Butters et al., 1989; Germann et al., 1984; Larsson and Jarvis, 1999; Ritsema and

Dekker, 1998; Smith et al., 1995), chalk samples (e.g. Besien et al., 2000; Nativ et al., 1995) and plant tissues (e.g. Bowman et al., 1997; Kung, 1990; Russo and Karmarkar, 1998). Bowman et al. (1997) confirmed that the method allows quantitative extraction of bromide from soils, and Russo and Karmarkar (1998) stated that extraction in water of plant tissues leads to unaltered concentrations of major ions. The method chosen for this study was the equilibration method in water.

Before extraction, the oven-dried soil samples were roughly pulverized with pestle and mortar to ensure maximum contact area. Similarly, the oven-dried chalk samples were crushed with a hammer into pieces of maximum 1 cm diameter. A sub-sample of around 10 g of soil or chalk was transferred to a 100 ml beaker with 50 ml of ultra-pure water and kept stirring for 15 hours. The suspension was then transferred to a centrifuge tube and centrifuged for 15 minutes at 1500 rpm. From there the centrifugate was filtered over a Whatman n°5 paper filter into a 100 ml flask, and the flask was filled up to volume with ultra-pure water.

The extraction method for the plant material was identical to the method used for soil and chalk, except for the preceding drying procedure, which was achieved by freeze-drying. The moist grass leaves and roots were weighed in a beaker and were then frozen. The frozen samples were transferred to the freeze drier, which establishes a temperature between –55 and -60°C under vacuum. This makes the frozen water sublime into water vapour, and this drying process makes the plants more brittle than conventional oven drying does. The dried material was then cut in centimetre-long pieces and roughly pulverised with pestle and mortar. A sub-sample of between 0.5 and 1 g of plant material was transferred to a 100 ml beaker with 50 ml of ultra-pure water and kept stirring for 15 hours. Finally the suspension was centrifuged and filtered equally as for the soil and chalk samples.

5.6.1.2 Bromide analysis

The bromide concentrations in the water extracts obtained from soil, chalk and plant samples were measured by ion chromatography. The same procedure was followed for the water samples collected at the lysimeter drainage.

Ion chromatography is a form of liquid chromatography that uses a column of ion-exchange resins to separate atomic or molecular ions based on their interaction with the resin. The anions are separated based on their affinity for the low capacity, strongly basic anion exchanger. Once separated, the anions pass through a chemical suppresser where they are converted into their highly conductive acid forms, while the eluent is converted into a weakly conductive acid. The separated anions are measured by conductivity and identified on the basis of their retention time as compared to standards. Finally the conductivity is converted to anion concentration based on calibration with standards.

A Dionex 2000i separator column (Dionex Corporation, 1983) was used with a carbonate-bicarbonate eluent as mobile phase (1.8 mM Na_2CO_3, 1.7 mM $NaHCO_3$). With a syringe, 5 ml of the water sample were injected through a 0.2 μm filter into the manual injection port. The retention time for bromide was approximately 2.6 minutes. A typical chromatogram is shown in Figure 5-10. For high bromide concentrations, occasionally the measured conductivity was beyond the calibration curve. In this case the water samples were diluted, and analysis was repeated until the conductivity was well within the appropriate range.

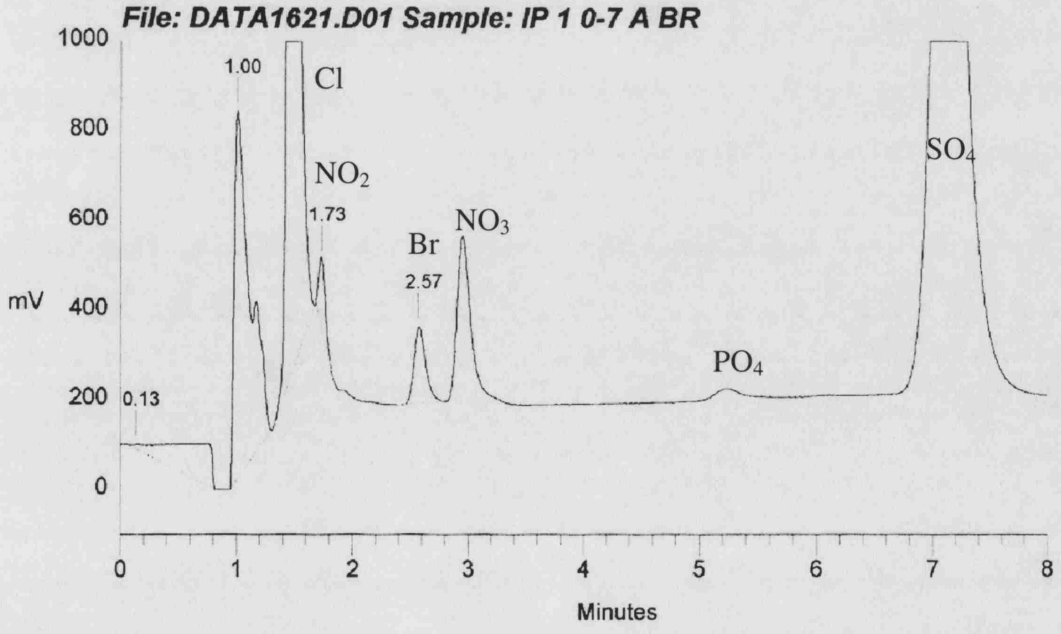

Figure 5-10 Typical chromatogram obtained after bromide analysis of a Fleam Dyke soil extract.

5.6.1.3 Bromide results

5.6.1.3.1 Bromide in the lysimeter drainage

The background level of bromide in the drainage from Fleam Dyke lysimeter was monitored regularly for two weeks prior to the tracer application. Concentrations were fairly constant, varying between 35 and 40 µg/l. This is at the lower end of data collected by Edmunds (1996), who reported values between 20 and 1140 µg/l for Chalk groundwater. Following the tracer application on 11 February 2002, the bromide concentration in the drainage remained at the same level, and remained like that during the rest of the recharge season (Figure 5-11). During the summer no data were available, as the lysimeter drainage ceased and no samples could be taken. When drainage started again in December 2002, sudden rises in bromide concentration were measured. This was initially attributed to the breakthrough of tracer in the lysimeter drainage. However, later it was noticed that the battery of the automatic water sampler had become faulty and overheated. As a result some of the water samples, which were arranged in a tray around the battery, became considerably warm as well. In addition, it was noticed that some of the sample bottles adjacent to the battery were only partially filled, instead of containing the standard 150 ml. This suggested that the sudden rises in bromide may not originate from bromide tracer, but may instead be caused by evaporation, leading to concentration of background bromide in the sample bottles.

On one sampling round the volumes of sample collected were recorded, and later it was shown that the sample bottles with the smallest volume had the highest bromide concentration. Correction factors were then calculated for each sample bottle, based on the proportion of the sample volume that had evaporated. These corrected data are also plotted in Figure 5-11, and it is shown that, by applying this correction, the concentrations are largely reduced back to background levels. A small number of higher concentrations remain in December 2002 and January 2003, but the correction factor is here highly uncertain because the volume of sample collected was not recorded. At the beginning of April 2003, the battery was replaced, and no further elevated bromide concentrations were recorded until the drainage ceased again in

May 2003. It can thus be concluded that, as the bromide concentration in the drainage water has remained constant, it is unlikely that any tracer bromide has migrated to the lysimeter drain.

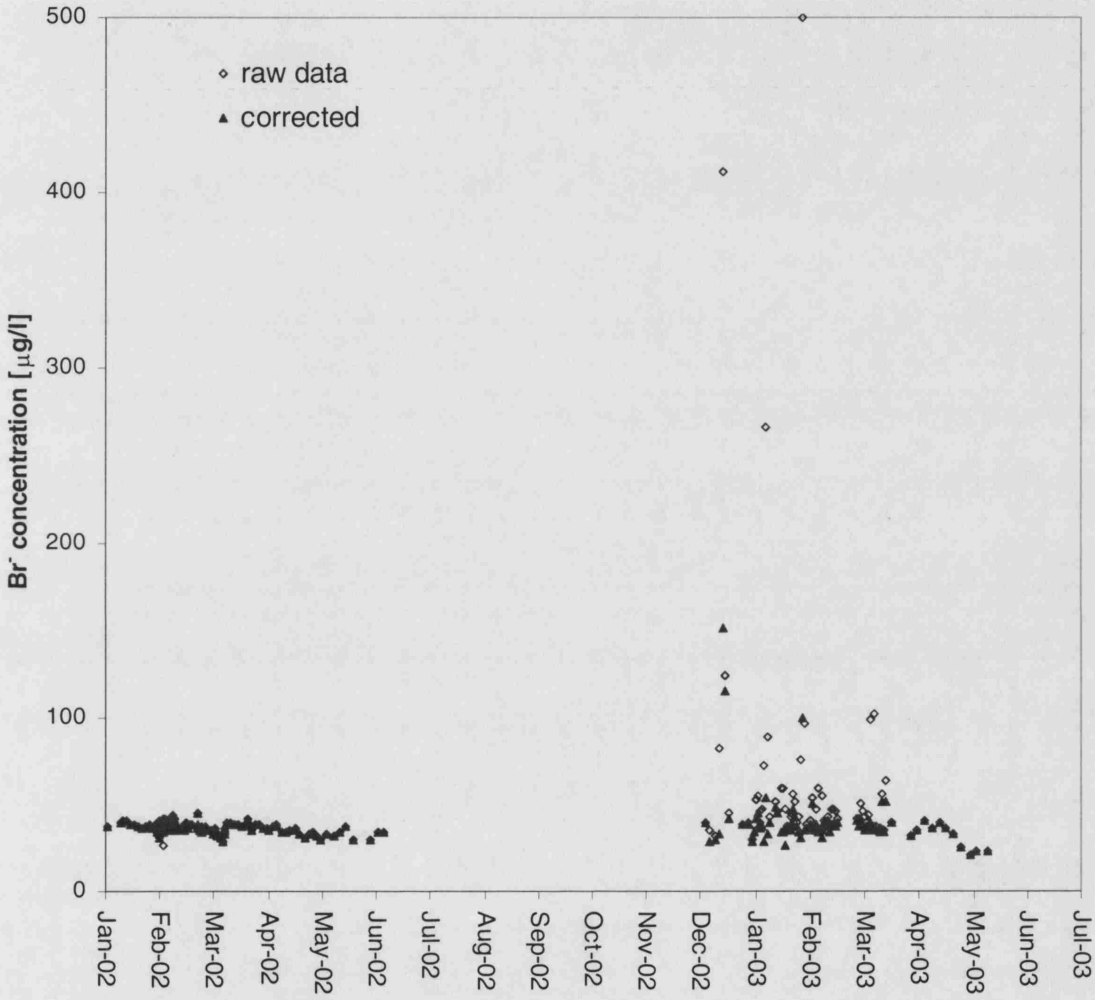

Figure 5-11 Bromide concentrations measured in drainage samples from Fleam Dyke lysimeter. In addition to the raw data, the figure shows corrected data that account for the concentration effect through evaporation of the samples.

5.6.1.3.2 Bromide in the core profiles

Bromide concentrations measured in the cores taken on the 4 × 4 m plot in May and July 2002 are shown in Figure 5-12 and Figure 5-13. The profiles show high bromide levels (up to 20,000 µg/l) in the soil layer, and lower concentrations (but still exceeding 2,000 µg/l) in the chalk underneath. Differences between profiles taken on the same date are apparent, suggesting lateral heterogeneity. Background bromide concentrations, measured on profiles taken on the Fleam Dyke research site outside of the tracer-irrigated area, are shown in Figure 5-14. Background concentrations typically exceeded 5,000 µg/l in the upper metre of the profile, and exceeded 2000 µg/l below. Moreover, the background concentrations were found to be highly variable between different profiles.

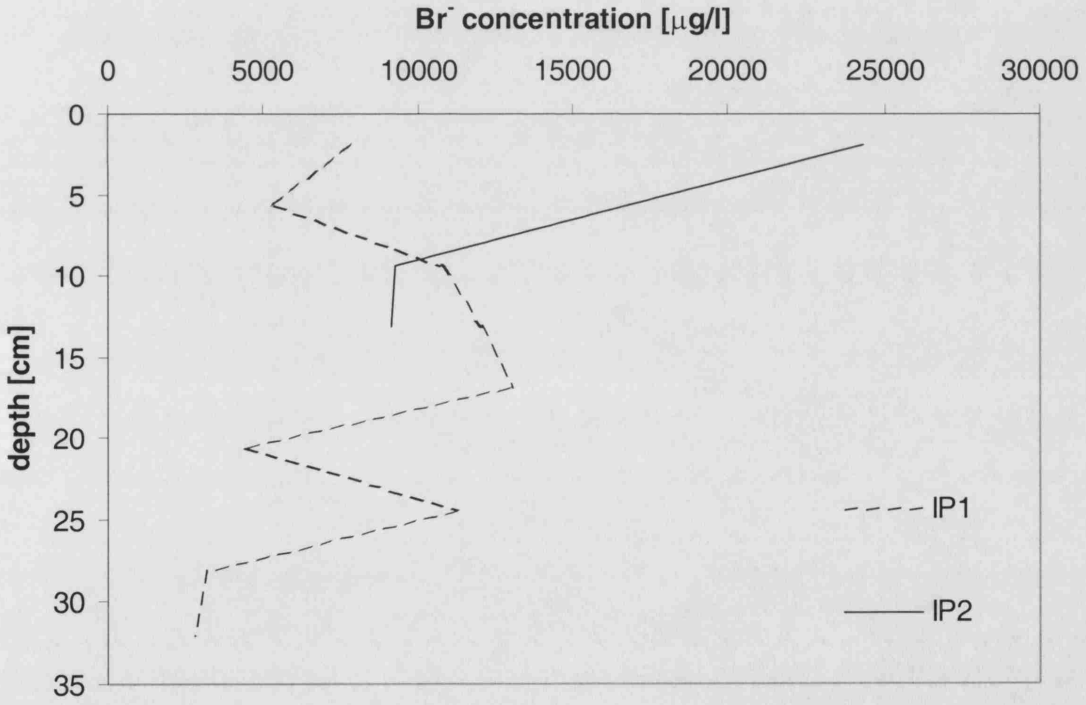

Figure 5-12 Bromide concentrations measured in two core profiles taken at the Fleam Dyke research site on 22 May 2002.

The high background bromide concentrations and their variability complicate the analysis of the bromide tracer migration. This is illustrated in Figure 5-15, which plots averages of profiles measured in May and July 2002 together with the average

background concentrations. The bromide level in the background profiles is of the same order of magnitude as the bromide level in the profiles taken from the tracer-irrigated plot. Below 40 cm depth, the average concentrations in the background profiles were even higher. The tracer bromide is thus masked by the background bromide, making any interpretation of the tracer bromide difficult.

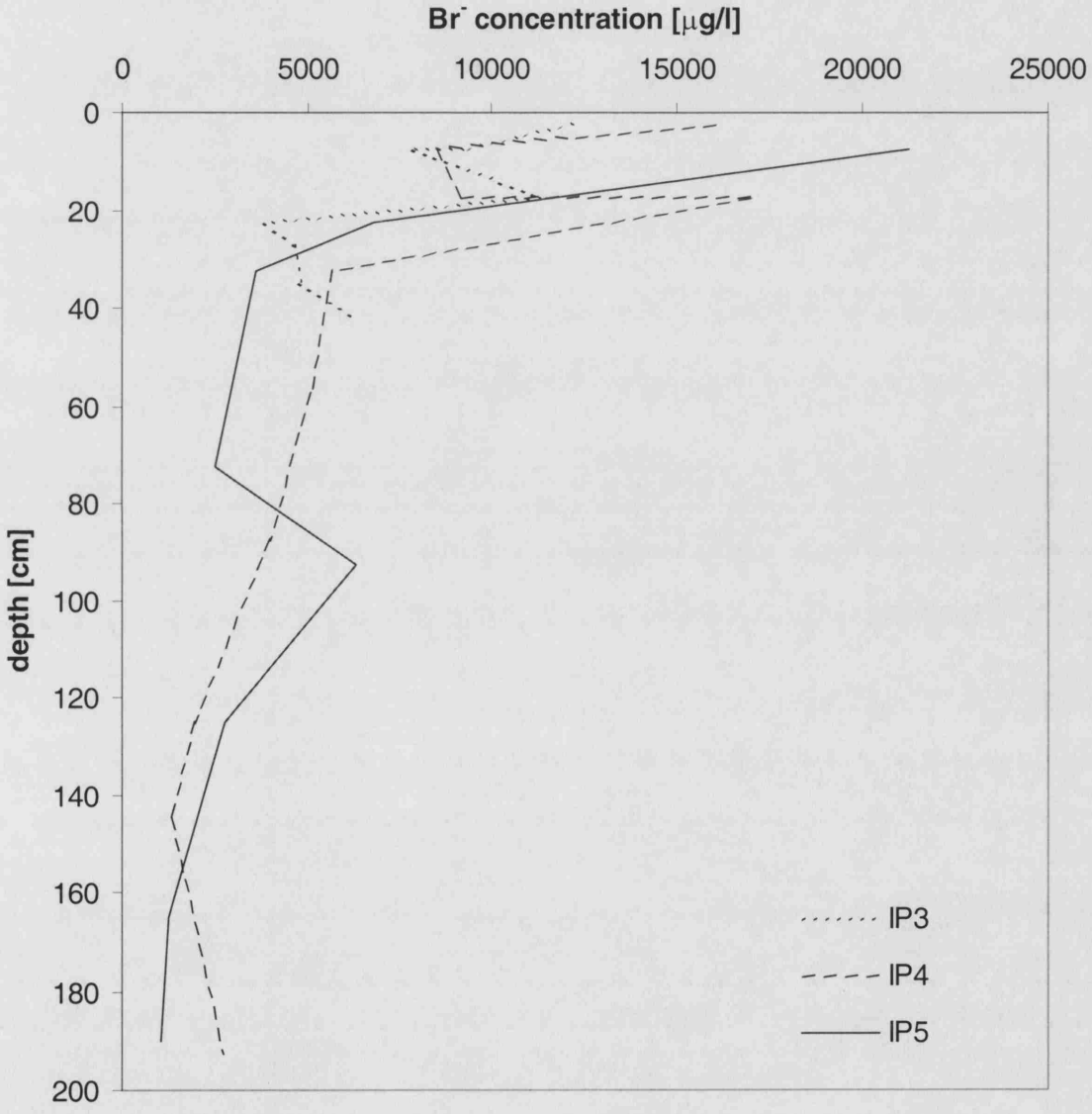

Figure 5-13 Bromide concentrations measured in three core profiles taken at the Fleam Dyke research site on 3 July 2002.

The average bromide recovery in the profiles was 0.70 g/m^2 in May 2002, and 2.03 g/m^2 in July 2002. Ignoring the background concentrations, this would lead to an average tracer recovery of 23.4% in May 2002 and 67.8% in July 2002. The low tracer recovery in May 2002 can be explained by the shallow core profiles down to 34 cm depth, with probably more tracer present deeper in the unsaturated chalk. Additional tracer is expected to be present inside the grass (see later section 5.6.1.3.4).

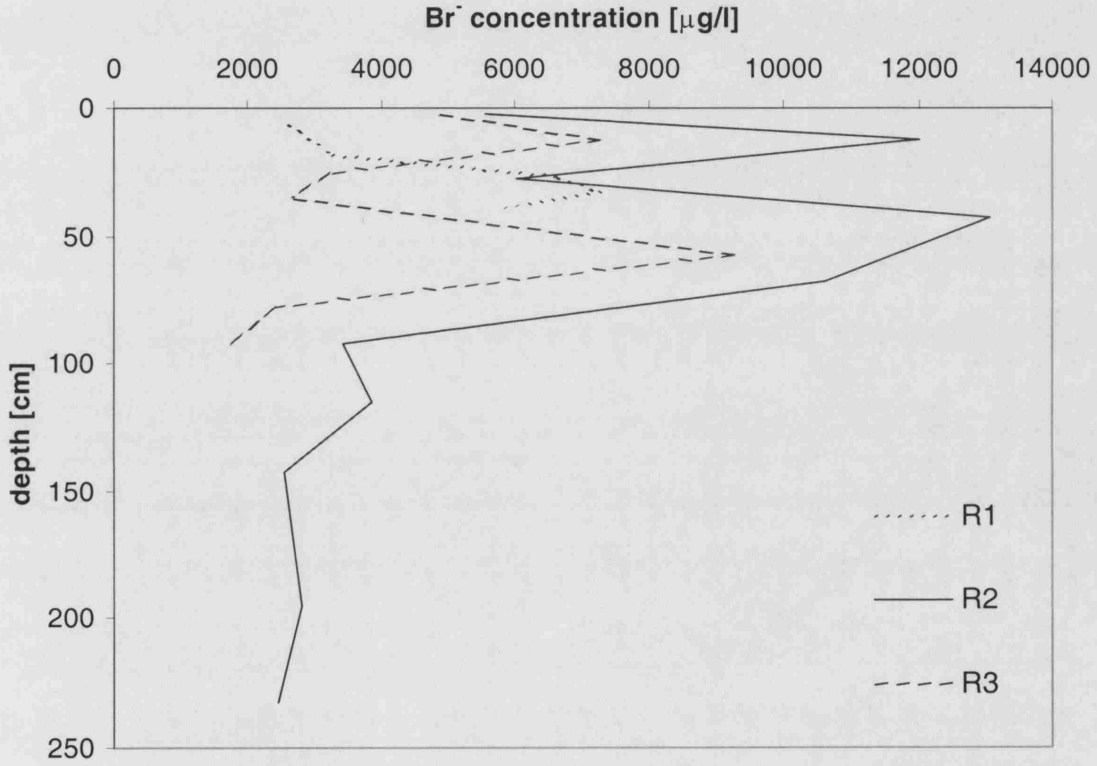

Figure 5-14 Background bromide concentrations measured in three reference core profiles taken at the Fleam Dyke research site (R1 drilled on 22 May 2002, R2 and R3 drilled on 3 July 2002).

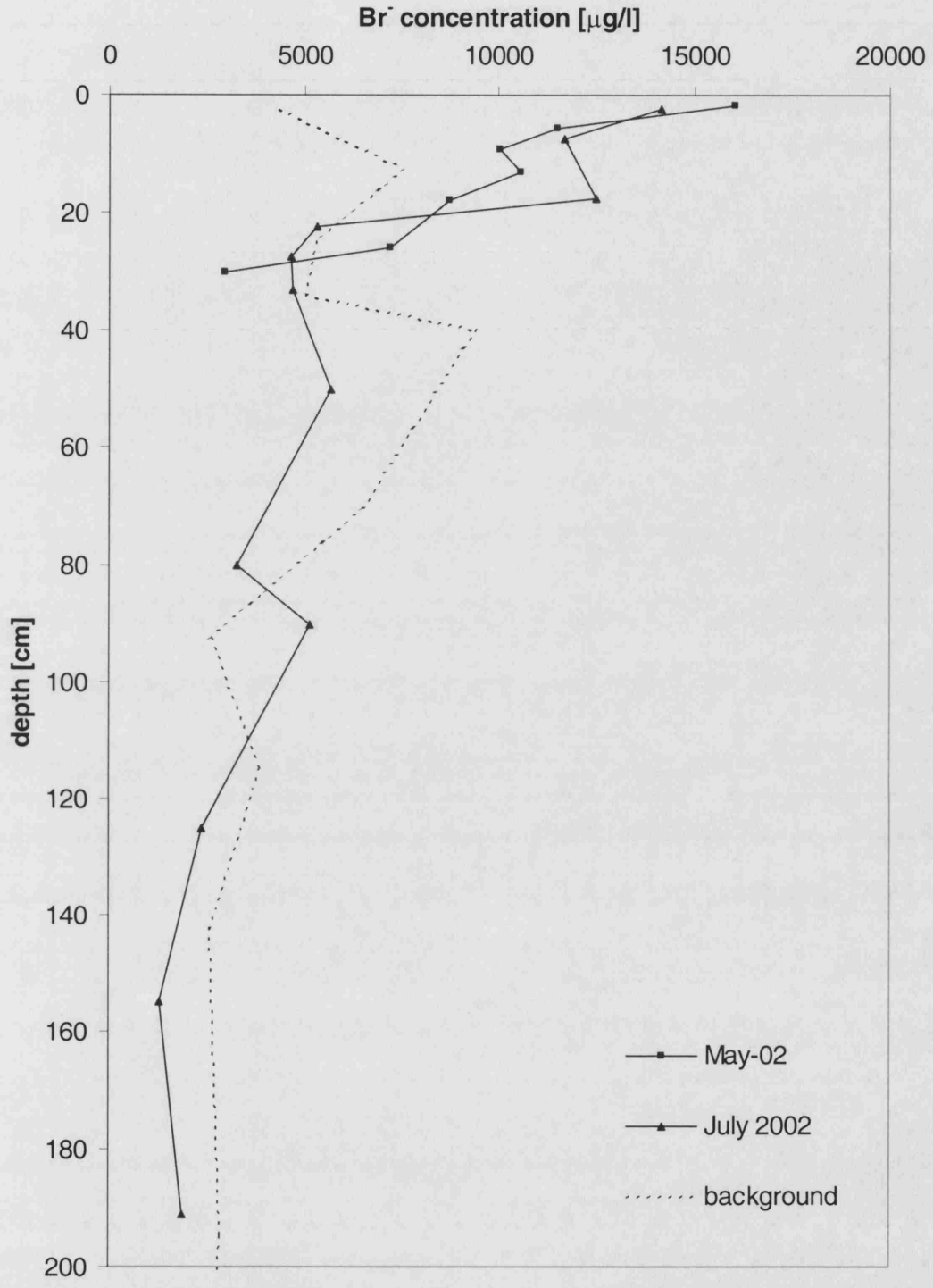

Figure 5-15 Average bromide profiles measured from cores taken at the Fleam Dyke research site.

The high bromide background concentrations were not anticipated. Bromide concentrations in the lysimeter drainage had been monitored prior to the tracer

application, and had been shown to be limited to the range of 35 to 40 µg/l. Bromide levels in rainfall had been measured on several occasions as well, and were always lower than 10 µg/l. For instance, a composite sample from the Fleam Dyke rain gauge over the period June 2002 - May 2003 had a bromide concentration of 4.3 µg/l (by comparison, Edmunds (1996) reported bromide concentrations in UK rainfall between 19 and 50 µg/l). There is thus a discrepancy of two to three orders of magnitude between the concentrations in the core profiles on the one hand (> 2000 µg/l), and the concentrations in the rain water and the lysimeter drainage on the other hand (< 50 µg/l). Three possibilities may be suggested to explain this difference:

1. *There is an error in the analysis method, and the actual background bromide concentrations in the core profiles are much lower.*

   Several steps were taken to test the validity of the chromatography method. It was suggested that the peak in the chromatogram around 2.6 minutes (Figure 5-10) may have been erroneously attributed to bromide, and may instead be caused by organic acids. This hypothesis was tested by placing several sub-samples in the furnace at 850°C for one hour. This effectively volatilizes all organic matter, and would thus remove the peak in the chromatogram if it were caused by organic acids. After cooling, the sub-samples were treated identically as sub-samples that had not undergone the furnace treatment. All sub-samples were stirred for 15 hours in ultra-pure water and were analyzed by ion chromatography. No difference in peak definition was observed between furnaced and non-furnaced samples, and the hypothesis of interference with organic acids was therefore rejected. Interference of any other ions at the same retention time as bromide is unknown in literature.

   Further independent testing of the ion chromatography analysis was attempted by measuring the bromide levels in the core extracts with a bromide specific electrode. Initial results indicated high bromide concentrations as well. However, the bromide specific electrode is primarily designed for concentrated bromide solutions. Therefore the measurements fell outside the optimal range for the electrode, and the results proved unreliable.

The main argument for the validity of the ion chromatography analysis method is that the core extracts, the drainage samples and the rainfall samples were all analyzed using the same methodology. The results indicated high concentrations in the core profiles and low concentrations in the lysimeter drainage and the rainfall, so the discrepancy cannot be due to the analysis method.

2. *There is an error in the extraction method, and the actual background bromide concentrations in the pore water are much lower.*

The extraction method by stirring in ultra-pure water was subjected to several tests. In a first approach, an independent extraction method was attempted, by wet grinding of the soil and chalk material with a micronizing mill (see Appendix VI). The resulting bromide concentrations were on average almost twice as high by the grinding method than by the stirring method. The additional bromide extracted by grinding is thought to originate from bromine that is incorporated inside the soil minerals, and which is not normally water-extractable. Hence the extraction method by stirring in ultra-pure water is likely to lead to a more representative value for the bromide concentration in the pore water. Nevertheless, the fact that both methods yielded high bromide concentrations confirms that there is a source of high bromide levels present in the soil.

Both extraction methods were subjected to a blank test, by following the whole extraction procedure using ultra-pure water without any soil sample (see Appendix VI). The results confirmed that the extraction method itself did not lead to bromide contamination.

For the extraction method by stirring in ultra-pure water, the influence of the extraction time was tested as well (see Appendix VI). Sub-samples of soil and chalk material were left stirring for times ranging from 20 minutes to 45 hours. The resulting bromide concentrations in the extracts showed no clear dependence on extraction times, and in general it appeared that 20 minutes was sufficient to attain diffusive equilibrium.

A review of the literature found that high bromide contents in soils may not be a rare phenomenon. Data are limited, but Flury and Papritz (1993) reported a typical natural bromide content in soils of 1 mg Br^- kg^{-1}. Similarly, Maw and Kempton (1982) stated that soils could contain water-extractable inorganic bromide up to 2 mg Br^- kg^{-1}. Yet it is not clear how much of this bromide is present in the pore water, or at what rate it would be released into the pore water. If one assumes that all the bromide reported is in solution in the pore water, and based on a gravimetric water content of 0.25, this would lead to a pore water concentration of 4000 and 8000 µg/l, respectively. This corresponds well with the bromide levels measured on the background cores at Fleam Dyke. However, it can be expected that the high bromide levels in soils as reported in literature mainly originate from bromide associated with the soil particles themselves. Adsorption to the soil minerals is unlikely, as bromide is generally regarded as conservative (Levy and Chambers, 1987). Alternatively, the bromide may be incorporated in the soil minerals themselves, or adsorbed to organic matter in the soil. Davis et al. (1998) reported sorption of up to 10% of the dissolved bromide on organic matter in the soil. As a result, the total bromide concentration in the soil may be larger than the bromide concentration in the pore water.

This finally leads to doubts about the validity of the bromide extraction method of stirring the soil for 15 hours in ultra-pure water. The stirring may lead to disintegration of soil particles and to extraction of bromide that was not initially present in the pore water. Hence the extraction method may yield a value for the total bromide in the soil, rather than for the bromide dissolved in the pore water. In the case of the extracts from the Fleam Dyke cores, this may suggest that the bromide concentrations in the pore water were actually much lower than the values measured. Yet high concentrations (> 2000 µg/l) were measured not only in the soil, but also in the chalk down to 2 metres depth. No data were found on bromide levels in unsaturated chalk, but the association of bromide with the $CaCO_3$ skeleton is highly unlikely, and the organic matter content of the chalk at Fleam Dyke was too low to function as a considerable adsorbant. Batch experiments with bromide on chalk samples have indicated a weak sorptive

behaviour (FRACFLOW, 1999), but the authors admitted that their results needed to be confirmed by more experiments.

To conclude, the extraction method by stirring in ultra-pure water could not be proved wrong, but uncertainty remains. As described above (section 5.6.1.1), the method is widely used and has a proven track record. As recommendations for the future, it is suggested that the method may be improved by shaking the sample rather than stirring, to minimize disintegration of the mineral particles. Finally, the method could be further tested against other methods, like extraction by squeezing or by centrifugation. However this work is outside the scope of the present study.

3. *The high bromide concentrations in the pore water are a recent phenomenon, which has not yet reached the depth of the lysimeter base.*

This would imply that the high bromide levels in the upper 2 metres originate from an exceptional bromide source that was only released over the last few years. The most likely anthropogenic sources of bromide are agricultural fertilizers or pesticides, e.g. 1,2-dibromoethane or methyl bromide (Flury and Papritz, 1993). The Fleam Dyke research site is adjacent to an agricultural field, and there is a possibility that application of fertilizers or pesticides on the field may lead to significant spreading of bromide onto the research site. However, inspection of the products used by the farmer over the last years revealed that none of them contained bromide. Any other anthropogenic sources of bromide seem very unlikely. A previous unreported tracer test using bromide may be possible. Yet high bromide levels were measured in all three background cores. The cores were drilled at a mutual distance of around 10 metres, so this rules out a very localized bromide input.

If there is indeed a bromide plume down to 2 metres depth that is gradually moving downwards, then this has strong implications for the transport mechanism of solutes through the chalk. Indeed, one would expect that, during high recharge rates when the fractures are active, some of the bromide would diffuse from the matrix into the fractures. Rapid transport through the fractures would then lead to

sudden rises in bromide concentration in the lysimeter drainage. However, the bromide level of the lysimeter drainage stayed very constant. An obvious explanation would be that the fractures always stay empty, but in section 4.3.3 it was shown that the hydraulic conductivity of the matrix alone is not sufficient to conduct higher recharge rates. A more likely explanation may be that the diffusive exchange between fractures and matrix is so fast that diffusive equilibrium is reached (Figure 3-9 a), or that the fractures are only active over short distances (Figure 3-9 d). On the whole, however, given that there is no likely source for the bromide, the uncertainty remains if the high bromide concentrations measured in the pore water are genuine.

5.6.1.3.3 Comparison with major anions

Apart from bromide, the concentrations of the major anions chloride, nitrate and sulphate were measured in water samples from Fleam Dyke. The same ion chromatography method was used, and the aim was to test if any anomalous concentrations occurred.

Table 5-5 shows averages of anion concentrations measured in rainfall, unsaturated pore water and lysimeter drainage at the Fleam Dyke site. A detailed profile of the anion concentrations measured in water extracts of core profile IP1 is also shown in Figure 5-16. Maximum concentrations of chloride, nitrate and sulphate measured in the topsoil were 275 mg/l, 60 mg/l and 370 mg/l, respectively. A nationwide survey of major anion concentrations in the unsaturated zone had been carried out in the 1980s, and included the agricultural field adjacent to the Fleam Dyke lysimeter (Coleby et al., 1998). In comparison, the concentrations measured for profile IP 1 are relatively high, especially for sulphate. This is unexpected, given the fact that the Fleam Dyke lysimeter site is unfertilized grassland, compared to the adjacent fertilized field. The anion concentrations in the rainfall and the lysimeter drainage in Table 5-5 are much lower. Hence it appears that a similar paradox exists for the major anions as for bromide, although less pronounced: the concentrations in the unsaturated pore water are unexpectedly high, especially compared with the concentrations in rainfall and in the lysimeter drainage.

Table 5-5 Major anion concentrations for the Fleam Dyke site in samples of rainfall, unsaturated pore water and lysimeter drainage. All values shown are averages of three or four samples.

	Cl (mg/l)	NO_3 (mg/l)	SO_4 (mg/l)	Cl/Br (-)
Rainfall	2.7	4.1	7.4	447
Unsaturated pore water [1]	179.7	30.3	174.9	46
Lysimeter drainage	15.2	2.7	34.4	445

[1] concentrations shown are measurements from water extracted from the upper 35 cm of core profile IP1 (see Figure 5-16), except for the Cl/Br ratio, which was calculated with the average Br concentrations measured in the background profiles.

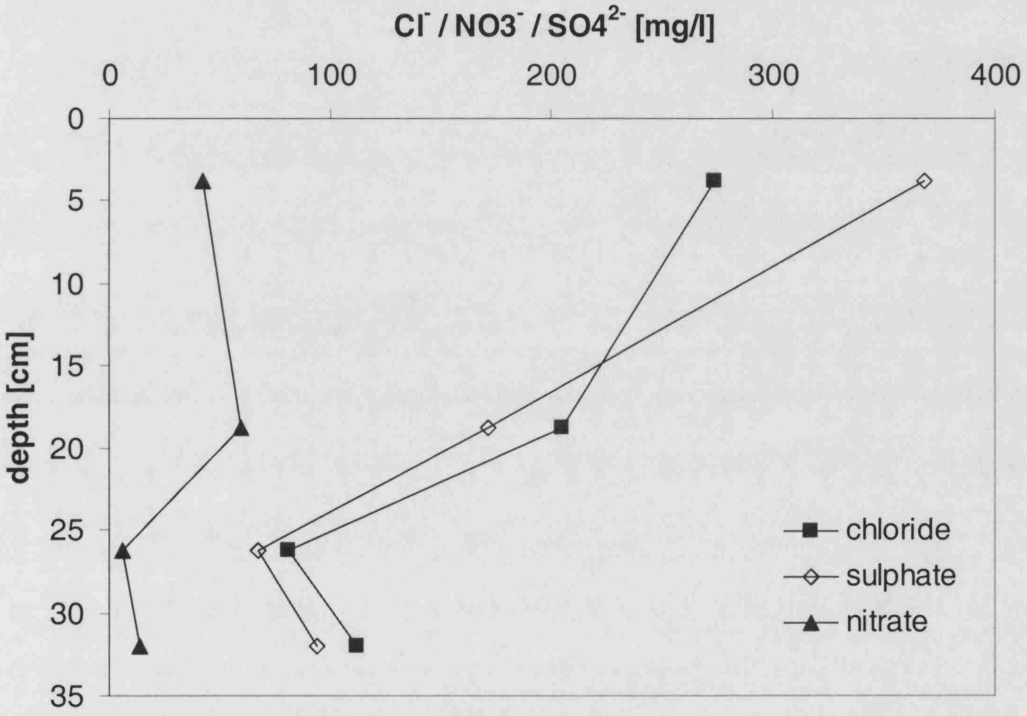

Figure 5-16 Concentrations of chloride, nitrate and sulphate measured in pore water from core profile IP1 taken at the Fleam Dyke research site on 22 May 2002.

Table 5-5 also shows the average Cl/Br ratios measured in the water samples. The Cl/Br ratios in the rainfall and in the lysimeter drainage are very similar, around 445. For rainfall, this value appears to be very high, caused by the low bromide concentrations (Davis et al. (1998) reported Cl/Br ratios in rain below 200 for the U.S.A.; Gerritse and George (1988) reported an average of 300 for Australian rain).

For the lysimeter drainage, the Cl/Br ratio of 445 is plausible, as Edmunds (1996) cited values between 220 and 500 for Chalk groundwater in the UK. The Cl/Br anomaly in Table 5-5 occurs once again for the unsaturated pore water, with a ratio of 46, which is one order of magnitude smaller than the ratios for the rainfall and the lysimeter drainage. A similar phenomenon has been observed by Gerritse and George (1988), who reported that the Cl/Br ratio decreased from 300 to 10 during infiltration of rainfall in an Australian soil. They explained their observation by the release of bromide by organic matter, which is enriched in bromide relative to chloride. This mechanism may partly explain the difference in the Cl/Br ratio between rainfall and the unsaturated pore water at Fleam Dyke. However, it cannot explain why the ratio increases again in the lysimeter drainage.

5.6.1.3.4 Bromide in the grass

The results of the bromide analysis of the grass extracts are shown in Table 5-6. High bromide contents were obtained from grass leaves and roots collected from the tracer-treated plot, showing the ability of the grass to take up bromide from the soil and concentrate it in its plant tissue. The bromide content in the plant material from the tracer-treated plot was two to three orders of magnitude higher than in the plant material from the background samples. This is in contrast with the bromide concentrations measured from the core profiles, where the concentrations in the tracer profiles were of the same order of magnitude as the background concentrations. It indicates that there was clearly a difference between the tracer-treated plot and the background sites in availability of bromide for plant water uptake. Where tracer had been applied, large amounts of bromide could be taken up by the grass, compared to only a small fraction of this at the background sites. This suggests that the majority of the bromide measured in the soil from the background cores may actually not be available for plant water uptake. This supports the hypothesis described above, that the high bromide background measured from the cores might not reflect the pore water concentrations, but might rather originate from bromide associated with the soil particles.

Table 5-6 Bromide concentrations and recovery in samples of grass leaves and roots taken at the Fleam Dyke research site on 10 May 2002. All values shown are averages of two samples.

	Background	Tracer-treated plot
Br^- content per dry mass of grass leaves [µg/g]	3	2127
Br^- content per dry mass of grass roots [µg/g]	2	407
Dry mass of grass leaves per unit area [g/m^2]	n/a	318
Dry mass of grass roots per unit area [g/m^2]	n/a	321
Br^- mass in grass leaves per unit area [g/m^2]	n/a	0.662
Br- mass in grass roots per unit area [g/m^2]	n/a	0.131
Br^- tracer recovery in grass leaves [%]	n/a	22.1
Br^- tracer recovery in grass roots [%]	n/a	4.4

Table 5-6 further shows the total mass of bromide per unit area recovered from the plant material. The majority of the bromide is stored in the above-ground plant material (grass leaves), rather than in the grass roots. In total, of the 3 g m^{-2} of bromide tracer applied 3 months earlier, about 26% was recovered from the grass.

5.6.1.3.5 Conclusion

Two problems were encountered with the bromide tracer, both complicating the analysis of the tracer transport. First, the samples from the lysimeter drainage had been subject to considerable evaporation due to a faulty battery. What was initially observed as tracer breakthrough, was later shown to be due to evaporative enrichment of the tracer in the sample bottle. After correction, it was concluded that no tracer had been detected in the lysimeter drainage.

A second problem was encountered with the bromide concentrations measured in the background profiles. The extracted pore water from these background profiles showed bromide levels up to 12 mg/l, which masked the bromide tracer in the other core profiles. The bromide background was higher than anticipated, and several possible explanations were investigated. No flaw could be found in the bromide

analysis method, and there was no likely secondary source of bromide. A more plausible explanation could be a flaw in the extraction technique, even though the procedures used were standard methods. The elutriation method by stirring in distilled water might bring bromide in solution that was not originally present in the pore water. Two further observations supported this hypothesis. First, elevated concentrations in the unsaturated pore water were also found for major anions. Second, bromide contents in grass leaves were low for the background profiles, suggesting that most of the bromide measured in these core profiles is not available for plant water uptake.

5.6.2 Deuterium

5.6.2.1 Deuterium extraction

Water was extracted from the soil, chalk and plant samples by azeotropic distillation with toluene in a 'Dean-Stark' apparatus (Figure 5-17). The method is based on the principle that toluene and water form an azeotropic mixture at 81.4°C (Revesz and Woods, 1990). This means that when a mixture of toluene and water is heated, the toluene-water azeotrope will boil at 81.4°C, a significantly lower temperature than the boiling point of toluene (110°C) and water (100°C). The Dean-Stark apparatus leads the gaseous azeotrope to a condenser and makes the condensate accumulate into a receiving funnel, where toluene and water separate again. Any excess toluene then flows back into the distillation flask. The receiving funnel is graded so the amount of water extracted can be quantified, and a tap allows easy collection of the extract. Revesz and Woods (1990) showed that, when applied to soil samples, the method does not affect the isotopic composition of the extracted soil water.

To extract the water from the soil samples for deuterium analysis, between 20 and 40 g of moist soil were heated with 100 to 200 ml of toluene in a 250 ml flask. The soil had been sealed in zip-lock polythene bags and stored at 4°C prior to treatment to prevent any changes in water content or isotopic composition of the soil water. The distillation process was performed with an electrical heating element under the fume cupboard to reduce the risks associated with toluene. Distillation took 1 to 2 hours

and was continued for fifteen minutes after the cloudiness of the liquid in the Dean-Stark apparatus disappeared, indicating that all water had been distilled. The volume of water was recorded (typically between 2 and 15 ml) to give an estimate of the gravimetric water content of the soil. The water extract was then collected from the receiving funnel into a McCartney bottle.

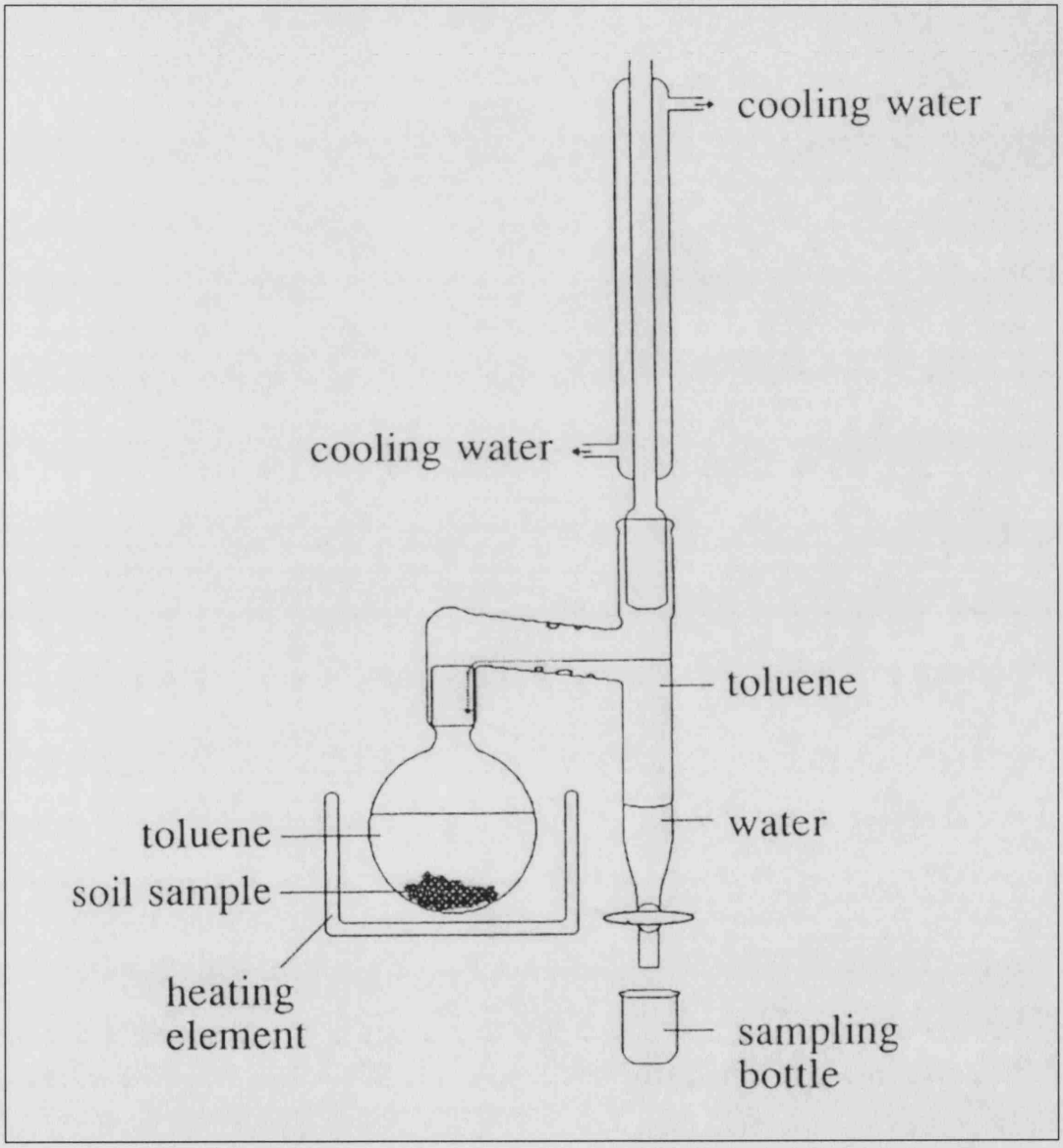

Figure 5-17 Dean-Stark apparatus for water extraction (after Revesz and Woods, 1990).

To remove any remaining traces of toluene from the water extract prior to analysis, wax was added to the McCartney bottle. The water was then warmed in the closed bottle on a heating plate to 60-70°C, to dissolve the remaining toluene into the melted

wax. The bottles were then cooled so the wax solidified at the top, and with a pipette, after penetrating the wax, the water was transferred to a new McCartney bottle.

The same method was used for water extraction of the chalk and grass samples. The chalk samples were first reduced in block size with a hammer to a characteristic length of maximum 5 mm before the chalk was introduced into the distillation flask. The azeotropic distillation method has been successfully applied on chalk samples before by Nativ et al. (1995). For the grass samples, distillation of the complete sample was needed to calculate the total amount of tracer present in the grass per surface unit. Therefore the complete contents of the polythene bag were transferred to the distillation flask and any remaining grass or condensed water inside the bag was transferred by rinsing with toluene.

To test the efficiency of the extraction method, 4 ml of HPLC-grade water were added to a mass of oven-dried soil in the distillation flask, and distillation was performed as above. The volume of extract collected was exactly 4 ml (within measuring errors), hence it was concluded that extraction by this method was complete. It is recognized that the ease of water extraction might be different for water contained within the matrix pores of the chalk samples. However, because the chalk samples were small and distillation was continued for fifteen minutes after visual clearness of the distillate, it is assumed that extraction was complete for the chalk samples as well. Regarding the water extraction from plant samples, Thorburn et al. (1993) have demonstrated the effectiveness of the method for *Eucalyptus* trees, so it can be assumed that for softer tissue such as grass the method is equally effective.

5.6.2.2 Deuterium analysis

The water samples (collected directly from the lysimeter drainage or obtained after azeotropic extraction from chalk, soil or plant samples) were analyzed for deuterium by mass spectrometry.

The majority of the analyses were run by the British Geological Survey (Wallingford), following a methodology described in Coleman et al. (1982). A

volume of 10 µl of the water sample was added to a tube containing 1 g of zinc shot, upon which the tube was sealed. The tube was immersed in liquid nitrogen for 1 minute to freeze the water, and the air was evacuated until a vacuum of better than 0.1 mbar was obtained. The tube was then allowed to warm up to room temp, before being placed in a heating block at 475°C for one hour. At this temperature the water is converted into H_2 gas by reduction with the Zn metal. A good reaction was marked by the formation of a zinc 'mirror' inside the tube. The reacted tubes were finally attached to the multi-port inlet of a VG Optima mass spectrometer operating in dual inlet mode, and the contents were analyzed for the isotopic ratio of hydrogen.

Samples collected from May 2002 onwards were analyzed for deuterium at the Bloomsbury Environmental Isotope Facility (BEIF) in University College London, by the following method. One ml of the water sample was pipetted into a septum-sealed vial. Repeated analyses were made of this sub-sample by continuous-flow mass spectrometry, using a pyrolysis method originally proposed by Prosser & Scrimgeour (1995). An aliquot of 2 ml from the septum-sealed vial was injected automatically into the pyrolysis furnace of a ThermoQuest High Temperature Conversion / Elemental Analyzer (TC/EA), where the water was reduced over glassy carbon at 1400°C in an atmosphere of pure helium to form H_2 and CO gases. These were separated on the TC/EA's gas chromatography column, and the separated gases swept by a 120 ml/min stream of carrier He into an open split device, from which a steady flow was admitted to a Delta Plus XP mass spectrometer. The $^2H/^1H$ ratio for each aliquot was determined by integration of peak areas, and compared with ratios measured on two pulses of reference hydrogen from a tank, to determine a delta value.

5.6.2.3 Deuterium results

5.6.2.3.1 Deuterium in the lysimeter drainage

The deuterium content in the drainage samples from the Fleam Dyke lysimeter was measured regularly, both before and after the tracer application in February 2002 (Figure 5-18). Concentrations were initially fairly constant, with δ^2H varying between -50 and –40‰ VSMOW (see Appendix III for a definition of the units used).

This is in correspondence with measurements of natural deuterium levels in the Fleam Dyke lysimeter drainage in the 1980s by Darling and Bath (1988). It also is a good reflection of the yearly average rainfall composition. A composite rainfall sample from the Fleam Dyke rain gauge over the period June 2002 - May 2003 had a δ^2H value of –46.4‰ VSMOW. However, Darling and Bath (1988) had also shown that the rainfall exhibited daily δ^2H variations of up to 70‰ VSMOW, and average seasonal variations of the same amplitude, with isotopically enriched summer rainfall relative to winter rainfall. Figure 5-18 shows that these variations were averaged out in the lysimeter drainage in 2002. This suggests either that rapid bypass flow from the surface to 5 metres depth did not take place, or that there was sufficient time for solute exchange between the rapid flow component and the bulk pore water.

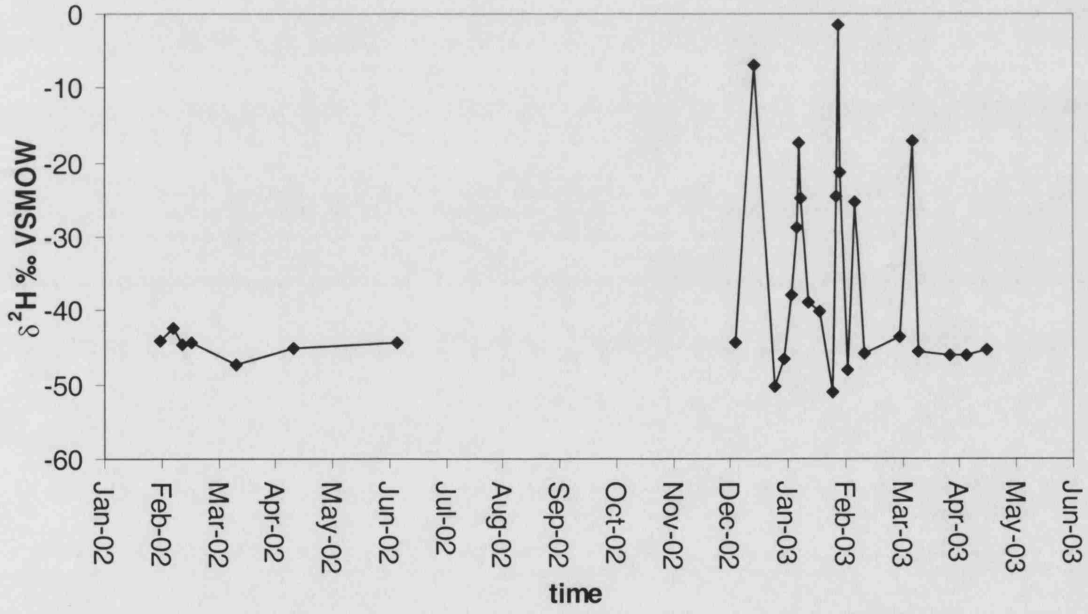

Figure 5-18 Deuterium contents measured in drainage samples from Fleam Dyke lysimeter. The high deuterium values in 2003 are most likely due to evaporative enrichment of the samples.

As shown in Figure 5-18, sudden rises in δ^2H were observed in the winter and spring of 2003. These coincided with peaks in bromide concentration. As explained in section 5.6.1.3.1, the increased bromide levels could be attributed to evaporation of the water samples, caused by overheating of the battery of the automated sampler.

Correction factors were calculated based on the volume of sample lost, and it was shown that this reduced the bromide levels in the drainage back to background concentrations. Similarly, the sudden rises in δ^2H may be due to evaporative enrichment in the water samples, as contrasting evaporative rates of the heavier ^2HHO and the lighter H_2O lead to isotopic fractionation. In theory, correction factors could be calculated for deuterium based on the process of Rayleigh distillation, describing an exponential increase in the isotopic ratio as the water reservoir diminishes in size (Clark and Fritz, 1997). In practice, the Rayleigh distillation is dependent on the humidity and the temperature, and as both factors were unknown, the calculation of reliable correction factors was not possible.

Whether the high deuterium concentrations were due to tracer arrival or evaporative enrichment was tested by analyzing selected samples for their ^{18}O content. In natural fresh waters, there is a relationship between ^{18}O and ^2H, known as the global meteoric water line (Clark and Fritz, 1997):

$$\delta^2 H = 8.13\,\delta^{18}O + 10.8 \qquad \textit{Eq. 5-1}$$

This is a global average, and small deviations of the global meteoric water line can be measured locally. Darling and Bath (1988) obtained the following relationship after monitoring the isotopic composition of rainfall at Fleam Dyke in the 1980s:

$$\delta^2 H = 7.30\,\delta^{18}O + 4.04 \qquad \textit{Eq. 5-2}$$

If the lysimeter drainage contained deuterium tracer, then this would increase δ^2H without increasing $\delta^{18}O$, i.e. it would translate the meteoric water line upwards. On the contrary, if higher deuterium concentrations were obtained by evaporative enrichment of the samples, then this would result in a deviation from the meteoric water line along a line with a lower slope (Clark and Fritz, 1997). Selected samples from the lysimeter drainage that contained high levels of deuterium were analysed for ^{18}O [(10)], and the results are shown in Figure 5-19. The samples show a good correlation between δ^2H and $\delta^{18}O$ (R^2=0.97), plotting along a line with a slope of

[(10)] Analysis of ^{18}O was performed by mass spectrometry at the School of Environmental Sciences, University of East Anglia.

5.25. This is a typical slope for evaporative enrichment under humid conditions (Clark and Fritz, 1997). It confirms that the high concentrations observed in the lysimeter drainage are an artefact, and are not due to tracer breakthrough. It can thus be concluded that, up to 15 months after the tracer application at the surface, none of the tracer could be detected in the lysimeter drainage at 5 metres depth.

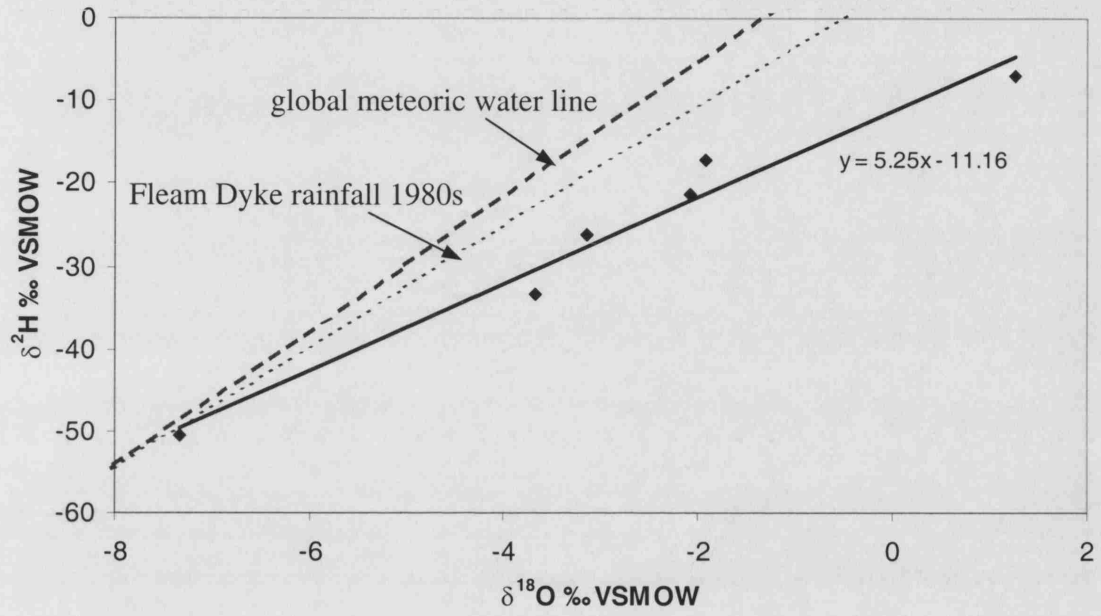

Figure 5-19 The relationship of δ^2H versus $\delta^{18}O$ for selected drainage samples that showed high deuterium enrichment. The deviation from the meteoric water line indicates evaporative enrichment of the samples.

5.6.2.3.2 Deuterium in the core profiles

The results of the deuterium analysis of the core profiles are shown for each sampling date in Figure 5-20 until Figure 5-23. The δ^2H values obtained for the chalk pore water are considered to represent the deuterium concentrations in the chalk matrix, rather than in the fractures. Core sampling provides a measure of the resident concentrations, i.e. volume-averaged concentrations. In the chalk, the majority of the pore volume resides in the matrix, which has a porosity that is at least 50 times larger than the fracture porosity. Moreover, because pore water was extracted from crushed

chalk fragments obtained from cores with a limited diameter (between 3 and 7 cm), the sampling of significant fracture water is not that likely.

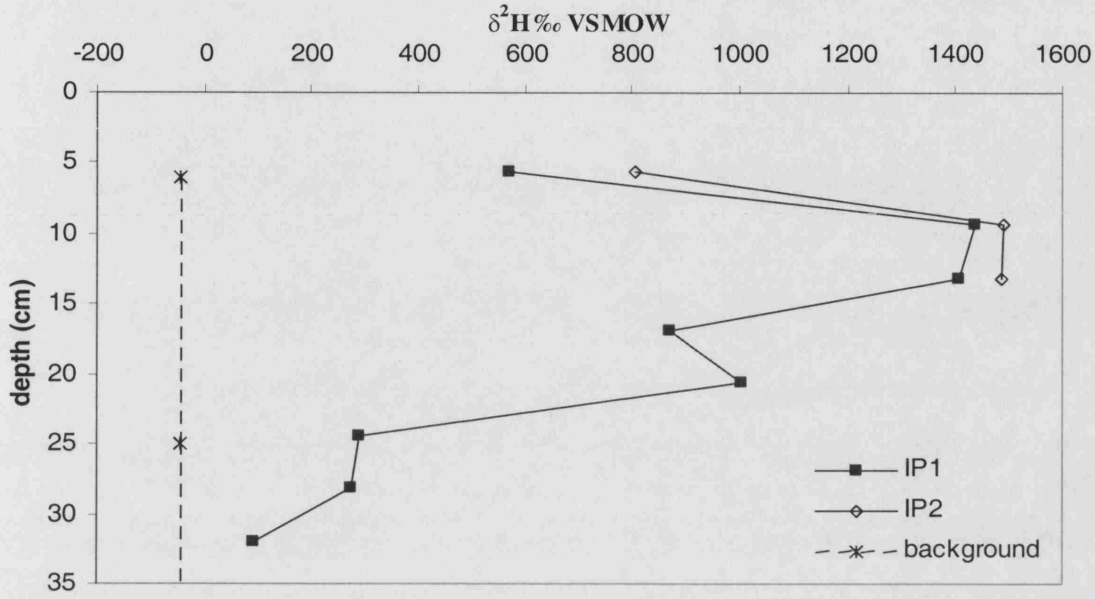

Figure 5-20 Deuterium concentrations measured in two core profiles taken at the Fleam Dyke research site on 10 May 2002.

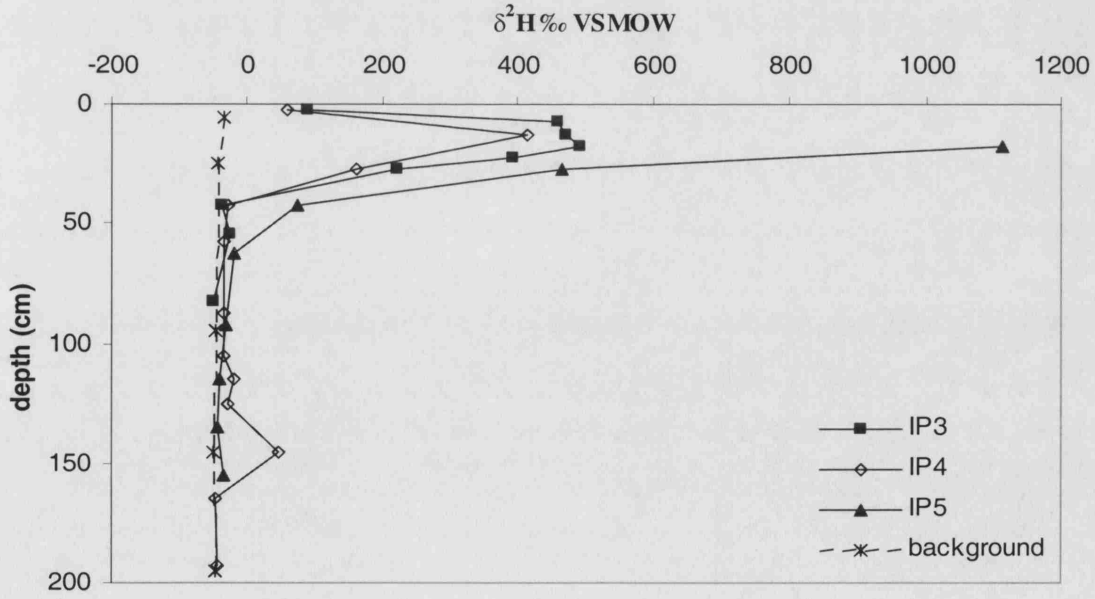

Figure 5-21 Deuterium concentrations measured in three core profiles taken at the Fleam Dyke research site on 3 July 2002.

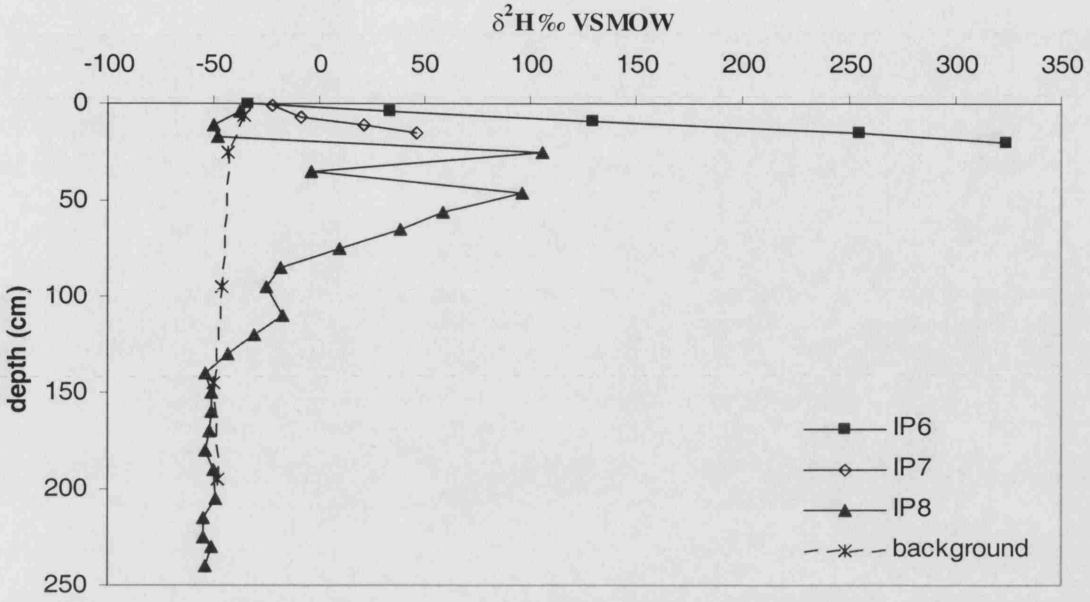

Figure 5-22 Deuterium concentrations at the Fleam Dyke research site, measured in core profiles IP6 and IP7 taken on 23 October 2002, and core profile IP8 taken on 13 December 2002.

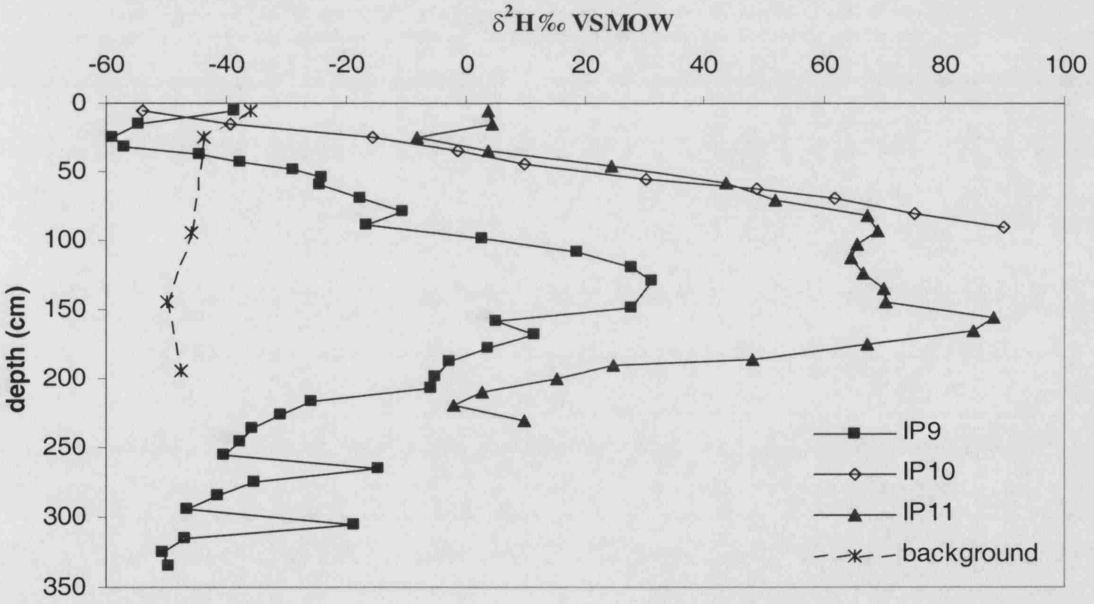

Figure 5-23 Deuterium concentrations measured in three core profiles taken at the Fleam Dyke research site on 22 May 2003.

The deuterium background concentrations in the chalk pore water were fairly uniform, varying between –50 and –40 ‰ VSMOW, at the same level as the deuterium measured in the lysimeter drainage. In the topsoil, a higher concentration of –35 ‰ VSMOW was measured in May 2002. This is in accordance with higher deuterium contents often reported in rainfall during spring and summer (Darling and Bath, 1988). In general, background concentrations of deuterium were low and constant, allowing clear differentiation of the tracer profiles.

From Figure 5-20 until Figure 5-23 it is apparent that a set of cores drilled on the same date sometimes yielded widely varying tracer profiles. Although the cores were all drilled within a few metres of each other and care had been taken to assure a uniform tracer application at the surface, significant differences in vertical tracer distribution were observed between core profiles. This suggests lateral heterogeneity of transport pathways. In Figure 5-5 it had already been shown that the stratification of the weathered chalk showed strong lateral heterogeneity, and it is clear that this must have an effect on flow and solute transport. Moreover, the fractures in the unweathered chalk impose additional heterogeneity on the transport pathways. Rapid transport may be possible through vertical fractures, combined with lateral diffusion into the matrix blocks. Due to the limited diameter of the core gouges, the core profiles do not necessarily provide a representative sample of this fracture-matrix continuum. The deuterium concentration measured in an individual core profile may thus be dependent on the specific stratification of the chalk in that profile, and on the accidental presence of active fractures in or around the core.

Envelopes of deuterium profiles for all sample dates are shown in Figure 5-24. Up until July 2002, the bulk of the tracer stayed in the soil and the weathered chalk underneath, maintaining a clear peak definition. The tracer profile gradually shifted downwards, suggesting a slow piston-like transport mechanism. After December 2002, when the tracer started reaching the unweathered chalk and when infiltration rates were high, the profile became more dispersed. This suggests that piston flow through the matrix, if occurring at all, was certainly not the only flow mechanism in the unweathered chalk. It may be an indication of fracture flow, allowing the deuterium to partially bypass the matrix, thereby increasing dispersion. This suggestion is confirmed by the occasional appearance of secondary peaks in the

profiles, e.g. around 150 cm depth for profile IP4 and around 260 and 300 cm depth for profile IP11. These secondary peaks appear isolated from the bulk of the tracer above, and seem to indicate the occurrence of some bypass flow mechanism. They suggest rapid flow of tracer through vertical fractures, without time for diffusive equilibrium with the surrounding chalk matrix. The secondary peaks then indicate the level where the tracer is slowed down and re-introduced to the chalk matrix. This may occur where a vertical fracture is intersected by a horizontal fracture, forcing the tracer to move laterally through the horizontal fracture, and thus slowing down the tracer and allowing diffusion into the surrounding matrix.

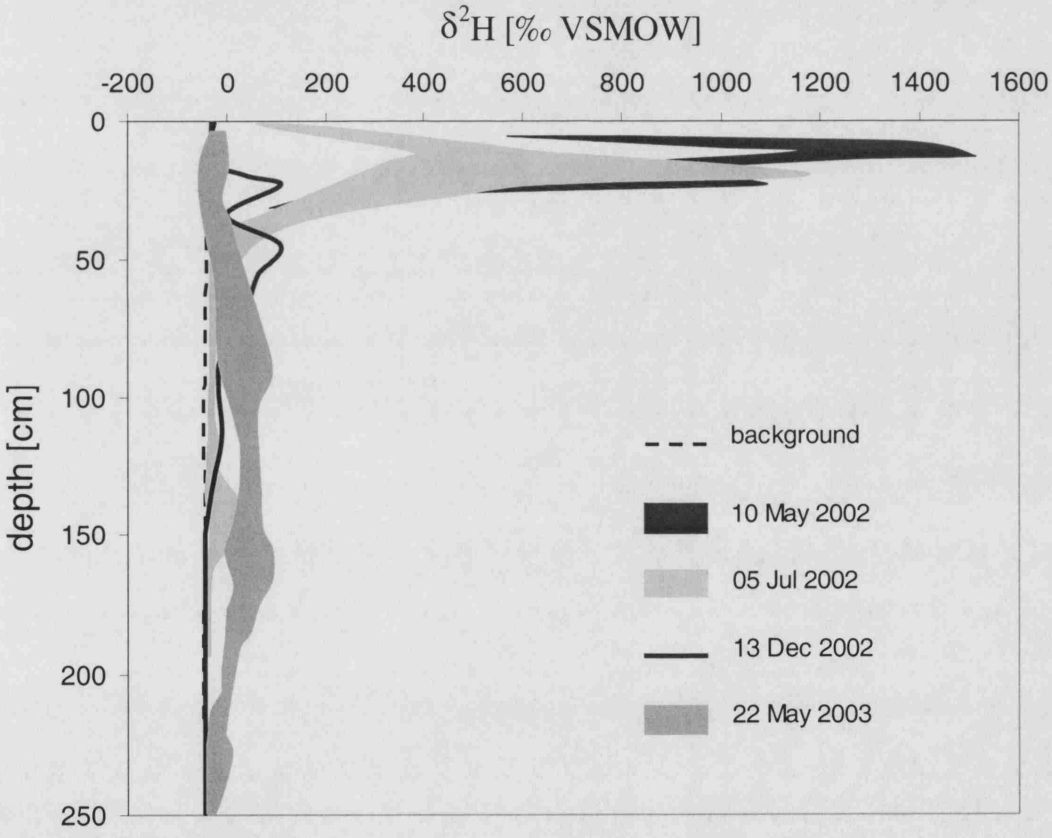

Figure 5-24 Envelopes of deuterium concentrations in multiple core profiles taken at the Fleam Dyke site in 2002-2003.

A quantitative measure of the tracer velocity, recovery and dispersion can be obtained by spatial moments analysis. The i^{th} spatial moment of the concentration distribution is given by (Freyberg, 1986):

$$M_i(t) = \int_0^\infty \theta(z,t) C(z,t) z^i dz \qquad \text{Eq. 5-3}$$

where $C(z,t)$ is the deuterium concentration (expressed in g/m^3, above background), $\theta(z,t)$ is the volumetric water content and z is the depth (in metres, measured positive downwards). For sample dates when multiple profiles had been measured, laterally-averaged deuterium profiles were calculated, and the averages corrected for background concentrations. The zeroth, first and second moments were then calculated from these averaged profiles (Table 5-7). This was done by approximating the integral in Eq. 5-3 by discrete steps associated with the core sections for which deuterium concentrations had been measured:

$$M_i(t) = \sum_{j=1}^{N} \theta(z_j,t) C(j,t) \left(\frac{(z_{j,l})^{i+1}}{i+1} - \frac{(z_{j,u})^{i+1}}{i+1} \right) \qquad \text{Eq. 5-4}$$

where j is the number of the core section, and $z_{j,l}$ and $z_{j,u}$ are the lower and upper boundary of the jth core section. The zeroth moment M_0 defines the deuterium mass recovered from the core profiles, and was used to calculate the total tracer recovery. The first moment M_1, when normalized, defines the location of the centre of mass z_c of the deuterium plume:

$$z_c = \frac{M_1}{M_0} \qquad \text{Eq. 5-5}$$

The second moment M_2 allows calculation of the spatial variance σ_z^2 [L^2], which is a measure for the spread of the concentration distribution around the centre of mass:

$$\sigma_z^2 = \frac{M_2}{M_0} - z_c^2 \qquad \text{Eq. 5-6}$$

Tracer recovery rates are shown in Table 5-7. In May 2002, three months after the tracer application at the surface, the recovery rate was only 8.7%. The explanation for this low recovery is tracer loss through evapotranspiration. The deuterium tracer had been applied in an equivalent of 1 mm water, without any additional irrigation. This facilitated tracer losses, through evaporation of tracer intercepted by the grass leaves and evaporation from the soil surface. Moreover, as can be seen in Figure 5-24, the bulk of the tracer remained in the root zone until at least July 2002, being continuously subject to tracer uptake by the grass roots. The tracer recovery gradually

decreased over time, reaching 2.4% in December 2002. An anomaly occurred in May 2003, when the recovery rate rose again to 6.0%. This inconsistency appears to be due again to the lateral heterogeneity of the transport process. The recovery rate of 2.4% in December 2002 was calculated from a single profile, and is therefore likely to be a poor representation of the average recovery. In May 2003, profiles IP9 and IP10, drilled on the same date, gave a deuterium recovery of 3.8% and 7.6%, respectively. It shows that the tracer profiles should be interpreted with caution, being essentially only point measurements of a whole range of transport behaviour. Additional uncertainty is due to the limited depth of the core profiles, making it possible that some tracer present at greater depth is not sampled by the coring.

Table 5-7 Moment analysis of deuterium profiles taken at the Fleam Dyke research site.

Date	Elapsed time	M_0	M_1	M_2	Tracer recovery	z_c	σ_z^2
	[d]	[g/m^2]	[g/m]	[g]	[%]	[m]	[m^2]
10/05/02	87	10.4	1.44	0.26	8.7	0.14	0.006
05/07/02	141	6.9	2.85	2.66	5.8	0.41	0.216
13/12/02	304	2.9	1.63	1.10	2.4	0.56	0.066
22/05/03	464	7.2	9.92	16.67	6.0	1.39	0.409

The evolution of the vertical position of the centre of mass as a function of time is shown in Figure 5-25. As can be expected, the velocity of the tracer plume is not constant. Recharge through the unsaturated zone in England has a strong seasonal character, causing the tracer to move most during the winter months, and to be almost stationary during the summer months. On average, Figure 5-25 indicates a vertical tracer velocity of 3.7 mm/d, while between May 2002 and May 2003, a value of 4.4 mm/d is obtained. This is considerably higher than the velocity of 1.8 mm/d that can be inferred from the environmental tritium profiles measured at Fleam Dyke in 1979 (Figure 4-8). One reason may be that the 4.4 mm/d obtained for the deuterium tracer test mainly covers transport through the weathered chalk. It may be an indication that the weathered chalk has a lower effective porosity than the unweathered chalk underneath, thereby increasing the effective velocity of the deuterium tracer. A lower

porosity in the upper few metres of the Fleam Dyke profile has also been reported by Foster and Bath (1983).

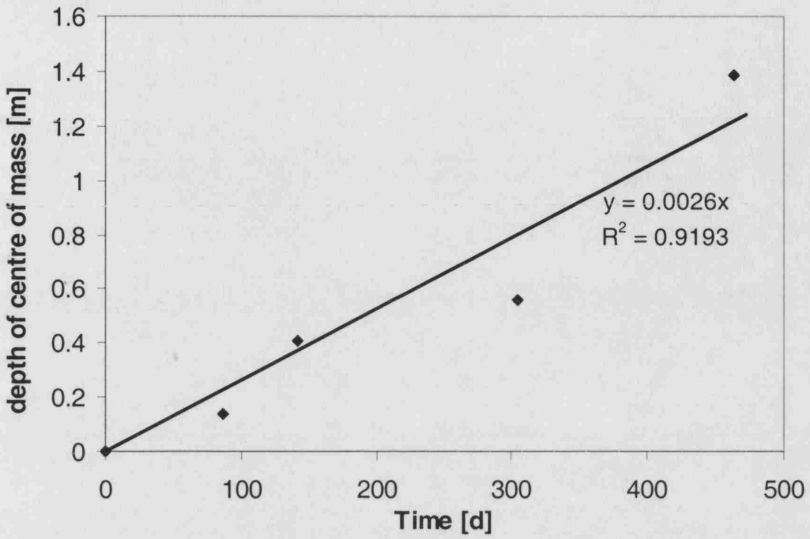

Figure 5-25 Vertical displacement of the centre of mass of the deuterium profiles as a function of time since tracer application.

From the spatial variance σ_z^2, the effective dispersion coefficient D_{eff} [L^2 T^{-1}] and the effective dispersivity α_{eff} [L] can be derived as follows (Garabedian et al., 1991):

$$D_{eff} = \frac{1}{2}\frac{d\sigma_z^2}{dt} \qquad \textit{Eq. 5-7}$$

$$\alpha_{eff} = \frac{1}{2}\frac{d\sigma_z^2}{dz_c} \qquad \textit{Eq. 5-8}$$

The evolution of the spatial variance with time and depth of the centre of mass is shown in Figure 5-26. The spatial variance does not show a clear upgoing trend, which is explained by the stratification of the profile in soil, weathered chalk and chalk, leading to non-uniform dispersive behaviour. A weighted least-squares regression can still be calculated, with the weights based on the number of cores that were used to calculate the average tracer profiles. This leads to an effective dispersion coefficient of 4.6×10^{-9} m^2/s and an effective dispersivity of 15 cm. Alternatively, the gradients of Eq. 5-7 and Eq. 5-8 can be approximated for each sample date by averaging the slopes from the origin, as shown in Table 5-8. This

gives an effective dispersion coefficient ranging between 0.4×10^{-9} and 8.8×10^{-9} m^2/s, and an effective dispersivity between 2 and 26 cm.

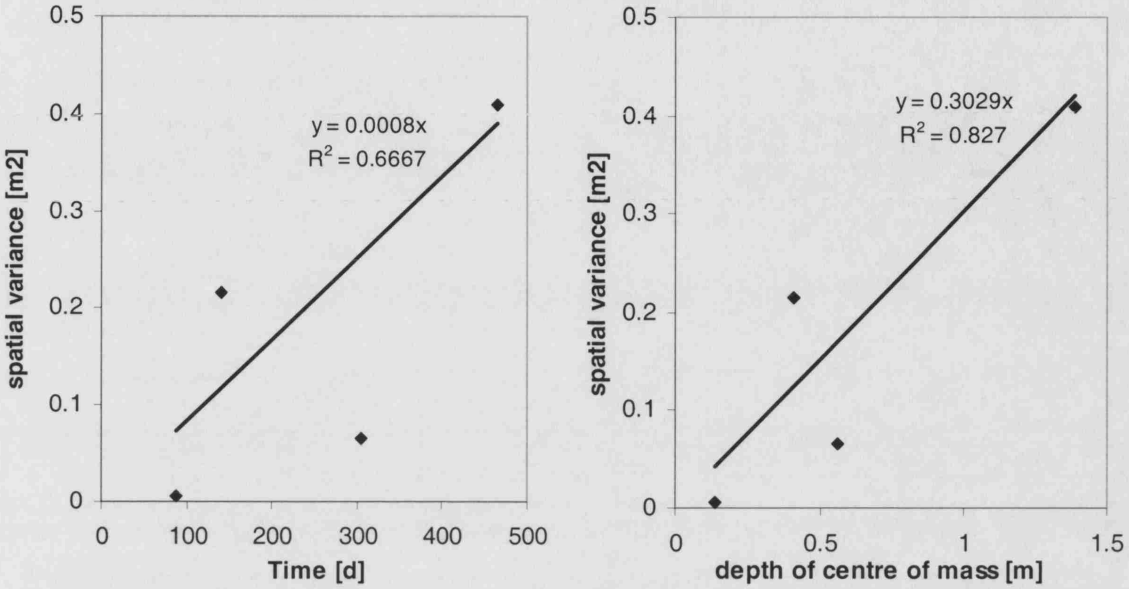

Figure 5-26 Spatial variance as a function of time since tracer application, and as a function of the depth of the centre of mass. The regression lines are weighted for the number of cores used to calculate the average tracer profile at each sample date.

Table 5-8 Effective dispersion coefficients and effective dispersivities obtained from the deuterium profiles by spatial moment analysis.

Date	t	z_c	$D_{eff} = \frac{1}{2}\frac{\sigma_z^2}{t}$	$\alpha_{eff} = \frac{1}{2}\frac{\sigma_z^2}{z_c}$	$\frac{\alpha_{eff}}{z_c}$
	[d]	[m]	[m^2/s]	[m]	[-]
10/05/02	87	0.14	0.4×10^{-9}	0.02	0.14
05/07/02	141	0.41	8.8×10^{-9}	0.26	0.63
13/12/02	304	0.56	1.3×10^{-9}	0.06	0.11
22/05/03	464	1.39	5.1×10^{-9}	0.15	0.11

The free-water diffusion coefficient for deuterium at 10°C is estimated at 1.48×10^{-9} m^2/s, and the effective diffusion coefficient in chalk is assumed to be around 25% of this value (Muller, 1987, see Appendix I), or 0.37×10^{-9} m^2/s. The average effective

dispersion coefficient obtained by spatial moment analysis is thus around one order of magnitude larger than the effective diffusion coefficient. This indicates that molecular diffusion only plays a minor role in the spreading of the deuterium tracer, and that other dispersive processes are dominant here. Apart from mechanical dispersion, these processes may include advective exchange of tracer between the fractures and the matrix.

Table 5-8 also gives the ratio of the effective dispersivity to the travel distance, α_{eff}/z_c. An average value of 0.25 is obtained. For the last two sampling dates, the ratio is 0.11. This corresponds well with the rule of thumb that states that the longitudinal dispersivity is about 10% of the travel distance (e.g. Spitz and Moreno, 1996).

5.6.2.3.3 Deuterium in the grass

The results of the deuterium analysis of the grass extracts are shown in Table 5-9. Deuterium analysis was only carried out for the grass leaves and not for the root system. A δ^2H value of +670‰ VSMOW was obtained for the grass leaves from the tracer-treated plot, which corresponds with the deuterium content measured in the topsoil. This confirms that deuterium is readily taken up by the grass roots. In the grass leaves from the background samples, a δ^2H value of –8.8‰ VSMOW was obtained. This is significantly higher than the deuterium concentrations measured in the soil from the background cores, and higher than concentrations normally measured in spring rainfall. The difference is likely to be caused by evaporative enrichment in the grass leaves, through preferential evaporation of H_2O over ^2HHO.

Table 5-9 Deuterium concentrations and recovery in samples of grass leaves, taken at the Fleam Dyke research site on 10 May 2002. All values shown are averages of two samples.

	Background	Tracer-treated plot
Deuterium concentration in grass leaves [‰ VSMOW]	-8.8	670
Deuterium tracer mass in grass leaves per unit area [g/m^2]	n/a	0.067
Tracer recovery in grass leaves [%]	n/a	0.056

The average tracer recovery in the grass leaves, 3 months after application, was only 0.056%. This is in clear contrast with bromide where recovery was 22.1% in the grass leaves. The reason is that deuterium is incorporated in the water molecules, and evaporates during transpiration in the plant leaves. The majority of the deuterium tracer is thus lost to the atmosphere.

5.7 Conclusion

The Fleam Dyke tracer test has provided an important dataset of transport through unsaturated chalk. The experiments were conducted in the field under natural gradient conditions, and should help to improve the understanding of the physical processes involved in flow and solute transport through the chalk as a fractured porous medium.

The experimental work has clearly illustrated lateral heterogeneity, even at the metre-scale. Visual inspection of cores revealed irregular stratification of the weathered chalk, with limited lateral consistency between profiles. As a result, permeameter measurements showed significant variations in the field-saturated hydraulic conductivity of the weathered chalk. This evidence of heterogeneity was confirmed by tracer analysis of the pore water from core samples, where tracer profiles showed considerable lateral variability. This heterogeneity in flow and transport behaviour is consistent with expectations of flow and transport in the fractured dual permeability system of the Chalk.

For 15 months after the application of the tracer at the surface, none of the tracer has been detected in the lysimeter drainage at 5 m depth. Nevertheless, 2002 was a relatively wet year, with a total rainfall amount of 709 mm, or 12% in excess of the local average[11]. The implication is that even under relatively wet conditions there was no fast-transport pathway providing a direct connection between the surface and the chalk at 5 m depth. It suggests that the Chalk aquifer at Fleam Dyke is not excessively vulnerable to pollution. This result illustrates the protective capacity of

[11] Yearly averaged rainfall for the Fleam Dyke site was estimated at 631 mm, based on the years for which good quality data were available, i.e. the periods 1980-1985 and 1996-2002.

the soil and the weathered chalk, having a buffering effect on high-intensity rainfall events and causing a delay before solutes can enter chalk fractures. Similar observations have been reported in the past. Wellings and Cooper (1983) compared recharge on various locations of the English Chalk and concluded that the likelihood of fracture flow was strongly influenced by the thickness of the soil cover and the depth of disturbance of the Chalk. Similarly, Brouyère et al. (2004), in a study of a chalk aquifer in Belgium, stressed the importance of a protective cover to prevent the fractures becoming active.

A problem was encountered with the interpretation of the bromide profiles. The bromide background concentrations were higher than expected, and this problem could not be fully resolved. Better information about the tracer transport was obtained from the deuterium profiles. The rate of transport was relatively low, at an average vertical tracer velocity of 4.4 mm/d (1.2 m/year). Considerable dispersion was observed once the tracer reached the unweathered chalk, and occasionally secondary peaks were observed between 150 and 300 cm depth. This suggests the occurrence of fracture flow, allowing some tracer to bypass the chalk matrix. Still, none of the tracer was detected in the lysimeter drainage at 5 m depth, indicating that the transport pathways through the fractures had only a limited vertical extent. This confirms the conclusions from previous work at the Fleam Dyke research site (section 4.3.3), i.e. that two possible conceptual models can be conceived for solute transport through the chalk fractures at Fleam Dyke. First, the fractures may be active over the whole depth of the unweathered chalk, but the tracer may gradually diffuse from the fractures into the matrix while travelling downwards through the fracture (Figure 3-9 c). This would induce some dispersion on the tracer profile, and could allow the fracture water reaching the lysimeter drainage to be almost free of tracer. Second, the fractures may only be active over limited depth (Figure 3-9 d). The water may be sucked back from the fractures into the matrix where the fracture aperture increases or where the hydraulic conductivity of the matrix increases, leading to advective exchange of tracer. Which of these two processes is dominant should be clarified by using the data in a modelling context, which will be pursued in Chapter 8.

6 Description of MACRO 5.0

6.1 Introduction

Modelling was undertaken to gain more insight into the unsaturated flow and transport process through the Chalk. As the unsaturated chalk was conceptualized as a dual-permeability medium (section 3.3), a model was needed that could adequately simulate this dual-permeability behaviour in the unsaturated zone. Furthermore, a total water balance was required, including plant water uptake. The model MACRO 5.0 was finally selected, and is described in this chapter.

MACRO 5.0 is a physically based, one-dimensional numerical model of variably saturated water flow and reactive solute transport (Larsbo and Jarvis, 2003; Stenemo and Jarvis, 2003). It was developed at the Swedish University of Agricultural Sciences (SLU, Uppsala) specifically for macroporous soils. A schematic overview of the flow components in the model is shown in Figure 6-1. The soil porosity is divided into two flow domains (macropores and micropores), so the model can be classified as a dual permeability model. Each flow domain is characterized by a flow rate and solute concentration, with the division between the two flow domains being defined by a given pressure head and a corresponding water content and hydraulic conductivity. In the micropores, unsaturated water flow and solute transport are modelled by Richard's equation and the advection-dispersion equation. For the moisture retention relation and the unsaturated hydraulic conductivity function in the micropores, a modified form of the van Genuchten equation is used. Unsaturated water flow in the macropores is treated as a non-capillary, gravity-driven process, with the hydraulic conductivity in the macropores expressed as a power function of the degree of saturation in the macropores (kinematic wave approach). Solute transport through the macropores is treated as a purely advective process. Water exchange between the flow domains is modelled as a first order process and solute

exchange between the flow domains is treated as a combination of a diffusion component (using a quasi-steady-state approach) and a mass flow component. The model calculates the full water balance, including water and solute uptake by crops, and contains optional modules for irrigation, flow to tile drains and heat conduction. When reactive solutes are simulated, adsorption is modelled according to the Freundlich isotherm, while degradation follows first-order kinetics.

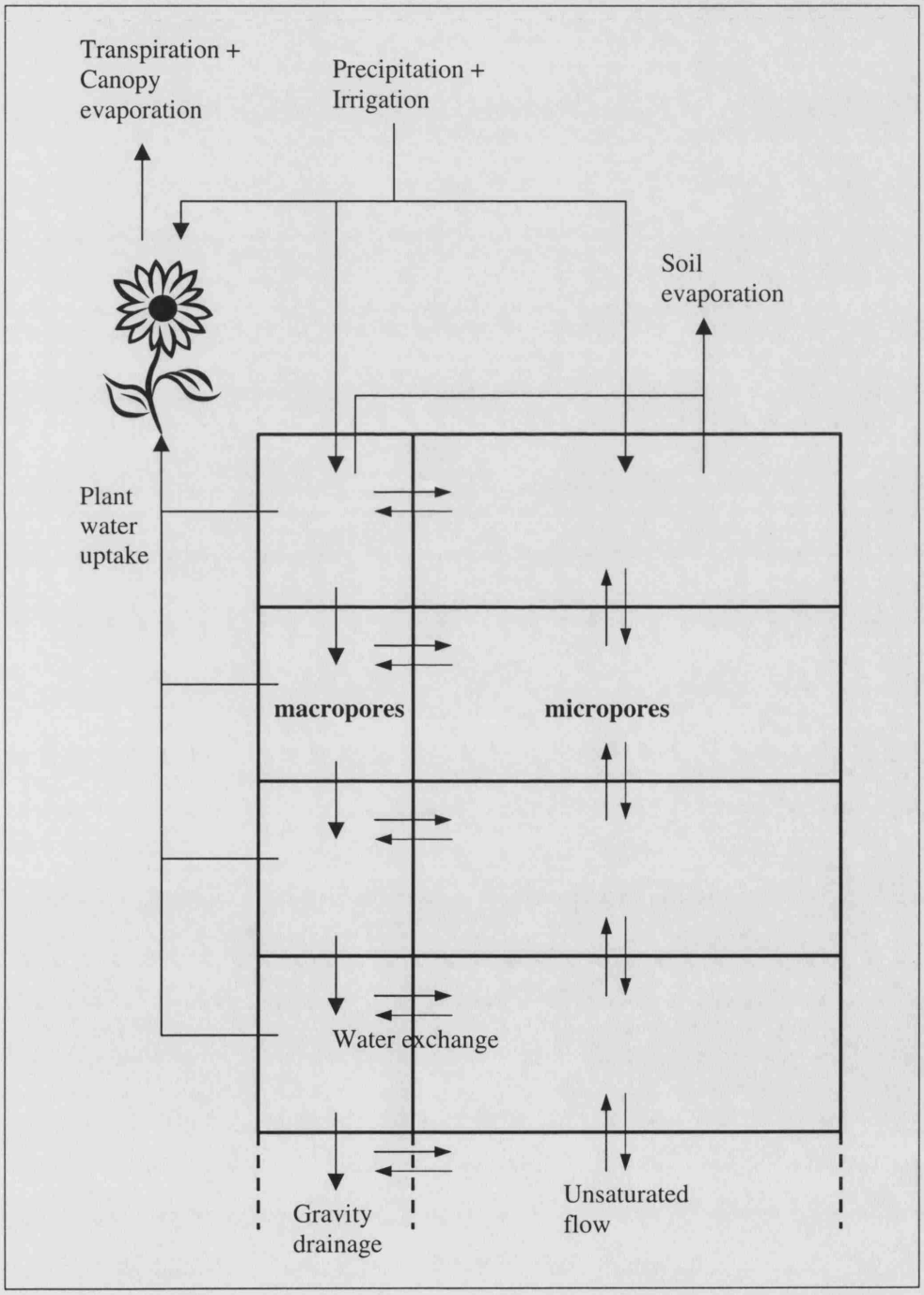

Figure 6-1 Schematic overview of the flow components in MACRO 5.0.

The main processes in MACRO 5.0 are described in more detail in the following sections, with an emphasis on the processes relevant to the simulation of the Fleam Dyke lysimeter data. The next section is largely based on the MACRO 5.0 manual by Larsbo and Jarvis (2003).

6.2 Processes, equations and numerical formulation

6.2.1 Evapotranspiration and canopy processes

Part of the precipitation that is added to the system is lost to the atmosphere through evapotranspiration, which is a combination of three separate processes: soil evaporation, root water uptake with subsequent transpiration, and wet canopy evaporation. For the plant cover, three options are available in the model: no crop (bare soil), a perennial crop, or an annual crop.

6.2.1.1 Annual crop development

The development of an annual crop is described by the total and green leaf area indices, *LAI* and *GLAI*, which vary as a function of the day number in the year. Prior to crop emergence and after harvest, both values are set to zero. Between crop emergence and a user-specified day number D_{min}, a linear development phase is assumed. Later, between D_{min} and the day of maximum leaf area D_{max}, the green leaf area index is given by:

$$GLAI = GLAI_{\min} + \left(GLAI_{\max} - GLAI_{\min}\right)\left(\frac{D^* - D_{\min}}{D_{\max} - D_{\min}}\right)^{x_1} \qquad \text{Eq. 6-1}$$

where $GLAI_{min}$ is the green leaf area index at D_{min}, $GLAI_{max}$ is the maximum green leaf area index, D^* is the current day number and x_1 is an empirical exponent. Similarly, the reduction in *GLAI* between the maximum value and harvest is given by:

$$GLAI = GLAI_{harv} + \left(GLAI_{\max} - GLAI_{harv}\right)\left(\frac{D_{harv} - D^*}{D_{harv} - D_{\max}}\right)^{x_2} \qquad \text{Eq. 6-2}$$

where $GLAI_{harv}$ is the green leaf area index at harvest and x_2 is an empirical exponent. The total leaf area index *LAI* is equal to *GLAI* for most of the year, except between

D_{max} and D_{harv} where *LAI* is maintained constant. For the root depth and the crop height of an annual crop, two linear development phases are assumed: first from zero at crop emergence to a user-specified value at D_{min}, and then between D_{min} and D_{max}.

For a perennial crop, *LAI* equals *GLAI* and is assumed constant over the whole year. The root depth and the crop height are assumed constant as well.

6.2.1.2 Soil evaporation

A total potential evapotranspiration rate PE_t [L T^{-1}] is supplied with a daily resolution by the user, and the potential soil evaporation rate PE_s [L T^{-1}] is then derived as:

$$PE_s = PE_t e^{-\alpha_f LAI} \qquad \textit{Eq. 6-3}$$

where α_f is the radiation attenuation factor [-] (fixed at a value of 0.6 as an average for vegetation). The actual soil evaporation rate E_s [L T^{-1}] is defined by comparing the potential rate with the maximum possible rate of upward water flux to the soil surface q_{max} [L T^{-1}]:

$$E_s = \min(q_{\max}, PE_s) \qquad \textit{Eq. 6-4}$$

where q_{max} is calculated by substituting the appropriate equation for the unsaturated hydraulic conductivity of the micropores into Darcy's law (see section 6.2.2.1).

6.2.1.3 Wet canopy evaporation

Precipitation, applied as daily input by the user, is assumed to be first diverted to the canopy, from where it can evaporate. A running water balance is calculated, so precipitation continuously fills up the canopy to a maximum amount, the canopy interception capacity $W_{c,max}$. Any precipitation in excess of this canopy capacity becomes effective precipitation and enters the upper layer of the soil profile. For an annual crop, the canopy interception capacity is assumed to increase linearly from

zero at crop emergence to a user-specified maximum at D_{max}, and it is set to zero again at harvest. The potential wet canopy evaporation rate [L T^{-1}] is calculated as:

$$PE_{wc} = c_f PE_t \left(1 - e^{-\alpha_f GLAI}\right) \qquad \textit{Eq. 6-5}$$

where c_f is an empirical correction factor to account for enhanced evaporation from wet canopy ($c_f \geq 1.0$) [-]. The actual wet canopy evaporation rate E_{wc} [L T^{-1}] is defined by comparing the potential rate with the amount of water stored on the canopy W_c [L]:

$$E_{wc} = \min\left(W_c, PE_{wc}\right) \qquad \textit{Eq. 6-6}$$

6.2.1.4 Root water uptake

The potential root water uptake rate PE_r [L T^{-1}] depends on the amount of water stored on the canopy W_c:

$$PE_r = \frac{PE_{wc} - W_c}{c_f} \qquad \textit{if } W_c < PE_{wc} \qquad \textit{Eq. 6-7}$$

$$PE_r = 0 \qquad \textit{if } W_c \geq PE_{wc} \qquad \textit{Eq. 6-8}$$

The ratio between actual and potential root water uptake rate is a function of a water stress index ω^* [-]:

$$\frac{E_r}{PE_r} = f\left(\omega^*\right) \qquad \textit{Eq. 6-9}$$

A threshold is set, such that root water uptake is only reduced when the root adaptability factor ω^*_c is exceeded (Figure 6-2). The total water stress index is calculated as:

$$\omega^* = \sum_{i=1}^{i=k} r_i \omega_i \qquad \textit{Eq. 6-10}$$

where k is the number of soil layers in the profile containing roots and r_i and ω_i are the proportion of the total root length and the water stress reduction factor in layer i respectively. The water stress reduction factor in each layer is a function of the water content. The water stress reduction factor is reduced to zero both at the saturated water content θ_s and also at the wilting point θ_w, and is considered to be at its maximum as

long as there is a minimum critical air content and the fraction of available water exhausted is below a threshold value (Figure 6-2).

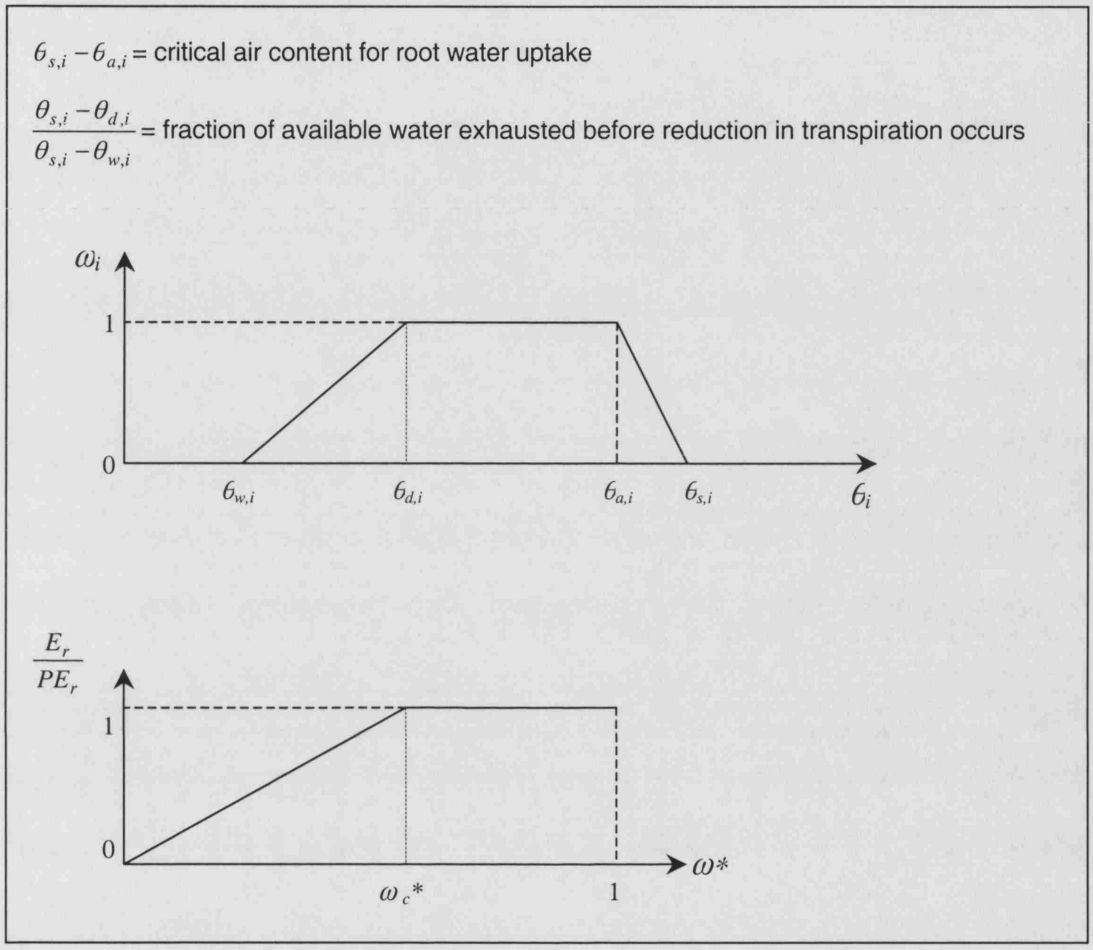

Figure 6-2 The water stress reduction factor for root water uptake.

The root length is assumed to be distributed logarithmically with depth, as defined by an empirical root distribution parameter ζ. The total water uptake is distributed over the root depth according to the stress in each layer. Hence the water uptake sink to be used in the flow equations is given by:

$$S_{r,i} = \left(\frac{E_r}{\Delta z_i}\right)\left(\frac{r_i \omega_i}{\omega^*}\right) \qquad \textit{Eq. 6-11}$$

where $S_{r,i}$ represents the root water uptake [T^{-1}] from layer i and Δz_i is the thickness of layer i [L]. Root water uptake always occurs preferably from the macropores; only when the macropores are empty is any excess demand taken from the micropores.

6.2.2 Flow description

6.2.2.1 Micropores

The vertical water flux through the micropores is calculated by the pressure-based form of Richards' equation (cf. Eq. 2-7):

$$C_{mi}\frac{\partial h_{mi}}{\partial t} = \frac{\partial}{\partial z}\left(K_{mi}(h_{mi})\left(\frac{\partial h_{mi}}{\partial z}+1\right)\right) - S_{r,mi} - \Gamma_{w,mi} \qquad \textit{Eq. 6-12}$$

where C_{mi} is the specific capacity of the micropores ($=d\theta_{mi}/dh_{mi}$) [L^{-1}], θ_{mi} is the water content in the micropores (expressed relative to the total volume) [-], t is the time [T], z is the vertical distance [L], K_{mi} is the hydraulic conductivity of the micropores [$L\ T^{-1}$], h_{mi} is the pressure head in the micropores [L], $S_{r,mi}$ is a sink term accounting for root water uptake [T^{-1}] and $\Gamma_{w,mi}$ is a source/sink term indicating water exchange between micropores and macropores (taken positive if flow is from the micropores into the macropores) [T^{-1}].

The total porosity is partitioned into micropores and macropores by a user-defined water content θ_b and a corresponding pressure head h_b and hydraulic conductivity K_b. In the micropores, the water retention relationship is expressed using a modified version of the van Genuchten equation (van Genuchten, 1980):

with:

$$h_{mi} = \frac{1}{\alpha}\left(S_{mi}^{-\frac{1}{m}} - 1\right)^{\frac{1}{n}} \qquad \textit{Eq. 6-13}$$

$$S_{mi} = \frac{\theta_{mi} - \theta_r}{\theta_s^* - \theta_r} \qquad \textit{Eq. 6-14}$$

$$m = 1 - \frac{1}{n} \qquad \textit{Eq. 6-15}$$

where α and n are empirical van Genuchten parameters and θ_r is the residual water content in the micropores [-]. The parameter θ_s^* is the fictitious saturated water content [-], obtained by extending the $h_{mi}(S_{mi})$ relationship beyond h_b as shown in Figure 6-3. It is used in the model to allow temporary oversaturation of the micropores, before the excess water is routed into the macropores.

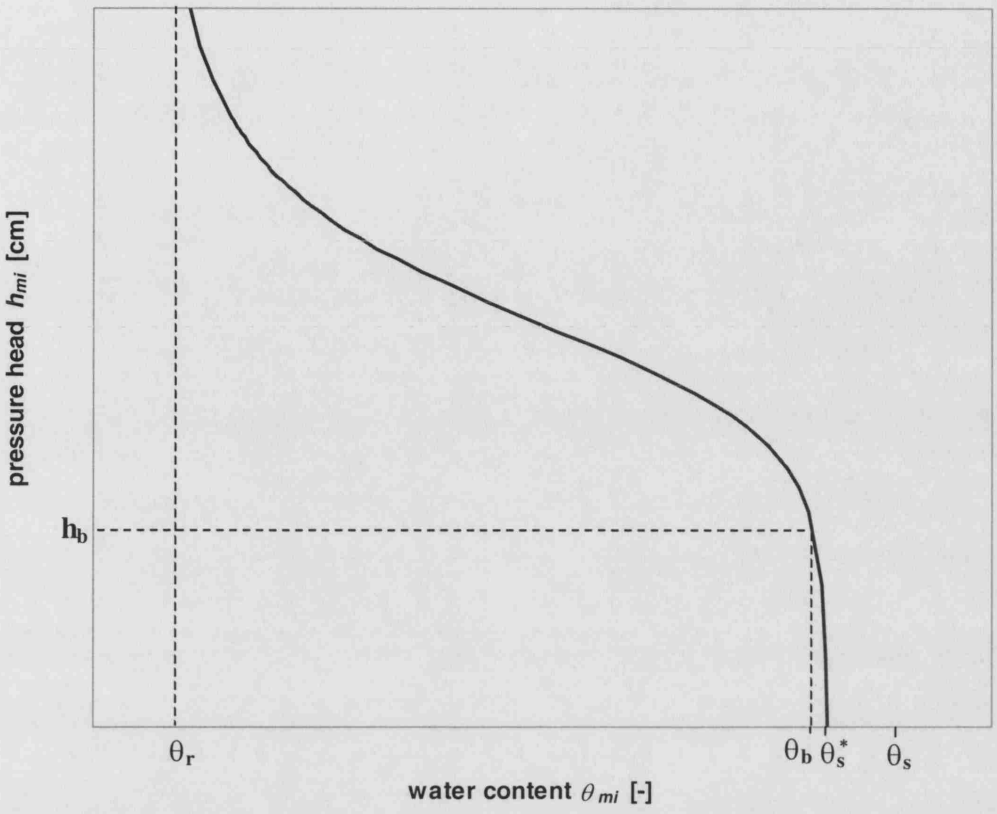

Figure 6-3 Modified van Genuchten model for the water retention curve (Eq. 6-13 to Eq. 6-15). θ_b is the true saturated water content of the micropores, θ_s^* is the fictitious saturated water content of the micropores, and θ_s is the total saturated water content including the macropores. Note that the pressure head is not defined in the macropores.

The unsaturated hydraulic conductivity function is derived according to a modified version of Mualem's (1976) model (Luckner et al., 1989):

$$K_{mi}(\theta_{mi}) = K_b\left(\frac{S_{mi}}{S_{mi(h_b)}}\right)^{\lambda}\left[\frac{1-\left(1-S_{mi}^{\frac{1}{m}}\right)^{m}}{1-\left(1-S_{mi(h_b)}^{\frac{1}{m}}\right)^{m}}\right]^2 \qquad \textit{Eq. 6-16}$$

where λ is the tortuosity factor in the micropores [-], and $S_{mi(hb)}$ is defined as:

$$S_{mi(h_b)} = \left[1+(\alpha h_b)^n\right]^{-m} \qquad \textit{Eq. 6-17}$$

K_b is the saturated hydraulic conductivity of the micropores, marking the boundary between micropores and macropores [L T^{-1}].

6.2.2.2 Macropores

For the unsaturated macropores, MACRO assumes gravity flow, ignoring capillary suctions:

$$\frac{dh_{ma}}{dz} = 0 \qquad \textit{Eq. 6-18}$$

$$\frac{dH_{ma}}{dz} = \frac{dh_{ma} + dz}{dz} = 1 \qquad \textit{Eq. 6-19}$$

As a result the pressure head is not required in the macropores. The governing equation for unsaturated flow in the macropores is then, based on the moisture-based form of Richards' equation (Eq. 2-8):

$$\frac{\partial \theta_{ma}}{\partial t} = \frac{\partial K_{ma}}{\partial z} - S_{r,ma} - \Gamma_{w,ma} \qquad \textit{Eq. 6-20}$$

where $\Gamma_{w,ma}$ is taken positive if the flow is from the macropores into the micropores ($\Gamma_{w,ma} = -\Gamma_{w,mi}$).

A kinematic wave approach is used, where the hydraulic conductivity function in the macropores is given as a simple power law expression of the degree of saturation in the macropores S_{ma} (Beven and Germann, 1981; Charbeneau, 1989):

$$K_{ma} = K_{ma,s}(S_{ma})^{n^*} \qquad \textit{Eq. 6-21}$$

with:

$$S_{ma} = \frac{\theta_{ma}}{\theta_s - \theta_b} \qquad \textit{Eq. 6-22}$$

where $K_{ma,s}$ is the saturated hydraulic conductivity of the macropores [L T^{-1}], θ_{ma} is the water content in the macropores [-], θ_s is the total saturated water content [-] and n^* is the pore size distribution index of the macropores [-].

6.2.2.3 Water exchange

Lateral water flow is possible between both flow domains, as introduced above by the exchange term Γ_w [T^{-1}]. Water exchange from macropores to micropores can occur when the macropores are active, but the micropores are not fully saturated. The exchange is based on a first-order approximation of the water diffusion equation,

assuming a rectangular-slab geometry for the aggregates (Gerke and van Genuchten, 1993b):

$$\Gamma_w = \left(\frac{3\,D\,\gamma_w}{a^2}\right)(\theta_b - \theta_{mi}) \qquad \textit{Eq. 6-23}$$

where a is the effective diffusion pathlength (i.e. half the slab width) [L] and γ_w is an empirical scaling factor obtained by comparing the first-order approach to a numerical solution of the horizontal diffusion equation [-]. Jarvis and Larsson (1998) obtained an average value of 0.8 for the scaling factor, and in MACRO γ_w is fixed to this value. D is the effective water diffusivity [$L^2\,T^{-1}$], given by:

$$D = \left(\frac{D_{\theta_b} + D_{\theta_{mi}}}{2}\right) S_{ma} \qquad \textit{Eq. 6-24}$$

S_{ma} is introduced to account for an incomplete wetted contact area between macropores and micropores, and $D_{\theta_{mi}}$ and D_{θ_b} are the water diffusivities at the current micropore water content and the boundary water content respectively [$L^2\,T^{-1}$], defined as (van Genuchten, 1980):

$$D_{\theta_{mi}} = \frac{(1-m)K_s^*}{\alpha m(\theta_s^* - \theta_r)} S_{mi}^{\lambda-1/m}\left[\left(1-S_{mi}^{1/m}\right)^{-m} + \left(1-S_{mi}^{1/m}\right)^{m} - 2\right] \qquad \textit{Eq. 6-25}$$

$$D_{\theta_b} = \frac{(1-m)K_s^*}{\alpha m(\theta_s^* - \theta_r)} S_{mi(h_b)}^{\lambda-1/m}\left[\left(1-S_{mi(h_b)}^{1/m}\right)^{-m} + \left(1-S_{mi(h_b)}^{1/m}\right)^{m} - 2\right] \qquad \textit{Eq. 6-26}$$

where λ is tortuosity factor of the micropores, $S_{mi(hb)}$ is defined by *Eq. 6-17* and K_s^* is the fictitious saturated hydraulic conductivity, obtained by extending the unsaturated hydraulic conductivity function of the micropores (Eq. 6-16) to saturated conditions ($S_{mi} = 1$):

$$K_s^* = K_b\left(\frac{1}{S_{mi(h_b)}}\right)^{\lambda}\left[1-\left(1-S_{mi(h_b)}^{1/m}\right)^{m}\right]^{-2} \qquad \textit{Eq. 6-27}$$

The water exchange term given by Eq. 6-23 is driven by the difference between the saturated water content of the micropores and the actual water content in the micropores. This is in contrast with the traditional approach, where the water exchange is driven by a pressure head gradient (Eq. 2-37). Although the pressure-

based approach is more physically based, it requires the water retention curve to be defined in both flow domains, which often proves problematic. Instead, Eq. 6-23 inherently assumes that, during water exchange from the macropores to the micropores, the interface instantaneously reaches pressure equilibrium at the air-entry pressure of the macropores (Simunek et al., 2003).

Water exchange in the opposite direction, from micropores to macropores, may occur when the micropores become saturated. This can happen at the soil surface or if the micropore hydraulic conductivity decreases with depth. In this situation, the excess water ($\theta - \theta_b$) is instantaneously routed into the macropores.

Note that in the present MACRO 5.0 version, the geometry of the dual permeability medium is fixed to rectangular slabs. It would be useful to include the possibility to simulate other geometries, such as cylindrical wormholes or spherical inter-aggregate pores. As a recommendation for a future version of MACRO, the user would be able to choose between different geometries, by adapting the factor 3 in Eq. 6-23 together with the scaling factor γ_w. The block geometry functions proposed by Barker (1985a) could be helpful in this respect.

6.2.3 Transport description

MACRO 5.0 has the ability to simulate reactive solutes, allowing for various formulations of sorption behaviour and for first-order degradation. In this context, however, only conservative solutes will be described, as used in the Fleam Dyke lysimeter experiments.

6.2.3.1 Micropores

Solute transport through the micropores is described by the advection-dispersion equation:

$$\frac{\partial(\theta_{mi(m)} c_{mi})}{\partial t} = \frac{\partial}{\partial z}\left(D_L \theta_{mi(m)} \frac{\partial c_{mi}}{\partial z} - q_{mi} c_{mi} \right) - U_{r,mi} - U_{s,mi} - U_{e,mi} \qquad \textit{Eq. 6-28}$$

where $\theta_{mi(m)}$ is the mobile water content in the micropores (accounting for an excluded water content due to anion exclusion)[-], c_{mi} is the solute concentration in the micropores [M L^{-3}], D_L is the longitudinal dispersion coefficient [L^2 T^{-1}], q_{mi} is the water flow rate through the micropores [L T^{-1}], $U_{r,mi}$ is a sink term accounting for uptake of solutes by the roots [T^{-1}], $U_{s,mi}$ is a sink term accounting for evaporation from the soil (only valid if deuterium or tritium are modeled) [T^{-1}] and $U_{e,mi}$ is a source/sink term indicating solute exchange between micropores and macropores (taken positive if exchange is from micropores into macropores) [T^{-1}].

The longitudinal dispersion coefficient is given by:

$$D_L = \alpha_L |v| + D_0 F \qquad \textit{Eq. 6-29}$$

where α_L is the longitudinal dispersivity [L], v is the effective pore water velocity (given as q_{mi}/θ_{mi}) [L T^{-1}] , D_o is the free-water diffusion coefficient [L^2 T^{-1}] and F is the formation factor [-], defined according to the Millington-Quirk model (1961):

$$F = \frac{\theta_{mi}^{10/3}}{\theta_b^{2}} \qquad \textit{Eq. 6-30}$$

The solute uptake by the roots is given by:

$$U_{r,mi} = f_c S_{r,mi} c_{mi} \qquad \textit{Eq. 6-31}$$

where f_c is a concentration factor varying between zero and unity (Boesten and Vanderlinden, 1991).

For evaporation of deuterium or tritium from the soil surface, the simplification is made that they evaporate at the same rate as the water:

$$U_s = E_s c_{mi,1} \qquad \textit{Eq. 6-32}$$

where $c_{mi,1}$ is the solute concentration in the micropores of the surface layer [M L^{-3}].

6.2.3.2 Macropores

Transport of solutes through the macropores is treated in the same fashion as was used for the micropores, with the exception that dispersion is neglected, so the advection-dispersion equation reduces to:

$$\frac{\partial(\theta_{ma} c_{ma})}{\partial t} = -\frac{\partial(q c_{ma})}{\partial z} - U_{r,ma} - U_{s,ma} - U_{e,ma} \qquad \textit{Eq. 6-33}$$

where θ_{ma} is the water content in the macropores [-] and c_{ma} is the solute concentration in the macropores [M L^{-3}]. The sink/source terms $U_{r,ma}$, $U_{s,ma}$ and $U_{e,ma}$ are treated equally as for the micropores, with $U_{e,ma} = -U_{e,mi}$.

6.2.3.3 Solute exchange

Solute exchange between micropores and macropores can occur both by diffusion and by advection:

$$U_{e,ma} = -U_{e,mi} = \left(\frac{3 D_E \theta_{mi}}{a^2}\right)(c_{ma} - c_{mi}) + \Gamma_{w,ma} c_x \qquad \textit{Eq. 6-34}$$

where $U_{e,ma}$ is taken positive for exchange from macropores into micropores and c_x is either the solute concentration in the macropores if the water flows from macropores to micropores, or the solute concentration in the micropores if vice versa (i.e. donor cell concept). As for water exchange, a rectangular slab geometry is assumed for the aggregates. For diffusion a quasi-steady-state approach is adopted, as it uses the average concentration c_{mi} over the whole micropore domain. D_E is the effective diffusion coefficient [L^2 T^{-1}], given by:

$$D_E = D_0 F S_{ma} \qquad \textit{Eq. 6-35}$$

6.2.4 Initial and boundary conditions

6.2.4.1 Initial condition

Two types of initial conditions can be specified. The user can specify initial water contents over the whole profile, or the profile can be considered in drainage equilibrium with a water table at the bottom.

6.2.4.2 Upper boundary condition

The boundary condition for water flow at the soil surface defines if infiltration will be directed into the micropores or macropores. The net precipitation rate (P_e = precipitation – interception) is first available for soil evaporation, and is then preferably directed into the micropores (I_{mi}). Any excess is directed into the macropores (I_{ma}):

$$I_{mi} = P_e - E_s \qquad \text{if} \quad P_e \le I_{\max} \qquad \text{Eq. 6-36}$$
$$I_{ma} = 0$$

$$I_{mi} = I_{\max} \qquad \text{if} \quad P_e > I_{\max} \qquad \text{Eq. 6-37}$$
$$I_{ma} = P_e - E_s - I_{mi}$$

where I_{max} is the infiltration capacity of the micropores [L T^{-1}], defined as:

$$I_{\max} = K_{top}\left[\frac{(h_{b,1} - h_1)}{\Delta z_1 / 2} + 1\right] \qquad \text{Eq. 6-38}$$

where the subscript *1* refers to the surface soil layer and K_{top} is given by the arithmetic mean of K_b and K_{mi} for the surface layer. When the micropores are saturated, I_{max} is simply given by K_b.

The solute concentration of water directed into the macropores c^*_{ma} [M L^{-3}] is calculated according to the "mixing depth" concept (Steenhuis and Walter, 1980), which assumes that the incoming net precipitation P_e is in instantaneous equilibrium with the water stored in a shallow layer down to the mixing depth z_d:

$$c^*_{ma}(t) = \frac{Q_d(t-\Delta t) + P_e(t)\,c_r(t)}{P_e(t) + z_d\,\theta_{mi,1}(t)} \qquad \textit{Eq. 6-39}$$

where Q_d is the amount of solute stored in the mixing depth [M L^{-2} T^{-1}], Δt is the time step, c_r is the solute concentration in the incoming rainfall [M L^{-3}] and $\theta_{mi,1}$ is the water content in the micropores of the upper soil layer [-]. The amount of solute added to, or removed from, the micropores in the top layer $Q_{mi,1}$ [M L^{-2} T^{-1}] is then calculated as:

$$Q_{mi,1} = P_e\,c_t - I_{ma}\,c^*_{ma} \qquad \textit{Eq. 6-40}$$

6.2.4.3 Lower boundary condition

Four different options are available for the bottom boundary condition of water flow:

1. *Known hydraulic gradient.*
2. *Lysimeter.* The pressure head at the bottom boundary is set to zero, but no upward flow is allowed.
3. *Known pressure head* (either constant or time-dependent).
4. *Water table located in the profile.*

For the first two boundary conditions, the solute flux out of the bottom layer is calculated by assuming zero dispersion. For the other boundary conditions, a constant solute concentration at the bottom boundary is assumed. When the solutes do not reach the lower boundary, as in the case of the Fleam Dyke tracer experiment, the choice of the lower boundary condition becomes less important.

6.2.5 Numerical procedure

For each time step, the calculations are decoupled with respect to the two flow domains. First, the water and solute fluxes in the micropores are calculated. A water balance is then constructed to determine the quantity of water directed into the macropores. Finally, the solute balance is computed using the fluxes from the water balance, to obtain the solute concentrations in the micropores and the macropores. Implicit solutions are used throughout the programme, and up to 200 computational layers are allowed, which normally ensures a high degree of numerical accuracy.

6.3 Inverse modelling procedure: SUFI

6.3.1 Parameter estimation and uncertainty

MACRO is a powerful modelling tool, as it comprises all the main processes involved in unsaturated flow and transport in dual permeability media. As a result of this, however, its main drawback is the high number of parameters to be estimated. For example, for one-dimensional simulation of conservative transport through a dual permeability medium consisting of one single layer, more than 20 parameters need to be defined. When modelling transport of reactive solutes through several layers with contrasting physical properties, the number of parameters to be estimated will be even higher. Hence site-specific measurements of physical and chemical properties are essential, supplemented by literature values and expert knowledge where necessary. However, direct measurement of some parameters can be either impossible or too costly, and expert knowledge often proves insufficient for site-specific behaviour. Thus, to deal with uncertainty in model input parameters, calibration of some key parameters often remains essential. For calibration of parameters in MACRO, the inverse modelling technique called SUFI has been provided. A description of the SUFI algorithm has been included in section 6.3.3, but first a short general overview of calibration techniques is presented.

6.3.2 Calibration techniques

Calibration of a mathematical model means the estimation of values for the model parameters. This involves measurements of dependent variables (e.g. water content, pressure head, solute concentration) and conditioning the model parameters (e.g. hydraulic conductivity, porosity, dispersivity) such that the simulated variables closely match the measured variables.

Two types of calibration techniques are commonly used: manual adjustment and automated calibration. With manual adjustment, also called trial-and-error calibration, the model is run repeatedly by the user and the parameters are changed by hand after each run, based on judgement by the user. On the other hand, automated

calibration, also called inverse modelling, uses a parameter optimization algorithm that guides the calculation of the parameter updates. The forward equation is solved repeatedly and the algorithm is based on the minimization of an objective function that describes the difference between simulated and measured variables (Zheng and Bennett, 1995). Several authors have presented reviews of inverse modelling in hydrogeology, either for the estimation of the permeability field in the saturated zone (e.g. de Marsily et al., 1999; McLaughlin and Townley, 1996; Sun, 1994; Yeh, 1986) or for the estimation of flow and transport parameters in the unsaturated zone (Kool et al., 1987). One of the most popular methods is the Gauss-Newton search algorithm (e.g. Jahns, 1966) and several modifications on this. An alternative is offered by gradient-based searches, like the functional steepest descent algorithm (e.g. Jacquard and Jain, 1965).

6.3.3 Description of SUFI

The inverse modelling technique linked to MACRO uses a very different approach to either the Gauss-Newton algorithm or gradient-based searches. SUFI stands for Sequential Uncertainty FItting, and is forward, sequential, iterative and Bayesian in nature (Abbaspour et al., 1997). It has been implemented and added to the shell program of MACRO 5.0. The method starts from prior uncertainty domains for each parameter, which can be based on literature values or expert knowledge. Subsequently the uncertainty is reduced by conditioning the model parameters on measured data through an objective function. This leads to a posterior uncertainty domain, where the prior uncertainty is reduced through calibration. A user-defined stopping rule imposed on the objective function defines when convergence has been reached.

At the start of the optimization problem a prior uncertainty domain needs to be defined for each parameter p_i (i=1,2...n), assuming a uniform distribution. This uncertainty domain is then divided into a user-defined number m_{pi} of equal-probability strata, with parameter values defined as the midpoint of each stratum. The next step consists in stratified sampling from the space of uncertain parameters and running MACRO for each sampled parameter combination. SUFI gives the option

between two types of sampling schemes. In the exhaustive stratified sampling, all possible parameter combinations are used, whereas in the random stratified sampling, only a randomly selected subset of the combinations are used. Exhaustive stratified sampling leads to a number of permutations $M = m_{p1} m_{p2} .... m_{pn}$, which can cause excessively long computation times, hence the use of random stratified sampling is often a more realistic option. After execution of MACRO for all the sampled parameter combinations, an objective function needs to be defined, which is a measure of the difference between measured and simulated variables. SUFI gives the option of choosing between the following objective functions:

Average model efficiency

$$g = \sum_{i=1}^{n} |x_m - x_s|_i \qquad \textit{Eq. 6-41}$$

Root-mean-square error (RMSE)

$$g = \sqrt{\frac{1}{n} \sum_{i=1}^{n} (x_m - x_s)_i^2} \qquad \textit{Eq. 6-42}$$

Logarithmic form of RMSE (LRMSE)

$$g = \sqrt{\frac{1}{n} \sum_{i=1}^{n} (\log x_m - \log x_s)_i^2} \qquad \textit{Eq. 6-43}$$

where x_m is the measured variable, x_s is the simulated variable and n is the number of measurements.

As the next step in the iteration procedure, the objective function is calculated for each model realization. A user-defined critical value is then selected for the objective function, and any realization leading to a value of the objective function below the critical value results in a hit and one point is added to the score for each parameter stratum of that realization. The scores are then counted up for each parameter stratum, and a frequency distribution is obtained for each parameter. Strata having a low number of hits are eliminated at both ends of the parameter domain, resulting in an updated, narrower domain with reduced uncertainty. The updated domain will then serve as the basis for the next iteration, and the whole procedure is repeated until the objective function cannot be reduced any further.

If more than one measured variable is being used as optimization target, then the objective functions of each variable need to be combined into the final objective function. Two different types of combined objective functions can be used, the additive function and the multiplicative function (Abbaspour et al., 1999):

Additive form

$$h = \sum_{i=1}^{n} w_i \, g_i \qquad \textit{Eq. 6-44}$$

Multiplicative form

$$h = \prod_{i=1}^{n} g_i \qquad \textit{Eq. 6-45}$$

where n is the number of variables, w_i is a weighting factor for variable i and g_i is a simple objective function for variable i (i.e. either of Eq. 6-41, Eq. 6-42 or Eq. 6-43). The advantage of the multiplicative form is that it eliminates the need for weighting factors. Abbaspour et al. (1999) showed that the multiplicative form could perform the same or better than the more traditional additive form. In addition to its use with MACRO, the multiplicative form in SUFI has also been successfully applied to inverse modelling with the simulation programs LEACHM (Schmied et al., 2000) and HYDRUS5 (Abbaspour et al., 2000; Sonnleitner et al., 2003).

An important feature of SUFI is that it is not a method of steepest descent, and therefore it is less prone to convergence problems (Abbaspour et al., 2000). Because it is a global search algorithm it is also less likely to fall into local minima (Roulier and Jarvis, 2003). For a complex simulation model like MACRO 5.0, it may therefore be more appropriate than a gradient method. To further avoid falling into local minima, the critical value of the objective function should be set high enough. The main drawback of the method is the high number of realizations needed, adding to computing time. As shown above, this can be reduced by choosing random stratified sampling instead of exhaustive stratified sampling.

6.4 Case studies of MACRO use

MACRO has found application in a wide range of field and lysimeter studies on unsaturated flow and transport. A selection of published studies is shown in Table 6-1. Applications have been mainly limited to soils, with occasional applications to landfills. The use of MACRO in studies of fractured rock has not previously been attempted.

Table 6-1 Overview of selected applications of MACRO.

Medium	Solute	Reference
Sand and clay soil	^{3}H and ^{36}Cl	Saxena et al. (1994)
Silt loam soil	herbicides	Jarvis (1995)
Glacial till soil	chloride	Villholth and Jensen (1998)
Sandy soil	bromide	Larsson et al. (1999)
Clay soil	bromide and bentazone	Larsson and Jarvis (1999)
Landfill	salt	Johnson et al. (2001b)
Humus-rich soil	bromide, chloride and ^{2}H	Kätterer et al. (2001)
Clay soil	herbicides	Cuevas et al. (2003)

6.5 Suitability for the unsaturated zone of the Chalk

The dual permeability approach adopted for macropores in MACRO appears to be equally applicable to a fractured porous medium as the Chalk, with the macropores representing the fractures and the micropores representing the matrix. The classical combination of advection dispersion equation and Richard's equation is used for the matrix, and gravity flow in the fractures is generated to drain any excess water once the matrix gets fully saturated. Diffusion of solutes between fractures and matrix is represented by a quasi-steady-state approach, by averaging the solute concentration over the width of a matrix block. A rectangular slab geometry is used for the macropores in MACRO, which corresponds well with the fracture geometry in the Chalk. In addition, MACRO allows for advective exchange between both flow

domains, occurring when the macropores are active but the micropores are not saturated or when the hydraulic conductivity of the micropores decreases with depth. Possibly this could allow for pressure-driven flow between fractures and matrix in the Chalk, as suggested by Price et al. (2000).

The application of MACRO 5.0 to a fractured porous medium also involves some challenges. First, the validity of the use of the van Genuchten equations for the hydraulic characterization of the chalk matrix is uncertain. The van Genuchten equations are primarily designed for soils, and may have limited use for porous rocks. Second, the quasi-steady-state approach for diffusive exchange between the fractures and the matrix may prove inadequate. It assumes that the changes in the fractures are slow compared to the time for approaching diffusive equilibrium (Barker, 1993). This could introduce errors at early times. Moreover, the ignoring of capillary suction and dispersion in the fracture domain may be overly simplistic. Finally, MACRO 5.0 can only simulate vertical fractures, but no horizontal fractures. In the chalk unsaturated zone, horizontal or sub-horizontal fractures, like bedding planes, are likely to occur. When a horizontal fracture is empty, it may form a capillary barrier for vertical flow through the matrix, the cross-flow being confined to the contact points between the matrix blocks. Mathias et al. (2004) stated that a connectivity between the matrix blocks of just 1% would be sufficient to allow non-restrictive flow across the matrix blocks. As the connectivity of fractures in the Chalk is likely to be greater than 1%, the presence of horizontal fractures may after all not have such a great influence on the matrix flow.

7 Flow simulation through unsaturated chalk using MACRO 5.0

7.1 Introduction

As was shown in Chapter 3 there remains significant uncertainty about recharge through unsaturated chalk, in particular the role of the fractures in the flow process. In this chapter flow through the unsaturated zone of the Chalk is modelled with MACRO 5.0, introduced in Chapter 6. A good quality dataset was available for the Fleam Dyke research site. At this site observations are available of lysimeter drainage, water contents and pressure heads for the period 1980-1981, and these were used to refine the developed model through calibration. The model was then validated against lysimeter drainage data for the period 1999-2003. This chapter starts with a description of the data inputs to the model, and is followed by a description of the flow calibration process and the results of calibration and validation.

7.2 Input data for MACRO simulation

7.2.1 Driving variables

The MACRO model was run for the period 4 June 1980 until 31 December 1981, covering one complete recharge season. For this period, the BGS had calculated potential evapotranspiration (PET) by the method of Penman-Monteith with a daily time step (section 7.2.1.1), based on meteorological data recorded on site. These daily PET data, together with daily rainfall data measured by the Fleam Dyke rain gauge, were used as driving variables for MACRO.

7.2.1.1 Potential evapotranspiration

Daily values of potential evapotranspiration (PET) are required as input for MACRO 5.0. Therefore PET was calculated from local daily meteorological data according to the Penman-Monteith equation, as documented in Allen et al. (1994):

$$PE_t = \frac{1}{\lambda_w}\left[\frac{\Delta(R_n - G) + 86.4\rho_a c_p \frac{e_s - e_d}{r_a}}{\Delta + \gamma_p\left(1 + \frac{r_s}{r_a}\right)}\right] \qquad \textit{Eq. 7-1}$$

where PE_t is the total potential evapotranspiration [mm d^{-1}]. Each of its components is now explained.

- λ_w is the latent heat of evaporation of water [MJ/kg] (Harrisson, 1963):

$$\lambda_w = 2.501 - 0.002361 T_w \qquad \textit{Eq. 7-2}$$

  where T_w = surface temperature of the water [°C]. In practice, T_w can be approximated by the air temperature T.

- Δ is the slope of the saturation vapour pressure curve [kPa $°C^{-1}$] (Murray, 1967):

$$\Delta = \frac{4098\ e_s}{(T + 237.3)^2} \qquad \textit{Eq. 7-3}$$

  where T = air temperature [°C]

- e_s is the saturated vapour pressure [kPa] (Wallace and Hobbs, 1977):

$$e_s = 0.6108\ \exp\left(\frac{17.27\ T}{237.3 + T}\right) \qquad \textit{Eq. 7-4}$$

- e_d is the actual vapour pressure [kPa] (Rosenberg et al., 1990):

$$e_d = e_{s,T_{wb}} - 0.000661\ P_a\ (T - T_{wb})(1 + 0.00115\ T_{wb}) \qquad \textit{Eq. 7-5}$$

  where P_a = atmospheric pressure [kPa]

  $e_{s,Twb}$ = saturated vapour pressure at the wet bulb temperature (kPa)

  T_{wb} = wet bulb temperature [°C]

- R_n is the net incoming radiation [MJ m^{-2} day^{-1}] (Shuttleworth, 1992):

$$R_n = (1-\alpha^*)S_t - \left(0.9\frac{n_s}{N_d}+0.1\right)\left(0.34-0.14\sqrt{e_d}\right)\sigma(273.3+T)^4 \qquad \textit{Eq. 7-6}$$

where α^* = albedo [-]

S_t = incoming solar radiation [MJ m^{-2} d^{-1}]

n_s = number of bright sunshine hours a day [h]

N_d = total day length [h]

e_d = vapour pressure [kPa]

σ = Stefan-Boltzmann constant = 4.903E-09 [MJ m^{-2} $K^{-4}day^{-1}$]

- G is the outgoing heat conduction into the soil [MJ m^{-2} day^{-1}], which for daily temperature fluctuations becomes (Shuttleworth, 1992):

$$G = 0.38\left(T_{s,day2} - T_{s,day1}\right) \qquad \textit{Eq. 7-7}$$

where $T_{s,\,day1}$ = soil temperature at day 1

$T_{s,\,day2}$ = soil temperature at day 2

- ρ_a is the atmospheric density [kg m^{-3}] (Shuttleworth, 1992):

$$\rho_a = 3.486\frac{P_a}{275+T} \qquad \textit{Eq. 7-8}$$

- c_p is the specific heat of moist air = 1.013 [kJ kg^{-1} $°C^{-1}$]

- γ_p is the psychrometric constant [kPa $°C^{-1}$], defined as (Brunt, 1952):

$$\gamma_p = 0.0016286\frac{P_a}{\lambda_w} \qquad \textit{Eq. 7-9}$$

- r_a is the aerodynamic resistance [s m^{-1}], given by (Shuttleworth, 1992):

$$r_a = \frac{\ln\left[\frac{(z_u-d)}{z_{om}}\right]\ln\left[\frac{(z_e-d)}{z_{ov}}\right]}{0.1681\,u} \qquad \textit{Eq. 7-10}$$

where z_u = height of the wind speed measurement [m]

z_e = height of the humidity measurement [m]

z_{om} = roughness parameter for momentum [m]

z_{om} = roughness parameter for heat and water vapour [m]

d = zero plane displacement of wind profile [m]

u = wind speed [m s^{-1}]

Estimates are made by assuming that $z_{om} = 0.123 \times h_c$ and $z_{ov} = 0.0123 \times h_c$ (Monteith and Unsworth, 1990), and that $d = 0.67 \times h_c$, where h_c is the mean vegetation height.

- r_s is the surface resistance [s m^{-1}], which can be approximated by (Allen, 1986):

$$r_s = \frac{200}{LAI} \qquad \textit{Eq. 7-11}$$

where LAI = total leaf area index [-]

7.2.2 Initial and boundary conditions

As initial conditions, water contents were provided as input for each numerical layer. Water contents for 4 June 1980 were available from the neutron probe measurements by the BGS in the Fleam Dyke lysimeter.

Upper boundary conditions were provided by daily PET and rainfall data as driving variables. As a lower boundary condition, the bottom lysimeter boundary condition was chosen (see section 6.2.4.3).

7.2.3 Crop parameters

The Fleam Dyke lysimeter is covered with grass, which is a perennial crop. The crop parameters required in MACRO are shown in Table 7-1. For the leaf area index, the value for a reference crop was chosen, i.e. an idealized grass crop (Shuttleworth, 1992). The values for the root depth and the root distribution were recommended by J. Finch (personal communication). For the critical air content and the canopy interception capacity, values were taken as suggested for grassland in the ANSWERS

model (Beasley and Huggins, 1991). Other parameters were set to their default values in MACRO.

Table 7-1 Parameter values for the grass crop.

Symbol	Description	Value
z_r	root depth [m]	0.8
LAI	leaf area index [-]	2.88
ζ	root distribution factor [(1)] [-]	70
$\frac{\theta_{s,i}-\theta_{d,i}}{\theta_{s,i}-\theta_{w,i}}$	fraction of available water exhausted before reduction in transpiration occurs [-]	0.5
$\theta_{s,i}-\theta_{a,i}$	critical air content for root water uptake [-]	0.75
ω^*_c	root adaptability factor [-]	0.5
c_f	correction factor for wet canopy evaporation [-]	1
$W_{c,max}$	canopy interception capacity [mm]	0.75

[(1)] percentage of the total root length present in the upper 25% of the root depth

7.2.4 Strata definition

The unsaturated profile at Fleam Dyke was divided into 5 strata (Table 7-2). The basis of this division were differences in water contents, pressure heads and hydraulic conductivities recorded by the BGS in the 1980s, as illustrated in Figure 7-1. The number of numerical layers was fixed at 60, and the model then automatically assigned these 60 layers over the 5 strata.

Table 7-2 Division of the unsaturated profile at Fleam Dyke into 5 strata

	soil	weathered chalk	chalk-1	chalk-2	chalk-3
Depth (cm)	0-20	20-65	65-150	150-270	270-500
Numerical layers	15	4	8	11	22

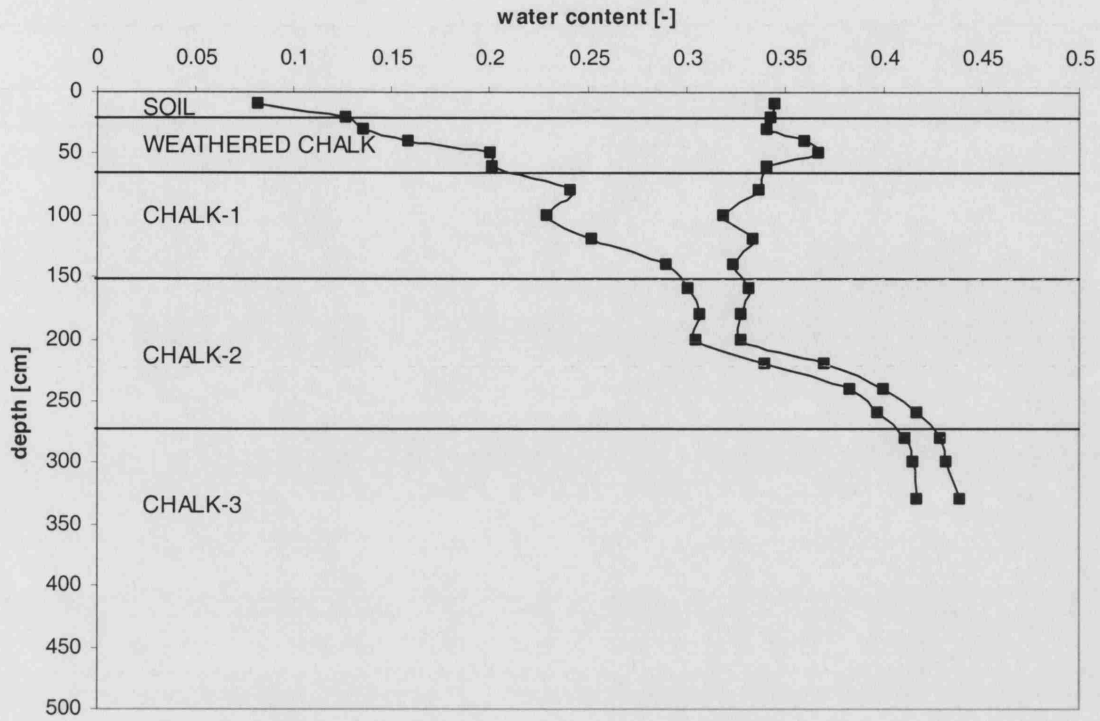

Figure 7-1 Minimum and maximum water contents measured in a grass plot on the Fleam Dyke site between 1978 and 1980 (Data courtesy of the BGS). Also shown is the division of the unsaturated profile in 5 strata, as used in MACRO.

7.2.5 Physical parameters

The use of Richard's equation as implemented in MACRO requires knowledge of two hydraulic functions. These are the water retention curve $h_{mi}(\theta_{mi})$ according to the van Genuchten model (Eq. 6-13) and the unsaturated hydraulic conductivity function $K_{mi}(h_{mi})$ according to the modified Mualem model (*Eq. 6-17*), both defined exclusively for the micropore domain.

Estimations of the van Genuchten-Mualem parameters for each stratum were made based on experimental data obtained in field and laboratory experiments, as explained in the following paragraphs. For the soil stratum, pedotransfer functions were used, whereas for the chalk strata the parameters were obtained by least-square fitting to measured hydraulic functions.

For the soil stratum, no measurements of pressure heads were available and the hydraulic functions had to be estimated by indirect methods. Therefore pedotransfer functions (PTFs) were employed, relating the hydraulic parameters to more readily available information such as particle size distribution and bulk density. The programme ROSETTA was used, which implements PTFs based on neural networks and which has been calibrated against a large database containing 2085 samples (Schaap et al., 1998). As input data the percentages of sand, silt and clay (section 5.5.3) and the bulk density (section 5.5.2) were used. This provided values for θ_s, θ_r, α and n. The tortuosity factor for the micropores λ was set to 0.5 (Mualem's approach). For the saturated hydraulic conductivity K_s, the value was taken from the permeameter measurements (section 5.5.4). For the soil at Fleam Dyke, it was assumed that macropore flow is negligible, i.e. the soil can be considered as a single porous medium. From the soil sampling, no aggregate structure had been observed, and drying cracks are unlikely because of the low clay content. It is still possible that bypass flow through the soil may occur through secondary structures such as decayed root holes and earthworm channels. However, because no data on macropore flow through the soil were available, this aspect was ignored. Macropore flow was thus excluded in the soil stratum by making the boundary hydraulic conductivity K_b approach the saturated hydraulic conductivity K_s. The resulting values for the hydraulic parameters are shown in Table 7-3.

Table 7-3 Estimated hydraulic parameters for use in the van Genuchten / Mualem functions (Eq. 6-13 until Eq. 6-17*)*

Stratum	θ_s^* [-]	θ_r [-]	n [-]	α [cm^{-1}]	λ [-]	K_b [mm/d]	K_s [mm/d]
soil	0.425	0.04	1.57	0.0071	0.5	265	266
weath. chalk	0.26	0	1.13	0.044	0.5	1.7	600
chalk-1	0.28	0	1.10	0.007	0.5	1.4	500
chalk-2	0.31	0	1.10	0.0011	0.5	0.083	100
chalk-3	0.425	0	1.88	0.00005	0.5	1.1	250

For the weathered chalk stratum and the three chalk strata underneath, direct measurements of the hydraulic functions were available for appropriate depths, thanks to the work by the BGS in the 1980s (see section 4.3.2). Water retention curves $h(\theta)$ had been measured on the Fleam Dyke lysimeter itself (Figure 4-10), and unsaturated hydraulic conductivity functions $K(h)$ had been measured on a grassland plot next to the lysimeter (Figure 4-11). For this study, an estimate of the hydraulic parameters for MACRO was obtained for each stratum by simultaneous least-squares fitting of the van Genuchten model and the modified Mualem model to the $h(\theta)$ and $K(h)$ data.

The van Genuchten function has been primarily designed for soils, and its application to a fractured porous rock like the chalk requires some consideration. Apart from its very small pore size and its resulting high capillary rise, the chalk matrix can be regarded as a similar porous medium as a soil. This means that the application of the van Genuchten function to the chalk matrix may be justified. Brouyère (2002) successfully used the van Genuchten function to describe the water retention relationship of both the chalk fractures and the matrix. The method involved two coupled van Genuchten functions, and Mualem's model was used to analytically derive the unsaturated hydraulic conductivity function from the combined water retention relationship. Brouyère's (2002) approach provides an elegant solution for the complex nature of the hydraulic behaviour of the Chalk. However, it assumes pressure equilibrium between matrix and fractures and does not allow for bypass flow. To describe highly transient flow behaviour, the dual permeability approach in MACRO may therefore be more appropriate. In MACRO a simplified gravity flow approach is used for the fractures, without defining the pressure head in the fractures. A single van Genuchten / Mualem function is then used for the matrix only.

Simultaneous fitting of the $\theta(h)$ and $K(h)$ functions was achieved by minimizing the following weighted least squares with the Solver function in Microsoft® Excel:

$$f = \frac{1}{\overline{\theta}}\sqrt{\frac{1}{N_\theta}\sum_{i=1}^{N_\theta}(\theta_{s,i}-\theta_{m,i})^2} + \frac{1}{\overline{K}}\sqrt{\frac{1}{N_K}\sum_{j=1}^{N_K}(K_{s,j}-K_{m,j})^2} \qquad \textit{Eq. 7-12}$$

where $\overline{\theta}$ is the average measured water content, $\overline{K}$ is the average measured hydraulic conductivity, N is the number of data points, and the subscripts s and j refer to fitted

and measured data points respectively. The inverses of the average measured data values were used as weights, as an alternative to the variance, which was unknown here. To reduce the number of fitting parameters, the residual water content θ_r was fixed at zero, and the tortuosity factor for the micropores λ was set to 0.5 (Mualem's approach). Fitting of the hydraulic functions was confined to that part of the data that was thought to describe the matrix component, i.e. for pressure heads below the inflection point in the $K(h)$ function. The saturated hydraulic conductivity K_s (i.e. including the macropore/fracture component) was taken as the hydraulic conductivity that was measured when the pressure head approached zero.

The resulting hydraulic parameters for each stratum are shown in Table 7-3. Figure 7-2 shows the result of the fitting of the hydraulic functions to the data for the weathered chalk at 0.6 m depth. The weathered chalk may be conceptualized as consisting of pebbles of chalk matrix separated by macropores. As such, the weathered chalk resembles a classic aggregated porous medium, whereas the unweathered chalk is a fractured porous medium. From the hydraulic conductivity function in Figure 7-2, a sudden rise is observed at a pressure head of -55 cm H_2O, which is thought to represent the transition between the matrix in the chalk pebbles and the macropores. Fitting of the hydraulic functions was therefore confined to pressure heads below -55 cm H_2O. Obtaining a good fit for both the $\theta(h)$ and $K(h)$ data proved difficult, as can be seen in Figure 7-2. The van Genuchten and Mualem functions share the same parameters n and α, which complicates simultaneous fitting of both functions. Also, it is recognized that the measured hydraulic conductivity function at such shallow depth as 0.6 m must be regarded with some scepticism (Cooper, D., personal communication). Irrigation for the steady state infiltration experiment (section 4.3.2.2) had been applied by a network of nozzles at finite spacing, and this may have introduced non-uniform infiltration conditions at shallow depth. The values obtained for the weathered chalk stratum (Table 7-3) are therefore taken as first estimates, and further calibration of the hydraulic parameters for the weathered chalk stratum is pursued in the next section.

Figure 7-3 shows the fitted hydraulic functions for the chalk-1 stratum. The results show some similarities with the weathered chalk stratum, suggesting that the chalk-1

stratum (65-150 cm depth) may be partly weathered too. This confirms the observations from the core profiles at Fleam Dyke (Figure 5-5), where weathering was detected down to a maximum depth of 165 cm. Figure 7-3 shows a poor fit for the $K(h)$ function, and the hydraulic parameter values are once again used as first estimates for calibration.

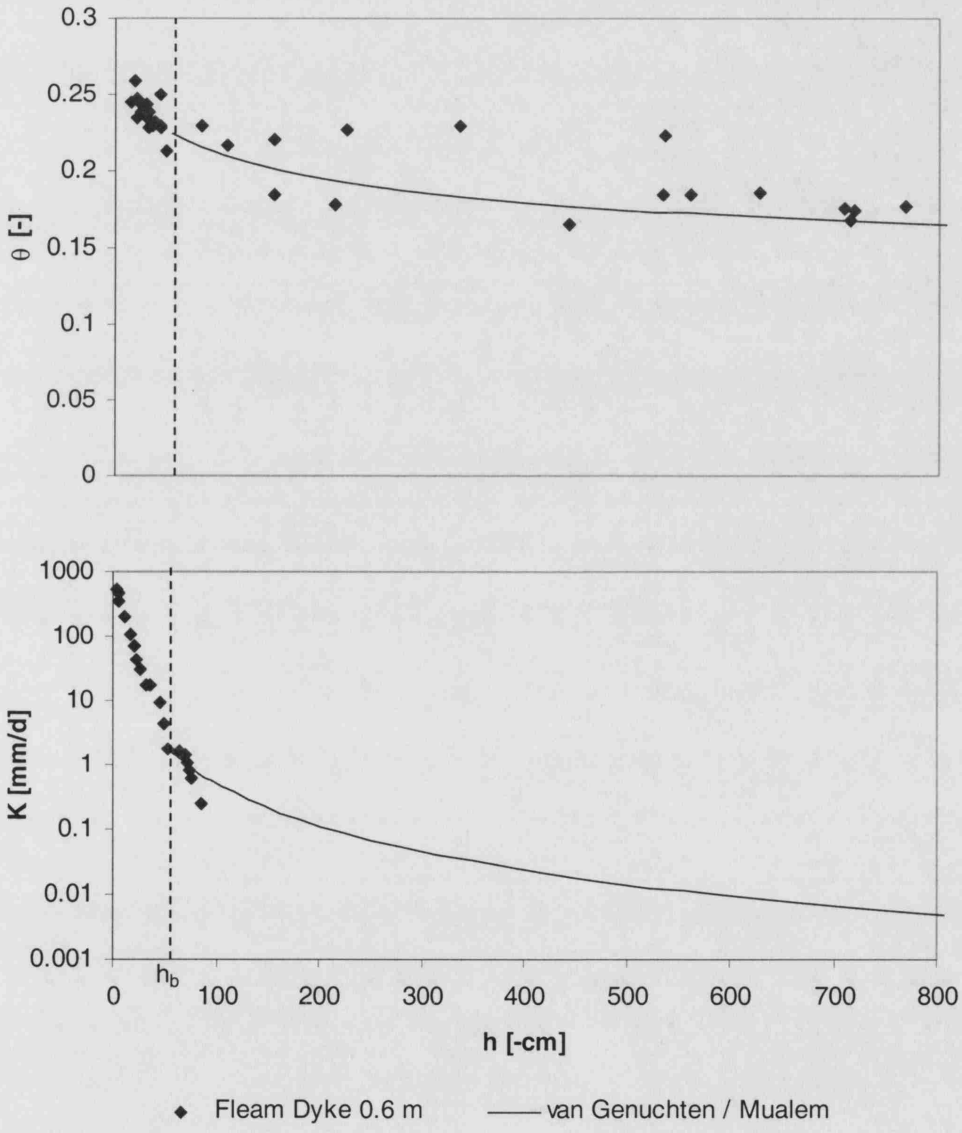

Figure 7-2 Fitting of the van Genuchten function and Mualem's model to the water retention curve and the unsaturated hydraulic conductivity function for the weathered chalk at Fleam Dyke at 0.6 m depth.

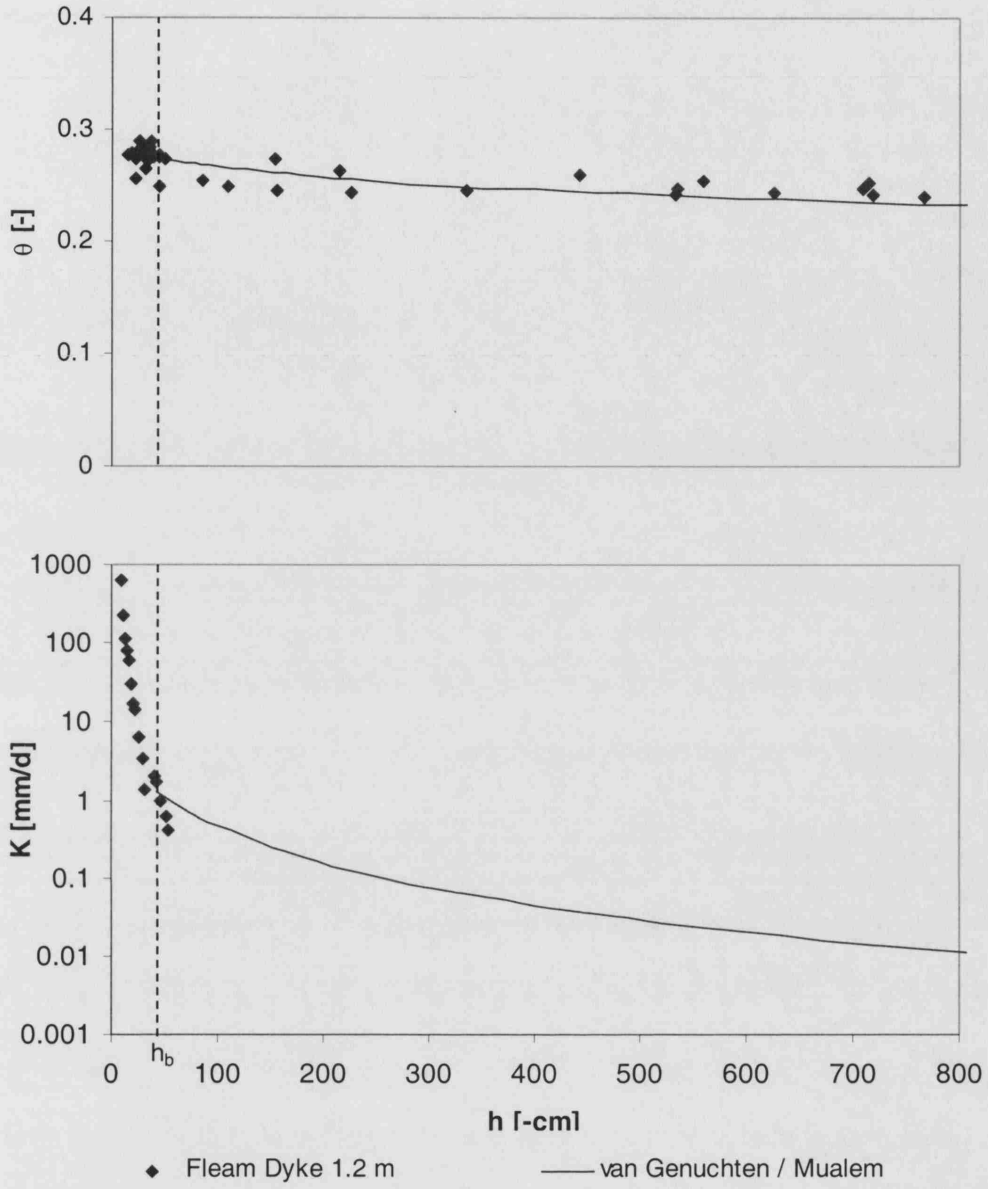

Figure 7-3 Fitting of the van Genuchten function and Mualem's model to the water retention curve and the unsaturated hydraulic conductivity function for the chalk at Fleam Dyke at 1.2 m depth (stratum chalk-1).

A different picture emerges for the strata chalk-2 and chalk-3 (Figure 7-4, Figure 7-5). Here the transition between the chalk matrix and the fractures is more pronounced, and a satisfactory fit is obtained for both the water retention curve and the unsaturated hydraulic conductivity function. Most of the values of the hydraulic parameters for these strata were therefore considered satisfactory, and for those parameters no further calibration was pursued.

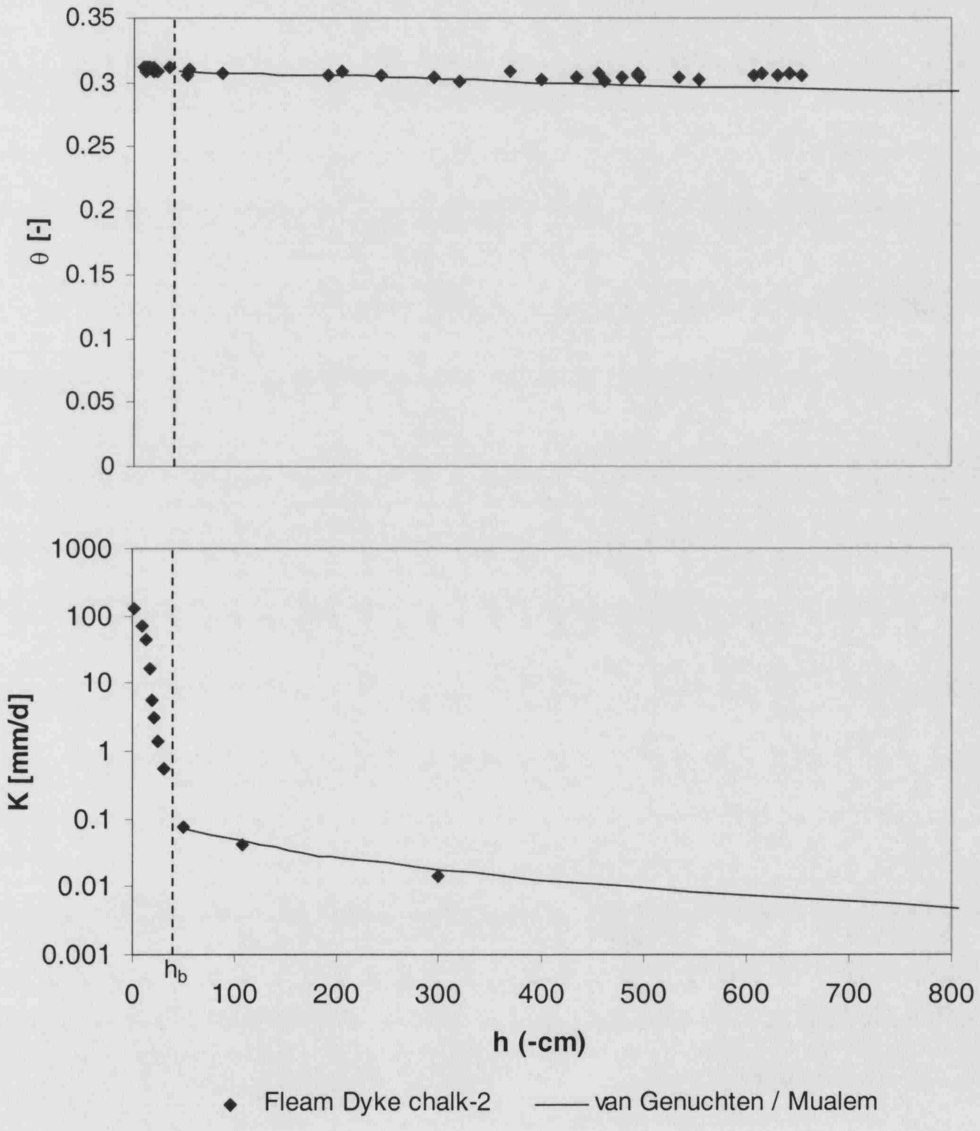

Figure 7-4 Fitting of the van Genuchten function and Mualem's model to the water retention curve and the unsaturated hydraulic conductivity function for the chalk at Fleam Dyke in stratum chalk-2. (The data points for θ(h) are from 2.1 m depth, whereas the data points for K(h) are averages of 1.8, 2.1 and 2.4 m depth).

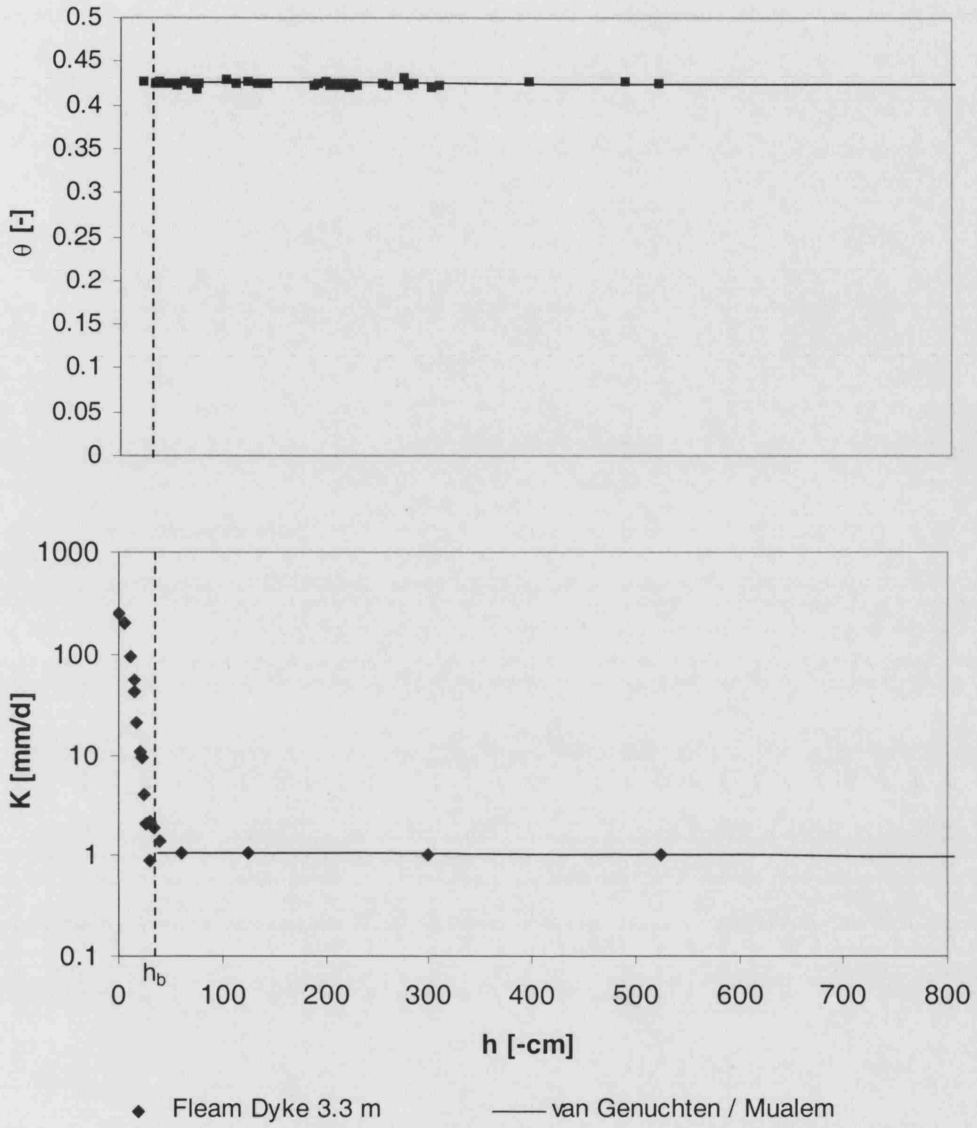

Figure 7-5 Fitting of the van Genuchten function and Mualem's model to the water retention curve and the unsaturated hydraulic conductivity function for the chalk at Fleam Dyke at 3.3 m depth (stratum chalk-3).

In addition to the hydraulic parameters given in Table 7-3, some more physical parameters needed to be defined for each stratum (Table 7-4). The total saturated water content θ_s for the soil was set to approach the fictitious saturated water content θ_s^* of the micropores, to exclude macroporous effects in the soil. In the chalk strata, θ_s was chosen such that the difference between θ_s and θ_s^* was 0.01, i.e. assuming a fracture porosity of 1% for the Chalk. The wilting point θ_w in each stratum was defined as the water content corresponding to a pressure head of –15,000 cm, as found by applying the van Genuchten function (Eq. 6-13) with the parameters in Table 7-3. For the tortuosity factor of the macropores n^*, an intermediate value of 3 was chosen for the weathered chalk, and a low value of 2 for the fractured chalk strata. The diffusion pathlength a represents the aggregate size: for the weathered chalk an aggregate size of 50 mm was chosen, whereas for the chalk strata a matrix block size of 100 mm was chosen. The boundary pressure head h_b for the soil stratum was set close to zero, to minimize macroporous effects. For the chalk strata, h_b was chosen as the inflection point in the unsaturated hydraulic conductivity curve, as shown in Figure 7-2 until Figure 7-5.

Table 7-4 Physical parameters for use in the flow simulation of MACRO, where θ_s is the total saturated water content, θ_w is the wilting point, n^* is the tortuosity factor for the macropores, a is the effective diffusion pathlength and h_b is the boundary pressure head.

Stratum	θ_s [-]	θ_w [-]	n^* [-]	a [mm]	h_b [cm]
soil	0.425	0.07	4	1	0.01
weath. chalk	0.27	0.11	3	50	55
chalk-1	0.29	0.18	2	100	40
chalk-2	0.32	0.24	2	100	40
chalk-3	0.435	0.34	2	100	35

7.3 Initial comparison with measurements

After all parameters values were provided as input to the model, a first run of the unsaturated flow model over the period 4 June 1980 until 31 December 1981 was performed. These prior results are shown in Figure 7-6 until Figure 7-8. Even with these initial parameter estimates, the MACRO model simulated the observations reasonably well. The seasonal occurrence of lysimeter drainage was well described, and generally the simulated water contents closely followed the observed water contents. The model was less successful in simulating the pressure heads, as it failed to predict the low pressure heads observed in the chalk strata during the summer. On closer inspection, the MACRO model also showed limitations in predicting the observed drainage peaks, and it underestimated the cumulative drainage. The dynamics of the water content in the weathered chalk at 0.6 m depth were also not accurately reproduced. In an attempt to improve the model performance, calibration by varying some key parameters is presented in the next section.

7.4 Calibration

7.4.1 Calibration process

The MACRO model involves a large number of parameters, and their values are often either unknown or uncertain. Calibration is therefore essential. For the Fleam Dyke study, the inverse modelling module SUFI was used, which is embedded in MACRO 5.0 (see section 6.3.3). Parameters were selected for calibration where no data were available, or where fitting of the van Genuchten / Mualem parameters to measured hydraulic functions had proved unsatisfactory (see section 7.2.5). Included were the hydraulic parameters for the weathered chalk and the chalk-1 stratum. Other parameters selected for calibration were the tortuosity of the macropores n^*, the fracture porosity θ_s-θ_s^*, the aggregate size a and the root adaptability factor ω^*_c (Table 7-6).

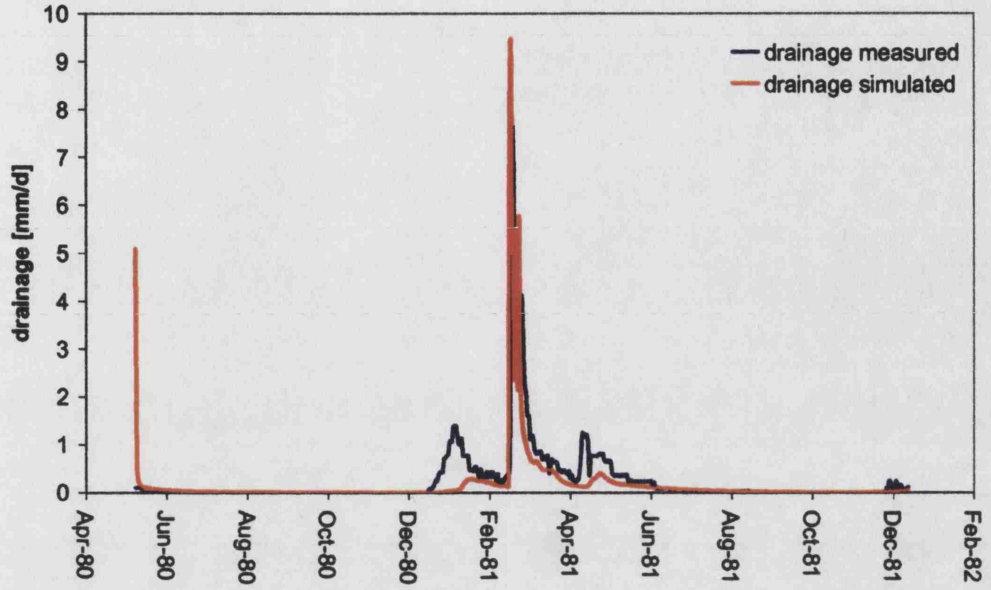

Figure 7-6 Prior results of flow modelling with MACRO 5.0, showing measured versus simulated drainage from the Fleam Dyke lysimeter.

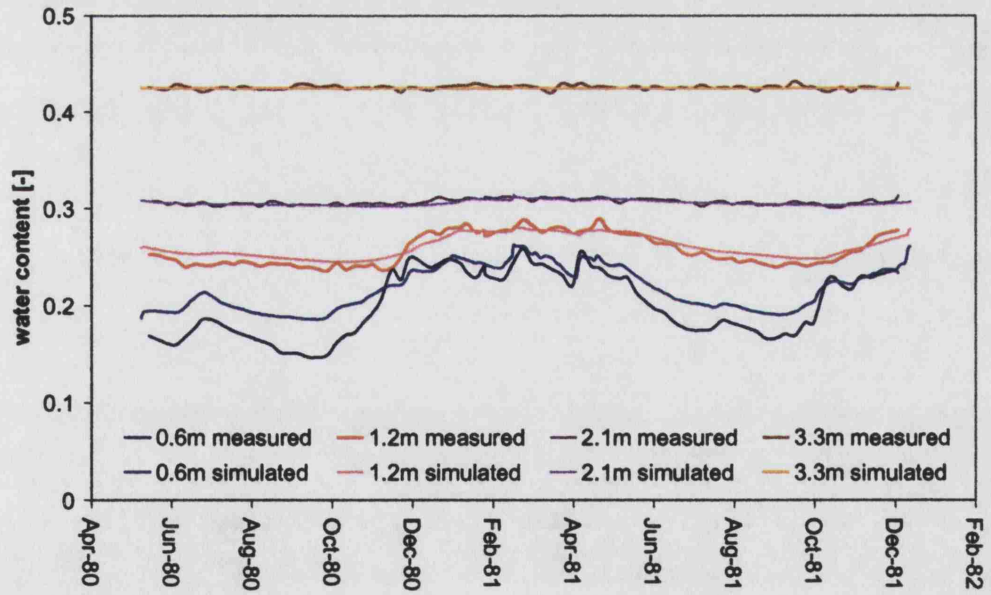

Figure 7-7 Prior results of flow modelling with MACRO 5.0, showing measured versus simulated water contents in the Fleam Dyke lysimeter.

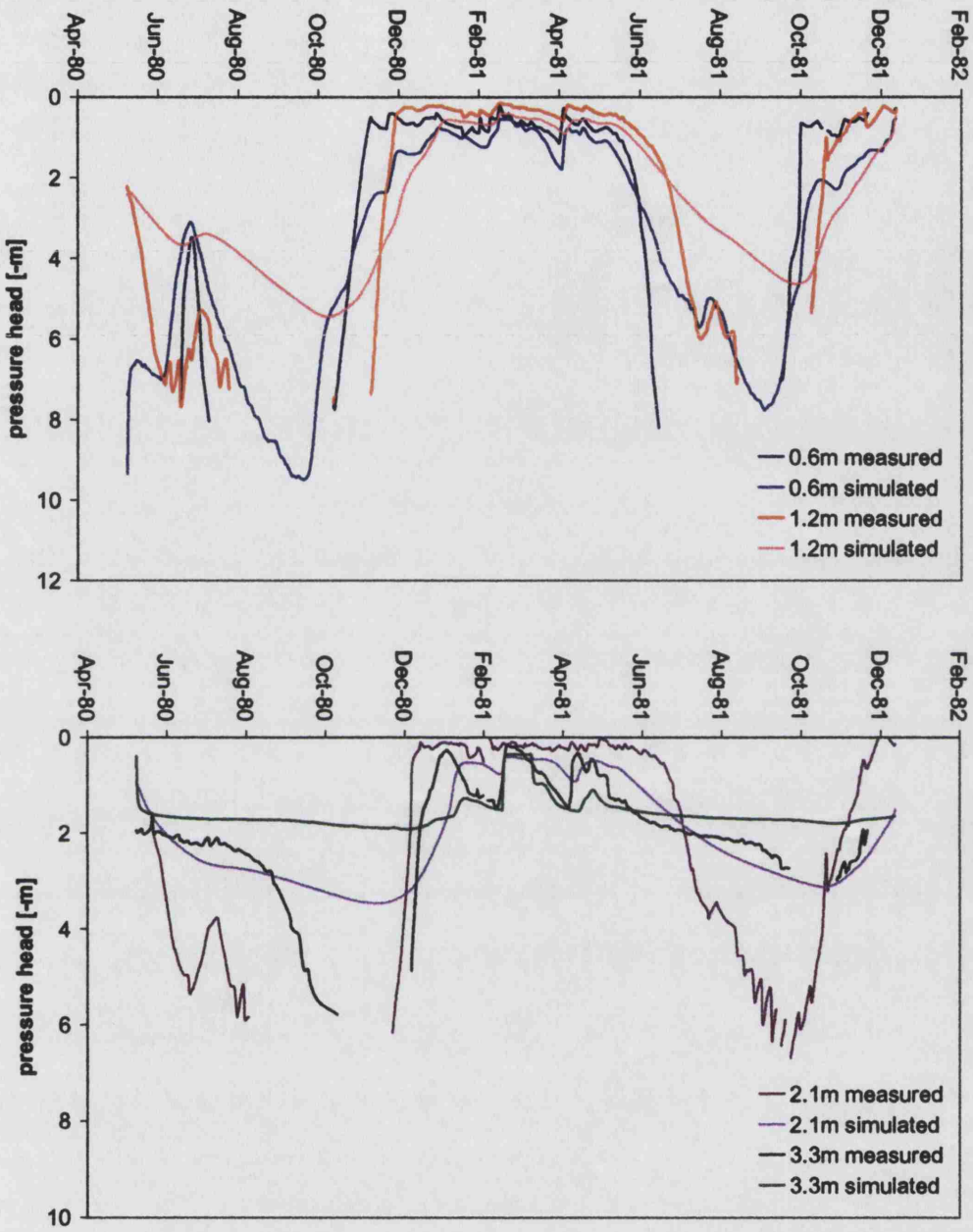

Figure 7-8 Prior results of flow modelling with MACRO 5.0, showing measured versus simulated pressure heads in the Fleam Dyke lysimeter (note that in the summer/autumn period, pressure head data are often missing because the tensiometers went off scale).

As calibration targets, daily data were available of the drainage from the lysimeter and of water contents and pressure heads in each of the four chalk strata. For the soil stratum, no water contents and pressure heads were available, but the parameter estimates for the soil were considered reliable. The objective function was defined as the root-mean-square error between simulated and observed data. A combined objective function was then calculated as the following multiplicative form:

$$O.F. = \sqrt{\frac{1}{N_d}\sum_{t=1}^{N_d}\left(d_s^{(t)} - d_m^{(t)}\right)^2} \times \sqrt{\frac{1}{\sum_{i=1}^{4} N_{\theta i}}\sum_{i=1}^{4}\sum_{t=1}^{N_{\theta i}}\left(\theta_{si}^{(t)} - \theta_{mi}^{(t)}\right)^2} \times \sqrt{\frac{1}{\sum_{j=1}^{4} N_{hj}}\sum_{j=1}^{4}\sum_{t=1}^{N_{hj}}\left(h_{sj}^{(t)} - h_{mj}^{(t)}\right)^2}$$

Eq. 7-13

where d is the lysimeter drainage, N is the number of data points, the subscripts s and m refer to simulated and measured data respectively, i is an index for the water content data in the four chalk strata and j is an index for the pressure head data in the four chalk strata.

Prior uncertainty domains were defined for each parameter included in the calibration (Table 7-6), mainly based on expert knowledge. For the van Genuchten / Mualem parameters, the prior uncertainty domain was based on the range of parameter values that still provided a reasonable fit to the measured hydraulic functions. As a total of 21 parameters were to be estimated, simultaneous calibration of all these parameters was not feasible due to the prohibitive number of simulations involved. It was therefore decided to calibrate the model stratum by stratum, starting on top with the weathered chalk. Random stratified sampling was used, where a subset of between 25 and 60% of all possible parameter combinations is simulated for each iteration. An overview of the iteration process is shown in Table 7-5. Parameters were optimized stratum by stratum, and this procedure was followed twice.

The evolution of the total objective function during the flow calibration process is shown in Figure 7-9. The figure also plots the partial objective functions that make up the total objective function by multiplication (Eq. 7-13). The total objective function was reduced during the calibration by simultaneously improving the fit to the

measured lysimeter drainage and water contents. The figure shows however that the fit to the measured pressure heads could not be improved.

Table 7-5 Summary of iterations during flow calibration for the Fleam Dyke site, showing the parameters that were changed in each iteration and the number of runs for each iteration.

Iteration	Parameters	Runs	Comments
1	-	1	Prior parameter estimates
2	$\theta_{s,2}$; $K_{b,2}$; n_2 ; α_2	144	Hydraulic parameters for weathered chalk
3	ω^*_c	10	Root adaptability factor; resulted in increase in objective function, but chosen such that cumulative drainage was well described
4	$\theta_{s,2}$; $K_{b,2}$; n_2 ; n^*_2	120	Hydraulic parameters for weathered chalk
5	$\theta_{s,3}$; $K_{b,3}$; n_3 ; α_3	120	Hydraulic parameters for chalk-1
6	$\theta_{s,3}$; $K_{b,3}$; n_3 ; n^*_3	163	Hydraulic parameters for chalk-1
7	$K_{b,4}$; n^*_4 ; n^*_5	400	Macropore parameters for chalk-2 and chalk-3
8	$K_{b,2}$; n_2 ; α_2 ; n^*_2 ; $h_{b,2}$	488	Hydraulic parameters for weathered chalk
9	$K_{b,3}$; n_3 ; α_3 ; n^*_3	229	Hydraulic parameters for chalk-1
10	$K_{b,4}$; n^*_4 ; n^*_5	265	Macropore parameters for chalk-2 and chalk-3
11	$\theta_{s,2}$; a_2 ; $\theta_{s,3}$; a_3	64	Macropore parameters for weathered chalk and chalk-1
12	$\theta_{s,4}$; a_4 ; $\theta_{s,5}$; a_5	447	Macropore parameters for chalk-2 and chalk-3

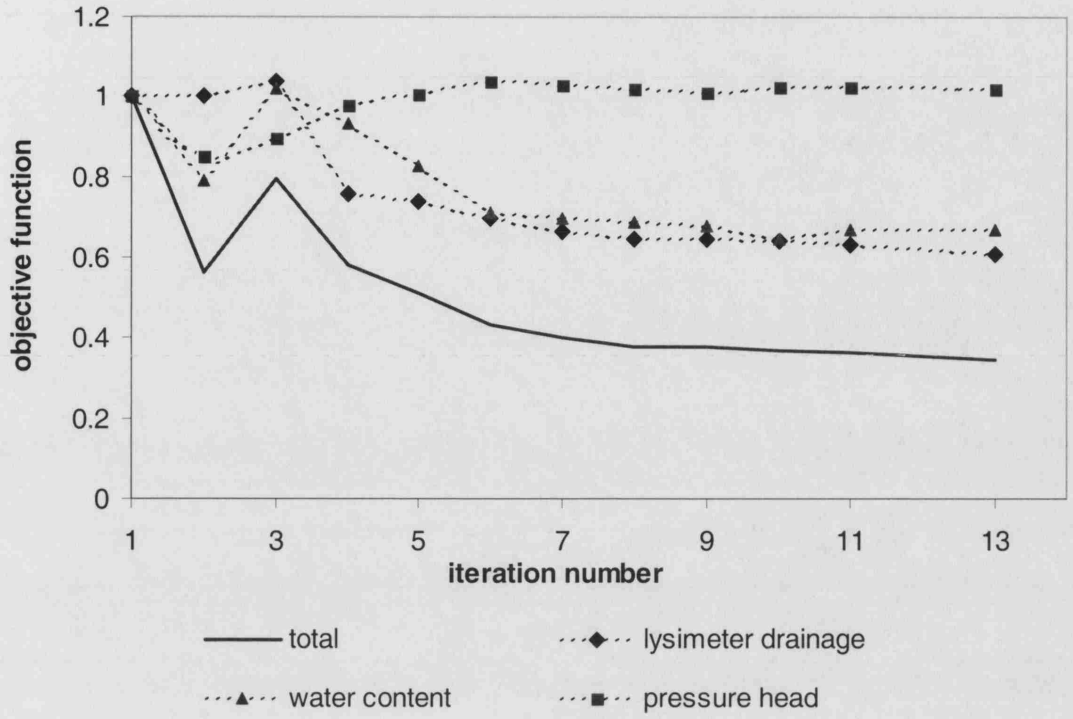

Figure 7-9 The progress of the total objective function (Eq. 7-13) and its partial objective functions during the flow calibration with SUFI of the Fleam Dyke tracer test for deuterium.

7.4.2 Calibration results

The resulting parameter values that provided the best fit are given in Table 7-6, together with their posterior uncertainty domain. Also shown is the coefficient of uncertainty for each parameter, which is a dimensionless number, obtained by dividing the width of the posterior uncertainty domain by its mean value. Large differences in coefficients of uncertainty exist between parameters. For instance, the van Genuchten parameter n was determined within a narrow interval, whereas the aggregate size a had a large coefficient of uncertainty that could not be reduced. Apparently the aggregate size is not a sensitive parameter in the flow calibration, where it only influences water exchange between fractures and matrix (Eq. 6-23). Possibly the aggregate size will be better constrained when solute transport is involved in the simulation, as it determines both diffusive and advective exchange of solutes (Eq. 6-34). Nevertheless, Roulier and Jarvis (2003) had also experienced that,

after flow and transport calibration with MACRO, there remained significant uncertainty for some key parameters governing macropore flow.

Table 7-6 Results of flow calibration of MACRO 5.0 for the Fleam Dyke research site. Included are the prior and posterior uncertainty domains and the coefficient of uncertainty for each calibrated parameter (subscripts in the parameters refer to the stratum number).

Parameter	Unit	Prior UD[1]	Posterior UD[1]	Best fit	COU[2] (%)
ω^*_c	[-]	(0.1, 0.8)	(0.7, 0.8)	0.75	13
$\theta_{s,2}$	[-]	(26.2, 28.5)	(27.0, 28.2)	27.2	4
$h_{b,2}$	[cm]	(25, 60)	(50, 60)	55	18
n_2	[-]	(1.1, 1.3)	(1.25, 1.28)	1.275	2
$K_{b,2}$	[mm/d]	(1.0, 5.0)	(3.6, 4.6)	3.8	24
n^*_2	[-]	(2, 6)	(2.5, 3.5)	3	33
a_2	[mm]	(5, 75)	(5, 75)	35	173
α_2	[cm^{-1}]	(0.015, 0.1)	(0.04, 0.06)	0.044	40
$\theta_{s,3}$	[-]	(28.1, 29.4)	(28.4, 29.4)	29.3	6
n_3	[-]	(1.05, 1.20)	(1.08, 1.11)	1.10	3
$K_{b,3}$	[mm/d]	(0.5, 2.5)	(1.2, 1.7)	1.4	33
n^*_3	[-]	(2, 6)	(2, 4)	3.5	67
a_3	[mm]	(10, 140)	(50, 140)	70	95
α_3	[cm^{-1}]	(0.0035, 0.02)	(0.009, 0.02)	0.02	76
$\theta_{s,4}$	[-]	(31.1, 32.3)	(31.3, 31.9)	31.45	2
$K_{b,4}$	[mm/d]	(0.02, 0.20)	(0.10, 0.14)	0.115	40
n^*_4	[-]	(2, 6)	(2, 2.5)	2	22
a_4	[mm]	(10, 140)	(10, 70)	20	150
$\theta_{s,5}$	[-]	(42.6, 44)	(43.6, 44)	43.7	1
n^*_5	[-]	(2, 6)	(2, 4)	3.4	67
a_5	[mm]	(10, 140)	(20, 75)	60	116

[1] UD = uncertainty domain

[2] COU = coefficient of uncertainty

The results of the flow calibration are shown in Figure 7-10 until Figure 7-12. Compared to the prior modelling results, there is improvement in the simulation of the lysimeter drainage (Figure 7-10). However, the cumulative drainage is still underestimated, at only 86.4% of the drainage measured. This might be due to an overestimation of the potential evapotranspiration, related to the unreliability of the meteorological data. The actual evapotranspiration was 86.1% of the potential evapotranspiration. Of the actual evapotranspiration, 59.2% was transpiration, 20.9% was canopy evaporation and 19.9% was soil evaporation. After calibration, the variation of the water content in the weathered chalk is also better represented (Figure 7-11). However, simulation of the pressure heads is still not satisfactory, as was shown in Figure 7-9. There is some improvement in the pressure heads during winter, but the model fails to simulate the low pressure heads in the chalk strata observed during the summer (Figure 7-12). This may be due to the representation of the hydraulic functions for the chalk strata by the modified van Genuchten – Mualem functions. Specifically designed for soils, these functions may after all not be that suitable for the chalk matrix. Another reason for the limited success for the pressure heads might be the multiplicative formulation of the objective function in Eq. 7-13. The use of the additive form (as in Eq. 6-44) with a higher weight on the pressure head data might have proved more successful here.

Figure 7-13 shows the distribution of flow between the micropores (matrix) and the macropores (fractures) in each chalk stratum. It illustrates the intermittent nature of the fracture flow, which only occurs during high infiltration events. The matrix flow is more constant throughout the recharge season. The distribution of flow between the matrix and the fractures is mainly determined by the boundary hydraulic conductivity K_b. The flow passes through the matrix, until the capacity of the matrix is exceeded, leading to diversion of flow through the fractures. Large differences exist between the strata, related to differences in K_b. In the weathered chalk the matrix flow is significant and the fracture flow is confined to a short period, whereas in the chalk-2 stratum the matrix flow is minimal and fracture flow accounts for the majority of the flow.

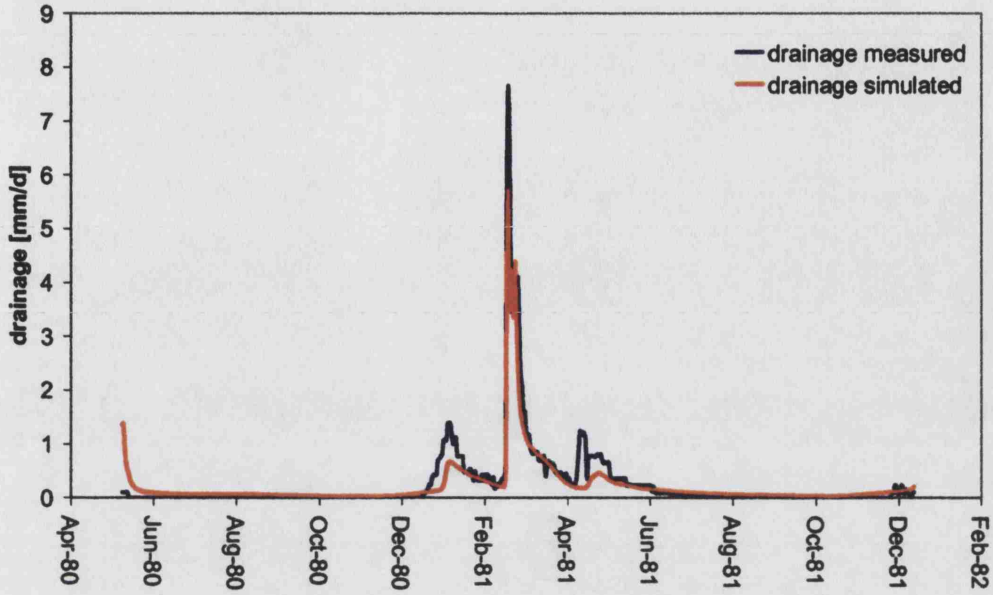

Figure 7-10 Results of flow modelling with MACRO 5.0 after calibration, showing measured versus simulated drainage from the Fleam Dyke lysimeter.

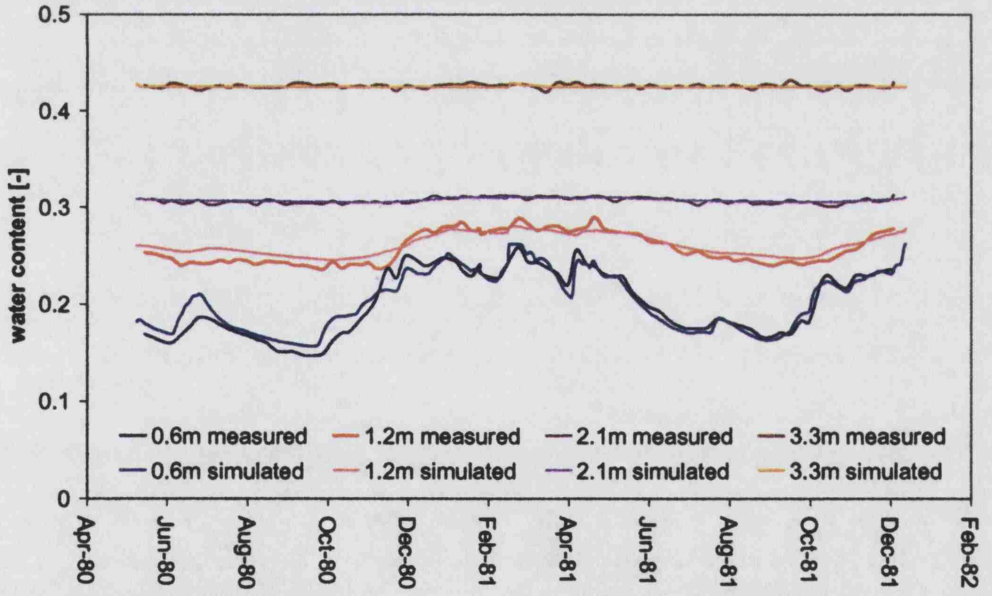

Figure 7-11 Results of flow modelling with MACRO 5.0 after calibration, showing measured versus simulated water contents in the Fleam Dyke lysimeter.

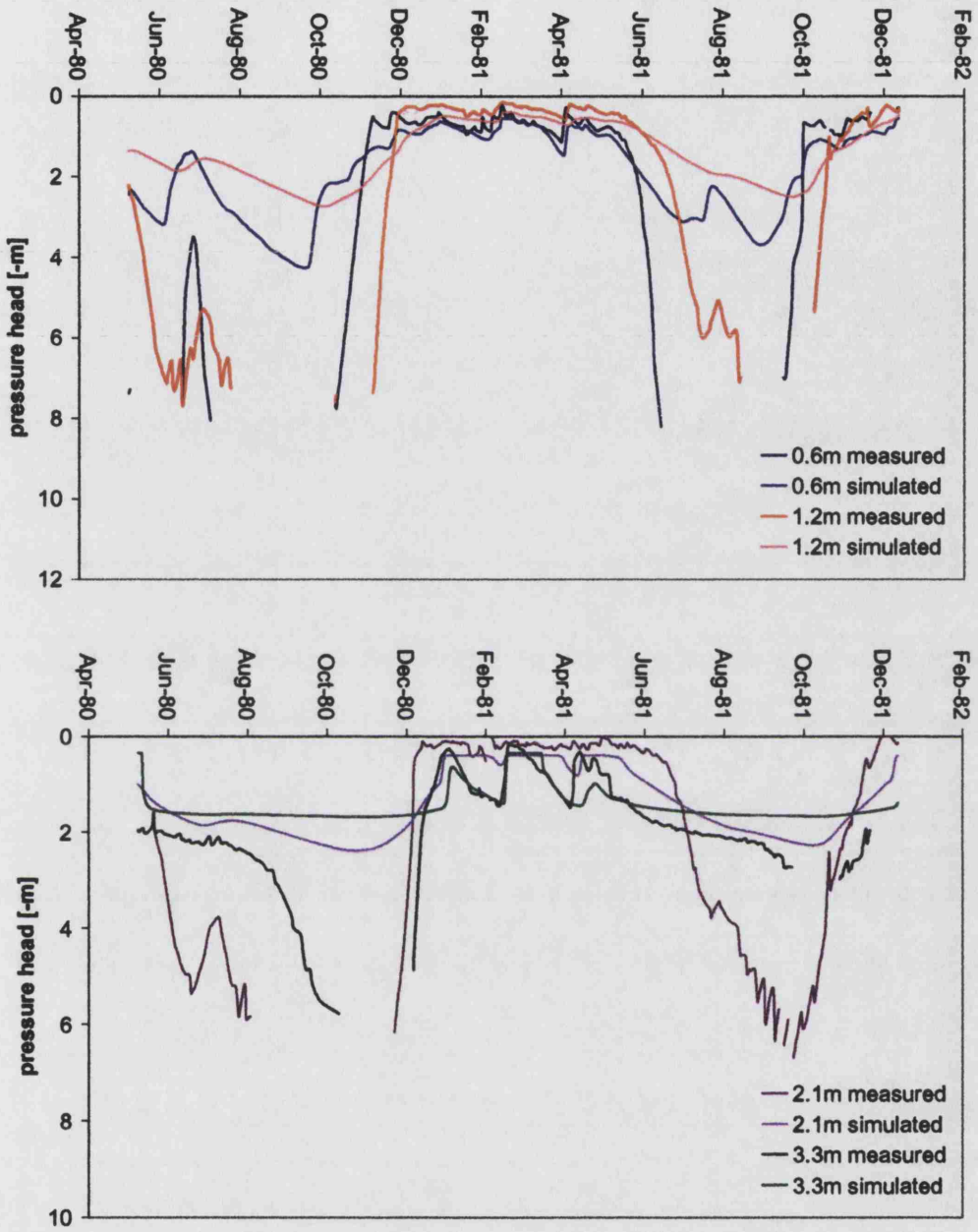

Figure 7-12 Results of flow modelling with MACRO 5.0 after calibration, showing measured versus simulated pressure heads in the Fleam Dyke lysimeter.

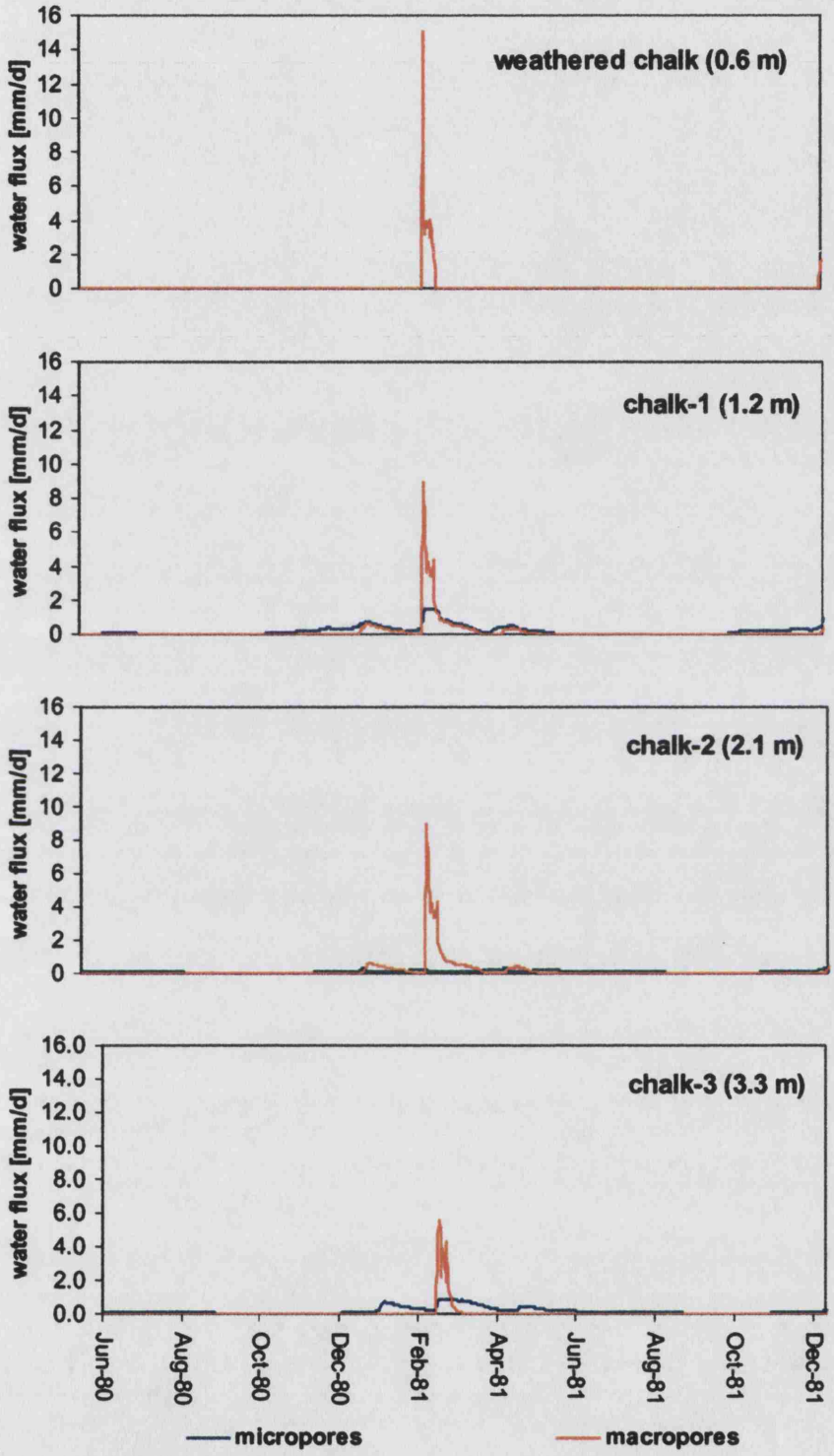

Figure 7-13 Occurrence of flow through the micropores (matrix) and the macropores (fractures) in different chalk strata of the Fleam Dyke site, as simulated by MACRO.

Note that for the weathered chalk and the chalk-1 stratum the van Genuchten parameters have been changed through calibration, so that the hydraulic functions of Figure 7-2 and Figure 7-3 are no longer valid. An updated version, using the best-fit parameters of Table 7-6, is shown in Figure 7-14 and Figure 7-15. For the weathered chalk, the hydraulic functions now significantly deviate from the measured data. This may be a cause for the limited success in the simulation of the pressure heads in Figure 7-12. The measured data are also subject to uncertainty, however: e.g. uncertainty in the calibration of the neutron probes for the water content measurements, and uncertainty in the unsaturated hydraulic conductivity function due to non-uniform infiltration conditions at shallow depth.

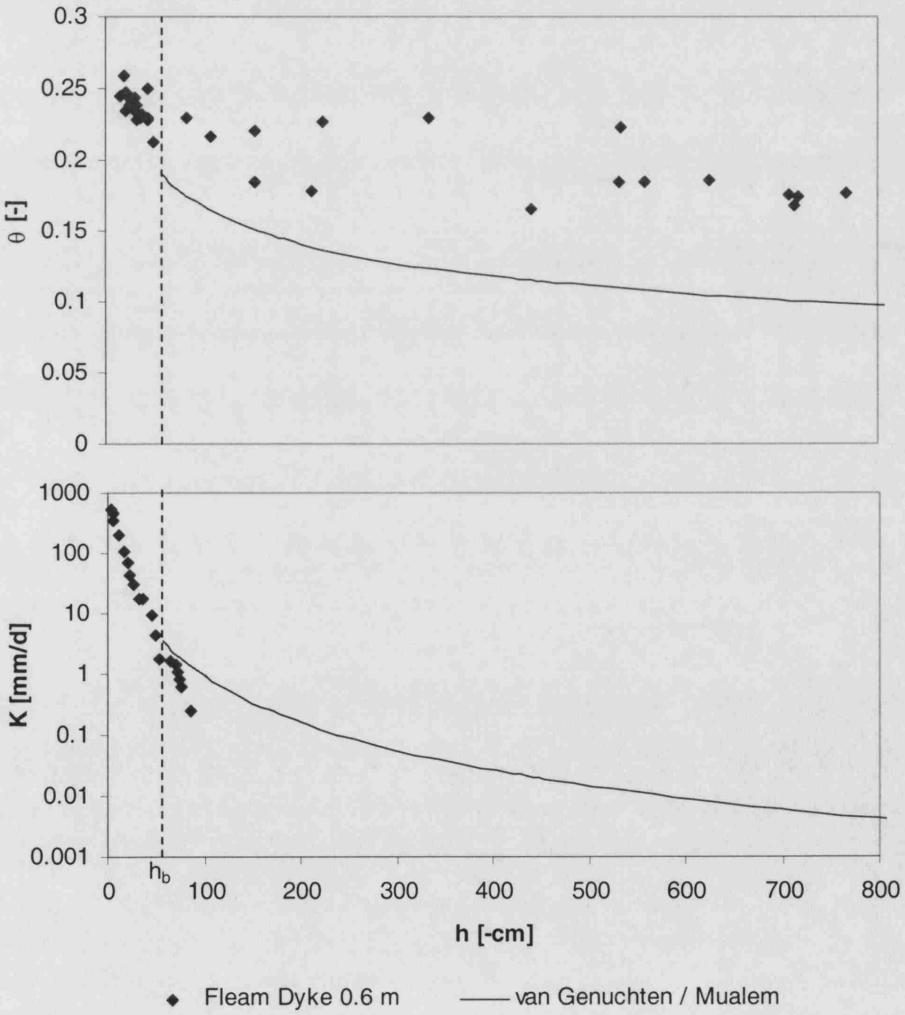

Figure 7-14 Fit of the van Genuchten function and Mualem's model to the water retention curve and the unsaturated hydraulic conductivity function for the weathered chalk at Fleam Dyke at 0.6 m depth, after flow calibration.

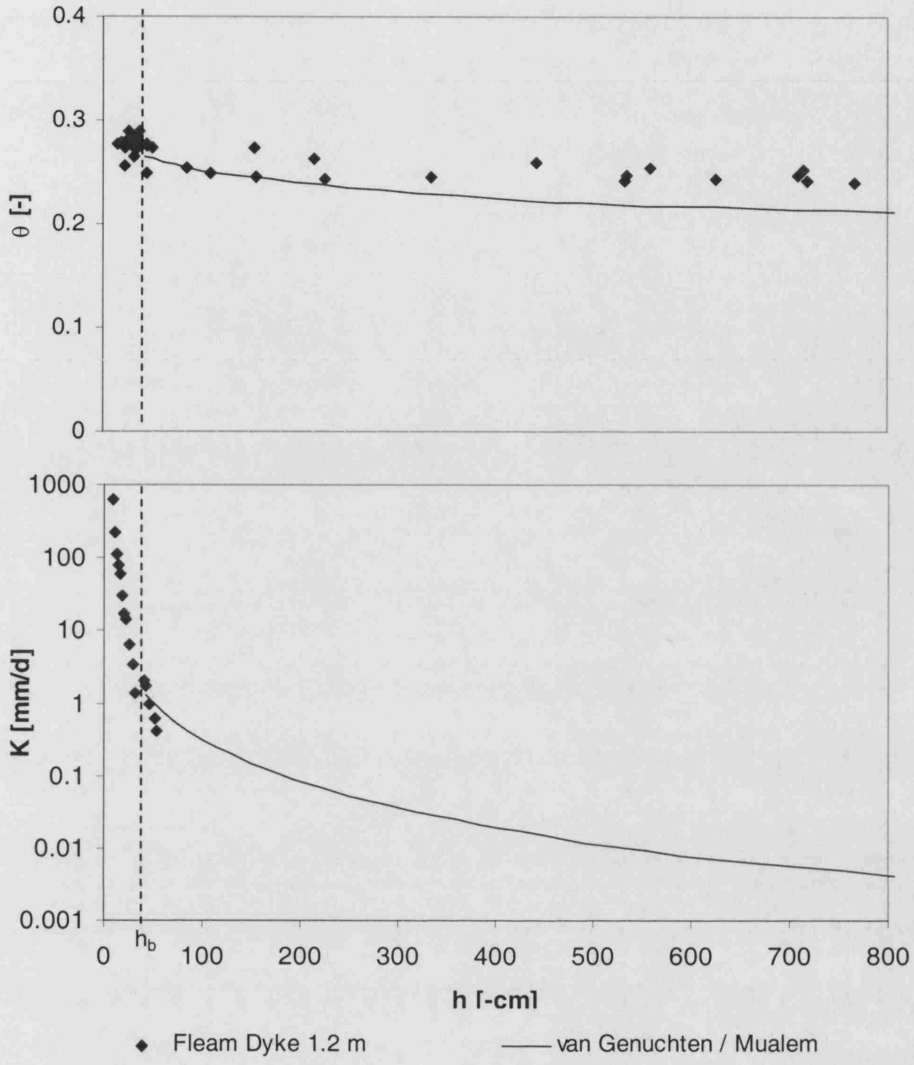

Figure 7-15 Fit of the van Genuchten function and Mualem's model to the water retention curve and the unsaturated hydraulic conductivity function for the chalk-1 stratum at Fleam Dyke at 1.2 m depth, after flow calibration.

7.5 Validation

To test the flow calibration of MACRO for the Fleam Dyke research site, validation of the model was performed on an independent dataset. The period from 1 January 1999 to 30 July 2003 was selected, i.e. 20 years after the period used for calibration and comprising a variety of recharge conditions. For this period, data were only available for the lysimeter drainage, and not for water contents and pressure heads.

7.5.1 Data input

All parameters were fixed to the values that provided the best fit for the flow calibration with the 1980-1981 dataset (Table 7-6). For the initial water contents, on 1 January 1999, no data were available. The initial water contents were therefore set to the values measured on 1 January 1981. Daily rainfall data for the whole period were available from the rain gauge on site.

Daily values of PET were calculated from meteorological data. A Visual Basic code was written by the author (Appendix VII), to implement the Penman-Monteith equations of section 7.2.1.1. Daily data of most meteorological variables were available from the weather station on site, but upon inspection several of the variables gave unreliable data. Only dry bulb temperature, wind speed and soil temperature were used from the weather station at Fleam Dyke. For other variables, data were used from the British Atmospheric Data Centre from nearby weather stations. The wet bulb depression was taken from Cambridge Botanic Garden (9 km from Fleam Dyke), the daily number of sunshine hours was taken from Cambridge Niab (12 km from Fleam Dyke), radiation was taken from Bedford Saws (49 km from Fleam Dyke), and atmospheric pressure was taken from Honington (40 km from Fleam Dyke). The *LAI* was fixed at 2.88 and the crop height h_c at 0.12 m.

7.5.2 Results

The results of the flow validation with MACRO are shown in Figure 7-16. Only the lysimeter drainage is shown, because no measurements of water contents or pressure heads were available. The simulated drainage fits the measured drainage remarkably well, both for the position of the peaks and the tail after each peak flow event. However, MACRO appears to overestimate the size of extreme recharge events, shown by the high peaks in Figure 7-16. It is possible that the lack of these high peaks in the measured lysimeter drainage is an artefact due to the presence of the lysimeter itself. When drainage reaches the lysimeter base with an area of 25 m^2, it needs to flow sub-horizontally towards the centre and run through the collecting trough to reach the tipping bucket. This may delay and smooth the detection of high

recharge events, leading to a reduction in peak size. On the other hand, the overestimation of the peaks in the MACRO output must, at least in part, be due to shortcomings in the first-order approach of the water exchange (Eq. 6-23). Water exchange from the fractures into the matrix is approximated by averaging the gradient over the matrix block. In reality, the local gradient at the fracture-matrix interface can be much higher. Therefore the first-order approach may underestimate the water exchange and overestimate the fracture flow events.

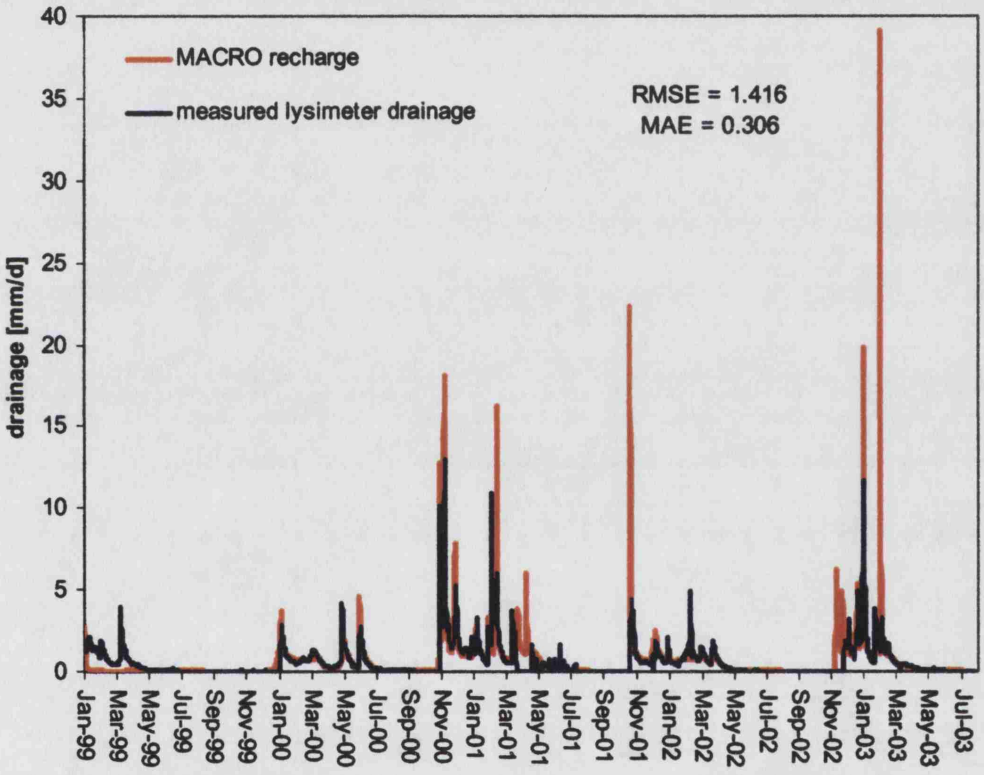

Figure 7-16 Result of flow validation with MACRO 5.0, showing measured versus simulated lysimeter drainage from the Fleam Dyke lysimeter.

The cumulative drainage from the lysimeter was overestimated at 125.5% of the measured drainage. In contrast, for the 1980-1981 data the drainage was underestimated (see section 7.4). These differences could be a result of having to use different weather stations for the meteorological variables. As described above, for

the period 1999-2003 the weather station at the Fleam Dyke research site was not fully functional and data from other stations had to be used for several meteorological variables. Howard and Lloyd (1979) had emphasized that the Penman equations are particularly sensitive to the wet bulb temperature. For the Fleam Dyke modelling for the period 1999-2003 the wet bulb depression was taken from a site 9 km away, and this might have affected the PE_t and eventually also the recharge simulation.

A quantitative measure of the model performance on the lysimeter drainage is shown in Figure 7-16 by the root means square error (RMSE) and the mean absolute error (MAE) for both models. The MAE is defined as:

$$MAE = \frac{1}{N}\sum_{t=1}^{N}\left|d_s^{(t)} - d_m^{(t)}\right| \qquad \textit{Eq. 7-14}$$

where d_s is the simulated recharge, d_m is the measured lysimeter drainage and N is the number of data points. The high value for the RMSE (1.416 mm/d) reflects the contribution of the high drainage peaks. Overall, the validation of the model for the lysimeter drainage can be judged satisfactory, which adds weight to the calibration of the 1980-1981 data set. No additional calibration of the combined data sets could be carried out since water contents and pressure heads were unavailable for the second modelling period.

7.6 Conclusion

Simulation of unsaturated flow through the Chalk at Fleam Dyke was attempted with MACRO 5.0. After calibration, the model successfully simulated the drainage from the lysimeter. The model repeatedly overestimated extreme recharge events, which must, at least in part, be due to the first-order approach to the water exchange term. Water contents were also well represented, but the model failed to reproduce the low pressure heads observed during the summer. Overall, the results suggest that the MACRO model can reliably simulate recharge through the chalk.

Fracture flow appeared to be confined to high infiltration events. Regarding the importance of fracture flow, large differences were observed between the chalk strata. In general, the distribution of flow between the matrix and the fractures was mainly

determined by the boundary hydraulic conductivity K_b in each stratum. These issues will be further discussed in the Chapter 8, together with the solute flux.

8 Transport simulation through unsaturated chalk using MACRO 5.0

8.1 Introduction

The previous chapter has described the calibration of the numerical model MACRO 5.0 against unsaturated-zone flow data from the Fleam Dyke research site. In the present chapter, this calibrated flow model will be used as the basis for simulation of solute transport at the same site. First the data from the tracer experiment at the Fleam Dyke lysimeter are applied to further calibrate the transport model. This calibrated model is then used to simulate the profiles of environmental deuterium and tritium from the 1980s. Finally conclusions are made regarding the flow and solute transport processes in the Chalk unsaturated zone.

8.2 Modelling of the Fleam Dyke tracer test (2001-2003)

8.2.1 Deuterium tracer

8.2.1.1 Model input

The modelling of the Fleam Dyke tracer test covered the period 1 January 2001 until 30 July 2003. The driving variables of rainfall and potential evapotranspiration were the same as used for the flow validation[12]. The initial water contents on 1 January 2001 were set to the values obtained from the flow validation. The initial deuterium contents of the pore water over the whole unsaturated profile were set to -47.5‰ VSMOW, which is the average deuterium content measured in the background cores.

[12] The reader is reminded that the flow calibration used data from 1980 until 1981, and the flow validation used data from 1999 until 2003 (section 7.5.1).

For the deuterium content of the rainfall, monthly values were available from the BGS from measurements in Wallingford, Oxfordshire (Figure 8-1). From simultaneous measurements in the 1980s it had been shown that the deuterium content of the rainfall in Fleam Dyke closely followed that of Wallingford (G. Darling, personal communication).

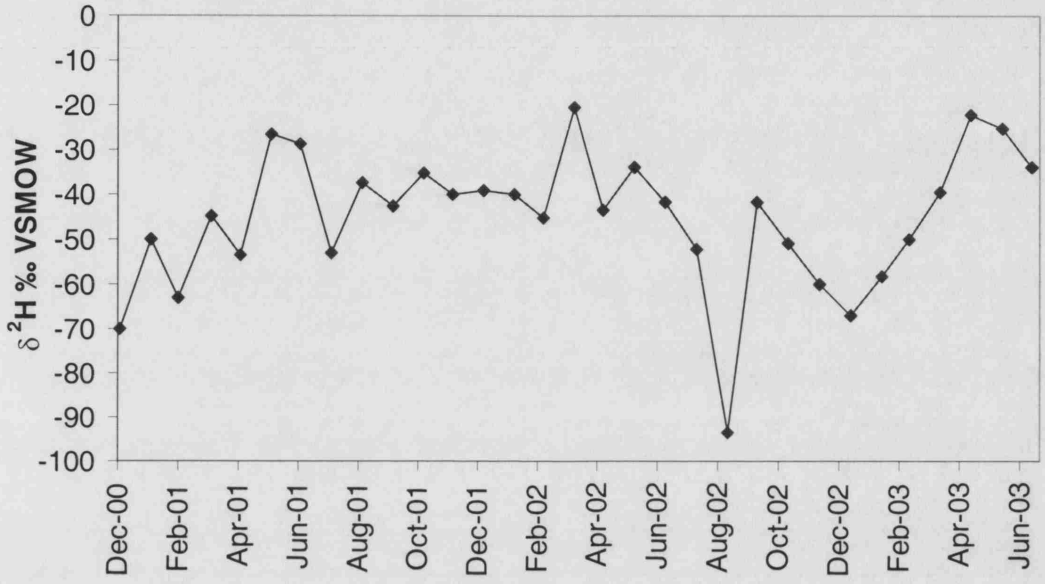

Figure 8-1 Deuterium content of rainfall from Wallingford, Oxfordshire for the period 2001-2003

As the bottom boundary condition, the 'lysimeter boundary condition' was maintained (i.e. the pressure head is zero at the bottom, and upwards flux is not allowed). This is appropriate for the simulation of the deuterium concentrations in the lysimeter drainage, as these conditions are expected at the lysimeter bottom. However, this boundary condition is not as physically representative for the simulation of the deuterium profiles, obtained from cores drilled in the plot adjacent to the lysimeter. The imposition of zero pressure head at 5 metre depth is not realistic. A time-dependent non-zero pressure head would be more appropriate, but no pressure head data were available for the simulation period. By default, the lysimeter boundary condition was used. A study by the British Geological Survey (1984) had shown that there were considerable differences in pressure head between the inside and the outside of the lysimeter below 2.1 m depth, but that above 2.1 m

depth the pressure heads were remarkably similar. As the bulk of the tracer movement still occurred above 2.1 m depth, the nature of the bottom boundary condition at 5 m depth may therefore not be that important.

All the flow parameters were fixed to the values that gave the best fit for the flow calibration in the previous chapter. The exception was the canopy interception capacity $W_{c,max}$ which was reduced from 0.75 mm to zero during the transport simulation. The reason is that MACRO does not allow evaporation of deuterium from the canopy. Interception of deuterium in rainfall by the canopy would therefore lead to concentration of deuterium on the canopy and a subsequent overestimation of the deuterium input into the profile. The effect of the suppression of canopy interception on the flow simulation was investigated. In fact, the resulting lysimeter drainage was almost identical, as the decreased evaporation from the canopy was compensated by increased plant water uptake and evaporation from the soil surface.

The suppression of canopy interception has a large impact on the evaporation of deuterium tracer. The tracer was distributed over the grass in an irrigation depth of only 1 mm. The canopy interception capacity of the grass is estimated at 0.75 mm, and it is therefore to be expected that a large proportion of the applied tracer was intercepted by the grass. The actual evapotranspiration on 11 February 2002, the day of the tracer application, was estimated at 0.76 mm by the flow validation described in the previous chapter. This means that a large proportion of the deuterium tracer may have escaped to the atmosphere even before entering the profile. With a transport model where canopy interception is suppressed, this implies that the amount of applied tracer used as input to the model should be artificially reduced. Therefore, in a first approach, the amount of the tracer solution applied was reduced from 1 mm to 0.5 mm. An irrigation depth of 0.5 mm was introduced as input to the model, applied on 11 February 2002 between 1:00 and 1:05 pm. The deuterium concentration in the irrigation water was set to +874,483‰ VSMOW (= 12% ^2H_2O), and the full irrigation amount was set to reach the soil surface, without any interception by the grass.

Additional parameters were required specific to the deuterium transport, as shown in Table 8-1. The mixing depth, which defines the amount of solute routed into the macropores at the surface, was kept at its default value of 1 mm. Because macropore

flow in the soil stratum was minimized in the model, this parameter has no significant effect. The longitudinal dispersivity was estimated at 10 cm as a first approach. This is based on the moment analysis presented in section 5.6.2.3.2, where an effective dispersivity of 15 cm was obtained. Because this value comprised both longitudinal dispersion and diffusion, a lower value of 10 cm was chosen for the longitudinal dispersivity.

Table 8-1 Parameter values for deuterium transport.

Symbol	Description	Value
z_d	mixing depth [mm]	1
D_0	free-water diffusion coefficient [m^2/s]	1.473×10^{-09}
α_L	Longitudinal dispersivity [cm]	10

8.2.1.2 Prior results

The deuterium profiles obtained after initial transport modelling of the Fleam Dyke tracer test are depicted in Figure 8-2. What is shown are the modelled deuterium contents in the micropores, not the macropores. This is because the deuterium contents measured in the core extracts are more likely to reflect the composition of the matrix water rather than the fracture water. The magnitudes of the peaks in the deuterium profiles are well represented. However, the profiles exhibit too much dispersion at early times, and the total tracer recovery is larger than what was measured in the field.

The modelled deuterium contents in the lysimeter drainage are shown in Figure 8-3. The model simulates a small breakthrough of deuterium tracer around January 2003. After two small pulses of tracer the deuterium content goes down again, but still stays slightly above the background level. The figure also shows measured deuterium contents, with elevated values around the same period. However, in section 5.6.2.3.1 it was shown that these measured high deuterium concentrations were due to evaporative enrichment of environmental deuterium in the sample bottles. The most likely conclusion is that no deuterium tracer appeared in the lysimeter drainage at all.

Still, there is some room to doubt whether some of these higher concentrations are partly caused by tracer breakthrough. Simulation with MACRO has endorsed these doubts. In what follows, however, it will be assumed that there was no breakthrough. This means that, despite the coincidence with the measured higher concentrations, the modelled peaks in Figure 8-3 indicate a flaw in the transport modelling (e.g. in the conceptual model or in the parameterization).

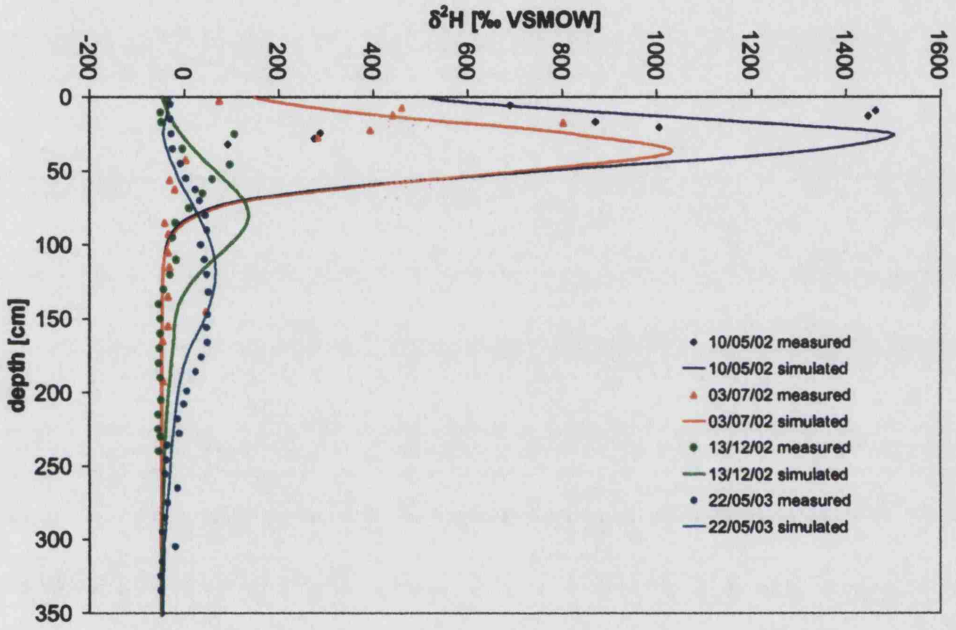

Figure 8-2 Prior results of transport modelling with MACRO 5.0, showing measured versus simulated deuterium contents in the unsaturated zone at Fleam Dyke. The simulated profiles give the deuterium content in the micropores.

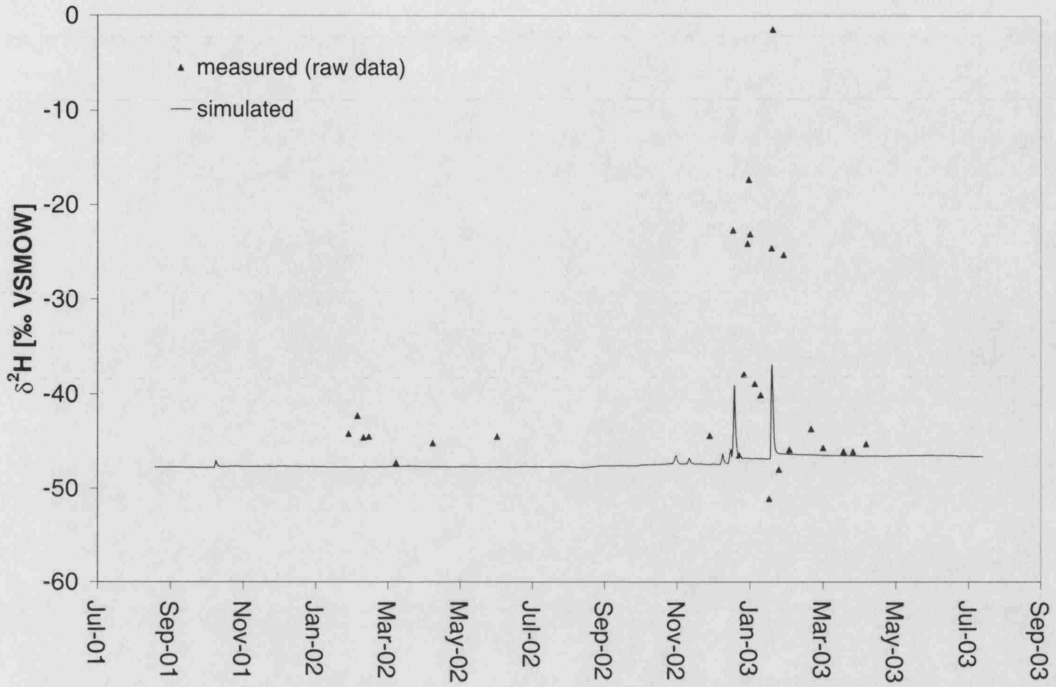

Figure 8-3 Prior results of transport modelling with MACRO 5.0, showing measured versus simulated deuterium contents in the Fleam Dyke lysimeter drainage. The elevated deuterium contents that were measured are most likely due to evaporative enrichment in the sample bottles.

8.2.1.3 Calibration

Calibration of the transport model for some key parameters was pursued to improve the fit between modelled and measured deuterium contents. Parameters selected for calibration included the longitudinal dispersivity α_L and the irrigation depth of the tracer solution *AMIR* (reduced from its actual value to account for evaporation of deuterium after interception by the grass). Other parameters set for calibration were the root depth z_r and the empirical root distribution ζ (= percentage of total root length in upper 25% of root depth), as those appeared to have a significant influence on the vertical distribution of solutes in the upper layers of the profile. Finally the tortuosity of the macropores n^* and the aggregate size a (i.e. half the slab width) of the chalk strata were included, because they retained a large posterior uncertainty domain after the flow calibration and they play an important role in solute transport.

The inverse modelling procedure SUFI was used again for the transport calibration. As calibration targets, a combination was chosen of lysimeter drainage, deuterium contents in the lysimeter drainage and deuterium contents in the matrix pore water. The daily data of lysimeter drainage were included to assure that the transport calibration would not upset the flow calibration. For the deuterium contents in the lysimeter drainage, it was assumed that no tracer breakthrough occurred at all. Therefore the calibration target was set at a constant background of -47.5‰ VSMOW, i.e. at the same level as the initial deuterium contents in the profile. For the deuterium contents in the matrix pore water, vertical profiles were available for 4 dates, and for a maximum of 27 depths. The combined objective function was then calculated by the multiplicative form of the root mean square errors:

$$O.F. = \sqrt{\frac{1}{N_t}\sum_{t=1}^{N_t}\left(d_s^{(t)} - d_m^{(t)}\right)^2} \times \sqrt{\frac{1}{N_t}\sum_{t=1}^{N_t}\left(c_{d,s}^{(t)} - c_{d,m}^{(t)}\right)^2} \times \sqrt{\frac{1}{\sum_{t=1}^{4} N_z}\sum_{t=1}^{4}\sum_{i=1}^{N_z}\left(c_{si}^{(t)} - c_{mi}^{(t)}\right)^2} \qquad \textit{Eq. 8-1}$$

where d is the lysimeter drainage, c_d is the deuterium content in the lysimeter drainage, c is the deuterium content in the matrix pore water, N_t is the number of days, N_z is the number of depths for which data are available, and the subscripts s and m refer to simulated and measured data respectively.

Prior uncertainty domains for each parameter are shown in Table 8-2. The prior uncertainty domains for the tortuosity of the macropores and for the aggregate size were set to the posterior uncertainty domains obtained from the flow calibration. This ensures that the model remains within the boundaries of the flow calibration. Because calibration of all parameters simultaneously would lead to a prohibitive number of model runs, the parameters were calibrated step by step and stratum by stratum (Table 8-3). A combination of exhaustive stratified sampling and random stratified sampling was used.

Table 8-2 Results of the transport calibration of MACRO 5.0 for the Fleam Dyke tracer test with deuterium. Included are the prior and posterior uncertainty domains and the coefficient of uncertainty for each calibrated parameter (subscripts in the parameters refer to the stratum number).

Parameter	Unit	Prior UD[1]	Posterior UD[1]	Best fit	COU[2] (%)
α_L	[cm]	(0.1, 30)	(0.5, 0.62)	0.5	21
AMIR	[mm]	(0.1, 0.9)	(0.35, 0.42)	0.38	18
z_r	[m]	(0.5, 1.0)	(0.50, 0.59)	0.52	17
ζ	[%]	(60, 80)	(74, 80)	80	8
n^*_2	[-]	(2.5, 3.5)	(2.5, 3.5)	3.5	30
a_2	[mm]	(5, 75)	(45, 75)	75	50
n^*_3	[-]	(2, 4)	(3, 4)	4	29
a_3	[mm]	(50, 140)	(50, 140)	50	95
a_4	[mm]	(10, 70)	(10, 25)	10	86
n^*_5	[-]	(2, 4)	(3, 4)	3.5	29
a_5	[mm]	(20, 75)	(20, 40)	20	67

[1] UD = uncertainty domain

[2] COU = coefficient of uncertainty

Table 8-3 Summary of iterations during transport calibration of the Fleam Dyke tracer test with deuterium, showing the parameters that were changed in each iteration and the number of runs for each iteration.

Iteration	Parameters	Runs	Comments
1	-	1	Prior parameter estimates
2	*AMIR*	10	Irrigation depth
3	α_L	10	Longitudinal dispersivity
4	z_r ; ζ	10	Parameters describing root distribution
5	n^*_2 ; a_2	109	Macropore parameters for weathered chalk
6	n^*_3 ; a_3	30	Macropore parameters for chalk-1
7	a_4 ; a_5 ; n^*_5	105	Macropore parameters for chalk-2 and chalk-3
8	*AMIR*	10	Irrigation depth
9	α_L ; z_r ; ζ	120	Longitudinal dispersivity and root parameters
10	α_L ; z_r	119	Longitudinal dispersivity and root depth

The evolution of the total objective function during the transport calibration process is shown in Figure 8-4. The figure also plots the partial objective functions that make up the total objective function by multiplication (Eq. 8-1). The total objective function gradually decreased during the calibration, until no further significant improvement could be made. The strongest contribution to the reduction in the total objective function comes from a better fit for the drainage concentrations. The deuterium concentrations in the unsaturated profile were also significantly improved, whereas the fit for the lysimeter drainage stayed largely the same.

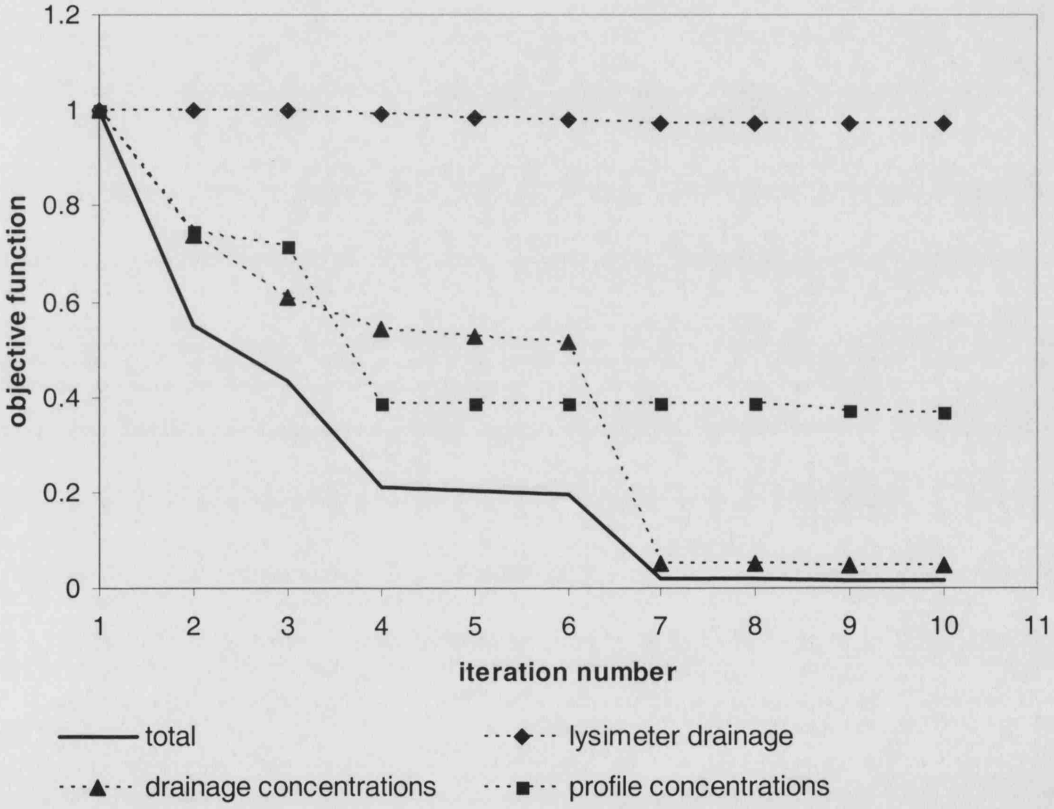

Figure 8-4 The progress of the total objective function (normalized from Eq. 8-1) and its partial objective functions during the transport calibration with SUFI of the Fleam Dyke tracer test for deuterium.

Resulting parameter values are shown in Table 8-2. A value of 0.5 cm was obtained for the longitudinal dispersivity. This is a low value compared to the effective dispersivities between 2 and 26 cm that were derived from the measured profiles by

moment analysis (section 5.6.2.3.2). The longitudinal dispersivity used in the model only refers to dispersion due to vertical transport through the micropores. Its low value suggests that transport through the matrix occurs in a piston-like manner with very little dispersion. The dispersion will be further discussed in section 8.2.1.5.

The irrigation depth of the tracer solution was set to 0.38 mm, as opposed to the actual applied irrigation of 1 mm. This implies that more than 60% of the deuterium tracer was lost by evaporation from the grass before it even reached the soil surface. Table 8-2 further shows that the transport calibration maximized the tortuosity of the macropores n^* for chalk strata 2 and 3, within the boundaries set by the flow calibration. This maximizes the hydraulic conductivity in the macropores, allowing solutes to travel faster through the fractures. The aggregate size a was maximized for the weathered chalk, and minimized for the three underlying chalk strata, again within the boundaries set by the flow calibration. This means that solute exchange between the macropores and the micropores (both by advection and diffusion) was minimized for the weathered chalk and maximized for the chalk strata underneath. In general however, the aggregate size a did not seem to be such a sensitive parameter in the model, as it retained a high coefficient of uncertainty in each chalk layer.

The resulting deuterium profiles after calibration are shown in Figure 8-5. Compared to the prior results (Figure 8-2), the fit between measured and simulated deuterium profiles is significantly improved, especially at early times. However, the improvement in the fit in the root zone appears to be at the expense of the fit below the root zone. That no good fit could be obtained need not be surprising. Each measured deuterium profile shown in Figure 8-5 is an average of up to 3 core profiles, which showed considerable lateral heterogeneity between them. Simulation with a one-dimensional transport model cannot resolve these heterogeneities. A better model performance could possibly be obtained by allowing vertical stratification of the longitudinal dispersivity α_L. In the MACRO 5.0 model, a single value of α_L was to be used for all strata. A lower α_L in the soil and the weathered chalk, as opposed to a higher α_L in the underlying chalk strata could possibly improve the model fit. Another reason for the limited success of the transport model may be the quasi-steady-state assumption of the diffusive exchange between the fractures and the

matrix. MACRO inherently assumes that the variation in the solute concentrations across a matrix block is linear. A better fit between measured and simulated deuterium concentrations may be obtained if a fully-diffusive model is used (section 2.3.2.2.1), where the concentration variation across the matrix block is modelled explicitly.

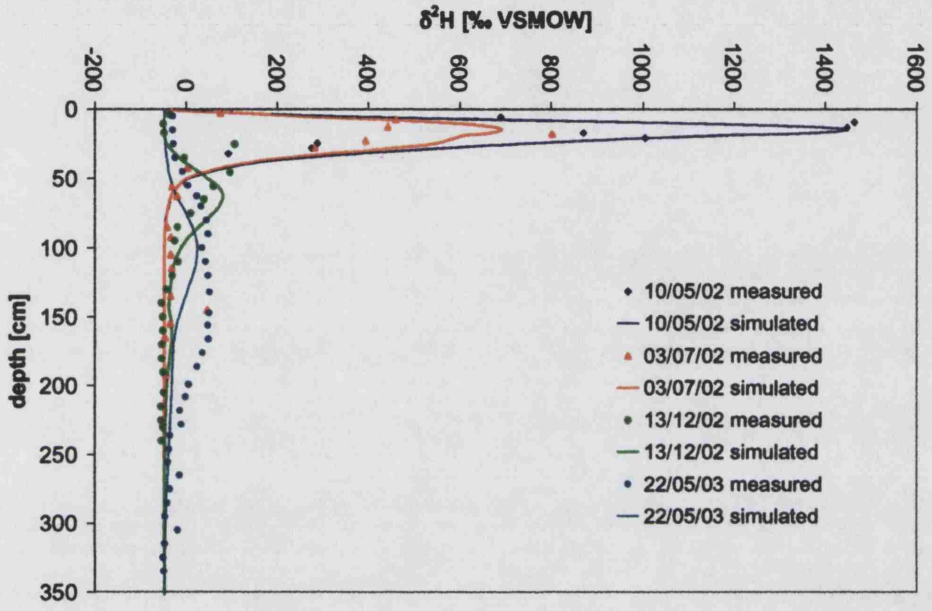

Figure 8-5 Results of transport modelling with MACRO 5.0 after calibration, showing measured versus simulated deuterium contents in the unsaturated zone at Fleam Dyke. The simulated profiles give the deuterium content in the micropores.

The deuterium contents in the lysimeter drainage obtained after the transport calibration are shown in Figure 8-6. The breakthrough that was obtained with the prior results in Figure 8-3 has completely disappeared, leaving the deuterium content at background level during the whole simulation period. This proves that the calibration target of zero breakthrough could easily be achieved, while still using realistic parameter values. Note that the simulated values are very close to the calibration target, but still result in a non-zero least-square difference. This ensured that, while the disappearance of the breakthrough greatly reduced the total objective

function of Eq. 8-1, the calibration remained sensitive to the deuterium profiles and the lysimeter drainage as well, as shown in Figure 8-4.

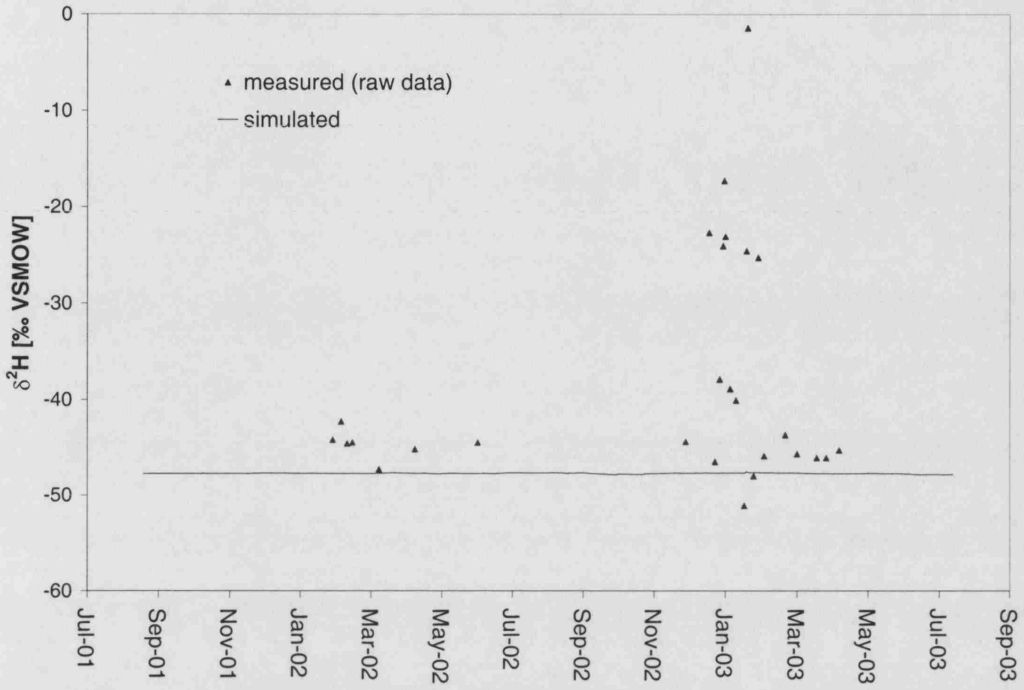

Figure 8-6 Results of transport modelling with MACRO 5.0 after calibration, showing measured versus simulated deuterium contents in the Fleam Dyke lysimeter drainage. The elevated deuterium contents that were measured are most likely due to evaporative enrichment in the sample bottles.

It was checked whether the transport calibration upset the flow calibration. Therefore the flow model was run again for the period 1980-1981, with the parameters of Table 7-6 that showed the best fit in the flow calibration. This time, however, the values for the root distribution parameters, the tortuosity of the macropores and the aggregate size were substituted by those values that provided the best fit for the transport calibration (Table 8-2). The objective function of the flow calibration (Eq. 7-13) was evaluated again, and it was shown that the objective function rose from 0.000124 to 0.000142. Visual inspection of the output graphs revealed that the changes in lysimeter drainage, water contents and pressure heads were minimal.

8.2.1.4 Prediction

Once the transport model had been calibrated, it could be used to make tentative predictions about the further progress of the deuterium tracer through the unsaturated zone at Fleam Dyke. Therefore the model was run from 2001 until 2020, using the parameter values that provided the best fit in the calibration of section 8.2.1.3. For each year until 2020, data of daily rainfall and daily PET were used from the year 2002. The repetition of input data from a single year was preferred rather than using average data. Averaging would remove the occurrence of extreme rainfall events, which are thought to be important in the generation of fracture flow. The year 2002 was chosen as it was a relatively wet year (a total rainfall amount of 709 mm, or 12% in excess of the local average), with an average distribution of heavy rainfall events. This would provide a conservative estimate for the transport velocities through the unsaturated zone. Deuterium concentrations in rainfall were set to a constant value of -47.5‰ VSMOW, ignoring seasonal variations.

Figure 8-7 shows the resulting deuterium concentrations in the profile until the year 2016. The bulk of the deuterium tracer starts reaching the base of the lysimeter at 5 m depth in the year 2006. The tracer peak becomes more and more dispersed, and by 2016 the complete tracer pulse has passed through the lysimeter and concentrations are back at background levels throughout the profile.

Figure 8-8 shows the corresponding breakthrough curve of the deuterium tracer in the lysimeter drainage. The deuterium content reaches a maximum of –27.2‰VSMOW in January 2010. The irregular jumps in the breakthrough curve are associated with the initiation of a new recharge season. Over the whole simulation period, only 2.6% of the applied deuterium tracer is predicted to appear in the lysimeter drainage. The remainder is lost through evapotranspiration. The results confirm the low transport velocities through the chalk unsaturated zone. The peak of the deuterium tracer takes 9 years to reach 5 m depth. Figure 8-8 further suggests that it would be useful to keep monitoring the deuterium content of the lysimeter drainage over the coming ten years to verify the predictions made by MACRO.

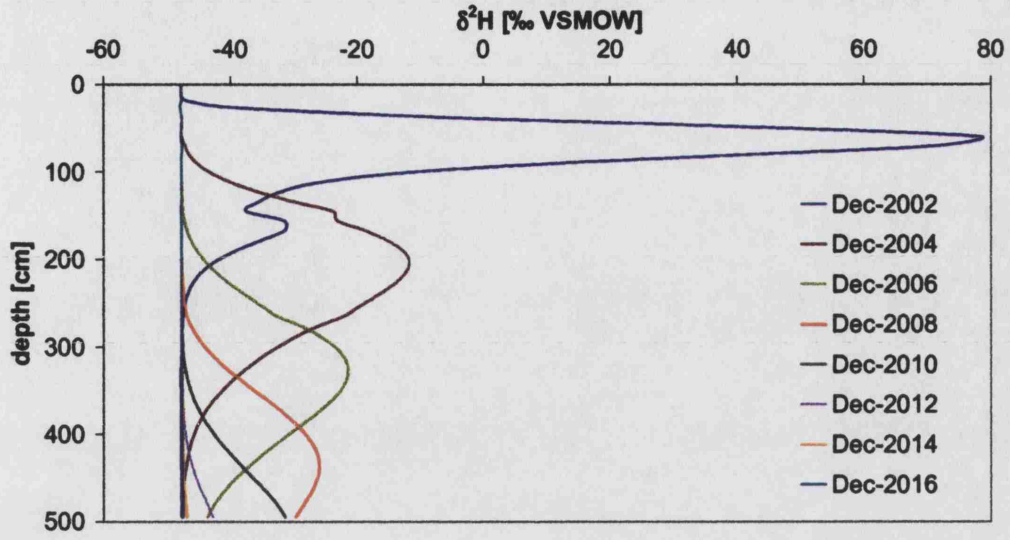

Figure 8-7 Deuterium contents in the unsaturated zone at Fleam Dyke until the year 2016, as predicted by MACRO 5.0.

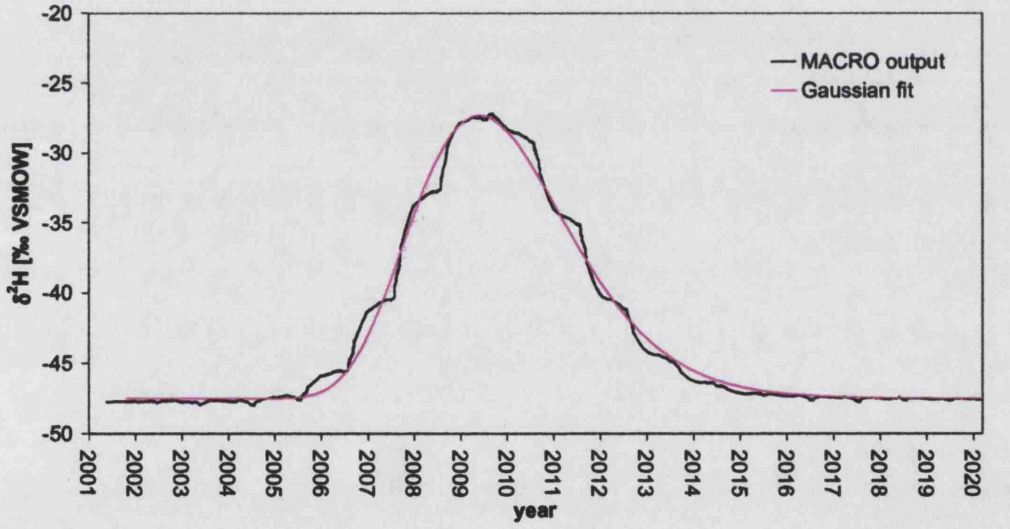

Figure 8-8 Deuterium contents in the drainage from the Fleam Dyke lysimeter until the year 2020, as predicted by MACRO 5.0. A Gaussian distribution is fitted to the breakthrough curve.

Figure 8-8 shows a spatially Gaussian distribution that is fitted to the breakthrough curve (using the Solver function in Microsoft® Excel), according to the formula (adapted from Bear, 1979):

$$C(z,t) = \frac{C_{0*}}{\sqrt{4\pi D_{eff}\, t}} e^{-\frac{(z-vt)^2}{4Deff\, t}} - 47.5‰\text{VSMOW} \qquad \textit{Eq. 8-2}$$

where C_{0*} is the input mass per unit area, t is the time (days), D_{eff} is the effective dispersion coefficient (m^2/s), z is the depth (set to 5 m = depth of lysimeter drainage), v is the transport velocity (m/s) and the factor 47.5‰VSMOW is subtracted to account for the background deuterium. This yields an effective dispersion coefficient D_{eff} of 2.5×10^{-9} m^2/s and a transport velocity v of 1.8 mm/d, leading to an effective dispersivity $\alpha_{eff} = D_{eff}/v$ of 12.64 cm.

That the model output of the drainage concentrations against time approaches a Gaussian distribution is remarkable. MACRO 5.0 is a dual permeability model, simulating flow and transport through the fractures and the matrix for the Fleam Dyke site. In the simulation shown in Figure 8-8 there was significant diffusive and advective exchange of tracer between the fractures and the matrix (as will be shown in section 8.5.3). However, apparently this did not lead to a deviation from the Gaussian distribution. The reason may be that the concentrations in the fractures and the matrix approach diffusive equilibrium – a concept introduced by Foster (1975) to explain the conservation of the environmental tritium profiles (see also section 3.2.1).

8.2.1.5 Discussion of dispersion

The dispersion obtained in the output of the MACRO model needs further attention. As shown in the previous section, a Gaussian distribution was fit to the tracer breakthrough curve, leading to an effective dispersivity α_{eff} of 12.64 cm. This is of the same order of magnitude as the effective dispersivities that were obtained by moment analysis of the measured deuterium profiles (Table 5-8). However, α_{eff} is much larger than the longitudinal dispersivity α_L of 0.5 cm that was supplied as input to the model. Therefore the question arises what the cause is of the dispersion in the model output, apart from longitudinal dispersion. The influence of the longitudinal dispersion was investigated by varying the value of α_L supplied to the model and

looking at the value of α_{eff} obtained from the fitted Gaussian distribution, as shown in Figure 8-9. For values of α_L larger than 0.5 cm, a linear response is obtained. For values of α_L below 0.5 cm, the model encountered numerical oscillations and overshoot problems, and this generated values of α_{eff} that deviated from the linear trend. The intercept of the trend line is at 12.55 cm, i.e. very close to the value of 12.64 obtained for α_L = 0.5 cm. This confirms that the majority of the dispersion in the MACRO output is caused by factors other than longitudinal dispersion.

The factors that can contribute to dispersion in the model output are:

- Longitudinal dispersion
- Diffusive exchange between the fractures and the matrix
- Advective exchange between the fractures and the matrix
- Numerical dispersion

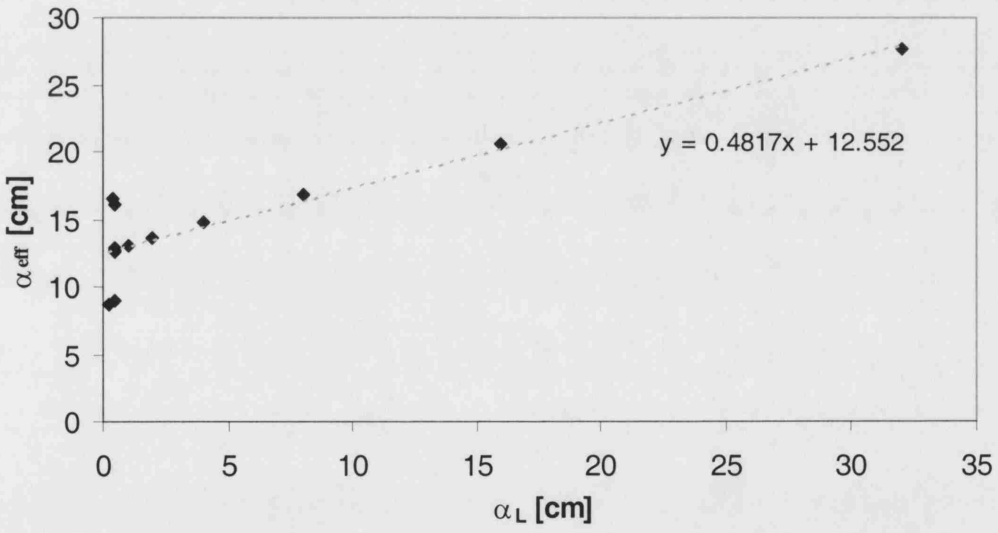

Figure 8-9 The effective dispersivity α_{eff} obtained from fitting a Gaussian distribution to the modelled breakthrough curve, as a function of the longitudinal dispersivity α_L supplied as input.

For a dual permeability model as MACRO, the dispersion caused by advective and diffusive exchange between the flow domains is difficult to quantify. Numerical dispersion is more predictable. A criterion to minimize numerical errors is to ensure a low Courant number (Spitz and Moreno, 1996):

$$Co = \frac{\Delta t\, v}{\Delta z} \leq 1 \qquad \textit{Eq. 8-3}$$

where Δt is the timestep, v is the velocity and Δz is the spatial discretization. In the Fleam Dyke simulation with MACRO, Δt was 30 minutes, v in the matrix was about 1 mm/d and Δz varied between 0.3 and 11.25 cm. This gives a maximum Courant number of 0.069, which is well within the limit. However, this does not eliminate numerical dispersion. In MACRO, the advection term in the advection-dispersion equation for the micropores (Eq. 6-28) is solved using a Crank-Nicholson finite difference scheme with upstream weighting. This introduces numerical dispersion, and an apparent dispersion coefficient associated with numerical dispersion can be calculated as (Zheng and Bennett, 1995):

$$D_{num} = \frac{1}{2} v \Delta z \qquad \textit{Eq. 8-4}$$

For a maximum Δz of 11.25 cm, this gives a numerical dispersion coefficient of 6.5×10^{-10} m^2/s. In comparison, the longitudinal dispersion coefficient (calculated by Eq. 6-29 for $\alpha_L = 0.5$ cm) is only 3.5×10^{-10} m^2/s.

In MACRO, numerical dispersion is minimized using an empirical correction factor, based on comparisons with an analytical solution (Larsbo and Jarvis, 2003). This correction factor is subtracted from the longitudinal dispersion coefficient before solving the advection-dispersion equation. If the corrected dispersion coefficient becomes negative, then a central weighting scheme is used instead. This eliminates numerical dispersion, but it makes the solution method more vulnerable to artificial oscillation problems. This is controlled by the Peclet criterion:

$$Pe = \frac{v \Delta z}{D_L} \leq 2 \qquad \textit{Eq. 8-5}$$

Depending on the spatial discretization Δz, which varied between numerical layers, this gives a Peclet number between 0.01 and 3.68 for the MACRO simulation of Fleam Dyke. Thus the Peclet criterion is not always met, leading to possible oscillation and overshoot problems. This is probably what happens in Figure 8-9 for values of $\alpha_L < 0.5$ cm. In this case the correction factor for numerical dispersion becomes larger than the longitudinal dispersion coefficient. This makes the solution method switch to central weighting, which introduces numerical oscillation.

8.2.1.6 Uncertainty and sensitivity

The model of the Fleam Dyke site has been calibrated in two steps. First the flow model was calibrated against data of lysimeter drainage, water contents and pressure heads (section 7.4). Next, this flow model was used to calibrate the transport model against data of lysimeter drainage, deuterium contents in the lysimeter drainage and deuterium contents in the matrix pore water (section 8.2.1.3). This has led to a solution of the flow and transport problem with an optimized parameter set. At this point, one may ask what the uncertainty of this solution is, and if the solution is unique.

Because the model was calibrated by multi-objective optimization, the problem was very well constrained. However, Yapo et al. (1998) showed that the solution of a multi-objective problem is generally not unique (the set of optimal solutions are called Pareto solutions). The inverse modelling procedure that was used for the Fleam Dyke model is a global search algorithm. This makes it less likely to fall into local minima. Moreover, the calibration employed a high number of model runs: 2451 in the flow calibration and another 496 in the transport calibration. This suggests that the parameter space was well explored, but one should keep in mind that a large number of parameters were involved in the calibration. For instance, the flow calibration simultaneously optimized 21 parameters, making the parameter space essentially 21-dimensional.

To conclude, there is some uncertainty about the uniqueness of the solution, but this uncertainty cannot be quantified. In contrast, the uncertainty of the parameter values is expressed explicitly in their posterior uncertainty domain (Table 7-6 and Table 8-2). An indication of the uncertainty of the model solution can then be given by performing a sensitivity analysis of the model parameters. This is illustrated in Figure 8-10 for two parameters: the root depth z_r [m] and the root distribution factor ζ [%] (= percentage of the total root length in the upper 25% of the root depth). The calibrated values of these parameters were, respectively, 0.52 m and 80%. Figure 8-10 indicates that the model fit could be slightly improved by decreasing the root depth and increasing the root distribution factor. However, field inspection had shown that roots persisted down to at least 50 cm depth at Fleam Dyke, and that a

significant proportion of the roots was present below the upper 20 cm of soil. Hence the borders of the prior uncertainty domains for these parameters were set at 0.5 m and 80%, respectively, and the calibrated parameters were set at these boundary values (see Table 8-2).

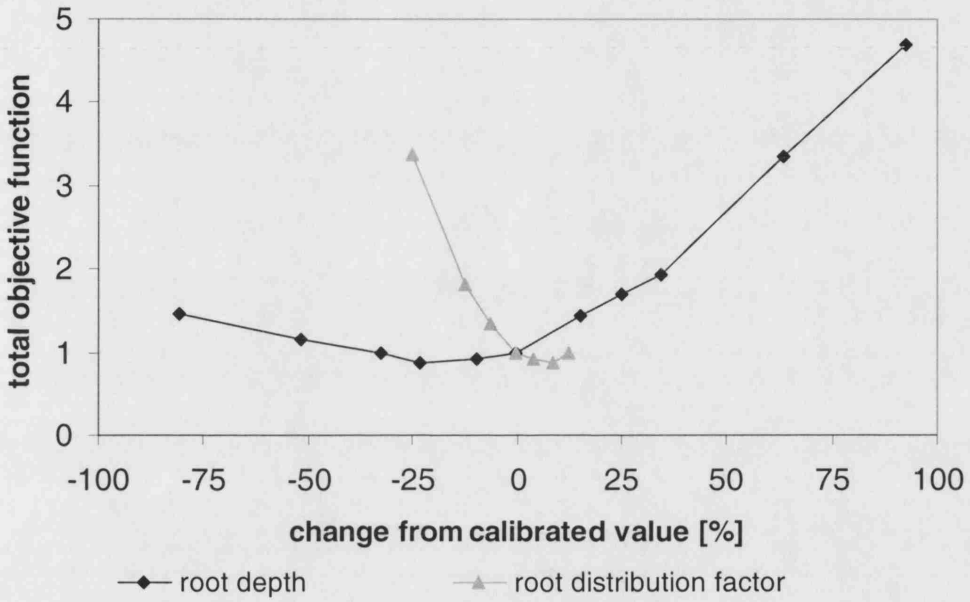

Figure 8-10 Results of sensitivity analysis of the root depth and the root distribution factor, showing the change in the total objective function (normalized from Eq. 8-1) as a function of the relative change in the parameters.

Figure 8-10 shows that the model is more sensitive to the root distribution factor than to the root depth, as indicated by the steepness of the curve. To achieve a full assessment of the uncertainty of the model solution as a function of the model parameters, all parameters should be varied simultaneously within their posterior uncertainty domain. Given the number of parameters involved, this would lead to a prohibitive number of model runs.

8.2.2 Bromide tracer

After calibration of the transport model for the deuterium tracer, the model was run for the bromide tracer. The diffusion coefficient was changed to 1.31×10^{-9} m^2/s and the bromide concentration in the irrigation water was set to 3 g/l. The concentration in the rainfall was fixed to a constant value of 4.3 µg/l, the concentration that was measured in a composite sample from the Fleam Dyke rain gauge over the period June 2002 - May 2003. The initial bromide concentrations in the profile were set to 37.5 µg/l, at the same level as the background concentrations measured in the lysimeter drainage. The concentration factor for plant tracer uptake f_c was set to 1, i.e. complete passive uptake of bromide by the plant roots.

Bromide is a fully conservative solute, and evaporation of bromide from the canopy is not an issue as it was for deuterium. Therefore canopy interception was restored for modelling the bromide tracer. The canopy interception capacity was set to 0.75 mm, and the irrigation depth of the tracer solution was kept at its actual value of 1 mm. The fraction of the irrigation intercepted by the grass was set to 0.5. The solute stored on the canopy is then calculated by a running solute balance, assuming complete mixing of solute on the canopy with solute from rainfall.

The bromide concentrations in the micropores obtained with MACRO are shown in Figure 8-11. No good fit was obtained between measured and simulated concentrations. However, the measured concentrations in Figure 8-11 are questionable. In section 5.6.1.3.2 it was shown that the background concentrations in the unsaturated profile were highly uncertain. It is likely that the simulated concentrations in Figure 8-11 are a better representation of reality than the measured concentrations shown.

The bromide concentrations in the lysimeter drainage are shown in Figure 8-12. The model predicted no breakthrough of bromide tracer, in accordance with the deuterium results. The measured bromide concentrations shown in Figure 8-12 have been corrected for evaporative enrichment of bromide in the sample bottles (section

5.6.1.3.1). The small number of elevated measured bromide concentrations in Figure 8-12 are probably due to the use of inaccurate correction factors.

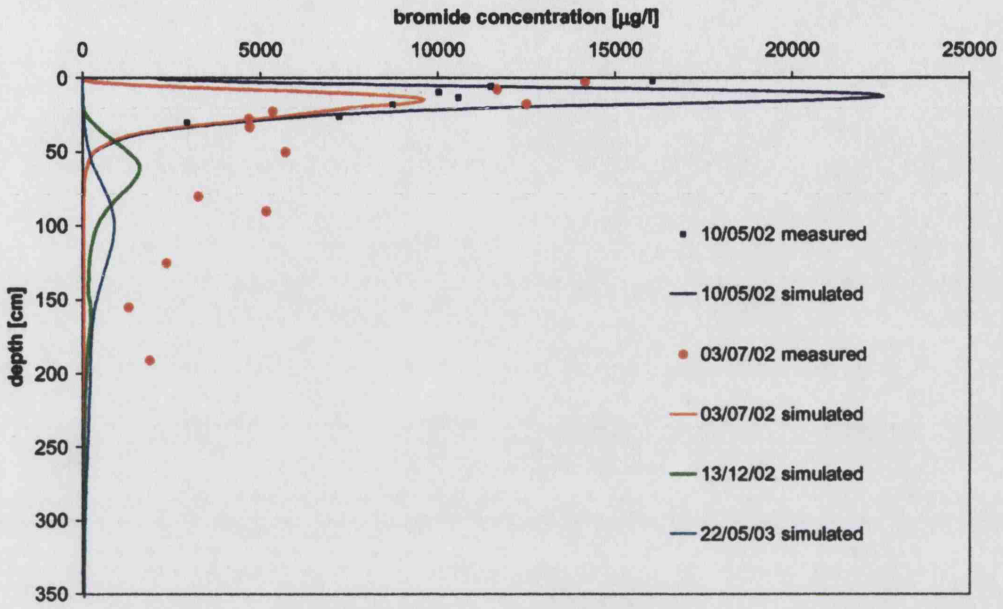

Figure 8-11 Results of transport modelling with MACRO 5.0, showing measured versus simulated bromide concentrations in the unsaturated zone at Fleam Dyke. The simulated profiles give the bromide concentrations in the micropores (matrix).

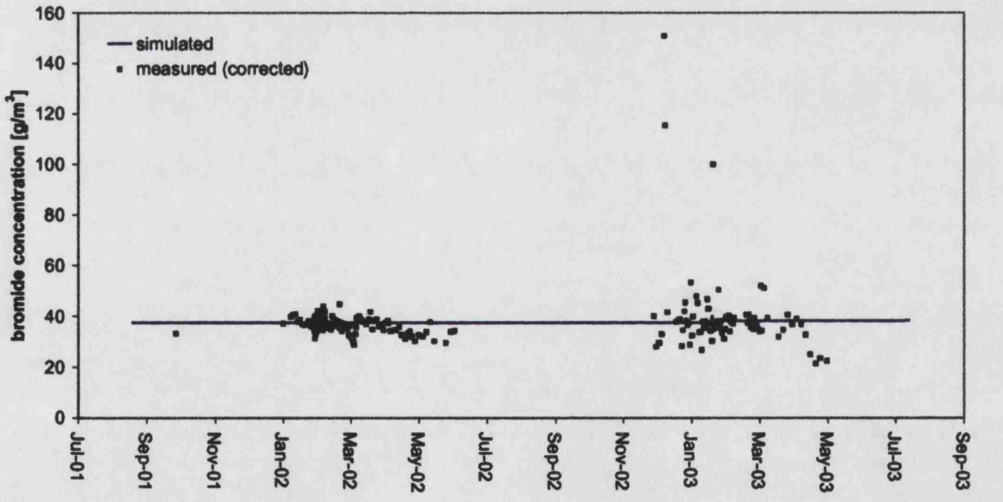

Figure 8-12 Results of transport modelling with MACRO 5.0, showing measured versus simulated bromide concentrations in the Fleam Dyke lysimeter drainage. The measured bromide concentrations have been corrected to account for evaporative enrichment in the sample bottles.

8.3 Modelling of environmental tritium profiles at Fleam Dyke (1954-1981)

After calibration of the transport model for the Fleam Dyke site, the model was used to simulate the environmental tritium profiles measured at Fleam Dyke between 1979 and 1981 (Figure 4-8). MACRO 5.0 was run over the period 1 January 1954 until 1 December 1981, with tritium concentrations in rainfall as input.

8.3.1 Model input

Daily rainfall data from a rain gauge at the Fleam Dyke site were available for the period 1954-1960 and 1970-1981. For the period 1961-1969, data were used from a rain gauge at Saffron Walden (17 km from Fleam Dyke). Monthly tritium concentrations in UK rainfall were available from Otlet (1978) and Cambray et al. (1982). For the period 1965-1981, they had calculated tritium in rainfall as averages of data from British monitoring stations in Milford Haven, Orfordness and Eskdalemuir. Tritium data before 1965 had been obtained by correlation with data from Ottawa (Canada) and Valentia (Ireland). The tritium concentrations show peaks in the summer of 1963 and 1964, which function as an environmental tracer in the unsaturated zone (Figure 8-13).

The depth of the profile was changed from 5 metres to 14 metres (the maximum depth of the tritium measurements), by increasing the depth of the chalk-3 stratum. Accordingly, the number of numerical layers in the model was increased from 60 to 200. As the bottom boundary condition, the lysimeter boundary condition was again maintained. This implies the imposition of a zero pressure head at 14 metres depth, which is not realistic. However, the peak of the tritium profiles was measured around 7 metres higher than this bottom boundary. Hence it is argued that the nature of the bottom boundary condition would have little effect on the progression of the tritium front.

The free-water diffusion coefficient for tritium was fixed at 1.50×10^{-9} m^2/s (Mills, 1973, value at 5°C corrected to 10°C by the Stokes-Einstein equation). The initial

tritium concentrations in the pore water were set to a background of 20 TU over the whole profile. The initial water contents on 1 January 1954 were set to the values obtained from the modelling of the Fleam Dyke tracer test for 1 January 2002. The MACRO model was finally set to the option of tritium as a tracer, which allows free plant uptake and evaporation of the tritium, and includes degradation of the tritium with a half-life of 12.4 years.

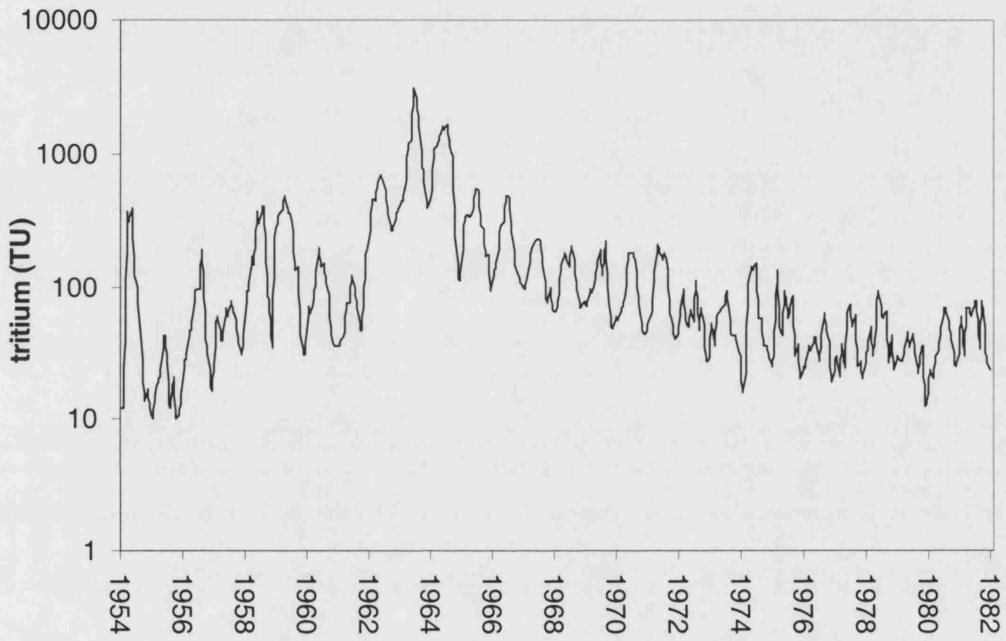

Figure 8-13 Monthly tritium concentrations in UK rainfall (assembled from Otlet (1978) and Cambray et al. (1982)).

All other parameters were set to the values that provided the best fit in the transport calibration of the Fleam Dyke tracer test (section 8.2). An exception was made for the crop parameters, because the parameter values for a perennial grass crop were no longer appropriate. The environmental tritium profiles had been measured from cores drilled in the arable field adjacent to the Fleam Dyke lysimeter. Between 1940 and 1980, a variety of cereal crops had been farmed on the field, of which spring barley was the most frequent and most representative (Cooper, 1985; Foster and Bath, 1983). Therefore the crop parameters needed to be adapted to an annual rotation of spring barley (Table 8-4). Extra parameters were needed for the annual crop development

(see section 6.2.1.1). Values for the maximum GLAI, the maximum rooting depth and the timing of the crop rotation were taken from Thompson et al. (1981). The maximum crop height of 0.8 m was obtained from Cooper (1985). The value of 0.25 for the albedo was taken from Shuttleworth (1992). Other crop parameters were either retained from the model calibration with the grass crop, or fixed to default values. Canopy interception was again disabled. This was done to avoid the concentration effect of tritium on the canopy, as MACRO does not allow for evaporation of tritium from the canopy.

As the crop height and the green leaf area index (GLAI) vary throughout the year, they affect the potential evapotranspiration (PET). Therefore the PET had to be calculated internally by MACRO, based on meteorological variables supplied as input. Because no local meteorological data were available for the period 1954-1981, monthly climate averages were used instead. Daily maximum and minimum temperatures were obtained from the Met Office as monthly averages for Cambridge over the period 1961-1990. Monthly averages of radiation, wind speed and vapour pressure deficit were calculated from the local data collected for the flow validation over the period 1998-2003 (section 7.5.1).

8.3.2 Results

The results of the transport modelling with tritium are shown in Figure 8-14. MACRO simulates the depth of the tritium peak remarkably well, indicating that the advective tracer velocity is well represented. However, the total tritium content in the profile is clearly underestimated by the model. The simulated tritium concentrations are lower than the measured concentrations, especially at shallow depth. The high measured tritium concentrations in the upper most 3 m of the profiles had also been identified as problematic by Foster and Bath (1983). As shown in Figure 8-13, reported values for tritium concentrations in UK rainfall after 1975 were typically around 80 TU in summer and around 20 TU in winter. On the other hand, the tritium concentrations in the upper most 3 m of the Fleam Dyke profiles were typically around 100 TU. This is contradictory. A possible explanation may be isotopic fractionation of tritium during evaporation of infiltrating rainfall from the soil surface.

However, Zimmerman et al. (1966) showed that this could only lead to an enrichment of maximum 2%.

Table 8-4 Parameter values for spring barley

Symbol	Description	Value
D_{emerg}	day of crop emergence	78 (17 Mar)
D_{min}	day of intermediate stage between emergence and maximum GLAI	79 (18 Mar)
D_{max}	day of maximum GLAI and root depth	180 (27 Jun)
D_{harv}	day of harvest	211 (28 Jul)
x_1	factor controlling the rate of increase of GLAI between crop emergence and maximum GLAI	1.5
x_2	factor controlling the rate of decrease of GLAI between maximum GLAI and harvest	0.7
$GLAI_{min}$	green leaf area index at intermediate stage [-]	0.1
$GLAI_{max}$	maximum green leaf area index [-]	5
$GLAI_{harv}$	green leaf area index at harvest [-]	5
$z_{r,min}$	root depth at intermediate stage [m]	0.05
$z_{r,max}$	maximum root depth [m]	1.2
$h_{c,min}$	crop height at intermediate stage [m]	0.1
$h_{c,max}$	maximum crop height [-]	0.8
ζ	root distribution [-] (1)	80
$\frac{\theta_{s,i} - \theta_{d,i}}{\theta_{s,i} - \theta_{w,i}}$	fraction of available water exhausted before reduction in transpiration occurs [-]	0.5
$\theta_{s,i} - \theta_{a,i}$	critical air content for root water uptake [-]	0.75
ω^*_c	root adaptability factor [-]	0.75
α^*	albedo	0.25
c_f	correction factor for wet canopy evaporation [-]	1
$W_{c,max}$	canopy interception capacity [mm]	0

(1) Percentage of the total root length that is present in the upper 25% of the root depth

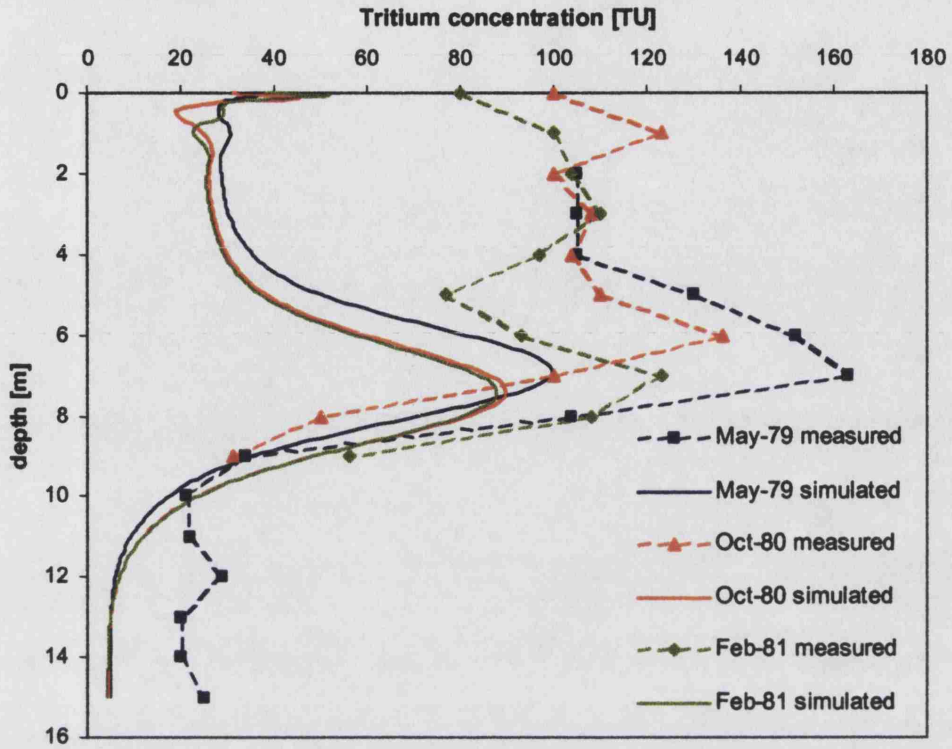

Figure 8-14 Measured versus simulated tritium concentrations in the matrix pore water at the Fleam Dyke site during the period 1979-1981.

Foster and Smith-Carington (1980) tried to reconcile the tritium concentrations in the rainfall and in the core profiles. They assumed a mechanism where isotopic equilibration between summer rainfall and soil moisture occurred. Even so, this could not explain the tritium concentrations around 100 TU measured in the top few metres at the Fleam Dyke site. Another important factor may be the uncertainty of the local tritium concentrations in rainfall at the Fleam Dyke site. The average concentrations in UK rainfall as shown in Figure 8-13 are subject to uncertainty, and considerable differences occur between locations within the UK (Foster and Smith-Carington, 1980). The uncertainty is especially high for the critical period of 1962-1964, when the UK concentrations were derived from correlation with measurements in Valentia (Ireland). This could explain the lack of fit between measured and simulated peak concentrations in Figure 8-14.

Figure 8-14 also shows a large discrepancy between measured and simulated tritium concentrations below 12 m depth. Simulated concentrations were at 5 TU or lower, indicating that the water below 12 m depth concerns 'old' water that has been subject to significant tritium decay. The measured profiles show concentrations around 20 TU at the same depth, suggesting that the older water is mixed with younger water that has bypassed the higher chalk layers. Apparently the model underestimates the bypass of solutes through the fractures in the chalk above and around 12 m depth. Further differentiation of the chalk profile into strata with different properties could possibly resolve this.

The modelling of the environmental tritium profiles at Fleam Dyke was subject to several limitations. First, the use of monthly climate averages for the meteorological variables restricts the accuracy of the PET, which may be particularly relevant during the critical 1962-1964 period. Second, there is considerable uncertainty in some of the crop parameters for spring barley shown in Table 8-4. Finally, little is known about the hydraulic properties of the chalk below 5 m depth, which might be different from the properties of the chalk-3 stratum obtained after calibration of the Fleam Dyke tracer test. Similarly, the hydraulic properties of the soil on the arable plot at Fleam Dyke might be different from those of the grass-covered soil at Fleam Dyke lysimeter. Even if all these uncertainties could be resolved, a satisfactory simulation of the measured tritium profiles would most likely still not be possible. The reason is the anomaly between the tritium concentrations in post-1975 UK rainfall and the tritium concentrations measured at shallow depth. This is probably related to an error in the tritium input function. Therefore further calibration of the model was not pursued.

8.4 Modelling of environmental deuterium profiles at Fleam Dyke (1979-1981)

The calibrated model was used to simulate the environmental deuterium profiles measured at Fleam Dyke between 1979 and 1981 (Figure 4-7). Therefore MACRO 5.0 was run over the period of 1 May 1979 until 30 September 1981, with deuterium concentrations in rainfall as input.

8.4.1 Model input

Daily rainfall data were available from the Fleam Dyke rain gauge. Monthly data of deuterium concentrations in rainfall were taken from Darling and Bath (1988), who measured deuterium contents of samples from the Fleam Dyke rain gauge (Figure 8-15). The initial water contents on 1 May 1979 were taken from neutron probe measurements performed by the BGS on the arable field next to Fleam Dyke lysimeter on that day. The initial deuterium contents in the pore water were set to the measured profile in May 1979 as shown in Figure 4-7.

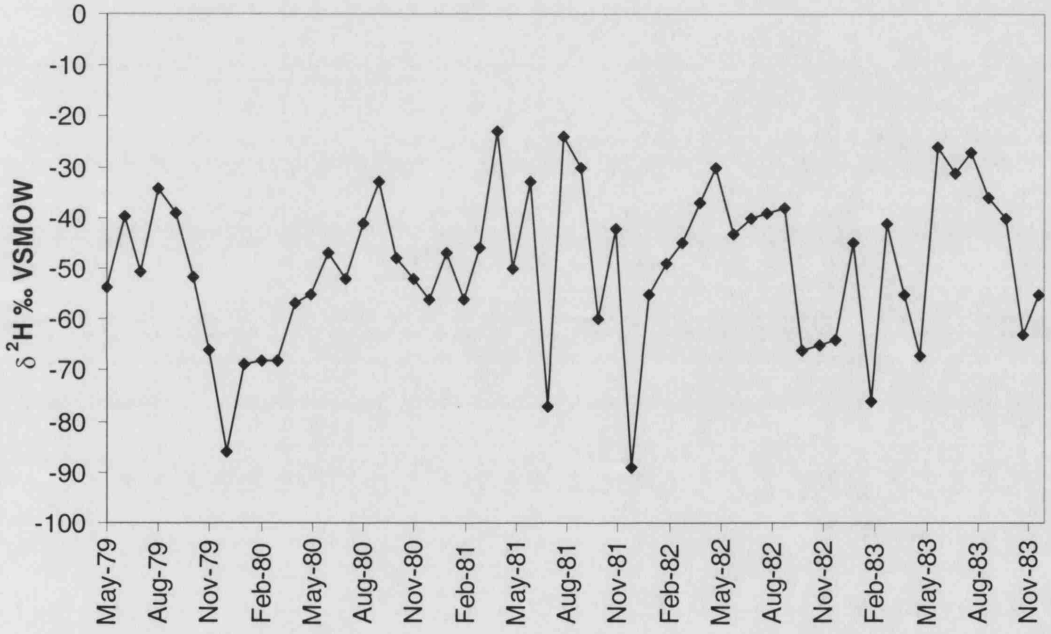

Figure 8-15 Monthly deuterium concentrations in rainfall from the Fleam Dyke site.

The depth of the profile was kept at 14 metres, with a total of 200 numerical layers. As the bottom boundary condition, the lysimeter boundary condition was maintained. As with the tritium simulation, the nature of the bottom boundary condition at 14 m depth was shown to have little effect on the transport of the solute in the upper metres.

The free-water diffusion coefficient for deuterium was fixed at 1.48×10^{-9} m^2/s (Table 5-1), and degradation of solute was disabled. The profiles of environmental deuterium had been measured on the arable plot adjacent to the Fleam Dyke

lysimeter. Therefore the annual development of spring barley needed to be included in the model again, and all parameters were fixed to the same values as in the tritium simulation of section 8.3.

PET needed to be calculated internally by MACRO, as it is dependent on the annual crop development of spring barley. Local data for the period 1979-1981 were only available for the air temperature and the incoming solar radiation. For the wind speed and the vapour pressure deficit, monthly averages were calculated from the local data collected for the flow validation over the period 1998-2003 (section 7.5.1).

8.4.2 Results

The resulting deuterium profiles are shown in Figure 8-16. For each sampling date, the simulated deuterium contents are smaller than the measured deuterium contents in the upper 2 m of the profile. Earlier, Figure 8-15 had shown that rainfall is on average isotopically enriched in summer and isotopically depleted in winter. This suggests that the model does not allow enough of the summer rainfall to contribute towards the repletion of the moisture store in the unsaturated profile. With the MACRO model, most of the summer rainfall evaporates, so it is the lighter winter rainfall that dominates the replenishment of the profile. In reality more mixing seems to occur between summer and winter rainfall. Foster and Bath (1983) came to a similar conclusion while discussing the deuterium profiles at Fleam Dyke, suggesting rapid penetration of summer rainfall and mixing with the soil moisture prior to evapotranspiration. This may be possible if bypass flow occurs in the soil during the summer, possibly by the presence of desiccating cracks or by tillage activity.

Most of the limitations in the transport model for the environmental tritium profiles (section 8.3.2) also apply to the environmental deuterium profiles. These are related to differences between the arable field and the grass-covered lysimeter site. There is uncertainty in some of the crop parameters for spring barley and in the hydraulic properties of the soil. Given the number of uncertainties and the limited availability of data, no further calibration was attempted.

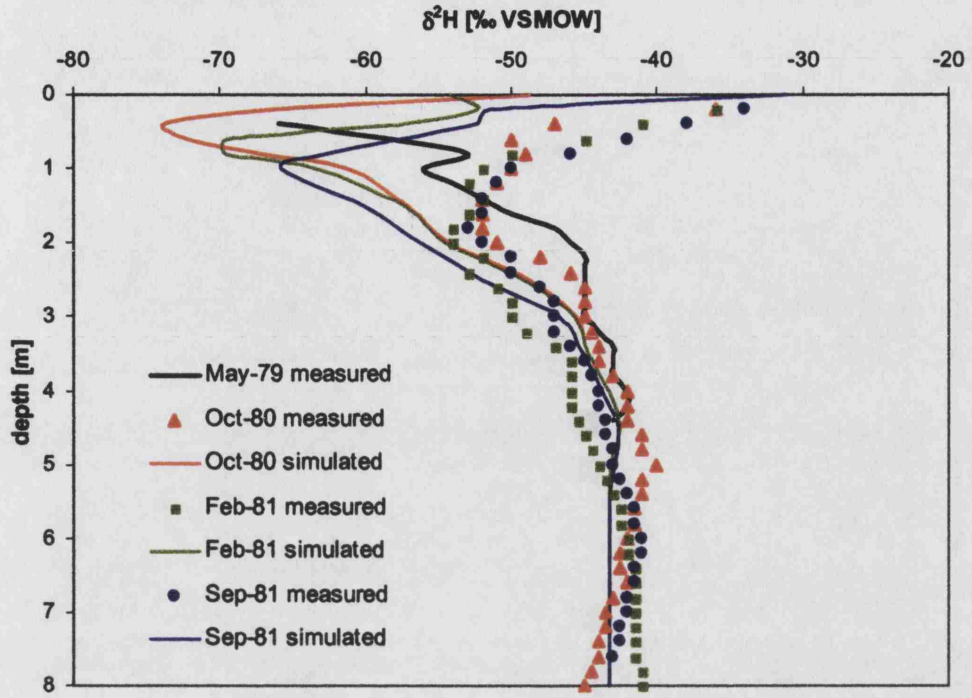

Figure 8-16 Measured versus simulated deuterium concentrations in the matrix pore water at the Fleam Dyke site during the period 1979-1981.

8.5 Discussion of the role of fractures and matrix

The last section of this chapter will look in more detail at the distribution of flow and solute transport between the fractures and the matrix, as simulated by MACRO. The following figures and discussion all rely on the calibrated transport model for the Fleam Dyke tracer test with deuterium as a tracer (section 8.2.1.3).

8.5.1 Flow velocity

Figure 8-17 shows the average flow velocities in the micropores (matrix) and macropores (fractures). Flow velocities in the fractures are about three orders of magnitude larger than those in the matrix. Values around 1000 mm/d are obtained for the fractures, compared to values around 1 mm/d for the matrix. This corresponds well with the literature values for chalk that were quoted in Table 3-1. Over the whole simulation period, the fractures never reached complete saturation. The saturation percentage of the fractures during times when the fractures are active was on average only about 15%, with maxima up to 60%.

8.5.2 Solute flux

Figure 8-18 shows the distribution of the solute flux between the matrix and the fractures for each chalk stratum. This figure is similar to Figure 7-13, which showed the distribution of the water flux. Figure 8-18 demonstrates the intermittent nature of the solute flux through the fractures, compared with the more continuous nature of the solute flux through the matrix. The movement of deuterium through the fractures is generally confined to periods of high infiltration rates. A different picture emerges for the chalk-2 stratum, which represents a hard band in the chalk at Fleam Dyke between 150 and 270 cm depth. Here the hydraulic conductivity of the matrix is so low (Table 7-6: 0.115 mm/d) that the solute flux through the matrix is minimal, and most of the solute flux occurs through the fractures.

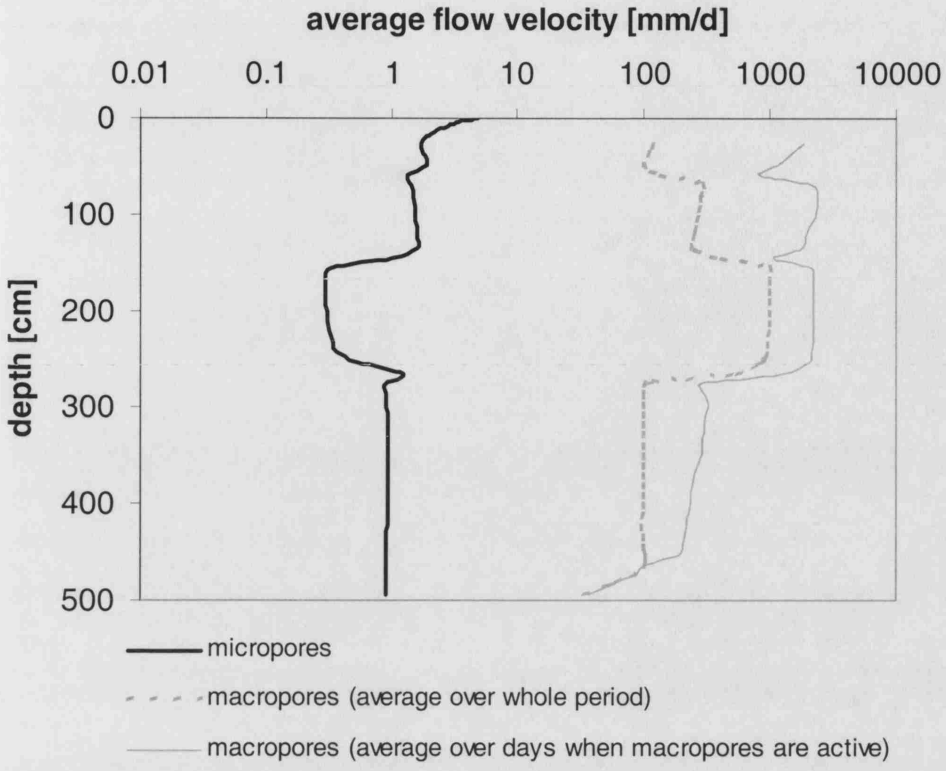

Figure 8-17 Average flow velocities in the micropores (matrix) and macropores (fractures), calculated with MACRO over the period 01/09/2001 until 30/07/2003.

8.5.3 Analysis of a high infiltration event

The occurrence of a high infiltration event is illustrated in Figure 8-19 until Figure 8-21. They cover the period of 6 November 2002 until 21 November 2002, which marked the start of the recharge season as modelled by MACRO. Figure 8-19 shows the percentage of the total water flux that passes through the macropores (fractures) at each depth, combined with the percentage of the total solute flux passing through the macropores. On 6 November, a first pulse of high infiltration reaches the weathered chalk at 20 cm depth, causing partial saturation of the fractures. This pulse of fracture flow quickly travels downwards, reaching the bottom of the lysimeter at 5 m depth in less than one week. The fracture component in the weathered chalk then fades away, whereas in the lower chalk strata the fracture component is more persistent.

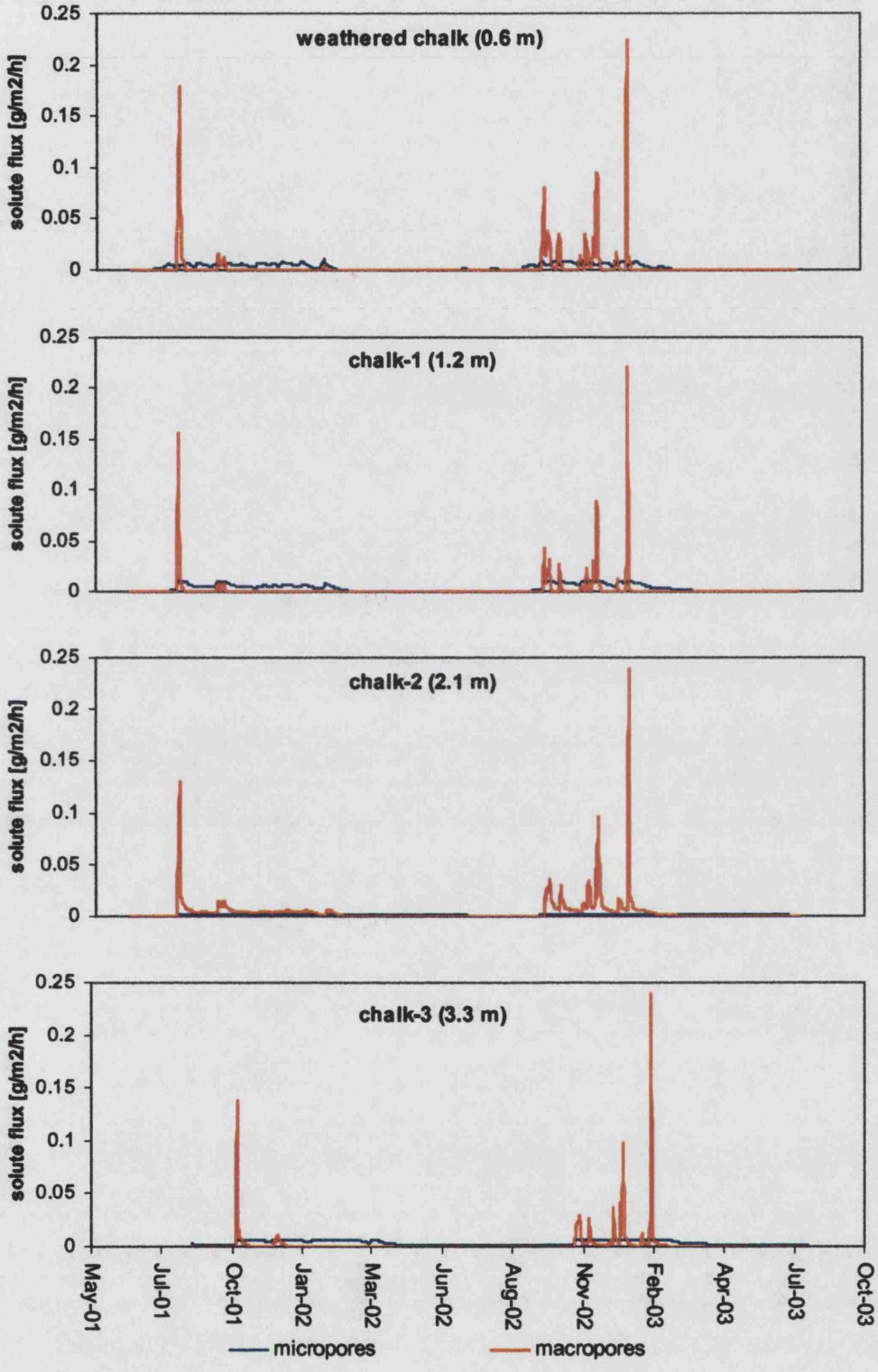

Figure 8-18 Occurrence of solute flux through micropores (matrix) and macropores (fractures) in different chalk strata of the Fleam Dyke site, as simulated by MACRO.

The initiation of this fracture flow component can also be followed on Figure 8-20, which shows the water exchange between the macropores (fractures) and the micropores (matrix). On 6 November water flows from the matrix to the fractures at 20 cm depth, at the top of the weathered chalk. Later on, there is additional flow from the matrix to the fractures at 65 cm depth, which marks the transition between the weathered chalk and the chalk-1 stratum. Deeper in the chalk-1 stratum, part of the fracture flow is initially sucked back into the matrix (Figure 8-20, 8 November), because the matrix is not yet fully saturated. From 12 November onwards, a stable water exchange mechanism is established around the chalk-2 stratum. This hard band of chalk between 150 and 270 cm depth forces the majority of the flow through the fractures, as can be seen from Figure 8-19. Water first flows through the matrix in the chalk-1 stratum and is then diverted towards the fractures of the chalk-2 stratum at 150 cm depth. At 270 cm depth, part of this fracture flow component is sucked back into the matrix of the chalk-3 stratum.

Figure 8-19 further shows the difference between the proportional water flux and solute flux passing through the macropores (fractures). Both curves generally follow the same course, although the solute flux component in the fractures is usually smaller than the water flux component in the fractures. The reason for this difference is additional diffusive transport of solutes through the matrix. In MACRO, diffusion of solutes is only modelled in the micropores, whereas in the macropores merely advective transport is assumed. As a consequence, diffusion increases the total solute flux in the matrix, and thereby decreases the proportion of the solute flux passing through the fractures. To test this hypothesis, the model was run with the diffusion coefficient set to zero. Indeed, in this case the curves of the water flux and the solute flux generally coincided.

At some instances however, the solute flux component in the fractures is actually larger than the water flux component. This occurs when the solute concentration in the fractures is larger than the solute concentration in the matrix. An example of this is shown in Figure 8-19, for 12 November around 100 cm depth. Here the deuterium concentration in the fractures of the chalk-1 stratum is larger than the deuterium concentration in the matrix. This in turn leads to diffusion of deuterium from the fractures into the matrix.

The deuterium concentrations in the fractures and the matrix are shown in Figure 8-21. On 6 November 2002, the peak of the deuterium tracer in the matrix had advanced to a depth of around 40 cm. When suddenly the fractures become active in the weathered chalk and the chalk-1 stratum, tracer is diverted from the matrix into the fractures. The tracer can then partially bypass the matrix by rapid transport through the fractures, leading to higher tracer concentrations in the fractures than in the matrix (Figure 8-21, 8 November). The tracer gradually moves back from the fractures to the matrix by advective exchange, in addition to diffusive exchange. The result of this bypass mechanism is that the peak of the tracer profile in the matrix is reduced, and that a secondary peak is introduced around 155 cm depth (Figure 8-21, 21 November).

Figure 8-21 shows that a concentration gradient between the fractures and the matrix occurs down to about 200 cm depth, whereas in the deeper chalk layers the concentrations in fractures and matrix are always the same. The reason for this different behaviour comes down to two main factors: the flow velocities in the fractures (Figure 8-17) and the matrix block size (parameter *a*, Table 8-2). The weathered chalk and the chalk-1 stratum feature average fracture flow velocities exceeding 2000 mm/d and a matrix block size of at least 50 mm. These conditions do not allow time for diffusive equilibrium between the fractures and the matrix. In contrast, the chalk-2 and chalk-3 strata feature average fracture flow velocities below 350 mm/d and a matrix block size of maximum 20 mm, allowing the fractures to approach diffusive equilibrium with the matrix.

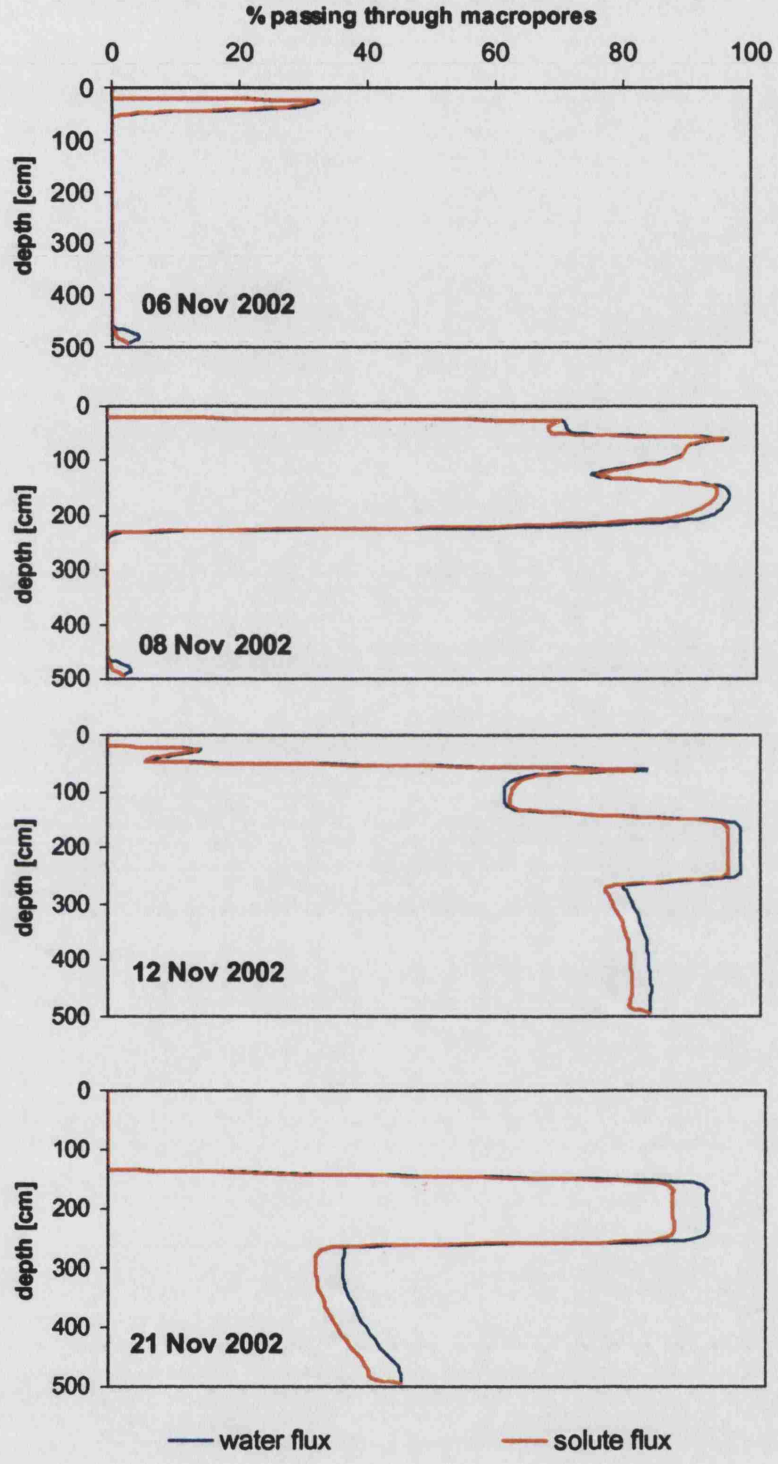

Figure 8-19 Percentages of the total water flux and solute flux passing through the macropores (fractures) as opposed to the micropores (matrix) at the Fleam Dyke site over the period of 6 to 21 November 2002, as simulated by MACRO.

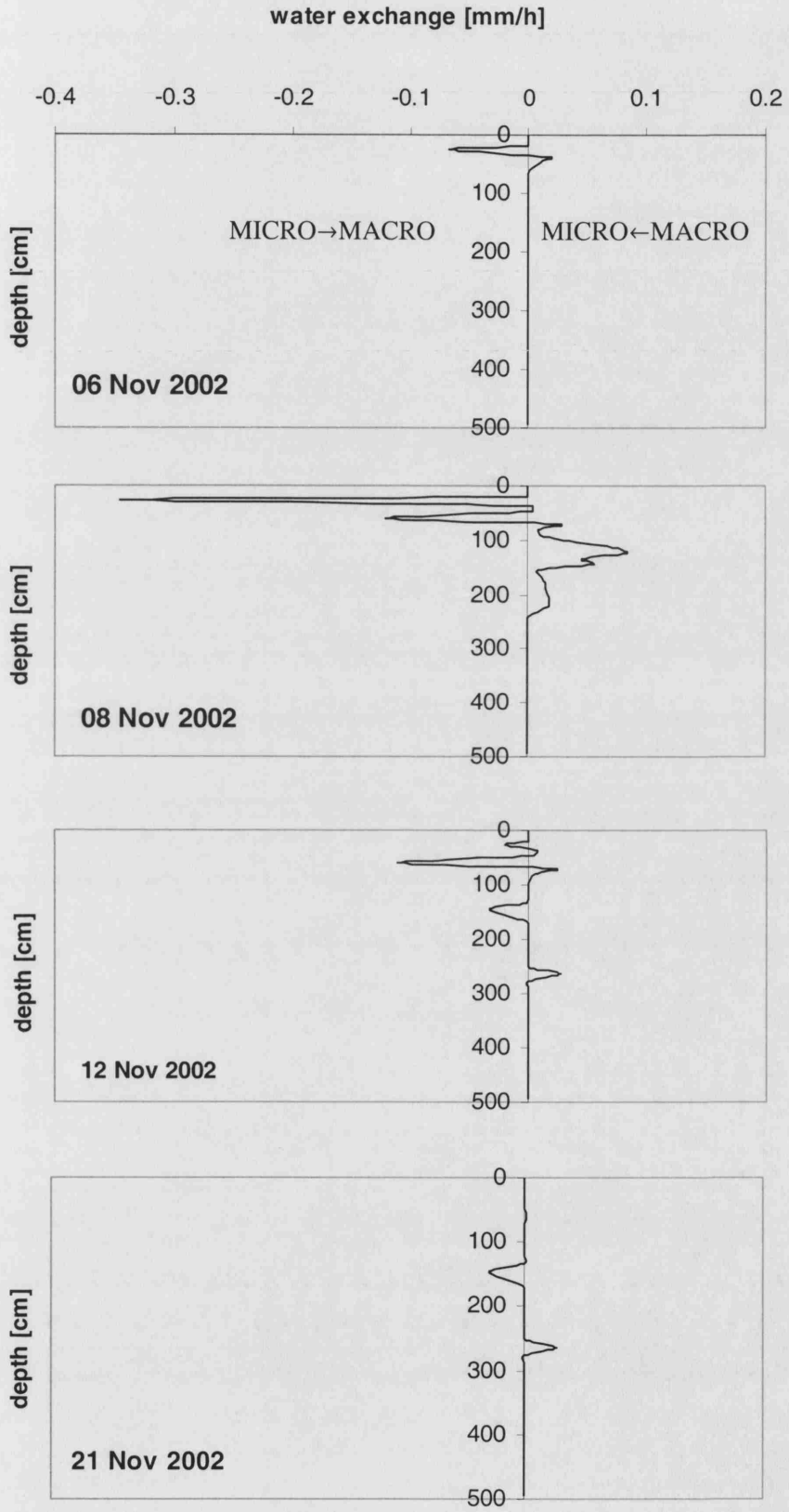

Figure 8-20 Water exchange between macropores (fractures) and micropores (matrix) at the Fleam Dyke site, as simulated by MACRO over the period of 6 to 21 November 2002; exchange is taken positive from the macropores into the micropores.

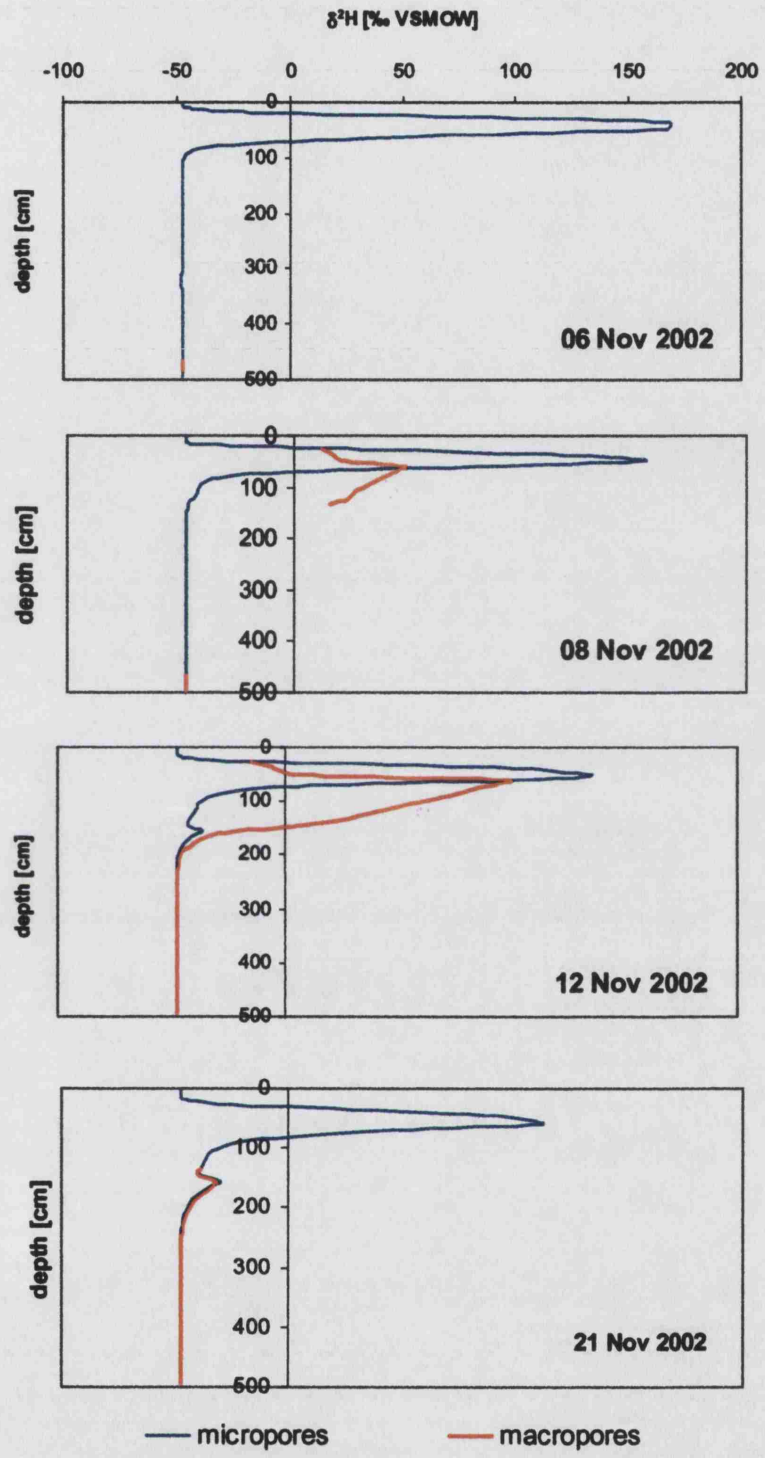

Figure 8-21 Deuterium concentrations in the macropores (fractures) and micropores (matrix) at the Fleam Dyke site, as simulated by MACRO over the period of 6 to 21 November 2002.

8.5.4 Revised conceptual model for flow and transport through the Chalk unsaturated zone

The fractions of the water flux and the solute flux that pass through the macropores can now be calculated relative to the cumulative fluxes over several years, as shown in Figure 8-22. This figure is analogous to Figure 8-19, but this time as an average over the period of September 2001 to July 2003. The difference between the solute flux and the water flux is again due to diffusion of solutes through the matrix. In this case the difference is larger than in Figure 8-19, because diffusion through the matrix continues during dry periods in the summer when the matrix water is essentially stagnant. From Figure 8-22 the relative importance of fracture flow at each depth in the chalk profile can easily be seen. In the chalk-1 and chalk-3 stratum, fracture flow accounts for about 45% of the total water flux. In the chalk-2 stratum, representing a hard band in the Chalk between 150 and 270 cm depth, this figure goes up to 85%. When examining drainage from the Fleam Dyke lysimeter in the 1980s, Jones and Cooper (1998) had suggested a value of around 30% for the proportion of fracture flow through the chalk. The present research suggests that a single value cannot give an accurate image. Rather, the importance of fracture flow shows significant variation between different strata in the same chalk profile.

This leads to a renewed conceptual model for flow and solute transport through the chalk at the Fleam Dyke site, as shown on the right in Figure 8-22. It shows a hypothetical plane-parallel fracture, intersecting the unsaturated profile from the surface down to 5 m depth. The average relative saturation of the fracture is variable along the profile, and the fracture never becomes completely saturated. Looking back at the four alternative conceptual models proposed in Chapter 3, this figure bears most resemblance with Figure 3-9 d, i.e. the conceptual model of advective exchange. Fracture flow is generated at various depths in the profile. This fracture flow component is derived from the matrix, and it may return to the matrix deeper in the profile where the hydraulic conductivity increases again.

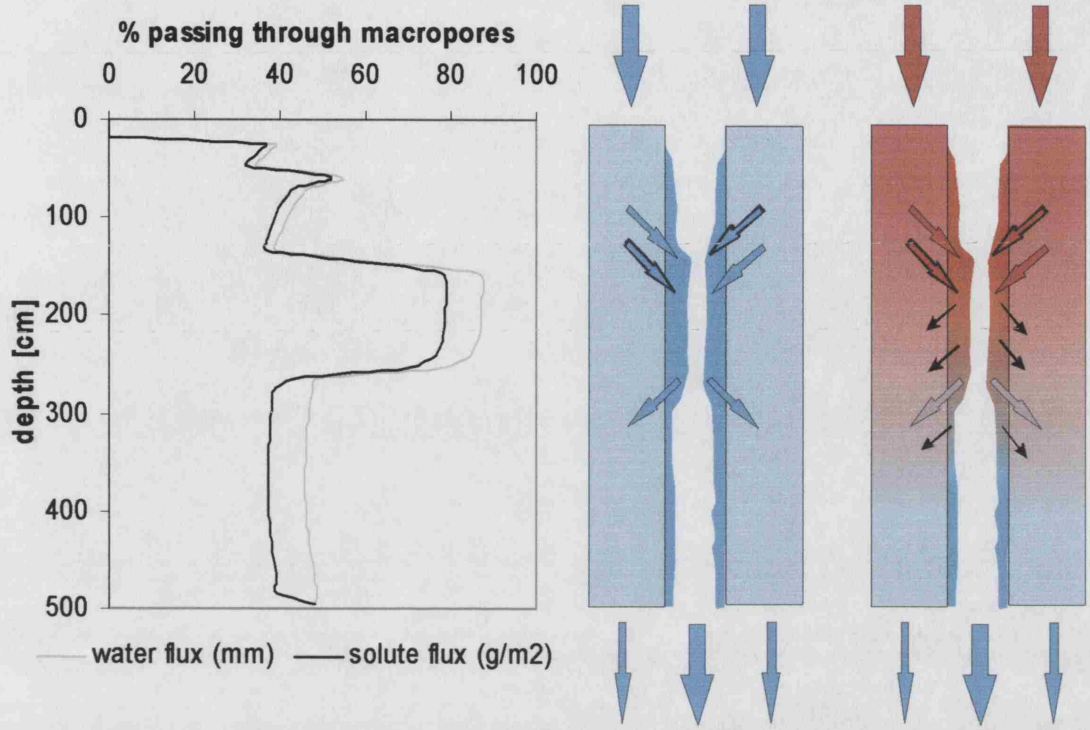

Figure 8-22 Percentages of the total cumulative water flux and solute flux passing through the macropores (fractures) as opposed to the micropores (matrix) at the Fleam Dyke site over the period of September 2001 until July 2003, as simulated by MACRO. A conceptual model for both the flow and transport behaviour is included on the right, showing a cross-section of chalk intersected by a vertical planar fracture. Clean water is represented in blue, solutes are represented in red, hollow arrows indicate water flow and black arrows indicate diffusion of solutes.

As the importance of fracture flow varies between different strata in the same chalk profile, large variations are also expected between different chalk sites. Unsaturated flow and transport through the Chalk in England exhibits significant regional differences, reflecting differences in geological, climatological and vegetational conditions. For instance, in section 3.2.2 it was shown that for some sites in the Upper Chalk fracture flow may be very unlikely. Hence the conceptual model shown in Figure 8-22 should merely be seen as a likely representation of the flow and transport behaviour at one particular chalk site. Care should be taken to extrapolate these results to other chalk sites. Therefore, over the whole Chalk in England, any of the conceptual models initially presented in Figure 3-9 may still be applicable.

9 Water balance method to calculate recharge through the Chalk

9.1 Introduction

Chapter 7 has illustrated how the MACRO model can be used to simulate recharge through the Chalk. The model was first calibrated for the Fleam Dyke site against data of water content, pressure head and lysimeter drainage for the period 1980-1981. The model was then validated for the same site against data of lysimeter drainage for the period 1999-2003. It was concluded that MACRO was satisfactory for describing the timing and daily variation of recharge through the Chalk (section 7.5.2). Such time series of recharge are often needed as input to simulate transient flow through the saturated zone.

MACRO is a complex model with high parameter requirements, and one could wonder if such complexity is needed when simulating only recharge, not transport. The principle of parsimony dictates that one should aim for a model that uses the smallest number of parameters necessary to describe the data adequately. Therefore the present chapter describes the use of a simple water balance method to simulate recharge through the chalk, and compares its performance against that of the MACRO model.

The water balance model called DFIDGWR (Finch, 2002) was chosen to simulate recharge at the Fleam Dyke site. The model requires meteorological data to calculate the PET internally, and these data were only available for the period 1999-2003. Therefore this period was chosen to calibrate the model, and validation with a second data set was not possible. Before proceeding to the model input and output, the next section provides an overview of the formulation of DFIDGWR.

9.2 Technical description of DFIDGWR

DFIDGWR is a water balance model that has been designed to give reliable estimates of groundwater recharge (Finch, 2002). The model calculates a mass balance with a daily time step, where soil drainage is the result of subtracting all the losses of water from the incoming rainfall. Therefore it consists of several sub-models dealing with canopy interception, runoff, interflow, soil moisture and evapotranspiration from vegetation and soil. Afterwards soil drainage is converted into recharge using a transfer function to describe the delay and smoothing occurring in the unsaturated zone. The model can be run in either point mode or regional mode. In point mode, the model is merely one-dimensional, whereas in regional mode, the model is fully spatially distributed, using a rectangular grid of cells to represent spatial variability.

The overall daily water balance is calculated as:

$$P = E_t + I_c + R_o + R_i + B + \Delta S \qquad \textit{Eq. 9-1}$$

where P is the precipitation rate [mm/d], E_t is the actual evapotranspiration [mm/d], I_c is the canopy interception [mm/d], R_o is the surface runoff [mm/d], R_i is the interflow [mm/d], B is the bypass flow [mm/d] and ΔS is the change in soil water content [mm/d]. Soil drainage is defined as the sum of the bypass flow and positive changes in the soil water content, once the field capacity has been exceeded. Canopy interception is only considered when the land cover is forest.

The main processes in DFIDGWR are described in more detail in the following sections, largely based on Finch (2001) and Finch (2002). Emphasis is on the processes relevant to the simulation of the Fleam Dyke lysimeter data. Hence canopy interception and interflow are not considered, and discussion of the model is limited to its operation in point mode.

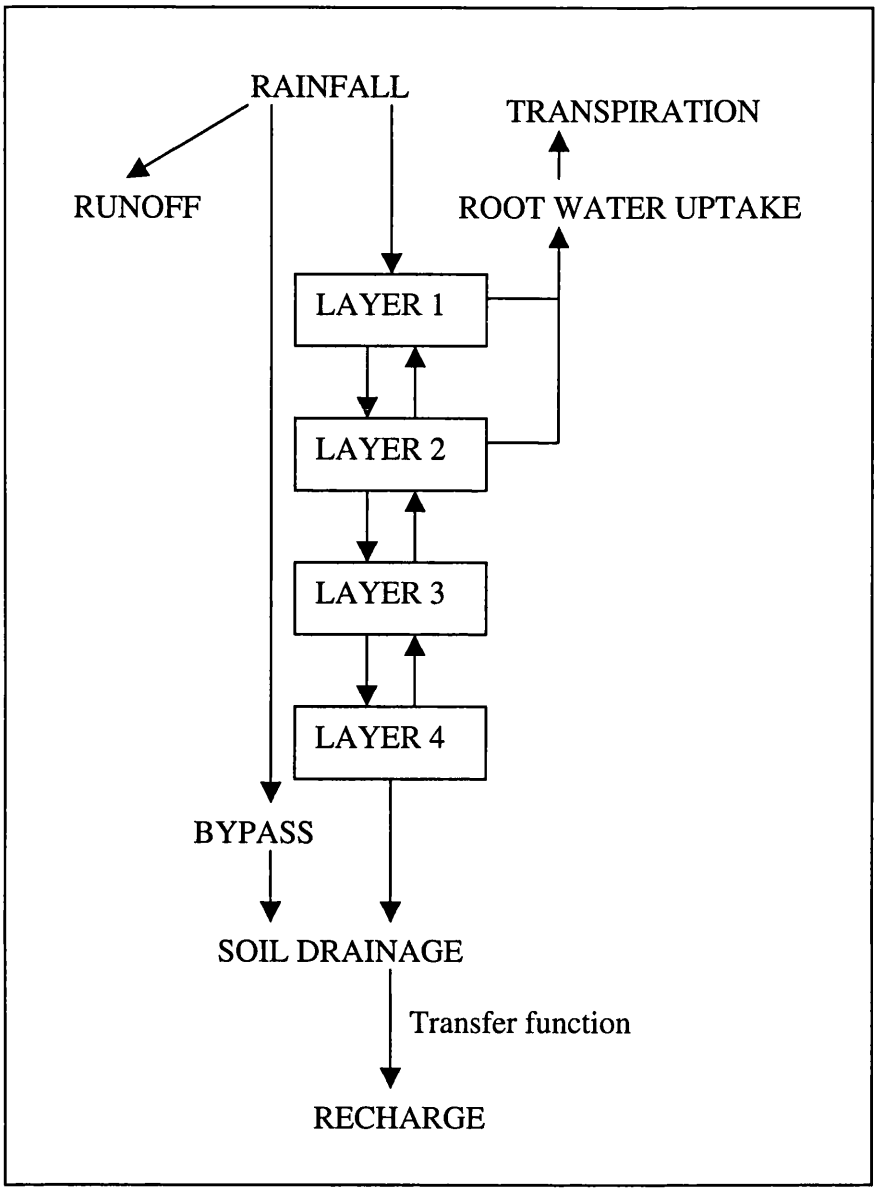

Figure 9-1 Schematic overview of the DFIDGWR model

9.2.1 Soil moisture model

The soil is here defined as "the zone, extending down from the surface, within which water is lost to evapotranspiration, i.e. the zone in which soil water deficits develop" (Finch, 2002). This is different to the definition used by a soil scientist, and implies that the "soil" can extend down to the unweathered bedrock.

In DFIDGWR, the soil is divided into four layers. The first and second layers represent the root zone from which root water uptake is possible. From layers three

and four, direct losses through evapotranspiration do not occur, but water can still be drawn upwards as a result of soil moisture deficits in the layers above.

Drainage between layers is based on a capacity approach, as introduced by Ragab et al. (1997). If the inflow into a layer increases its water content above its field capacity, then the excess water drains down to the layer underneath. The inflow into the upper layer, $q_{in,1}$, is equal to the effective rainfall P_e, defined as:

$$q_{in,1} = P_e = P - R_o - B - I_c \qquad \textit{Eq. 9-2}$$

For layers two until four, the inflow $q_{in,i}$ into each layer i is calculated as:

$$q_{in,i} = q_{in,i-1} - (\theta_{f,i-1} - \theta_{i-1})\Delta z_{i-1} \quad \textit{if} \quad q_{in,i-1} > (\theta_{f,i-1} - \theta_{i-1})\Delta z_{i-1} \qquad \textit{Eq. 9-3}$$

$$q_{in,i} = 0 \quad \textit{if} \quad q_{in,i-1} \le (\theta_{f,i-1} - \theta_{i-1})\Delta z_{i-1} \qquad \textit{Eq. 9-4}$$

where $\theta_{f,i}$ is the water content of layer i at field capacity [-], θ_i is the actual water content of layer i [-] and Δz_i is the thickness of layer i [mm]. The soil drainage Q_s leaving layer 4 is finally defined as:

$$Q_s = q_{in,4} - (\theta_{f,4} - \theta_4)\Delta z_4 \quad \textit{if} \quad q_{in,4} > (\theta_{f,4} - \theta_4)\Delta z_4 \qquad \textit{Eq. 9-5}$$

$$Q_s = 0 \quad \textit{if} \quad q_{in,4} \le (\theta_{f,4} - \theta_4)\Delta z_4 \qquad \textit{Eq. 9-6}$$

In addition to drainage between soil layers as described above, movement of water between soil layers in response to different water potentials is possible as well. This has been implemented in DFIDGWR using the model of Ben Mehrez et al. (1992):

$$\Delta\theta_i = -\Omega(\theta_i - \theta_{i+1}) \qquad \textit{Eq. 9-7}$$

where $\Delta\theta_i$ is the change in water content in layer i due to the gradient in water potential and Ω is the pseudodiffusivity [s^{-1}], defined as:

$$\Omega = \frac{2D_i[(\theta_i + \theta_{i+1})/2]}{(\Delta z_i + \Delta z_{i+1})\Delta z_i} \qquad \textit{Eq. 9-8}$$

and D_i is the diffusivity [m^2/s]. An expression for the diffusivity is found by defining the water retention relationship and the unsaturated hydraulic conductivity according to Campbell's (1974) formulation. This is analogue to the formulation of Brooks & Corey (1964) (Eq. 2-18 and Eq. 2-21), but with $\theta_r = 0$ and $b = 1/\lambda$:

$$h = h_e\left(\frac{\theta_s}{\theta}\right)^b \qquad \textit{Eq. 9-9}$$

$$K = K_s\left(\frac{\theta}{\theta_s}\right)^{2b+3} \qquad \textit{Eq. 9-10}$$

where K_s is the saturated hydraulic conductivity [m/s], θ_s is the saturated water content [-] and h_e is the air-entry pressure [m]. Taking the derivative of the water retention relationship to obtain the specific capacity:

$$\frac{\partial h}{\partial \theta} = -b\, h_e \theta_s{}^b\, \theta^{-b-1} \qquad \textit{Eq. 9-11}$$

and introducing this into the diffusivity (as in Eq. 2-10), this becomes:

$$D = K\frac{\partial h}{\partial \theta} = \frac{-bK_s h_e}{\theta}\left(\frac{\theta}{\theta_s}\right)^{b+3} \qquad \textit{Eq. 9-12}$$

9.2.2 Evapotranspiration and canopy processes

9.2.2.1 Potential evapotranspiration (PET)

PET is calculated in DFIDGWR by any of the models of Penman-Monteith, Penman, Priestley-Taylor or Makkink. The Penman-Monteith model is by far the most widely accepted, and was used for the simulation of the Fleam Dyke lysimeter data.

The Penman-Monteith equation implemented in DFIDGWR calculates PET based on daily meteorological data (Allen et al., 1994):

$$PE_t = \frac{1}{\lambda_w}\left[\frac{\Delta(R_n - G) + 86.4\rho_a c_p \frac{e_s - e_d}{r_a}}{\Delta + \gamma_p\left(1 + \frac{r_s}{r_a}\right)}\right] \qquad \textit{Eq. 9-13}$$

where PE_t is the total potential evapotranspiration rate [mm/d], λ_w is the latent heat of evaporation of water [MJ/kg], Δ is the slope of the saturation vapour pressure curve [kPa/°C], e_s is the saturated vapour pressure [kPa], e_d is the actual vapour pressure [kPa], R_n is the net incoming radiation [MJ/m^2/day], G is the outgoing heat conduction into the soil [MJ/m^2/day], γ_p is the psychrometric constant [kPa/°C], c_p is the specific heat of moist air [= 1.013 kJ/kg/°C], r_s is the surface resistance [s/m] and r_a is the aerodynamic resistance [s/m].

This equation is identical to the Penman-Monteith equation implemented in Visual Basic for use in the MACRO model, and the reader is referred to section 7.2.1.1 for a description of its components. All components are calculated identically as for the Visual Basic model, with exception for the surface resistance r_s [s/m] which is calculated as:

$$r_s = \frac{r_l}{0.5LAI} \qquad \textit{Eq. 9-14}$$

where r_l is the stomatal resistance of a single leaf [s/m] and LAI is the leaf area index [-].

9.2.2.2 Actual evapotranspiration

For permanent short vegetation, as in the case of the Fleam Dyke lysimeter, evapotranspiration is taken to occur exclusively by transpiration, while evaporation directly from the soil and from canopy interception are assumed negligible. The relation between actual root water uptake $E_{r,i}$ and total potential evapotranspiration PE_t in each model layer i is governed by the stress factor ω_i, which is a function of the water content (Figure 9-2):

$$E_{r,i} = PE_t\ \omega_i\ r_i \qquad \textit{Eq. 9-15}$$

with:

$$\omega_i = \frac{\theta_i - \theta_{w,i}}{\theta_{d,i} - \theta_{w,i}} \qquad \textit{if } 6_{w,i} < 6_i < 6_{d,i} \qquad \textit{Eq. 9-16}$$

$$\omega_i = 0 \qquad \textit{if } 6_i \le 6_{w,i} \qquad \textit{Eq. 9-17}$$

$$\omega_i = 1 \qquad \textit{if } 6_i \ge 6_{d,i} \qquad \textit{Eq. 9-18}$$

where r_i is the fractional proportion of roots in layer i [-], $\theta_{w,i}$ is the water content for layer i at wilting point and $\theta_{d,i}$ is the water content for layer i below which evaporation is reduced below potential.

The total root mass is divided between the two upper layers, and the proportion in each layer, as well as the thickness of each layer, is defined by the user.

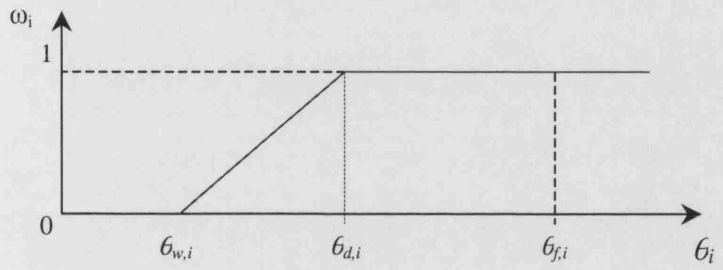

Figure 9-2 The stress factor ω_i for root water uptake

9.2.3 Surface runoff

Runoff is effective rainfall that is lost through overland flow and is considered unavailable for recharge. The amount of runoff is taken to be a function of the water content of the upper layer:

$$R_o = P_e - \Delta z_1(\theta_{s,1} - \theta_1) \quad if \quad P_e > \Delta z_1(\theta_{s,1} - \theta_1) \qquad Eq.\ 9\text{-}19$$

$$R_o = 0 \quad if \quad P_e \le \Delta z_1(\theta_{s,1} - \theta_1) \qquad Eq.\ 9\text{-}20$$

where R_o is the runoff [mm/d], Δz_1 is the thickness of the surface layer [mm], $\theta_{s,1}$ is the saturated water content of the surface layer [-] and θ_1 is the actual water content of the surface layer [-].

9.2.4 Bypass flow

Bypass flow is effective rainfall that is routed directly to the soil drainage, with disregard of the actual water content of the soil. It is calculated as:

$$B = f P_e \quad if \quad P_e > P_B \qquad Eq.\ 9\text{-}21$$

$$B = 0 \qquad if \quad P_e \leq P_B \qquad \text{Eq. 9-22}$$

where B is the bypass flow [mm/d], f is the proportion of effective rainfall diverted to bypass flow [-] and P_B is the threshold of effective rainfall above which bypass flow is initiated [mm/d].

9.2.5 Unsaturated-zone transfer function

The water balance model described above takes account of all the losses that reduce the incoming rainfall to the soil drainage, i.e. the total water available for recharge. However, a simple water balance model cannot describe the exact timing of the recharge, with recharge being defined as the water arriving at the water table. Therefore, to simulate the temporal distribution of recharge, one needs to describe the infiltration through the unsaturated zone that converts soil drainage $Q_s(t)$ into recharge $Q(t)$. Instead of resolving the exact unsaturated flow equations (like MACRO does), DFIDGWR uses a simplified approach, where the impact of the unsaturated zone is modelled through a transfer function, described as a "black box" process (Besbes and de Marsily, 1984).

The soil drainage $Q_s(t)$ can be approximated by a series of pulses:

$$Q_s(t) = \sum_{i=0}^{N} Q_i \Delta t \, \delta(t - i\Delta t) \qquad \text{Eq. 9-23}$$

where N is the number of time steps of duration Δt and Q_i is the average value of $Q_s(t)$ over the interval $i\Delta t$ to $(i+1)\Delta t$. Recharge as a function of time $Q(t)$ can be related to the soil drainage $Q_s(t)$ through the unit response function σ:

$$Q(t) = \int_0^t Q_s(t-u)\sigma(u)du \qquad \text{Eq. 9-24}$$

This becomes:

$$Q(t) = \int_0^t \sum_{i=0}^{N} Q_i \Delta t \, \delta(u - i\Delta t)\sigma(u)du \qquad \text{Eq. 9-25}$$

which gives:

$$Q(t) = \Delta t \sum_{i=0}^{N} Q_i \, \sigma(i\Delta t) \qquad \text{Eq. 9-26}$$

For the unit response function σ, which accounts for both the delay and the smoothing occurring in the unsaturated zone, the unit hydrograph model of Nash (1959) was

chosen. This assumes that the unsaturated zone may be represented by a series of horizontal layers, with the outflow of one layer being the inflow into the next layer. A parameter m corresponds to the number of layers and thus the thickness of the unsaturated zone, whereas the storage characteristic j is a time constant. The response function can then be expressed as:

$$\sigma(t)=\frac{1}{j\Gamma(m)}\exp(-t/j)(t/j)^{m-1}H(t) \qquad \textit{Eq. 9-27}$$

where $\Gamma(m)$ is a gamma function and $H(t)$ is the Heaviside step function.

This approach has several inherent assumptions. The transfer through the unsaturated zone is considered conservative, i.e. the long term average soil drainage and recharge are identical. Implicitly this means that flow in the unsaturated zone is only downward and that there is no upward migration between the water table and the bottom of the soil. Further it is assumed that the transfer through the unsaturated zone is a linear process: more precisely, the unsaturated hydraulic conductivity does not vary significantly with time. Calver (1997) successfully used a similar transfer function approach to describe oscillations of unconfined aquifer water levels in the Chalk and Permo-Triassic Sandstones in England and Wales.

9.3 Data input

The DFIDGWR recharge model was executed for the Fleam Dyke site for the period of 1 January 1999 until 30 July 2003. Rainfall data and meteorological data for the calculation of PET were supplied as input with a daily resolution. The same dataset was used as for the flow validation of the MACRO model (section 7.5.1).

The division of the Fleam Dyke profile into 4 layers is shown in Table 9-1. The maximum rooting depth, marking the boundary between layers 2 and 3, was fixed at 80 cm depth, which was the initial estimate used in the MACRO model. The boundary between layer 1 and 2 was set to 20 cm depth, such that layer 1 represents the topsoil. The total depth of the profile, representing the total thickness of the capillary rise zone, was estimated at 250 cm. The model automatically allocates the

boundary between layers 3 and 4, and both layers must have identical hydraulic properties.

Table 9-1 Physical properties used in the recharge model DFIDGWR for the Fleam Dyke site.

Symbol	Description	Layer1	Layer2	Layers3+4
Δz	depth [cm]	0-20	20-80	80-250
θ_w	wilting point [-]	0.07	0.125	0.295
θ_f	field capacity [-]	0.30	0.235	0.308
θ_s	saturated water content [-]	0.425	0.26	0.312
K_s	saturated hydraulic conductivity [mm/d]	266	600	265
h_e	air-entry pressure [cm]	-78.6	-20	-50
b	empirical constant (Campbell) [-]	5.3	9	100

For layer 2 and layers 3&4, values for the parameters θ_s, h_e and b were obtained by fitting Campbell's function (Eq. 9-9) to measured water retention curves (Figure 9-3). Values for the wilting point θ_w were then obtained by applying Campbell's function for a pressure head of –15000 cm. For the topsoil of layer 1, no measured water retention curve was available. Instead, values for the parameters h_e and b were taken from Clapp and Harnberger (1978) as averages for silt loam.

Values for the field capacity for layer 2 and layers 3+4 were derived from time series of water contents, as shown in Figure 9-4. The field capacity, loosely defined as the water remaining in the soil after free drainage ceases, is estimated from the graphs as the level where the water content reaches a plateau. For layer 1, no time series of water contents was available, and the field capacity was estimated at 0.30 as an average for a loamy soil. For the parameters θ_s and θ_w of layer 1, the same values were used as defined in the MACRO model for the soil stratum at Fleam Dyke. Similarly, values for the saturated hydraulic conductivity K_s for each layer were adopted from the MACRO input (Chapter 7).

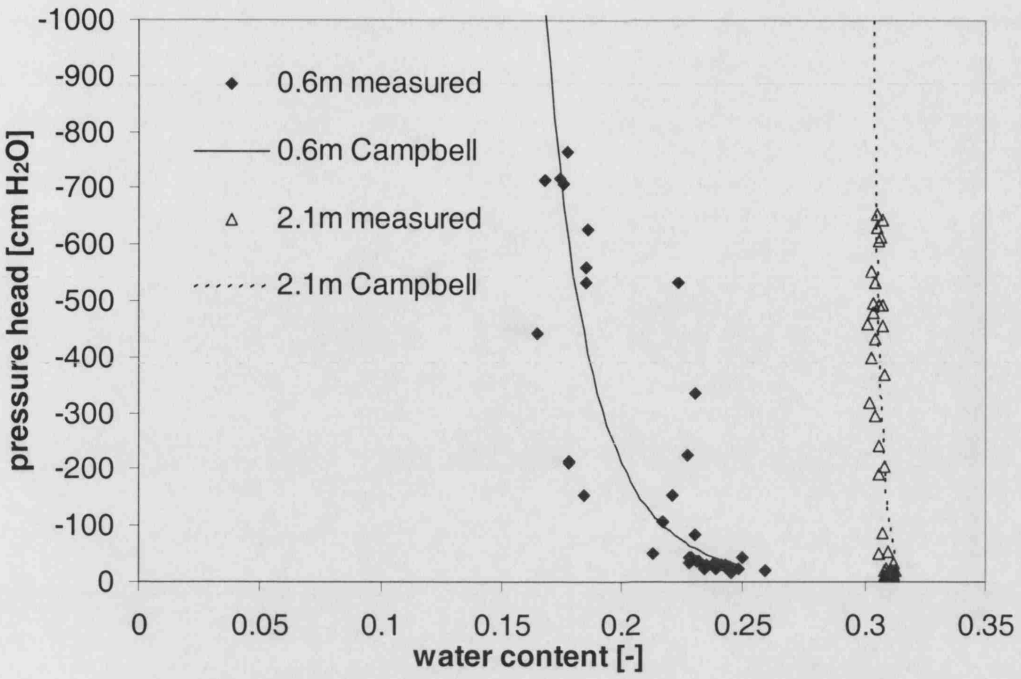

Figure 9-3 Fitting of the Campbell (1974) function to water retention curves measured in the Fleam Dyke lysimeter at 0.6 and 1.2 m depth.

More parameter values were required for the grass crop and for the calculation of the PET. The stomatal resistance of a single leaf r_l was set to 100 s/m, conforming with Allen (1986). The following parameter values for the grass crop were defined as in the MACRO application (Chapter 7): the leaf area index was set to 2.88, the canopy height was set to 0.12 m, the albedo was set to 0.23, the proportion of roots in the topsoil was set to 0.8 and the fraction of soil available water below which evaporation is reduced below potential was set to 0.5.

The proportion of effective rainfall that is diverted to bypass flow was set to zero. Bypass flow in DFIDGWR is generated irrespective of the soil moisture conditions, producing equal amounts of bypass flow in summer as in winter. This is not realistic for unsaturated chalk, where bypass flow through fractures is only thought to occur in the absence of a soil moisture deficit in the matrix.

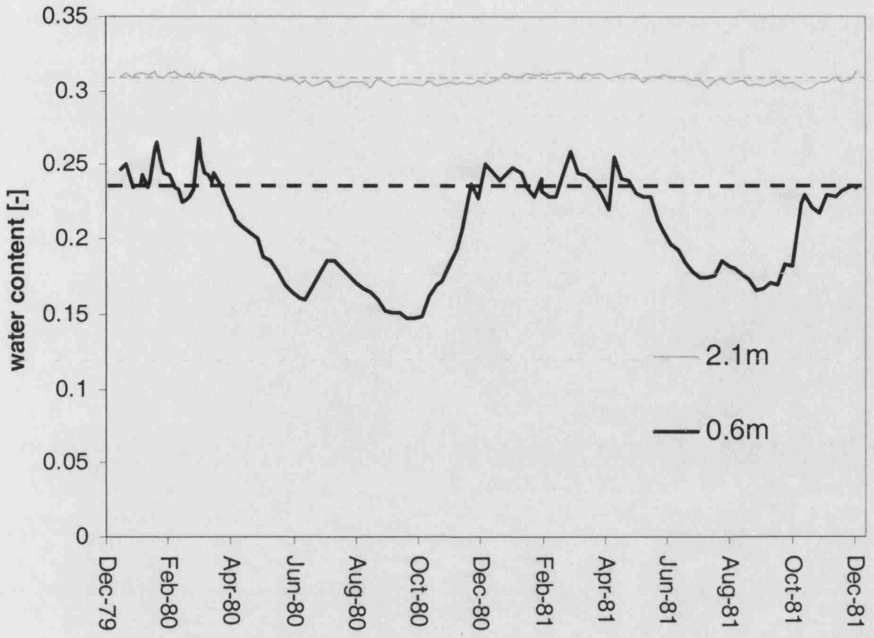

Figure 9-4 Evolution of the water content over time at different depths in the Fleam Dyke lysimeter, with an estimation of the field capacity shown as a dotted line.

The initial water contents in each layer were set to field capacity, which was considered appropriate for 1 January 1999. The final parameters that needed to be defined were the factors m and j in the unsaturated transfer function (Eq. 9-27). Because they are essentially empirical, both factors were initially set to their default value of 2.

9.4 Prior results

The results of the initial recharge modelling at the Fleam Dyke site with DFIDGWR are shown in Figure 9-5. A soil moisture deficit up to 200 mm builds up during the summer. Soil drainage is only generated when the soil moisture deficit ceases during the winter recharge season. The model simulates soil drainage as a collection of individual spikes. Figure 9-5 shows how the soil drainage is converted into recharge by a transfer function, accounting for the delay and smoothing occurring in the unsaturated zone. Figure 9-6 compares the simulated recharge with the drainage measured from the Fleam Dyke lysimeter. For a first model run without calibration,

the fit is encouraging. However, the initiation of recharge is simulated too early in the year. Moreover, the model does not properly represent the shape of the backward tailing in the recharge, possibly due to incorrect parameterization of the unsaturated transfer function.

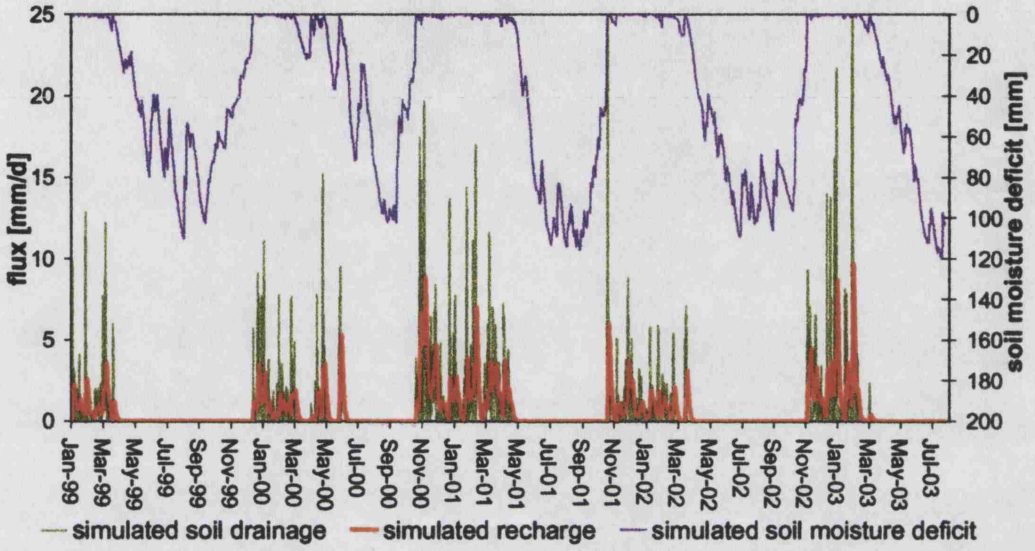

Figure 9-5 Prior results of flow modelling with DFIDGWR, showing simulated soil drainage, recharge and soil moisture deficits for the Fleam Dyke site.

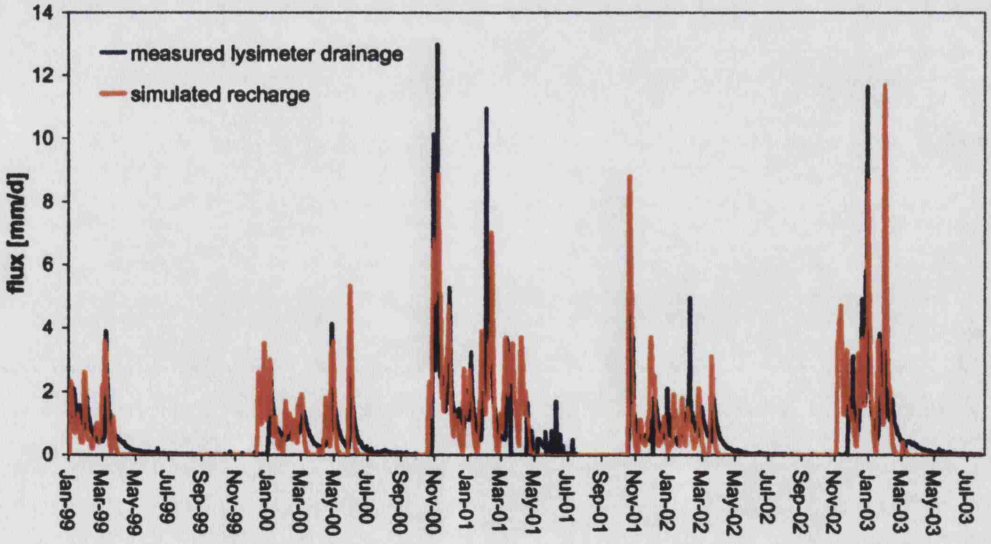

Figure 9-6 Prior results of flow modelling with DFIDGWR, showing simulated recharge versus measured drainage for the Fleam Dyke lysimeter.

9.5 Calibration

Limited calibration of the DFIDGWR model was pursued to improve its performance on the Fleam Dyke data. The objective function used to assess the model performance was the root mean square error (RMSE) between the simulated recharge and the measured lysimeter drainage, defined as:

$$RMSE = \sqrt{\frac{1}{N}\sum_{t=1}^{N}\left(d_s^{(t)} - d_m^{(t)}\right)^2} \qquad \textit{Eq. 9-28}$$

where d_s is the simulated recharge, d_m is the measured lysimeter drainage and N is the number of data points. The RMSE was calculated from daily data over the period of 1 August 1999 until 30 July 2003, with exclusion of the period of 22 March 2001 until 9 May 2001 when good quality drainage data were not available. For the prior results of Figure 9-6, a RMSE of 0.905 mm/d was obtained.

As a first step, the field capacity of the soil layer was optimized. This parameter had initially been estimated at 0.30 as a literature value for a loamy soil. It is subject to uncertainty, and Finch (1998) showed that the water balance model is particularly sensitive to the field capacity. Calibration by manual adjustment (trial-and-error) yielded a field capacity of 0.36 for the soil layer. This reduced the RMSE to 0.807 mm/d.

The second step in the model calibration was the optimization of the parameters m and j in the unsaturated transfer function (Eq. 9-27). Both parameters had initially been assigned a default value of 2. They have no influence on the cumulative recharge, but they largely determine the shape of the recharge hydrograph. Calibration was performed by manual adjustment and reached a minimum of 0.730 mm/d for the RMSE at m=1.2 and j=6. A response surface of the calibration process is shown in Figure 9-7.

As a final step, the field capacity of the soil layer was optimized once more. This provided a value of 0.34, with a RMSE of 0.715 mm/d.

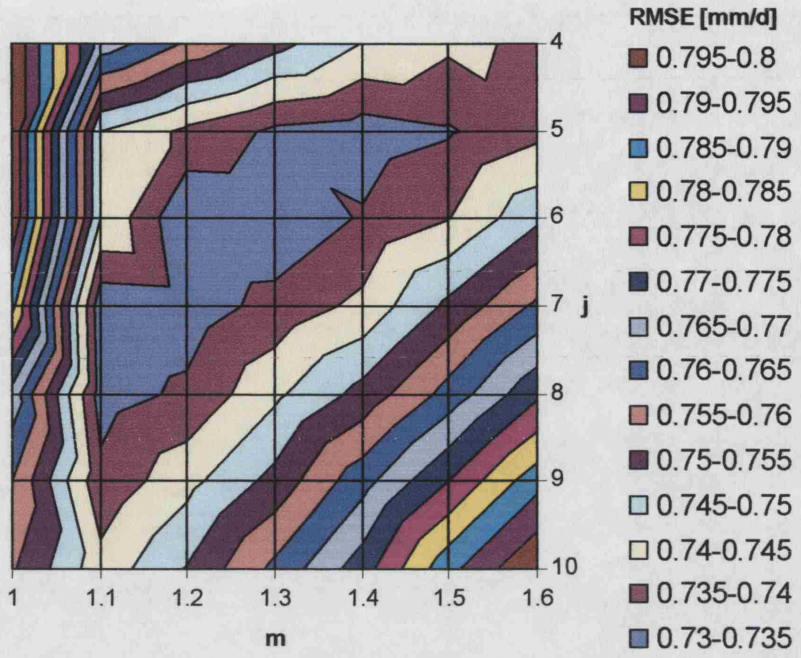

Figure 9-7 Response surface of the root mean square error (RMSE) between measured drainage from the Fleam Dyke lysimeter and simulated recharge as a function of the parameters m and j, as used in the unsaturated transfer function in the model DFIDGWR.

The results of the recharge modelling after calibration are shown in Figure 9-8. Compared to the prior results of Figure 9-6, the recharge hydrograph shows closer resemblance to the lysimeter drainage data, with a better representation of the backward tailing. The timing of the initiation of recharge is also slightly improved, although in the winter of 2001/2002 the initiation of recharge is now too late. The model simulated 71.5 mm of runoff over the simulation period, or 2.2% of the total rainfall.

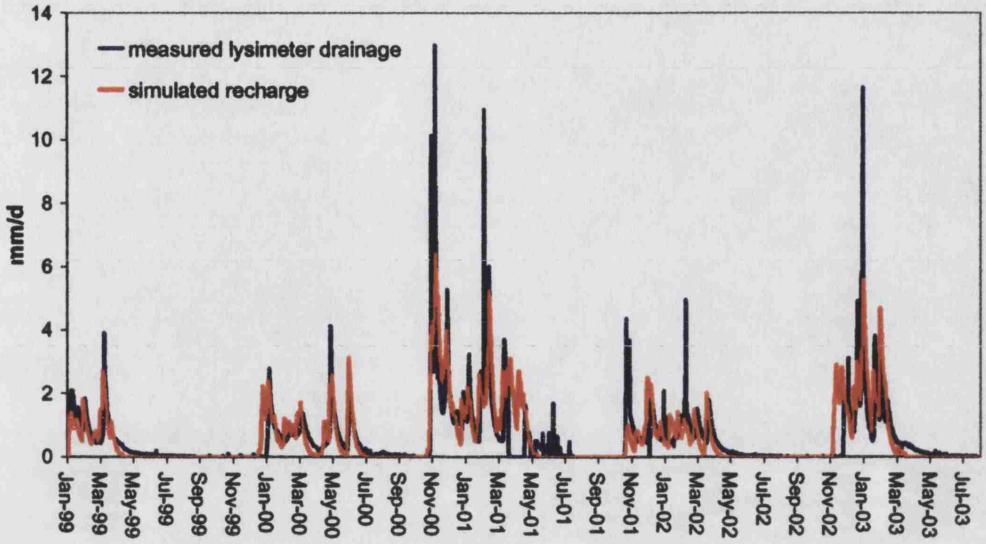

Figure 9-8 Results of recharge modelling with DFIDGWR, showing simulated recharge versus measured drainage from the Fleam Dyke lysimeter, after calibration.

9.6 Discussion

A comparison between the modelling of the Fleam Dyke recharge with DFIDGWR and MACRO is shown in Figure 9-9. Upon visual inspection, both models are comparable in their performance. MACRO appears superior in the timing and shape of the individual peaks, but it overestimates the size of extreme recharge events. In section 7.5.2 it was argued that the lack of high drainage peaks in the measured data may be an artefact due to smoothing at the lysimeter base. Figure 9-9 also shows the root mean square error (RMSE) and the mean absolute error (MAE) for both models. The MAE is defined as:

$$MAE = \frac{1}{N}\sum_{t=1}^{N}\left|d_s^{(t)} - d_m^{(t)}\right| \qquad \textit{Eq. 9-29}$$

where d_s is the simulated recharge, d_m is the measured lysimeter drainage and N is the number of data points. DFIDGWR performs better for the RMSE, whereas MACRO performs better for the MAE. The reason for the poor assessment of MACRO with the RMSE is the presence of the high peaks in the recharge, which lend a disproportionate contribution towards the square errors.

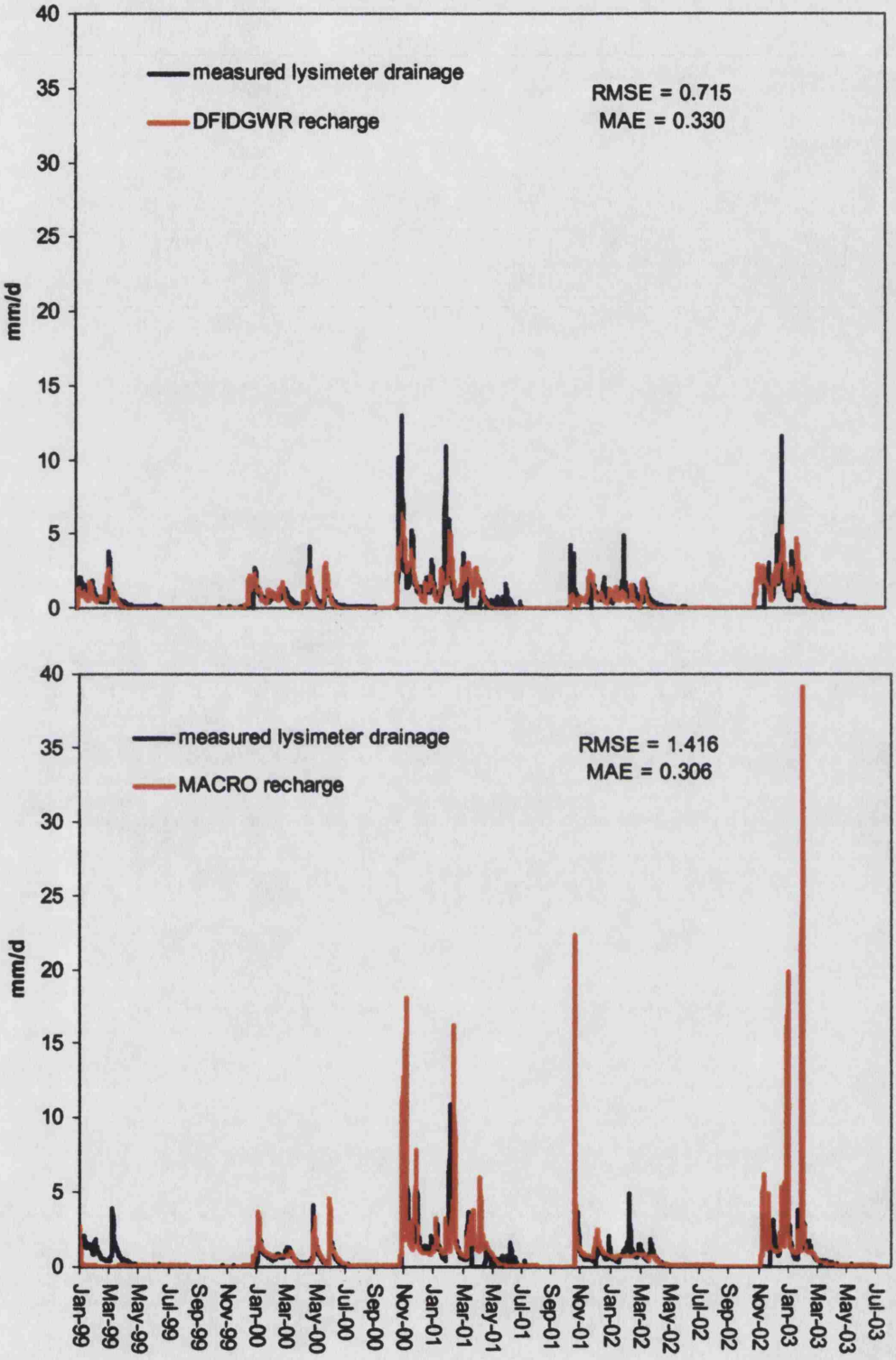

Figure 9-9 Measured drainage from the Fleam Dyke lysimeter versus simulated recharge, as obtained with the models DFIDGWR and MACRO 5.0.

Table 9-2 reports the values of cumulative recharge obtained with both models for selected recharge seasons. MACRO overestimates the recharge by 25% compared with the lysimeter drainage. These results come from a validation run with MACRO (section 7.5.2), after calibration on data that were gathered 20 years earlier. Moreover, MACRO was not specifically calibrated against cumulative recharge. Rather, it was calibrated to give reliable time series of water contents, pressure heads and recharge, which could serve as a base to model solute transport. This may explain the mediocre performance of MACRO on the cumulative recharge. In this respect DFIDGWR performs better, even without calibration. Subsequent calibration with only 3 parameters brought the cumulative recharge within 2% error of the measured drainage.

Table 9-2 Measured and modelled cumulative recharge through the Chalk at the Fleam Dyke site. A recharge season is defined from 1 October until 30 September.

recharge season	Lysimeter measured	MACRO	DFIDGWR Prior	DFIDGWR After calibration
1999/2000	151.6	169.3	176.2	162.0
2001/2002	173.3	198.4	171.0	141.6
2002/2003	200.3	291.8	261.5	231.3
average	175.1	219.8	202.9	178.3
% of lysimeter	100.0	125.5	115.9	101.8

To conclude, DFIDGWR appears to be successful in simulating recharge through unsaturated chalk. Its performance on the Fleam Dyke data was similar or better than MACRO. This stands in contrast with its relatively simple model formulation and moderate parameter requirements. Compared with the flow calibration of MACRO, which required optimization of no less than 21 parameters (Table 7-6), calibration of DFIDGWR was performed by changing only 3 parameters. Consequently, parsimonious considerations indicate that, when the aim is to model recharge through unsaturated chalk, DFIDGWR is preferable to MACRO. MACRO explicitly differentiates between fractures and matrix, but the results suggest that this is not important when only modelling recharge. However, the distinction between fractures

and matrix does become important when modelling solute transport. Exchange of solutes between fractures and matrix leads to large variations in transport velocities, and this affects the dispersion of the solute plume. A dual permeability model such as MACRO is needed to simulate such effects.

Note that the simulation of the Fleam Dyke recharge has previously been attempted by Ragab et al. (1997) with a rudimentary version of DFIDGWR called the Four Root Layers Model (FRLM). Their model considerably overestimated recharge at Fleam Dyke over the period 1978-1982, with cumulative values that were around 170% of the measured lysimeter drainage. Similarly, Bradford et al. (2002) used FRLM to simulate recharge in the Chalk catchment of the River Pang. They also came to the conclusion that FRLM overestimates recharge. The reason for the greater success of DFIDGWR must be the pseudodiffusivity function of Eq. 9-7, which was not included in FRLM. The pseudodiffusivity function causes upward flow in summer and extends the soil moisture deficit in late autumn. Therefore a larger part of the winter drainage is used in replenishing the soil moisture store, hence reducing the total recharge.

10 Conclusions and further research

10.1 Conclusions

This work has dealt with flow and solute transport through unsaturated chalk. In the present section, the main findings of the work are summarized, along with their implications for the vulnerability of the chalk aquifer.

A tracer test was performed under natural rainfall conditions on the unsaturated chalk at the Fleam Dyke research site, Cambridgeshire. Deuterium and bromide were distributed over a grass-covered lysimeter (a cube of colume 125 m^3) and an adjacent 4×4 m grass plot. Up until 15 months after the tracer application, none of the tracer was detected in the lysimeter drainage at 5 m depth. Repeated core profiling in the unsaturated zone revealed an average vertical tracer velocity of 4.4 mm/d (1.2 m/year) for the deuterium tracer. Significant differences in vertical tracer distribution were observed between core profiles, indicating lateral heterogeneity of transport pathways. Considerable dispersion was observed once the tracer reached the unweathered chalk, and occasionally secondary peaks were observed between 150 and 300 cm depth. A problem was encountered in the determination of the bromide tracer concentrations in the core profiles. The background profiles showed bromide levels up to 12 mg/l, which masked the bromide tracer in the other core profiles. The reason for these high background levels could not be resolved.

The tracer results suggested that the Chalk aquifer at Fleam Dyke is not particularly vulnerable to pollution. Even under relatively wet conditions, there was no evidence of fast-transport pathways providing direct connection between the surface and the chalk at 5 m depth. The results illustrated the protective capacity of the soil and the weathered chalk, having a buffering effect on high-intensity rainfall events and causing a delay before solutes can enter chalk fractures. However, the appearance of

secondary tracer peaks down to 300 cm depth showed that some bypass flow through fractures was occurring.

The Chalk is a fractured porous medium, and its unsaturated zone is best conceptualized by a dual permeability approach. Modelling of the unsaturated zone at Fleam Dyke was undertaken by MACRO 5.0, a numerical 1-D dual permeability model that was initially developed for macroporous soils. The flow model was calibrated against data of lysimeter drainage, water content and pressure head. A good fit was obtained for the drainage and water content, but the model fell short in simulating the low pressure heads in the chalk strata observed during the summer. The flow simulation illustrated the intermittent nature of the fracture flow, which was confined to periods of high rainfall in winter. Moreover, the model envisaged fracture flow to be highly variable between individual chalk strata in the same profile. The distribution of flow between the matrix and the fractures appeared to be mainly determined by the saturated hydraulic conductivity of the matrix.

Although the MACRO model is particularly useful for understanding flow and solute transport through the unsaturated chalk, it is overly complex when the aim is simply to predict time series of recharge to the chalk aquifer. This was illustrated by comparing MACRO with DFIDGWR, a simple four-layer water balance model. DFIDGWR appeared to be successful in simulating recharge through unsaturated chalk, with a performance on the Fleam Dyke data that was similar or better than MACRO. Given its relatively simple model formulation and moderate parameter requirements, DFIDGWR appears to be the preferred model to simulate recharge through unsaturated chalk.

After calibration of the flow, MACRO was used to simulate the tracer transport at the Fleam Dyke site. The fit to the tracer profiles was only moderate, even after extensive calibration. This could be related to lateral heterogeneity in transport behaviour, but it may also indicate shortcomings in the model. MACRO predicted the deuterium tracer to appear in the lysimeter drainage between 2006 and 2016.

Finally, MACRO was used to simulate the profiles of environmental isotopes measured at an arable plot at the Fleam Dyke site between 1979 and 1981. The model

was successful at predicting the depth of the measured tritium peaks, but it could not explain the high tritium concentrations measured at shallow depth. Simulation of the measured deuterium profiles was only partly successful, which may be due to the differences between the arable land and the grass plot.

Despite the uncertainties associated with the MACRO solution, the model offered good insight into the likely mechanisms that operate during flow and solute transport through unsaturated chalk. For the Fleam Dyke site, MACRO simulated flow velocities around 1 m/d for the fractures, compared to values around 1 mm/d for the matrix. The fractures never reached complete saturation. No single value could be given for the importance of fracture flow, as it varied with depth. At Fleam Dyke, between 40 and 80% of the cumulative flux passed through the fractures. Diffusion between the fractures and the matrix tended to equalize tracer concentrations in the fractures and the matrix, although bypass of tracer through the fractures occurred in some chalk strata. Whether diffusive equilibrium or bypass occurred seemed to be mainly dependent on the fracture flow velocity and on the matrix block size. Besides diffusion, the MACRO modelling stressed the importance of advective exchange of solutes between fractures and matrix. The advective exchange may even outweigh diffusive exchange.

The findings of the Fleam Dyke tracer test and the associated modelling results could help in the assessment of the vulnerability of the chalk aquifer. Traditionally, the Chalk aquifer is assumed to be very vulnerable to pollution because of the potential of the fractures as pathways for preferential transport. However, field experience has shown that actual pollution events of the chalk aquifer are less common than anticipated. The Fleam Dyke results may explain why. First, the presence of soil and weathered chalk on top of the Chalk has a buffering effect on high infiltration events. Second, diffusion between the fractures and the matrix can prevent preferential transport of solutes through the fractures. Finally, advective transport of solutes between the fractures and the matrix, as driven by a pressure gradient, may play an important role. Pressure-driven flow between the fractures and the matrix limits the vertical extent of the fracture flow trajectories. Note that these processes may disperse and delay the contaminants, but they do not necessarily remove the contaminants. For diffuse long-term pollution, such as nitrate, it is not so much the

transfer time to the water table that is relevant, but rather the concentration at which the pollutants can reach the water table. Therefore the Chalk at Fleam Dyke should still be regarded as having a high specific vulnerability to nitrate.

10.2 Recommendations for further research

MACRO 5.0 has proven to be a useful tool in modelling flow and solute transport through unsaturated chalk. From the modelling experience with the Fleam Dyke data, the following model improvements can be suggested:

- The model should allow the dispersivity α_L to be varied between different strata in the profile, to allow for vertical heterogeneity in transport behaviour;
- The model should allow evaporation of deuterium and tritium with water intercepted by the canopy;
- In the current version, the model conceptualizes aggregates as consisting of rectangular slabs. The introduction of a block geometry factor could extend this to other geometries, such as spheres or cylinders.

The last core profiling at Fleam Dyke in May 2003 showed that there was still a considerable amount of deuterium tracer present in the unsaturated chalk profile. Further core profiling over the coming years would provide more information on the tracer transport. MACRO predicted breakthrough of the deuterium tracer in the lysimeter drainage starting from 2006. It is therefore recommended that sampling of the lysimeter drainage continues, perhaps at a rate of only a few samples every recharge season. In addition to providing a clear answer to the transport velocity at Fleam Dyke, this would allow validation of the MACRO transport model.

There is scope for a second tracer test on the Fleam Dyke lysimeter. It would be preferable if the tracer could be introduced directly into the unweathered chalk below 2 m depth. This would prevent tracer loss by plant uptake, and it would avoid the dispersing effect of the soil and the weathered chalk. A method is proposed where a narrow access tube is drilled into the lysimeter down to 2 m depth and a point injection of tracer is realized from there. It is recommended that two tracers with contrasting diffusion coefficients should be used, as this would provide unequivocal

information on the diffusion exchange mechanism. Tracers to be considered should include fluorescein and lithium. Their ratio of molecular diffusion coefficients is 0.72 (FRACFLOW, 1999), they have very low and well-known toxicity characteristics, and batch sorption experiments on chalk fragments showed sorption to be minimal (Wilkinson, 2002).

The Chalk exhibits large regional differences, and care should be taken in extrapolating the results from the Fleam Dyke site to other chalk sites. Therefore it would be useful to conduct more tracer experiments at other locations on the English Chalk of different geological conditions, preferably accompanied by modelling work. Possible locations on the Upper Chalk are Bridget's Farm, Hampshire and West Ilsley, Berkshire, both well-documented sites because of research in the 1980s.

Eventually, the updated understanding of flow and solute transport through unsaturated chalk should lead to the development of an improved methodology for vulnerability mapping of the Chalk aquifer. Starting from the overlay method that is currently used in England and Wales, the way forward is for a more physically based approach, whilst keeping data requirements to a minimum. For instance, an assessment of the potential for preferential transport through the unsaturated chalk could be made based on estimates of parameters such as the fracture aperture and the saturated hydraulic conductivity of the matrix.

This work has focussed exclusively on transport of solutes. Another topic that increasingly draws attention is transport of particulate matter through the unsaturated zone. In particular, Cryptosporidium oocysts and the prion causing Bovine Spongiform Encephalopathy (BSE) are subjects of concern for English water sources at present. Tracer tests in the unsaturated chalk with microspheres or bacteriophage would be useful to investigate these issues.

References

Abbaspour, K., Kasteel, R. and Schulin, R., 2000. Inverse parameter estimation in a layered unsaturated field soil. Soil Science, 165(2): 109-123.

Abbaspour, K., Sonnleitner, M.A. and Schulin, R., 1999. Uncertainty in estimation of soil parameters by inverse modeling: example lysimeter experiments. Soil Science Society of America Journal, 63: 501-509.

Abbaspour, K.C., vanGenuchten, M.T., Schulin, R. and Schlappi, E., 1997. A sequential uncertainty domain inverse procedure for estimating subsurface flow and transport parameters. Water Resources Research, 33(8): 1879-1892.

Allen, D.J., Bloomfield, J.P. and Robinson, V.K., 1997. The physical properties of major aquifers in England and Wales. WD/97/34, British Geological Survey, Keyworth.

Allen, R.G., 1986. A Penman for all seasons. Journal of Irrigation and drainage engineering, 112: 348-368.

Allen, R.G., Smith, M., Pereira, L.S. and Perrier, A., 1994. An update for the calculation of reference evaporation. ICID Bulletin, 43: 35-92.

Aller, L., Bennett, T., Lehr, J.H., Petty, R.J. and Hackett, G., 1987. DRASTIC: a standardised system for evaluating groundwater pollution potential using hydrographic settings, US EPA Report 600/2-87-035.

Bai, M., Elsworth, D. and Roegiers, J.C., 1993. Multiporosity multipermeability approach to the simulation of naturally fractured reservoirs. Water Resources Research, 29(6): 1621-1633.

Bajracharya, K. and Barry, D.A., 1997. Nonequilibrium solute transport parameters and their physical significance: numerical and experimental results. Journal of Contaminant Hydrology, 24(3-4): 185-204.

Ballif, J.-L., 1998. Frange capillaire et tracés historiques du tritium et de l'azote dans la craie sénonienne en Champagne. Bulletin de la Société Géologique de France, 169: 203-209.

Banks, D., Davies, C. and Davies, W., 1995. The Chalk as a karstic aquifer - Evidence from a tracer test at Stanford-Dingley, Berkshire, UK. Quarterly Journal of Engineering Geology, 28: S31-S38.

Barenblatt, G.I., Zheltov, I.P. and Kochina, I.N., 1960. Basic concepts in the theory of seepage of homogeneous liquids in fissured rocks. Journal of Applied Mathematics and Mechanics, 24: 1286-1303.

Barker, J.A., 1982. Laplace transform solutions for solute transport in fissured aquifers. Advances in Water Resources, 5: 98-104.

Barker, J.A., 1985a. Block-geometry functions characterizing transport in densely fissured media. Journal of Hydrology, 77: 263-279.

Barker, J.A., 1985b. Modelling the effects of matrix diffusion on transport in densely fissured media, 18th Congress of the International Association of Hydrogeologists. Hydrogeology in the service of man, Cambridge.

Barker, J.A., 1991. Transport in fractured rock. In: R.A. Downing and W.B. Wilkinson (Editors), Applied groundwater hydrology. Clarendon Press, Oxford, pp. 199-216.

Barker, J.A., 1993. Modelling groundwater flow and transport in the Chalk. In: R.A. Downing, M. Price and G.P. Jones (Editors), The hydrogeology of the Chalk of North-West Europe. Clarendon Press, Oxford, pp. 59-66.

Barker, J.A. and Foster, S.S.D., 1981. A diffusion exchange model for solute movement in fissured porous rock. Quarterly Journal of Engineering Geology, 14(1): 17-24.

Barker, J.A., Wright, T.E.J. and Fretwell, B.A., 2000. A pulsed-velocity method of double-porosity solute transport modelling. In: A. Dassargues (Editor), TraM'2000 Conference. Tracers and modelling in hydrogeology, Liège, Belgium, pp. 297-302.

Barraclough, D., Gardner, C.M.K., Wellings, S.R. and Cooper, J.D., 1994. A tracer investigation into the importance of fissure flow in the unsaturated zone of the British Upper Chalk. Journal of Hydrology, 156(1-4): 459-469.

Bear, J., 1979. Hydraulics of groundwater. McGraw-Hill Inc., New York.

Bear, J. and Verruijt, A., 1990. Modelling groundwater and pollution. Reidel Publishing Company, Dordrecht.

Beasley, D.B. and Huggins, L.F., 1991. ANSWERS (Areal Nonpoint Source Watershed Environment Response Simulation) User's Manual. Agricultural Engineering Department, Purdue University, West Lafayette, Indiana.

Becker, M.W. and Coplen, T.B., 2001. Use of deuterated water as a conservative artificial groundwater tracer. Hydrogeology Journal, 9: 515-516.

Becker, M.W. and Shapiro, A.M., 2000. Tracer transport in fractured crystalline rock: Evidence of nondiffusive breakthrough tailing. Water Resources Research, 36(7): 1677-1686.

Belford, R.K., 1979. Collection and evaluation of large soil monoliths for soil and crop studies. Journal of Soil Science, 30: 363-373.

Bell, F.G., Culshaw, M.G. and Cripps, J.C., 1999. A review of selected engineering geological characteristics of English Chalk. Engineering Geology, 54(3-4): 237-269.

Ben Mehrez, M., Taconet, O., Vidalmadjar, D. and Sucksdorff, Y., 1992. Calibration of an energy flux model over bare soils during the Hapex-Mobilhy experiment. Agricultural and Forest Meteorology, 58(3-4): 257-283.

Berkowitz, B., 1994. Modelling flow and contaminant transport in fractured media. In: M.Y. Corapcioglu (Editor), Advances in porous media, Volume 2. Elsevier, Amsterdam.

Berkowitz, B., 2002. Characterizing flow and transport in fractured geological media: A review. Advances in Water Resources, 25: 861-884.

Besbes, M. and de Marsily, G., 1984. From infiltration to recharge: use of a parametric transfer function. Journal of Hydrology, 74: 271-293.

Besien, T.J., Williams, R.J. and Johnson, A.C., 2000. The transport and behaviour of isoproturon in unsaturated chalk cores. Journal of Contaminant Hydrology, 43(2): 91-110.

Beven, K. and Germann, P.F., 1981. Water flow in soil macropores, II. A combined model. Journal of Soil Science, 32: 15-29.

Black, J.H., Boreham, D., Bromley, J., Campbell, D.J.V., Mather, J.D. and Parker, A., 1979. Construction and instrumentation of lysimeters to study pollutant movement through unsaturated sand. Reports of the Institute of Geological Sciences, 79(6): 14-16.

Black, J.H. and Kipp, K.L., 1983. Movement of tracers through dual-dorosity media - Experiments and modeling in the Cretaceous Chalk, England. Journal of Hydrology, 62(1-4): 287-312.

Bloomfield, J., 1996. Characterisation of hydrogeologically significant fracture distributions in the Chalk: An example from the Upper Chalk of southern England. Journal of Hydrology, 184(3-4): 355-379.

Bloomfield, J.P., Brewerton, L.J. and Allen, D.J., 1995. Regional trends in matrix porosity and dry density of the Chalk of England. Quarterly Journal of Engineering Geology, 28: S131-S142.

Bodin, J., Delay, F. and de Marsily, G., 2003. Solute transport in a single fracture with negligible matrix permeability: 2. mathematical formalism. Hydrogeology Journal, 11(4): 434-454.

Boesten, J. and Vanderlinden, A.M.A., 1991. Modeling the influence of sorption and transformation on pesticide leaching and persistence. Journal of Environmental Quality, 20(2): 425-435.

Bowles, J.E., 1992. Engineering properties of soils and their measurement. Mc.Graw-Hill, Inc., New York.

Bowman, R.S., Schroeder, J., Bulusu, R., Remmenga, M. and Heightman, R., 1997. Plant toxicity and plant water uptake of fluorobenzoate and bromide tracers. Journal of Environmental Quality, 26: 1292-1299.

Bradford, R.B., Ragab, R., Crooks, S.M., Bouraoui, F. and Peters, E., 2002. Simplicity versus complexity in modelling groundwater recharge in Chalk catchments. Hydrology and Earth System Sciences, 6: 927-937.

British Geological Survey, 1984. Comparison between drainage measured by the BGS lysimeter and the IH method at Fleam Dyke lysimeter, Report of the Bristish Geological Survey, Wallingford.

Brooks, R.H. and Corey, A.T., 1964. Hydraulic properties of porous media, Hydrol. Papers No.3, Civ. Eng. Dep., Colorado State University, Fort Collins, U.S.A.

Brouyère, S., 2002. Etude et modélisation du transport et du piégage de solutés en milieu variablement saturé. PhD Thesis, Université de Liège, 572 pp.

Brouyère, S., Dassargues, A. and Hallet, V., 2004. Migration of contaminants through the unsaturated zone overlying the Hesbaye chalky aquifer in Belgium: a field investigation. Journal of Contaminant Hydrology, 72(1-4): 135-164.

Brunt, D., 1952. Physical and dynamical meteorology. University Press, Cambridge.

Brusseau, M.L., 1993. The influence of solute size, pore water velocity, and intraparticle porosity on solute-dispersion and transport in soil. Water Resources Research, 29(4): 1071-1080.

Brusseau, M.L., 1999. Nonideal transport of reactive solutes in porous media. In: M.B. Parlange and J.W. Hopmans (Editors), Vadose zone hydrology. Oxford University Press, New York, pp. 130-154.

Butters, G.L., Jury, W.A. and Ernst, F.F., 1989. Field scale transport of bromide in an unsaturated soil, 1. Experimental methodology and results. Water Resources Research, 25(7): 1575-1581.

Calver, A., 1997. Recharge response functions. Hydrology and Earth System Sciences, 1: 47-53.

Cambray, R.S., Playford, K. and Lewis, G.N.J., 1982. Radioactive fallout in air and rain. Results to end of 1981, UKAEA Atomic Energy Research Establishment, Harwell.

Campbell, G.S., 1974. A simple method for determining unsaturated conductivity from moisture retention data. Soil Science, 117: 6-11.

Charbeneau, R.J., 1989. Liquid moisture redistribution: hydrologic simulation and spatial variability. In: H.J. Morel-Seytoux (Editor), Unsaturated flow in hydrologic modeling. Kluwer, Dordrecht, pp. 127-160.

Childs, E.C., 1969. An introduction to the physical basis of soil water phenomena. John Wiley & Sons Ltd., London.

Clapp, R.B. and Hornberger, G.M., 1978. Empirical equations for some soil hydraulic properties. Water Resources Research, 16: 601-604.

Clark, I. and Fritz, P., 1997. Environmental isotopes in hydrogeology. Lewis Publishers, New York.

Coats, K.H. and Smith, B.D., 1964. Dead-end pore volume and dispersion in porous media. Society of Petroleum Engineers Journal, 4: 73-84.

Coleby, L.M., Kinniburgh, D.G., Merrin, P.D. and Chilton, P.J., 1998. Catalogue of nitrate, chloride and sulphate porewater profiles. Hydrogeology Series, Technical Report WD/98/12, British Geological Survey.

Coleman, M.L., Shepherd, T.J., Durham, J.J., Rouse, J.E. and Moore, G.R., 1982. Reduction of water with zinc for hydrogen isotope analysis. Analytical Chemistry, 54: 993-995.

Connell, L.D., 2002. A simple analytical solution for unsaturated solute migration under dynamic water movement conditions and root zone effects. In: R.M. Davison (Editor), Sustainable groundwater development. Geological Society, Special Publications, London, pp. 193: 255-264.

Connell, L.D. and Van den Daele, G.F.A., 2003. A quantitative approach to aquifer vulnerability mapping. Journal of Hydrology, 276: 71-88.

Connell, L.D. and Van den Daele, G.F.A., (in review). Simple models for subsurface solute transport that combine unsaturated and saturated pathways. Journal of Contaminant Hydrology.

Cooper, J.D., 1985. Estimation of aquifer recharge in the area of Fleam Dyke pumping station by soil physics methods, Department of the Environment.

Cooper, J.D., Gardner, C.M.K. and Mackenzie, N., 1990. Soil controls on recharge to aquifers. Journal of Soil Science, 41(4): 613-630.

Cooper, J.D., Shearer, T.R. and Kitching, R., 1986. Assessment of recharge to groundwater measured by the BGS lysimeters and the IH method at Fleam Dyke pumping station, Fulbourn, Cambridgeshire, Report to DoE. Institute of Hydrology, Wallingford, UK.

Council of European Communities, 1980. Directive on the protection of groundwater against pollution caused by certain dangerous substances (80/68/EEC). Official Journal of the European Community, L20.

Cuevas, M.V., Fernandez, J.E., Roulier, S., Calderon, M.J., Hermosin, M.C., Stenemo, F., Larsbo, M. and Jarvis, N., 2003. Comparing macro 4.3 with 5.0 for simulating the fate of chloridazon and lenacil in a clayey soil of southwest Spain, Pesticide in Air, Plant, Soil & Water System, pp. 517-526.

Dahan, O., Nativ, R., Adar, E.M., Berkowitz, B. and Ronen, Z., 1999. Field observation of flow in a fracture intersecting unsaturated chalk. Water Resources Research, 35(11): 3315-3326.

Daly, D., Dassargues, A., Drew, D., Dunne, S., Goldscheider, N., Neale, S., Popescu, I.C. and Zwahlen, F., 2002. Main concepts of the "European approach" to karst-groundwater- vulnerability assessment and mapping. Hydrogeology Journal, 10(2): 340-345.

Darcy, H., 1856. Les fontaines publiques de la ville de Dijon. Dalmont, Paris.

Darling, W.G. and Bath, A.H., 1988. A stable isotope study of recharge processes in the English Chalk. Journal of Hydrology, 101(1-4): 31-46.

Davis, S.N., Whittemore, D.O. and Fabryka-Martin, J., 1998. Uses of chloride/bromide ratios in studies of potable water. Ground Water, 36: 338-350.

de Marsily, G., Delhomme, J.-P., Delay, F. and Buoro, A., 1999. Regards sur 40 ans de problèmes inverses en hydrogéologie. Comptes Rendus de l'Académie des Sciences - Series IIA - Earth and Planetary Science, 329(2): 73-87.

De Smedt, F., Wauters, F. and Sevilla, J., 1986. Study of tracer movement through unsaturated sand. Journal of Hydrology, 85: 169-181.

De Smedt, F. and Wierenga, P.J., 1979. A generalized solution for solute flow in soils with mobile and immobile water. Water Resources Research, 15: 1137-1141.

Dionex Corporation, 1983. Dionex - Basic ion chromatography, training course manual, Sunnyvale.

Doerfliger, N., Jeannin, P.Y. and Zwahlen, F., 1999. Water vulnerability assessment in karst environments: a new method of defining protection areas using a multi-attribute approach and GIS tools (EPIK method). Environmental Geology, 39(2): 165-176.

Dowdell, R.J., Webster, C.P., Hill, D. and Mercer, E.R., 1984. A lysimeter study of the fate of fertilizer nitrogen in spring barley crops grown on shallow soil overlying Chalk - Crop uptake and leaching losses. Journal of Soil Science, 35(2): 169-181.

Downing, R.A., Price, M. and Jones, G.P., 1993. The making of an aquifer. In: R.A. Downing, M. Price and G.P. Jones (Editors), The hydrogeology of the Chalk of North-West Europe. Clarendon Press, Oxford, pp. 1-13.

Downing, R.A., Smith, D.B. and Warren, S.C., 1978. Seasonal variations of tritium and other constituents in groundwater in the Chalk near Brighton, England. Journal of the Institution of Water and Engineering Science, 32: 123-136.

Durner, W., 1994. Hydraulic conductivity estimation for soils with heterogeneous pore structure. Water Resources Research, 30: 211-223.

Dykhuizen, R.C., 1987. Transport of solutes through unsaturated fractured media. Water Resources, 21: 1531-1539.

Edmunds, W.M., 1996. Bromine geochemistry of British groundwaters. Mineralogical Magazine, 60: 275-284.

Edmunds, W.M. and Bath, A.H., 1976. Centrifuge extraction and chemical analysis of interstitial waters. Environmental Science and Technology, 10: 467-472.

Environment Agency, 1998. Policy and practice for the protection of groundwater, 2nd edition. Stationary Office, London.

Environment Agency, 2002. The Water Framework Directive - Guiding principles on technical requirements.

Fetter, C.W., 1994. Applied hydrogeology. Prentice-Hall, New Jersey.

Fetter, C.W., 1999. Contaminant hydrology. Macmillan Publishing Company, New York.

Finch, J.W., 1998. Estimating direct groundwater recharge using a simple water balance model - sensitivity to land surface parameters. Journal of Hydrology, 211(1-4): 112-125.

Finch, J.W., 2001. Estimating change in direct groundwater recharge using a spatially distributed soil water balance model. Quarterly Journal of Engineering Geology and Hydrogeology, 34: 71-83.

Finch, J.W., 2002. DFIDGWR: a spatially distributed water balance model for estimating direct groundwater recharge, Centre of Ecology and Hydrology, Wallingford.

Flury, M. and Papritz, A., 1993. Bromide in the natural environment: occurrence and toxicity. Journal of Environmental Quality, 22: 747-758.

Forbes, C.L., 1979. The Fleam Dyke lysimeters. Reports of the Institute of Geological Sciences, 79(6): 31-33.

Foster, S.S.D., 1975. The Chalk groundwater tritium anomaly - a possible explanation. Journal of Hydrology, 25: 159-165.

Foster, S.S.D., 1987. Fundamental concepts in aquifer vulnerability, pollution risk and protection strategy. In: W. van Duijvenbooden and H.G. van Waegeningh (Editors), Vulnerability of soil and groundwater to pollutants, TNO Committee on Hydrological Research, The Hague, Proceedings and Information No. 38.

Foster, S.S.D., 1993. The Chalk aquifer - its vulnerability to pollution. In: R.A. Downing, M. Price and G.P. Jones (Editors), The hydrogeology of the Chalk of North-West Europe. Clarendon Press, Oxford, pp. 93-112.

Foster, S.S.D. and Bath, A.H., 1983. The distribution of agricultural soil leachates in the unsaturated zone of the British Chalk. Environmental Geology, 5(2): 53-59.

Foster, S.S.D. and Smith-Carington, A., 1980. The interpretation of tritium in the Chalk unsaturated zone. Journal of Hydrology, 46: 343-364.

FRACFLOW, 1999. Second annual progress report: Contaminant transport, monitoring technique, and remediation strategies in cross European chalk.

Freeze, R.A. and Cherry, J.A., 1979. Groundwater. Prentice Hall, London.

Fretwell, B.A., 1999. Distribution of contaminants in the seasonally unsaturated zone of the Chalk aquifer. PhD Thesis, University College London, London.

Freyberg, D.L., 1986. A natural gradient experiment on solute transport in a sand aquifer. 2. Spatial moments and the advection and dispersion of nonreactive tracers. Water Resources Research, 22: 2031-2046.

Garabedian, S.P., LeBlanc, D.R., Gelhar, L.W. and Celia, M.A., 1991. Large-scale natural gradient tracer test in sand and gravel, Cape Cod, Massachussets. 2. Analysis of spatial moments. Water Resources Research, 27: 911-924.

Gardner, C.M.G., Bell, J.P., Cooper, J.D., Darling, W.G. and Reeve, C.E., 1991. Groundwater recharge and water movement in the unsaturated zone. In: R.A. Downing and W.B. Wilkinson (Editors), Applied groundwater hydrology. Clarendon, Oxford, pp. 54-76.

Gardner, C.M.G., Cooper, J.D., Wellings, S.R., Bell, J.P., Hodnett, M.G., Boyle, S.A. and Howard, M.J., 1990. Hydrology of the unsaturated zone of the chalk of south-east England. In: J.B. Burland, R.N. Mortimore, L.D. Roberts, D.L. Jones and B.O. Corbett (Editors), International Chalk Symposium 1989. Thomas Telford, Brighton Polytechnic, pp. 611-618.

Gaudet, J.P., Jegat, H., Vachaud, G. and Wierenga, P.J., 1977. Solute transfer, with exchange between mobile and stagnant water, through unsaturated sand. Soil Science Society of America Journal, 41: 665-671.

Geake, A.K. and Foster, S.S.D., 1989. Sequential isotope and solute profiling in the unsaturated zone of British Chalk. Hydrological Sciences Journal, 34(1): 79-95.

Gee, G.W. and Bauder, J.W., 1986. Particle-size analysis. In: A. Klute (Editor), Methods of soil analysis, Part 1. Physical and mineralogical methods. Agronomy series no. 9, Madison, Wisconsin.

Gerke, H.H. and van Genuchten, M.T., 1993a. A dual-porosity model for simulating the preferential movement of water and solutes in structured porous media. Water Resources Research, 29: 305-319.

Gerke, H.H. and van Genuchten, M.T., 1993b. Evaluation of a first-order water transfer term for variably saturated dual-porosity models. Water Resources Research, 29: 1225-1238.

Germann, P.F., Edwards, W.M. and Owens, L.B., 1984. Profiles of bromide and increased soil moisture after infiltration into soils with macropores. Soil Science Society of America Journal, 48: 237-244.

Gerritse, R.G. and George, R.J., 1988. The role of soil organic matter in the geochemical cycling of chloride and bromide. Journal of Hydrology, 101: 83-95.

Glass, R.J., Nicholl, M.J., Pringle, S.E. and Wood, T.R., 2002. Unsaturated flow through a fracture-matrix network: Dynamic preferential pathways in mesoscale laboratory experiments. Water Resources Research, 38: 1281.

Gogu, R.C. and Dassargues, A., 2000. Current trends and future challenges in groundwater vulnerability assessment using overlay and index methods. Environmental Geology, 39(6): 549-559.

Gogu, R.C., Hallet, V. and Dassargues, A., 2003. Comparison of aquifer vulnerability assessment techniques. Application to the Néblon river basin (Belgium). Environmental Geology, 44: 881-892.

Gooddy, D.C., 2002. Movement of leachate from beneath turkey litter sited over Chalk in Southern England. Journal of Environmental Science and Health, B37: 81-91.

Gooddy, D.C., Withers, P.J.A., McDonald, H.C. and Chilton, P.J., 1998. Behaviour and impact of cow slurry beneath a storage lagoon: II. Chemical composition of Chalk porewater after 18 years. Water, Air and Soil Pollution, 107: 51-72.

Grisak, G.E. and Pickens, J.F., 1980. Solute transport through fractured media, 1. The effect of matrix diffusion. Water Resources Research, 16: 719-730.

Haigh, N., 2003. Manual of environmental policy: the EU and Britain, Institute for European Environmental Policy, London.

Hall, E.S., Oakes, D.B. and Young, C.P., 1976. Nitrate in groundwater - studies on the Chalk near Winchester, Hampshire. Technical Report TR31, Water Research Centre, Stevenage.

Hancock, J.M., 1975. The petrology of the Chalk. Proceedings of the Geologists' Association, 86: 499-535.

Hancock, J.M., 1993. The formation and diagenesis of the Chalk. In: R.A. Downing, M. Price and G.P. Jones (Editors), The hydrogeology of the Chalk of North-West Europe. Clarendon Press, Oxford.

Haria, A.H., Hodnett, M.G. and Johnson, A.C., 2003. Mechanisms of groundwater recharge and pesticide penetration to a chalk aquifer in southern England. Journal of Hydrology, 275(1-2): 122-137.

Harris, R.C., 1998. Protection of groundwater quality in the UK : present controls and future issues. In: J. Mather, D. Banks, S. Dumpleton and M. Fermor (Editors), Groundwater contaminants and their migration. Publications. Geological Society, London, pp. 3-13.

Harrisson, L.P., 1963. Fundamentals concepts and definitions relating to humidity. In: A. Wexler (Editor), Humidity and moisture. Reinhold Publishing Co., New York.

Headworth, H.G., 1972. The analysis of natural groundwater fluctuations in the chalk of Hampshire. Journal of the Institution of Water and Engineering Science, 26: 107-124.

Hillel, D., 1971. Soil and water: physical principles and processes. Physiological Ecology Series. Academic Press, New York.

Hiscock, K.M., Lovett, A.A., Brainard, J.S. and Parfitt, J.P., 1995. Groundwater vulnerability assessment: two case studies using GIS methodology. Quarterly Journal of Engineering Geology, 28: 179-194.

Hollis, J.M., Bembridge, C. and Harrod, T.R., 1990. Moisture retention among uncommon soil texture classes, porous rocks and extremely calcareous substrates. SSLRC Research Contract 3802, Soil Survey and Land Research Centre, Silsoe, Bedford.

Hough, M., Palmer, S., Weir, A., Lee, M. and Barrie, L., 1995. The Meteorological Office Rainfall and Evaporation Calculation System: MORECS Version 2.0. An update to Hydrological Memorandum 45, Meteorological Office, Bracknell, UK.

Howard, K.W.F. and Lloyd, J.W., 1979. The sensitivity of parameters in the Penman evaporation equations and direct recharge balance. Journal of Hydrology, 41: 329-344.

Hu, Q. and Brusseau, M.L., 1995. Effect of solute size on transport in structured porous media. Water Resources Research, 31: 1637-1646.

Jacquard, P. and Jain, C., 1965. Permeability distribution from field pressure data. Society of Petroleum Engineers Journal, 5: 281-294.

Jahns, H.O., 1966. A rapid method for obtaining a two-dimensional reservoir description from well pressure response data. Society of Petroleum Engineers Journal, 6: 315-327.

Jarvis, N., 1995. Simulation of soil water dynamics and herbicide persistence in a silt loam soil using the MACRO model. Ecological Modelling, 81: 97-109.

Jarvis, N.J. and Larsson, M.H., 1998. The MACRO model (Version 4.1), Technical description.

Johnson, A.C., Besien, T.J., Bhardwaj, C.L., Dixon, A., Gooddy, D.C., Haria, A.H. and White, C., 2001a. Penetration of herbicides to groundwater in an unconfined chalk aquifer following normal soil applications. Journal of Contaminant Hydrology, 53(1-2): 101-117.

Johnson, C.A., Schaap, M.G. and Abbaspour, K.C., 2001b. Model comparison of flow through a municipal solid waste incinerator ash landfill. Journal of Hydrology, 243(1-2): 55-72.

Jones, H.K., 1992. Fleam Dyke lysimeter: Summary of results obtained from initial data analysis. Hydrogeology Series, Technical report WD/92/19, British Geological Survey, Keyworth, Nottinghamshire.

Jones, H.K. and Cooper, D.M., 1998. Water transport through the unsaturated zone of the Middle Chalk: a case study from Fleam Dyke lysimeter. In: N.S. Robins (Editor), Groundwater pollution, aquifer recharge and vulnerability. Special Publications. Geological Society, London, pp. 117-128.

Jury, W.A., 1982. Simulation of solute transport using a transfer-function model. Water Resources Research, 18(2): 363-368.

Jury, W.A. and Roth, K., 1990. Transfer functions and solute movement through soil. Birkhauser Verlag, Basel.

Kätterer, T., Schmied, B., Abbaspour, K.C. and Schulin, R., 2001. Single- and dual-porosity modelling of multiple tracer transport through soil columns: effects of initial moisture and mode of application. European Journal of Soil Science, 52(1): 25-36.

Kirkham, D. and Powers, W.L., 1972. Advanced Soil Physics. John Wiley & Sons, Toronto.

Kitching, R. and Shearer, T.R., 1982. Construction and operation of a large undisturbed lysimeter to measure recharge to the Chalk aquifer, England. Journal of Hydrology, 58(3-4): 267-277.

Koletzko, B., Demmelhair, H., Hartl, W., Kindermann, A., Koletzko, S., Sauerwald, T. and Szitanyi, O., 1998. The use of stable isotope techniques for nutritional and metabolic research in paediatrics. Early Human Development, 53: S77-S97.

Kool, J.B. and Parker, J.C., 1987. Development and evaluation of closed-form expressions for hysteretic soil hydraulic properties. Water Resources Research, 23: 105-114.

Kool, J.B., Parker, J.C. and van Genuchten, M.T., 1987. Parameter estimation for unsaturated flow and transport models -- A review. Journal of Hydrology, 91(3-4): 255-293.

Kung, K.-J.S., 1990. Influence of plant water uptake on the performance of bromide tracer. Soil Science Society of America Journal, 54: 975-979.

Larsbo, M. and Jarvis, N.J., 2003. MACRO 5.0. A model of water flow and solute transport in macroporous soil. Technical description. Emergo 2003:6 Report, Swedish University of Agricultural Sciences, Uppsala.

Larsson, M.H. and Jarvis, N.J., 1999. Evaluation of a dual-porosity model to predict field-scale solute transport in a macroporous soil. Journal of Hydrology, 215(1-4): 153-171.

Larsson, M.H., Jarvis, N.J., Torstensson, G. and Kasteel, R., 1999. Quantifying the impact of preferential flow on solute transport to tile drains in a sandy field soil. Journal of Hydrology, 215(1-4): 116-134.

Levy, B.S. and Chambers, R.M., 1987. Bromide as a conservative tracer for soil-water studies. Hydrological Processes, 1: 385-389.

Lewis, M.A., Jones, H.K., MacDonald, D.M.J., Price, M., Barker, J.A., Shearer, T.R., Wesselink, A.J. and Evans, D.J., 1993. Groundwater storage in British aquifers: Chalk. R&D Note 169, National Rivers Authority, Bristol.

Liu, H.H., Doughty, C. and Bodvarsson, G.S., 1998. An active fracture model for unsaturated flow and transport in fractured rocks. Water Resources Research, 34: 2633-2646.

Lloyd, J.W., 1993. The United Kingdom. In: R.A. Downing, M. Price and G.P. Jones (Editors), The hydrogeology of the Chalk of North-West Europe. Clarendon Press, Oxford, pp. 220-249.

Lloyd, J.W., Harker, D. and Baxendale, R.A., 1981. Recharge mechanisms and groundwater flow in the Chalk and drift deposits of southern East Anglia. Quarterly Journal of Engineering Geology, 14: 87-96.

Luckner, L., Van Genuchten, M.T. and Nielsen, D.R., 1989. A consistent set of parametric models for the two-phase flow of immiscible fluids in the subsurface. Water Resources Research, 25: 2187-2193.

Ma, L. and Selim, H.M., 1995. Transport of a nonreactive solute in soils: a two-flow domain approach. Soil Science, 159: 225-234.

MacDonald, A.M. and Allen, D.J., 2001. Aquifer properties of the Chalk of England. Quarterly Journal of Engineering Geology and Hydrogeology, 34: 371-384.

MacDonald, A.M., Brewerton, L.J. and Allen, D.J., 1998. Evidence for rapid groundwater flow and karst-type behaviour in the Chalk of southern England. In: N.S. Robins (Editor), Groundwater pollution, aquifer recharge and vulnerability. Special Publications. Geological Society, London, pp. 95-106.

Maclean, R.D., 1969. The effects of tipped domestic refuse on groundwater quality: a survey in north Kent. Proceedings of the Society of Water Treatment and Examination, 18: 18-34.

Mahmood-ul-Hassan, M. and Gregory, P.J., 2002. Dynamics of water movement on Chalkland. Journal of Hydrology, 257(1-4): 27-41.

Maloszewski, P., Herrmann, A. and Zuber, A., 1999. Interpretation of tracer tests performed in fractured rock of the Lange Barmke basin, Germany. Hydrogeology Journal, 7: 209-218.

Mathias, S.A., Butler, A.P., Wheater, H.S. and McIntyre, N., 2004. The significance of flow in the matrix of the Chalk unsaturated zone, Unpublished presentation, "The Chalk" meeting, Geological Society, London.

Maw, G.A. and Kempton, R.J., 1982. Bromine in soils and peats. Plant and Soil, 65: 103-109.

McLaughlin, D. and Townley, L.R., 1996. A reassessment of the groundwater inverse problem. Water Resources Research, 32: 1131-1161.

Millington, R.J. and Quirk, J.P., 1961. Permeability of porous solids. Transactions of the Faraday Society, 57: 1200-1207.

Mills, R., 1973. Self diffusion in normal and heavy water in the range 1-45. Journal of Physical Chemistry, 77: 665-688.

Monteith, J.L. and Unsworth, M., 1990. Principles of environmental physics. Edward Arnold, London, 291 pp.

Moreno, L. and Neretnieks, I., 1992. Fluid and solute transport in a network of channels, Scientific Basis for Nuclear Waste Management Xv. Materials Research Society Symposium Proceedings, pp. 691-698.

Mualem, Y., 1976. A new model for predicting the hydraulic conductivity of unsaturated porous media. Water Resources Research, 12: 513-522.

Muller, E., 1987. Modelling groundwater pollution at a site near Cambridge, Research report no. 7, NERC Water Research Unit, University of Newcastle-upon-Tyne.

Murray, F.W., 1967. On the computation of saturation vapor pressure. Journal of Applied Meteorology, 6: 203-204.

Nash, J.E., 1959. Systematic determination of unit hydrograph parameters. Journal of Geophysical Research, 64: 111-115.

Nativ, R., Adar, E., Dahan, O. and Geyh, M., 1995. Water recharge and solute transport through the vadose zone of fractured chalk under desert conditions. Water Resources Research, 31(2): 253-261.

Nitao, J.J. and Buscheck, T.A., 1991. Infiltration of a liquid front in an unsaturated, fractured porous medium. Water Resources Research, 27: 2099-2112.

Ogata, A. and Banks, R.B., 1961. A solution of the differential equation of longitudinal dispersion in porous media. US Geological Survey Professional Papers, 411-A: A1-A7.

Osborne-White, H.J., 1932. The Geology of the country near Saffron Walden. Memoirs of the Geological Survey of Great Britain. Her Majesty's Stationery Office, London.

Otlet, R.L., 1978. Tritium in rainfall, UKAEA Atomic Energy Research Establishment, Harwell.

Parker, B.L., Gillham, R.W. and Cherry, J.A., 1994. Diffusive disappearance of immiscible-phase organic liquids in fractured geologic media. Ground Water, 32(5): 805-820.

Passioura, J.B., 1971. Hydrodynamic dispersion in aggregated media, 1. Theory. Soil Science, 111: 339-344.

Perkins, T.K. and Johnson, O.C., 1963. A review of diffusion and dispersion in porous media. Society of Petroleum Engineers Journal, 3: 70-84.

Peters, R.R. and Klavetter, E.A., 1988. A continuum model for water movement in an unsaturated fractured rock mass. Water Resources Research, 24: 416-430.

Pickens, J.F. and Gillham, R.W., 1980. Finite element analysis of solute transport under hysteretic unsaturated flow conditions. Water Resources Research, 16: 1071-1078.

Poletika, N.N., Jury, W.A. and Yates, M.V., 1995. Transport of bromide, simazine, and Ms-2 coliphage in a lysimeter containing undisturbed, unsaturated soil. Water Resources Research, 31(4): 801-810.

Poulovassilis, A., 1969. The effect of hysteresis of pore-water on the hydraulic conductivity. Journal of Soil Science, 20: 52-57.

Poulovassilis, A., Krentos, V.D., Stylianou, Y. and Metochis, C., 1974. Soil water properties of layered soil determined *in situ*. In: IAEA (Editor), Isotope and radiation techniques in soil physics and irrigation studies, Vienna, pp. 205-224.

Price, M., 1976. Chalk pore size measurements and their significance. Water Services, 80: 596-600.

Price, M., 1987. Fluid flow in the Chalk of England. In: J.C. Goff and B.P.J. Williams (Editors), Fluid flow in sedimentary basins and aquifers. Special Publications, 34. Geological Society, London, pp. 141-156.

Price, M., 1990. Hydrogeology. In: J.B. Burland, R.N. Mortimore, L.D. Roberts, D.L. Jones and B.O. Corbett (Editors), International Chalk Symposium 1989. Thomas Telford, Brighton Polytechnic, pp. 553-554.

Price, M., Downing, R.A. and Edmunds, W.M., 1993. The Chalk as an aquifer. In: R.A. Downing, M. Price and G.P. Jones (Editors), The hydrogeology of the Chalk of North-West Europe. Clarendon Press, Oxford, pp. 35-58.

Price, M., Low, R.G. and McCann, C., 2000. Mechanisms of water storage and flow in the unsaturated zone of the Chalk aquifer. Journal of Hydrology, 233(1-4): 54-71.

Prosser, S.J. and Scrimgeour, C.M., 1995. High-precision determination of H-2/H-1 in H-2 and H2O by continuous-flow isotope ratio mass-spectrometry. Analytical Chemistry, 67(13): 1992-1997.

Pruess, K., 1998. On water seepage and fast preferential flow in heterogeneous, unsaturated rock fractures. Journal of Contaminant Hydrology, 30(3-4): 333-362.

Pruess, K., Faybishenko, B. and Bodvarsson, G.S., 1999. Alternative concepts and approaches for modeling flow and transport in thick unsaturated zones of fractured rocks. Journal of Contaminant Hydrology, 38(1-3): 281-322.

Pruess, K., Wang, J.S.Y. and Tsang, Y.W., 1990. On thermohydrologic conditions near high-level nuclear wastes emplaced in partially saturated fractured tuff, 2. Effective continuum approximation. Water Resources Research, 26: 1249-1261.

Ragab, R., Finch, J. and Harding, R., 1997. Estimation of groundwater recharge to chalk and sandstone aquifers using simple soil models. Journal of Hydrology, 190(1-2): 19-41.

Rawson, P.F., 1992. Cretaceous. In: P.M.D. Duff and A.J. Smith (Editors), Geology of England and Wales. The Geological society, London.

Reeves, M.J., 1979. Recharge and pollution of the English Chalk: some possible mechanisms. Engineering Geology, 14: 231-240.

Revesz, K. and Woods, P.H., 1990. A method to extract soil water for stable isotope analysis. Journal of Hydrology, 115: 397-406.

Ritsema, C.J. and Dekker, L.W., 1998. Three-dimensional patterns of moisture, water repellency, bromide and pH in a sandy soil. Journal of Contaminant Hydrology, 31: 295-313.

Roels, S., Vandersteen, K. and Carmeliet, J., 2003. Measuring and simulating moisture uptake in a fractured porous medium. Advances in Water Resources, 26: 237-246.

Rosenberg, N.J., Blad, B.L. and Verma, S.B., 1990. Microclimate. Second edition. John Wiley & Sons, New York.

Ross, P.J. and Smettem, K.R.J., 1993. Describing soil hydraulic properties with sums of simple functions. Soil Science Society of America Journal, 57: 26-29.

Ross, P.J. and Smettem, K.R.J., 2000. A simple treatment of physical nonequilibrium water flow in soils. Soil Science Society of America Journal, 64: 1926-1930.

Roulier, S. and Jarvis, N., 2003. Modeling macropore flow effects on pesticide leaching: Inverse parameter estimation using microlysimeters. Journal of Environmental Quality, 32(6): 2341-2353.

Rowe, R.K., Hammoud, A. and Booker, J.R., 1989. The effect of multi-directional matrix diffusion on contaminant transport through fractured systems. In:

Kobus and W. Kinzelbach (Editors), Contaminant transport in groundwater. Balkema, Rotterdam.

Russo, V.M. and Karmarkar, S.V., 1998. Water extraction of plant tissues for analysis by ion chromatography. Communications in Soil Science and Plant Analysis, 29: 245-253.

Saxena, R.K., Jarvis, N.J. and Bergstrom, L., 1994. Interpreting non-steady state tracer breakthrough experiments in sand and clay soils using a dual-porosity model. Journal of Hydrology, 162(3-4): 279-298.

Saxton, K.E., Rawls, W.J., Romberger, J.S. and Papendick, R.I., 1986. Estimating generalized soil-water characteristics from texture. Soil Science Society of America Journal, 50(4): 1031-1036.

Schaap, M.G., Leij, F.J. and van Genuchten, M.T., 1998. Neural network analysis for hierarchical prediction of soil hydraulic properties. Soil Science Society of America Journal, 62: 847-855.

Schmied, B., Abbaspour, K. and Schulin, R., 2000. Inverse estimation of parameters in a nitrogen model using field data. Soil Science Society of America Journal, 64(2): 533-542.

Schoen, R., Gaudet, J.P. and Bariac, T., 1999a. Preferential flow and solute transport in a large lysimeter, under controlled boundary conditions. Journal of Hydrology, 215: 70-81.

Schoen, R., Gaudet, J.P. and Elrick, D.E., 1999b. Modelling of solute transport in a large undisturbed lysimeter, during steady-state water flux. Journal of Hydrology, 215(1-4): 82-93.

Selroos, J.-O., Walker, D.D., Strom, A., Gylling, B. and Follin, S., 2002. Comparison of alternative modelling approaches for groundwater flow in fractured rock. Journal of Hydrology, 257(1-4): 174-188.

Shearer, T.R., 1979. Recharge measurement using lysimeters. Reports of the Institute of Geological Sciences, 79(6): 10-13.

Shearer, T.R., 1984. Recharge to the Chalk aquifer measured by lysimeter. Scientific Report, Hydrogeology Series WD/ST/84/10, British Geological Survey.

Shuttleworth, W.J., 1992. Evaporation. In: D.R. Maidment (Editor), Handbook of hydrology. McGraw-Hill, New York.

Simunek, J., Jarvis, N.J., van Genuchten, M.T. and Gardenas, A., 2003. Review and comparison of models for describing non-equilibrium and preferential flow and transport in the vadose zone. Journal of Hydrology, 272(1-4): 14-35.

Smith, D.B., Wearn, P.L., Richards, H.J. and Rowe, P.C., 1970. Water movement in the unsaturated zone of high and low permeability strata by measuring natural tritium, IAEA Symposium on Isotope Hydrology, Vienna, pp. 73-87.

Smith, E.A., Powers, W.L. and Shea, P.J., 1995. Relationship of bromide and atrazine movement in soil to pore-size distribution, compaction, and saturation cycles. Soil Science, 159(1): 23-31.

Soilmoisture Equipment Corp., 1986. Guelph Permeameter 2800KI: Operating instructions, Santa Barbara, USA.

Sonnleitner, M.A., Abbaspour, K.C. and Schulin, R., 2003. Hydraulic and transport properties of the plant-soil system estimated by inverse modelling. European Journal of Soil Science, 54(1): 127-138.

Spitz, K. and Moreno, J., 1996. A practical guide to groundwater and solute transport modeling. John Wiley & Sons, Inc., New York.

Steenhuis, T.S. and Walter, M.F., 1980. Closed form solution for pesticide loss in runoff water. Trans. ASEA, 23: 615-620.

Stenemo, F. and Jarvis, N.J., 2003. Users guide to MACRO5.0, a model of water flow and solute transport in macroporous soil. Emergo 2003:10 Report, Swedish University of Agricultural Sciences, Uppsala.

Sun, N.-Z., 1994. Inverse problems in groundwater modeling. Theory and applications of transport in porous media. Kluwer Academic Publishers, Dordrecht.

Tang, D.H., Frind, E.O. and Sudicky, E.A., 1981. Contaminant transport in fractured porous media: analytical solution for a single fracture. Water Resources Research, 17: 555-564.

Therrien, R. and Sudicky, E.A., 1996. Three-dimensional analysis of variably-saturated flow and solute transport in discretely-fractured porous media. Journal of Contaminant Hydrology, 23: 1-44.

Thompson, N., Barrie, I.A. and Ayles, M., 1981. The Meteorological Office rainfall and evaporation calculation system: MORECS, Memorandum 45, The Meteorological Office, UK.

Thorburn, P.J., Walker, G.R. and Brunel, J.P., 1993. Extraction of water from eucalyptus trees for analysis of deuterium and O-18 - Laboratory and field techniques. Plant Cell and Environment, 16(3): 269-277.

Tokunaga, T.K. and Wan, J.M., 1997. Water film flow along fracture surfaces of porous rock. Water Resources Research, 33(6): 1287-1295.

Tsang, Y.W. and Tsang, C.F., 1987. Channel model of flow through fractured media. Water Resources Research, 23: 467-479.

Tsang, Y.W., Tsang, C.F., Hale, F.V. and Dverstorp, B., 1996. Tracer transport in a stochastic continuum model of fractured media. Water Resources Research, 32: 3077-3092.

Tseng, P.H., Sciortino, A. and Vangenuchten, M.T., 1995. A partitioned solution procedure for simulating water-flow in a variably saturated dual-porosity medium. Advances in Water Resources, 18(6): 335-343.

UK Groundwater Forum, 1998. Groundwater, our hidden asset, British Geological Survey, Keyworth.

van der Zee, S.E.A.T.M. and van Riemsdijk, W.H., 1994. Transport of reactive solutes in soils. In: M.Y. Corapcioglu (Editor), Advances in porous media, Volume 2. Elsevier, Amsterdam.

van Genuchten, M.T., 1980. A closed-form equation for predicting the hydraulic conductivity of unsaturated soils. Soil Science Society of America Journal, 44: 892-898.

van Genuchten, M.T. and Alves, W.J., 1982. Analytical solutions of the one-dimensional convective-dispersive solute transport equation. U.S. Department of Agriculture, Technical Bulletin No. 1661.

van Genuchten, M.T. and Dalton, F.N., 1986. Models for simulating salt movement in aggregated field soils. Geoderma, 38: 165-183.

van Genuchten, M.T. and Wierenga, P.J., 1976. Mass transfer studies in sorbing media, I. Analytical solutions. Soil Science Society of America Journal, 40: 473-480.

Villholth, K.G. and Jensen, K.H., 1998. Flow and transport processes in a macroporous subsurface- drained glacial till soil - II. Model analysis. Journal of Hydrology, 207(1-2): 121-135.

Vogel, T., Gerke, H.H., Zhang, R. and Van Genuchten, M.T., 2000. Modeling flow and transport in a two-dimensional dual-permeability system with spatially variable hydraulic properties. Journal of Hydrology, 238(1-2): 78-89.

Vrba, J. and Zaporozec, A., 1994. Guidebook on mapping groundwater vulnerability. International Contributions to Hydrogeology, 16. Verlag Heinz Heise, Hannover.

Wagner, B., Tarnawski, V.R., Hennings, V., Muller, U., Wessolek, G. and Plagge, R., 2001. Evaluation of pedo-transfer functions for unsaturated soil hydraulic conductivity using an independent data set. Geoderma, 102(3-4): 275-297.

Wallace, J.M. and Hobbs, P.V., 1977. Atmospheric science: an introductory survey. Academic Press, San Diego.

Wang, J.S.Y. and Narasimhan, T.N., 1985. Hydrologic mechanisms governing fluid flow in a partially saturated, fractured, porous medium. Water Resources Research, 21: 1861-1874.

Ward, R.S., Harrison, I., Leader, R.U. and Williams, A.T., 1997. Fluorescent polystyrene microspheres as tracers of colloidal and particulate materials: Examples of their use and developments in analytical technique. In: A. Kranjc (Editor), Tracer Hydrology. Balkema, Rotterdam, pp. 99-103.

Ward, R.S., Lawrence, A.R., Williams, A.T. and Barker, J.A., 2001. Transport of microbiological contaminants in the unsaturated zone of the Chalk aquifer: investigation by tracer test. In: K.-P. Seiler and S. Wohnlich (Editors), New approaches characterizing groundwater flow. Balkema, Munich, pp. 221-224.

Watson, K.K., 1966. An instantaneous profile method for determining the hydraulic conductivity of unsaturated porous materials. Water Resources Research, 2: 709-715.

Wellings, S.R., 1984a. Recharge of the Upper Chalk aquifer at a site in Hampshire, England. 1. Water-balance and unsaturated flow. Journal of Hydrology, 69: 259-273.

Wellings, S.R., 1984b. Recharge of the Upper Chalk aquifer at a site in Hampshire, England. 2. Solute movement. Journal of Hydrology, 69: 275-285.

Wellings, S.R. and Bell, J.P., 1980. Movement of water and nitrate in the unsaturated zone of Upper Chalk near Winchester, Hants., England. 48: 119-136.

Wellings, S.R. and Cooper, J.D., 1983. The variability of recharge of the English Chalk aquifer. Agricultural Water Management, 6(2-3): 243-253.

Wilkinson, A.T., 2002. The role of sorption phenomena in the transport of contaminants and tracers in groundwater, MSci report, University College London.

Williams, A., Barker, J.A., Silgram, M.A., Mansour, M., Neumann, I. and Hughes, A.G., 2003. The use of flow modelling to assess the impact of agricultural control measures on abstracted groundwater quality, MODFLOW and more: Understanding through modelling. Poeter, Zheng, Hill and Doherty, pp. 446-450.

Withers, P.J.A., McDonald, H.C., Smith, K.A. and Chumbley, C.G., 1998. Behaviour and impact of cow slurry beneath a storage lagoon: I. Groundwater contamination 1975-1982. Water, Air and Soil Pollution, 107: 35-49.

Worssam, B.C. and Taylor, J.H., 1969. Geology of the country around Cambridge. Memoirs of the Geological Survey of Great Britain. Her Majesty's Stationery Office, London.

Yapo, P.O., Gupta, H.V. and Sorooshian, S., 1998. Multi-objective global optimization for hydrologic models. Journal of Hydrology, 204: 83-97.

Yeh, W.W.G., 1986. Review of parameter-identification procedures in groundwater hydrology - the inverse problem. Water Resources Research, 22(2): 95-108.

Young, C.P., 1981. The distribution and movement of solutes derived from agricultural land in the principal aquifers of the United Kingdom, with special reference to nitrate. Water Science and Technology, 13: 1137-1152.

Zaidman, M.D., Middleton, R.T., West, L.J. and Binley, A.M., 1999. Geophysical investigation of unsaturated zone transport in the Chalk in Yorkshire. Quarterly Journal of Engineering Geology, 32: 185-198.

Zheng, C. and Bennett, G.D., 1995. Applied contaminant transport modeling. Van Nostrand Reinhold, New York.

Zhuang, J., Nakayama, K., Yu, G.R. and Miyazaki, T., 2001. Predicting unsaturated hydraulic conductivity of soils based on some basic soil properties. Soil & Tillage Research, 59(3-4): 143-154.

Zimmerman, M.D., Bennett, P.C., Sharp, J.M. and Choi, W.-J., 2002. Experimental determination of sorption in fractured flow systems. Journal of Contaminant Hydrology, 58: 51-77.

Zimmerman, U., Ehhalt, D.H. and Munnïch, K.O., 1966. Soil-water movement and evapotranspiration: changes in the isotopic composition of the water. Proc. IAEA Symp. on Isotopes in Hydrology, IAEA, Vienna: 567-585.

Appendix I Diffusion coefficients

Diffusion of atoms or molecules in solution is the process whereby the solutes move from an area of higher concentration to an area of lower concentration, as a result of their random kinetic activity. Diffusion occurs even in the absence of a hydraulic gradient, and tends towards an even distribution of the solutes. It is characterized by a diffusion coefficient, and different types of diffusion coefficients can be defined, depending on their use. In literature there is considerable confusion over the different types, therefore their definition is included again in this Appendix. Some values for diffusion coefficients are included as well.

1. Types of diffusion coefficients

The distinction between the different types of diffusion coefficients is best illustrated by their uses in diffusion equations (Barker et al., 1995). The *free-water diffusion coefficient* D_0 (also called tracer diffusion coefficient) is valid in a free water body, for use in Fick's first law:

$$J = -D_0 \frac{\partial c}{\partial x}$$

where J is the diffusive flux of solutes in free water. In a porous medium, Fick's first law can still be used if D_0 is replaced by the *effective diffusion coefficient*, D_E:

$$J_m = -D_E \frac{\partial c}{\partial x}$$

where J_m is the diffusive flux of solutes in the porous medium (defined as the mass of solute passing across the total area per unit of time). The *apparent diffusion coefficient* D_A applies when Fick's second law is used:

$$\frac{\partial c}{\partial t} = D_A \frac{\partial^2 c}{\partial x^2}$$

Hence for dual continuum modelling, the effective diffusion coefficient is used for a quasi-steady-state approach, whereas the apparent diffusion coefficient is used for a diffusive-type approach.

The three types of diffusion coefficients are related through:

$$D_E = \phi_f D_A = \psi D_0$$

with

$$\phi_f = \phi R$$

$$\psi = \frac{\phi_D \delta}{\tau^2}$$

where ϕ_f is the rock capacity factor or the fictitious porosity [-], ϕ is the porosity [-], R is the retardation coefficient [-], ψ is the diffusibility [-], ϕ_D is the through-diffusion porosity [-], δ is the constrictivity [-] and τ is the tortuosity [-]. For an isotropic medium, the through diffusion porosity ϕ_D is equal to the porosity ϕ (Gooddy et al., 1996). The tortuosity τ is defined as the ratio of the path length in the porous medium to the distance in direction of the flow.

The diffusibility ψ allows the calculation of D_E for a specific porous medium, provided that D_0 is known. For the Chalk matrix, Muller (1987) suggested a diffusibility of 0.25. Alternatively, the ratio D_E/D_0 has been matched with the formation factor F, which can be calculated from the porosity by a power relation known as Archie's law (1942). Experimental work on chalk samples as part of the FRACFLOW project (2000) yielded a good fit for an exponent of 2.4, or:

$$F = \frac{D_E}{D_0} = \phi^{2.4}$$

For a porosity of 45%, this gives a formation factor of 0.15. It is to be expected that the formation factor, and thus also the effective diffusion coefficient, will be lower when the

medium is unsaturated. In this case, Baum (1998) recommends for the formation factor to be calculated by the Millington-Quirk model (1961):

$$F = \frac{\theta^{10/3}}{\phi^2}$$

where θ is the water content. For the unsaturated zone of the Chalk, the matrix is usually close to saturation, so θ is close to ϕ. For a porosity of 45%, this yields a formation factor of 0.35, which may be too high. Thus the Millington-Quirk model might not be a good approximation for the Chalk.

2. Formulae for the free-water diffusion coefficient

The free-water diffusion coefficient for a specific solute is not a constant, but is dependent on pressure and temperature (Wilbur et al., 1976). Therefore any reported value of the diffusion coefficient should be accompanied by the pressure and temperature at which it was measured. For ionic solutes, the free-water diffusion coefficient is also dependent on the concentration of the ion, as well as on the concentration of other ions present in the solution. It is common practice to report the diffusion coefficient for an infinite solution, which makes it independent of concentration.

The free-water diffusion coefficient is defined by the chemical properties of the diffusing species; hence formulae are available in literature to estimate D_0 from known parameters. These formulae provide limited accuracy, but when no measurements are available they can give a fair approximation.

For large spherical particles or molecules, the Stokes-Einstein equation can be used:

$$D_0 = \frac{kT_K}{6\pi\mu_w r_p}$$

where k is the Boltzmann constant (1.38×10^{-23} J K^{-1}), T_K is the absolute temperature [K], μ_w is the dynamic viscosity [M L^{-1} T^{-1}] and r_p is the radius of the diffusing solute [L].

For individual ions at infinite dilution, D_0 can be calculated from the Nernst equation:

$$D_0 = \frac{R_g T_K \lambda_0}{|Z| F_a^{\,2}}$$

where R_g is the gas constant (8.3144 J mol^{-1} K^{-1}), λ_0 is the equivalent ionic conductivity at infinite dilution [C^2 T kg^{-1} mol^{-1}], Z is the charge of the ion [-] and F_a is the Faraday constant (9.65×10^4 C mol^{-1}).

For organic solutes in water at 25°C, the Hayduk and Laudie relationship (1974) can be used:

$$D_0^{25°C} = \frac{13.26 \times 10^{-5}}{\mu_w^{\,1.4} V^{0.589}}$$

where μ_w is the dynamic viscosity (in centipoise) and V is the molar volume [L^3 mol^{-1}].

The temperature-dependence of the free-water diffusion coefficient can be expressed based on the Stokes-Einstein equation:

$$\left(\frac{D_0 \mu_w}{T_K}\right)_{T_{K,1}} = \left(\frac{D_0 \mu_w}{T_K}\right)_{T_{K,2}}$$

According to Li and Gregory (1974), this relationship holds well for all ions diffusing slower than fluoride.

3. Reported values for diffusion coefficients

Table A-I-1 shows some results of measurements of the diffusion coefficients for selected solutes. The values shown are for atmospheric pressure, and for high or infinite dilution. Diffusion coefficients for deuterium are for diffusion of deuterated water ($^2HH0$) in normal water (H_20). Diffusion coefficients for tritium are for diffusion of tritiated water ($^3HH0$) in normal water (H_20).

Table A-I-1. Reported values for diffusion coefficients

Solute	Type	T [°C]	Medium	D [$m^2 s^{-1}$]	Reference
bromide	D_0	0	N/A	1.05×10^{-9}	Li and Gregory (1974)
bromide	D_0	10	N/A	1.31×10^{-9}	Parker et al. (1994)
bromide	D_0	18	N/A	1.76×10^{-9}	Li and Gregory (1974)
bromide	D_0	25	N/A	2.01×10^{-9}	Li and Gregory (1974)
bromide	D_0	25	N/A	1.99×10^{-9}	Robinson and Stokes (1968)
bromide	D_E	20	Chalk Denmark	2.78×10^{-10}	Fracflow (1999)
bromide	D_A	20	Chalk Denmark	2.76×10^{-11}	Fracflow (1999)
bromide	D_A	25	Lower Chalk Suffolk	3.50×10^{-10}	Gooddy et al. (1996)
chloride	D_0	0	N/A	1.01×10^{-9}	Li and Gregory (1974)
chloride	D_0	18	N/A	1.71×10^{-9}	Li and Gregory (1974)
chloride	D_0	20	N/A	2.00×10^{-9}	Luckner & Schestakow(1991)
chloride	D_0	25	N/A	2.03×10^{-9}	Li and Gregory (1974)
chloride	D_0	25	N/A	2.02×10^{-9}	Robinson and Stokes (1968)
chloride	D_A	22	Lower Chalk Harwell	2.50×10^{-10}	Fretwell (1999)
chloride	D_A	25	Lower Chalk Suffolk	3.35×10^{-10}	Gooddy et al. (1996)
chloride	D_A	25	Middle Chalk Suffolk	6.08×10^{-10}	Gooddy et al. (1996)
chloride	D_E	20	Chalk England	$0.52\text{-}3.23\times10^{-10}$	Hill (1984)
deuterium	D_0	5	N/A	1.30×10^{-9}	Mills (1973)
deuterium	D_0	20	N/A	2.13×10^{-9}	Fracflow (2000)
deuterium	D_0	25	N/A	2.27×10^{-9}	Mills (1973)
deuterium	D_E	20	Chalk Denmark	4.03×10^{-10}	Fracflow (2000)
lithium	D_0	0	N/A	4.72×10^{-10}	Li and Gregory (1974)

lithium	D_0	18	N/A	8.69×10^{-10}	Li and Gregory (1974)
lithium	D_0	25	N/A	1.03×10^{-9}	Li and Gregory (1974)
lithium	D_E	20	Chalk Denmark	8.05×10^{-11}	Fracflow (2000)
lithium	D_A	20	Chalk Denmark	5.51×10^{-11}	Fracflow (1999)
tritium	D_0	5	N/A	1.27×10^{-9}	Mills (1973)
tritium	D_0	15	N/A	1.72×10^{-9}	Mills (1973)
tritium	D_0	25	N/A	2.24×10^{-9}	Mills (1973)
tritium	D_A	25	Lower Chalk Harwell	$1.7\text{-}2.9\times10^{-10}$	Brewer et al. (1992)
tritium	D_E	20	Chalk England	$0.60\text{-}3.51\times10^{-10}$	Hill (1984)
tritium	D_E	25	Lower Chalk Harwell	$2.7\text{-}4.6\times10^{-11}$	Brewer et al. (1992)

References

Archie, G.E., 1942. The electrical resistivity log as an aid in determining some reservoir characteristics. Trans. A.I.M.E., 146: 54-61.

Barker, J.A., Kinniburgh, D.G., MacDonald, D.M.J., Allen, D.J. and MacDonald, A.M., 1995. Groundwater modelling and modelling methodology, Appendix 1: Databases for groundwater modelling, National Rivers Authority, Bristol.

Baum, E.J., 1998. Chemical property estimation: theory and application. Lewis Publishers, Florida.

Brewer, R.J., Fellingham, L.R. and Jefferies, N.L., 1992. Groundwater contamination at Harwell laboratory, Progress report, November 1990 to April 1992., AEA Technology plc, Harwell, Didcot.

FRACFLOW, 1999. Second annual progress report: Contaminant transport, monitoring technique, and remediation strategies in cross European chalk.

FRACFLOW, 2000. Third annual progress report: Contaminant transport, monitoring technique, and remediation strategies in cross European chalk.

Fretwell, B.A., 1999. Distribution of contaminants in the seasonally unsaturated zone of the Chalk aquifer. PhD Thesis, University College London, London.

Gooddy, D.C., Kinniburgh, D.G. and Barker, J.A., 1996. Development of a rapid method for determining apparent diffusion coefficients for chloride in Chalk. Technical Report WD/95/66, Hydrogeology Series, British Geological Survey, Keyworth.

Hayduk, W. and Laudie, H., 1974. Prediction of diffusion coefficients for non-electrolytes in dilute aqueous solutions. Journal of the American Institute of Chemical Engineering, 20: 611-615.

Hill, D., 1984. Diffusion coefficients of nitrate, chloride, sulphate and water in cracked and uncracked Chalk. Journal of Soil Science, 35(27-33).

Li, Y.-H. and Gregory, S., 1974. Diffusion of ions in sea water and in deep-sea sediments. Geochimica Et Cosmochimica Acta, 38: 703-714.

Luckner, L. and Schestakow, W.M., 1991. Migration processes in the soil and groundwater zone. Lewis Publishers, Michigan.
Millington, R.J. and Quirk, J.P., 1961. Permeability of porous solids. Transactions of the Faraday Society, 57: 1200-1207.
Mills, R., 1973. Self diffusion in normal and heavy water in the range 1-45. Journal of Physical Chemistry, 77: 665-688.
Muller, E., 1987. Modelling groundwater pollution at a site near Cambridge, Research report no. 7, NERC Water Research Unit, University of Newcastle-upon-Tyne.
Parker, B.L., Gillham, R.W. and Cherry, J.A., 1994. Diffusive disappearance of immiscible-phase organic liquids in fractured geologic media. Ground Water, 32(5): 805-820.
Robinson, R.A. and Stokes, R.H., 1968. Electrolyte solutions. Butterworths, London.
Wilbur, D.J., DeFries, T. and Jonas, J., 1976. Self-diffusion in compressed liquid heavy water. Journal of Chemical Physics, 65: 1783-1786.

Appendix II Biostratigraphy of the Chalk at the Fleam Dyke research site

The geological map locates Fleam Dyke lysimeter on the outcrop of the lower beds of the Middle Chalk, i.e. the Lower Turonian. The Melbourn Rock, marking the transition between Middle and Lower Chalk, is shown on the map to crop out a short distance to the north and to the west. Kitching and Shearer (1982) had also classified the chalk at Fleam Dyke as Middle Chalk, based on their reported recovery of fragments of *Inoceramus labiatus* from local samples.

Biostratigraphy based on calcareous nannofossils contradicts this classification, and instead suggests that the Fleam Dyke site is located in the Upper Cenomanian, i.e. the Lower Chalk. Selected samples from cores IP9 and IP11, recovered from the Fleam Dyke site during the tracer experiment, were examined for nannofossils. This was done by Sudeep Kanungo from the Micropalaeontology Unit at University College London, and the results are shown in the following table. The well-established zonation schemes of Perch-Nielsen (1985) and Burnett (1998) were used to date the selected samples. The results unambiguously date the samples as Late Cenomanian, placing them in the lithostratigraphical unit of the Lower Chalk known as the Plenus Marls. This is shown by the presence of *Helenea chiastia*, a marker species that is known to have its extinction around the Cenomanian/Turonian boundary, and by the absence of Turonian biostratigraphic markers.

The nannofossil evidence thus contradicts the macrofossil evidence of Kitching and Shearer (1982). As nannofossils are known to be precise dating tools for the Cretaceous it can be concluded that the Fleam Dyke site belongs to the Upper Cenomanian, or Lower Chalk. The macrofossil *Inoceramus labiatus* does not occur in the Upper Cenomanian (C.J. Wood, personal communication). Its identification by Kitching and Shearer (1982) may thus be questioned. Finally, from the hydrogeological point of view, the difference

between Lower and Upper Chalk may not be that important. Bloomfield et al. (1995) had shown that the Lower and Middle Chalk of the East Anglia region are statistically indistinguishable in terms of porosity and permeability of core samples.

References

Bloomfield, J.P., Brewerton, L.J. and Allen, D.J., 1995. Regional trends in matrix porosity and dry density of the Chalk of England. Quarterly Journal of Engineering Geology, 28: S131-S142.

Burnett, J.A., 1998. Upper Cretaceous. In: P.R. Bown (Editor), Calcareous Nannofossil Biostratigraphy. Kluwer Academic, pp. 132-199.

Kitching, R. and Shearer, T.R., 1982. Construction and operation of a large undisturbed lysimeter to measure recharge to the Chalk aquifer, England. Journal of Hydrology, 58(3-4): 267-277.

Perch-Nielsen, K., 1985. Mesozoic calcareous nannofossils. In: H.M. Bolli, J.B. Saunders and K. Perch-Nielsen (Editors), Plankton Stratigraphy. Cambridge University Press, pp. 329-426.

SAMPLE	IP9, 56-64	IP9, 144-153	IP9, 193-203	IP9, 231-241	IP9, 320-330	IP11, 40-53	IP11, 98-108	IP11, 140-150	IP11, 225-235
PRESERVATION	G-M	G-M	M	G-M	G-M	M	G-M	G-M	G-M
ABUNDANCE	H	H	Me	Me	H	Me	H	H	H
TAXON									
Ahmuellerella cf. A. octoradiata			R	R					R
Amphizygus brooksii					R				
Axopodorhabdus albianus			R	F	C	VR			F
Axopodorhabdus dietzmannii									
Biscutum constans	R	F	C	F	C		R	F	F
Biscutum cf. *B. constans* (large)		F	F	F	F		R	F	F
Braarudosphaera africana			VR						
Braarudosphaera hockwoldensis	VR	VR	R		R		R	F	VR
Broinsonia cenomanicus									
Broinsonia enormis	F	C	C	C	C	R	R	C	C
Broinsonia galloisii									
Broinsonia cf. *B. matalosa*		VR	VR	?				VR	
Broinsonia stenostaurion									
Bukrylithus ambiguus			R	VR				R	
Calciosolenia fossilis									
Calculites anfractus									
Calculites percenis									
Chiastozygus cf. *C. bifarius*			R	VR	R				
Chiastozygus litterarius	VR	R		R	R				VR
Chiastozygus platyrhethus									
Chiastozygus spissus									
Chiastozygus cf. *C. synquadriperforatus*			R						
Chiastozygus trabalis									
Chiastozygus sp. (small)			VR						
Corollithion kennedyi									
Corollithion ? madagaskerensis									
Corollithion exiguum									
Corollithion signum									
Cretarhabdus conicus									
Cretarhabdus multicavus									
Cretarhabdus striatus			VR	VR	VR				VR
Cribrosphaerella ehrenbergii									?
Crucibiscutum hayi									
Cyclagelosphaera margerelii									
Cyclagelosphaera reinhardtii									
Cyclagelosphaera rotaclypeata									
Cylindralithus biarcus									
Cylindralithus nudus					R				
Cylindralithus sculptus		R	F	F	F	VR		R	F
Discorhabdus ignotus					?				
Eiffellithus gorkae	VR	VR	R					?	
Eiffellithus ? hancockii									
Eiffellithus monechiae									
Eiffellithus turriseiffelii	R	R	C	C	C	F	C	C	C
Eprolithus floralis (spiky)									
Eprolithus floralis (petal)	F	C	C	F	C	C	F	C	C
Flabellites oblongus	?						?	?	
Gartnerago chiasta									
Gartnerago cf. *G.nanum*									
Gartnerago nanum									?
Gartnerago praeobliquum									
Gartnerago cf. *G. praeobliquum*									
Gartnerago segmentatum	VR	VR		F	F	VR	VR	VR	VR
Gartnerago theta									
Grantarhabdus coronadventis				VR	VR			VR	

Haqius circumradiatus		VR	VR					VR	
Hayesites albiensis									
Helenea chiastia		R	F	R	R	R	R	R	R
Helicolithus compactus		VR	R	R	VR	VR		R	R
Helicolithus trabeculatus									
Hemipodorhabdus cf. *H. gorkae*									
Kamptnerius magnificus	VR								
Laguncula dorotheae									
Lapideacassis glans									
Lapideacassis mariae									
Lithraphidites acutus	VR								
Lithraphidites carniolensis	C	F	C	C	R	A	A	C	C
Lithraphidites pseudoquadratus									
Loxolithus armilla	VR	VR	R	F	F	R	R		R
Loxolithus sp. 1									
Manivitella pemmatoidea		VR	R	F	F			R	R
Manivitella sp. 1									
Microrhabdulus belgicus									
Microrhabdulus decoratus					?				
Octocyclus reinhardtii			VR						
Owenia hilli									
Percivalia fenestrata									
Percivalia ? howardii									
Placozygus cf. *P.fibuliformis*				R		VR			
Prediscosphaera columnata	R	?	F	F	C	R	F	C	C
Prediscosphaera cretacea	F	F	C	C	C	R	R	C	C
Prediscosphaera cf. *P. ponticula*	F	C	C	C	C	C	F	C	C
Prediscosphaera spinosa	VR			VR					VR
Prediscosphaera spinosa (small)									
Radiolithus cf. *R. planus*		R						?	
Radiolithus planus			VR						
Repagulum parvidentatum									
retecapsa rims	C	F	F		C	C	C		
Retecapsa crenulata	R	F	C	C	F	C	C	F	F
Retecapsa surirella	VR	VR	R	R		F			
Rhagodiscus achlyostaurion			R	R	?		VR	VR	?
Rhagodiscus achlyostaurion (thick spine)									
Rhagodiscus angustus			R	R					VR
Rhagodiscus asper		VR				?			
Rhagodiscus gallagheri									
Rhagodiscus hamptonii			R	VR	R				
Rhag. cf. *R. reniformis*									
Rhagodiscus splendens									
Rotelapillus crenulatus		VR		VR			VR	VR	VR
Seribiscutum primitivum									
Sollasites horticus									
Staurolithites gausorhethium		?							
Staurolithites glaber									
Staurolithites laffittei									
Staurolithites mutterlosei									
Staurolithites spp. (unicyclic/bicyclic)			VR						
Stoverius achylosus				VR					
Tegumentum stradneri (small/large)				VR					
Tetrapodorhabdus decorus								VR	VR
Tranolithus gabalus				F					
Tranolithus minimus									
Tranolithus orionatus	C	C	C	C	C	C	C	C	C
Tranolithus sp. 1									
Tubodiscus burnettiae									
Watznaueria barnesiae	A	A	A	A	A	A	A	A	A
Watznaueria biporta	R							R	
Watznaueria britannica									

Watznaueria fossacincta		F	F	R	F	R	F	C	C	
Watznaueria manivitiae s. l.	C	C	C	C	A	A	C	C	C	
Watznaueria ovata					VR		VR			
Zeugrhabdotus bicrescenticus	R	R	R	R	R			R	R	
Zeugrhabdotus diplogrammus	R	R	R	R	F	R		R	R	
Zeugrhabdotus embergeri	F	VR	R	F	F	F	R	R	R	
Zeugrhabdotus cf. *Z. embergeri* (small)										
Zeugrhabdotus howeii	F	C	C	C	C	C	C	C	C	
Zeugrhabdotus cf. *Z. howeii*	F	C	C	C	C	C			C	
Zeugrhabdotus xenotus										
NANNOFOSSIL EVENT	*L. acutus* present (very rare)	*H. chiastia* present	*A. albianus*, *C. striatus*, *B. africana* last seen		*C. kennedyi* absent	*A. albianus*, *H. chiastia* present, *L.acutus* not seen			*C. striatus* last seen, *C. kennedyi* absent	
NANNOFOSSIL ZONE (Burnett, 1998)			**UC3e-4b**				**UC4b-5a**			
NANNOFOSSIL ZONE (Perch-Nielsen, 1985)			**CC10a**				**CC10a**			
AGE (NANNOFOSSIL BASED)			**LATE CENOMANIAN**				**LATE CENOMANIAN**			
SAMPLE	IP9, 56-64	IP9, 144-153	IP9, 193-203	IP9, 231-241	IP9, 320-330	IP11, 40-53	IP11, 98-108	IP11, 140-150	IP11, 225-235	

KEY

Preservation:
G-Good
M-Moderate
Me-Medium
H-High
FOV-field of view

Relative Abundance:
R-Rare (1 specimen/>20 FOV's)
VR-Very Rare (1-2 specimens sighted)
F-Few (1 specimen/2-20 FOV's)
C-Common (1-10 specimens/FOV)
A-Abundant (>10 specimens/FOV)
? Questionable

Appendix III Units for isotopes

1. Tritium

The tritium concentration is commonly expressed in Tritium Units (TU). One TU corresponds to one ^3H atom per 10^{18} atoms of hydrogen.

2. Deuterium

The deuterium concentration is commonly expressed as a δ-value, i.e. as a parts per thousand or permil (‰) difference from a reference (Clark and Fritz, 1997):

$$\delta^2 H_{sample} = \left[\frac{\left(\frac{^2H}{^1H}\right)_{sample}}{\left(\frac{^2H}{^1H}\right)_{VSMOW}} - 1 \right] \times 1000‰ \text{ VSMOW}$$

The isotopic ratio $^2H/^1H$ represents the number of ^2H atoms divided by the number of ^1H atoms. The standard reference is VSMOW, which stands for Vienna Standard Mean Ocean Water. The isotopic ratio $^2H/^1H$ for VSMOW is:

$$\left(\frac{^2H}{^1H}\right)_{VSMOW} = (155.76 \pm 0.05) \times 10^{-6}$$

3. Oxygen-18

Like deuterium, the oxygen-18 concentration is expressed as a δ-value:

$$\delta^{18}O_{sample} = \left[\frac{\left(\frac{^{18}O}{^{16}O}\right)_{sample}}{\left(\frac{^{18}O}{^{16}O}\right)_{VSMOW}} - 1 \right] \times 1000\ ‰\ \text{VSMOW}$$

where the isotopic ratio $^{18}O/^{16}O$ for VSMOW is:

$$\left(\frac{^{18}O}{^{16}O}\right)_{VSMOW} = (2005.2 \pm 0.45) \times 10^{-6}$$

References

Clark, I. and Fritz, P., 1997. Environmental isotopes in hydrogeology. Lewis Publishers, New York.

Appendix IV Risk assessment for fieldwork at Fleam Dyke lysimeter

1. Site description

Fleam Dyke lysimeter is located at Cambridge Water Company's Fleam Dyke Pumping Station in Fulbourn, Cambridgeshire (National Grid Ref. TL 539 549). The lysimeter is essentially a 5×5×5 m block of chalk, contained in reinforced steel pilings such that drainage water can be collected at the base. The instrument chamber under the ground is accessible by means of a vertical steel ladder under a manhole cover to a depth of 6m below ground level. At the bottom, a reinforced concrete access passage, 1.5 m wide by 2 m high, leads around the base of the lysimeter.

2. Work plan

As part of the tracer test carried out on the Fleam Dyke lysimeter, a site visit needs to be done on a regular basis to collect drainage samples. This involves going down the lysimeter shaft into the instrument chamber in the lysimeter basis. There the samples are retrieved from the automatic sampler, the sampler is reprogrammed and the samples are brought along to the surface. The interval of these site visits varies between one week and several months, and presence in the lysimeter basis can be as short as five minutes and is never longer than one hour.

3. Identification of hazards

Fleam Dyke lysimeter has been classified as a confined space Category 2 and therefore is subject to the Confined Spaces Regulations 1997 as issued by the Health and Safety Executive.

The hazards that can be identified in this case are:

- Falling from the 5 metre deep ladder in the access shaft.
- Flooding of the lysimeter instrument chamber.
- Oxygen deficiency in the lysimeter chamber.
- Concentration of noxious gases (e.g. carbon dioxide, methane and hydrogen sulphide) entering the lysimeter chamber from the surrounding unsaturated chalk.

4. Identification of risks

- Falling from the ladder presents a moderate risk, as the ladder can be slippery when wet.
- Flooding of the lysimeter is not likely to occur, as the fractured chalk is sufficiently permeable for infiltration of recharge, and surface ponding is never observed.
- The risk of oxygen deficiency or development of methane or hydrogen sulphide is probably very low, because organic matter in the chalk matrix is almost absent.
- Carbon dioxide could be a risk as it can be produced by the acting of acid rain on chalk. A build-up of carbon dioxide is most likely after heavy rainfall and could further be influenced by fluctuations in the pumping rate of Fleam Dyke pumping station and by rapid changes in atmospheric pressure as governed by the weather conditions.

5. Control measures

1. As Fleam Dyke lysimeter has been classified as a category 2 confined space, a Confined Spaces Training Course has been completed by Gerd Van den Daele and Tim Atkinson in August 2001 at ESS Limited, Wellingborough.

2. For any access to the lysimeter chamber, a minimum of two people is always on site. One man may enter the confined space, while the other one remains outside

the confined space at the surface (called the 'top man'). The top man maintains communication at all times with the person entering the lysimeter.

3. For each site visit, before entry is made to the confined space, notice is given to both a person from the Environment Agency and a person from University College London, and a second notice is given when the field visit is completed. Mobile phones are carried on the site at all times.

4. To prevent the potential build-up of carbon dioxide in the lysimeter chamber, an extractor fan has been installed, which provides forced ventilation of the confined space. The fan operates on a regular time cycle with 5 minutes of ventilation every hour, 24 hours per day.

5. The manhole cover of the lysimeter access shaft is removed at least 10 minutes prior to entry to allow for ventilation. The extractor fan is switched to continuous operation and is kept in this position for as long as anyone is present in the lysimeter chamber.

6. During each site visit, the atmosphere in the lysimeter chamber is monitored continuously by a four-gas monitor that measures concentrations of CO_2, O_2, H_2S and flammable gasses. The atmosphere monitor must be tested prior to entry to ensure that it is working correctly. The atmosphere monitor is then gradually lowered into the lysimeter access shaft on a rope, obtaining readings at minimum three levels including top, middle and basis of the shaft over a period of at least two minutes. These readings are made after the 10 minutes period of continuous ventilation. If the gas detector gives no alarm, entry can be made into the confined space, with the atmosphere monitor strapped to the entrant and switched on at all times.

7. Safety footwear is worn by the entrant to minimize the risk of slipping from the ladder.

8. While climbing up and down the ladder through the access shaft, the entrant is secured with a harness to a winch operated by the top man.

9. An emergency alarm is present on the site, which can be easily activated from inside the lysimeter chamber.

Appendix V Methodology for particle size analysis of soil samples

Initially 100 g of air-dried soil were sieved over a 2 mm sieve and both fractions were dried in the oven for 12 hours at 105°C and weighed. Then 100 ml of water were added to 20 g of the fine soil (< 2 mm), and 10 ml of a 1M NaOAc solution were added to remove carbonates and soluble salts. This suspension was centrifuged for 10 minutes at 1500 rpm, the supernatant was discarded and the remaining soil was washed twice with 50 ml water and centrifuged again. After the carbonate removal, 25 ml of water were added to the soil, and the centrifuge bottle was shaken on a wrist action shaker. From there the soil was transferred to a 1000 ml beaker, and 5 ml of a 30% hydrogen peroxide solution were added to destroy any organic matter present. The beaker was kept covered until frothing had ceased, and then the beaker was heated to 90°C without cover to evaporate the excess water.

For the separation of the sand fractions, the treated fine soil (< 2 mm) was washed over a 45 μm sieve. The residue on the sieve was dried for 12 hours at 105°C and weighed, while the suspension with the fines was retained for further analysis. The dry residue was then sieved over a stack of sieves with mesh openings of 1000, 500, 270, 90 and 45 μm (shaken for 3 minutes) and each fraction was weighed.

For separation of the finest fractions (< 45 μm), Andreasen's pipette apparatus was used. This consists of a sedimentation cylinder in which a homogeneous soil suspension is left to settle, while removing samples from a certain depth by means of a pipette at fixed time intervals. Based on Stokes' law, the maximum diameter of the particles in each sample can be expressed as:

$$d_S = \sqrt{\frac{18\mu_w h}{gt(\rho_s - \rho_w)}}$$

where d_S is the maximum (Stokes) diameter [L], μ_w is the dynamic viscosity of the suspension [M L^{-1} T^{-1}], h is the depth below water surface [L], t is the sedimentation time [T], ρ_s is the density of the particles [M L^{-3}], and ρ_w is the density of the water [M L^{-3}].

To ensure optimal chemical dispersion of the soil suspension, 10 ml of a 50 g/l Na-hexametaphosphate solution (HMP) were added to the fine soil and the volume was made up to 1 litre with distilled water. The suspension was left several hours to equilibrate in the sedimentation cylinder and was then shaken thoroughly and the timer was started. At specified times and depths, 25 ml samples were withdrawn with a pipette (a total of 7 samples). The samples were dried in the oven for 12 hours at 105°C and their residue weighed. To the remaining suspension in the cylinder, 10 ml of 1M $CaCl_2$ and 1 ml of 1M HCl were added to prevent $CaCO_3$ formation. After flocculation had occurred, the clear solution was decanted off, and the residue was dried in the oven for 12 hours at 105°C and weighed.

The relative weights of all the separated fractions were combined to calculate the particle size fraction for each diameter range and to construct a cumulative particle size distribution curve. Finally the percentages of sand, silt and clay allowed the determination of the soil texture.

Appendix VI Testing of the bromide extraction method

1. Extraction by grinding with a micronizing mill

To test the efficiency of the extraction method by stirring of the soil and chalk samples in distilled water, a variant of the method was tested in parallel. This involved the wet grinding of the soil or chalk samples in a McCrone micronizing mill. This device breaks up the material by rubbing it between rotating, shaking agate rods. Therefore 2 to 4 g of oven-dried soil or chalk (pulverized with pestle and mortar or crushed with a hammer, respectively) were transferred to the mill with 25 ml of ultra-pure water. The suspension was ground for 20 minutes and subsequently collected in a centrifugation tube. Afterwards another 25 ml of ultra-pure water was added to the mill and shaken for 5 minutes to rinse the mill of the remaining material. The rinsing water was added to the suspension in the centrifugation tube and the rinsing procedure was repeated once more. From there the suspension was centrifuged for 15 minutes at 1500 rpm. Finally the centrifugate was filtered over a Whatman n°5 paper filter into a 100 ml flask, and the flask was filled up to volume with ultra-pure water.

Figure A-VI-1 shows a comparison of the bromide concentrations obtained after either extracting the bromide by stirring in distilled water, or after extraction by grinding the soil material with a micronizing mill. In both cases bromide was measured by ion chromatography. The measured concentrations were systematically higher after grinding than after stirring. Some of the bromide obtained from grinding might originate from bromide incorporated inside the soil particles.

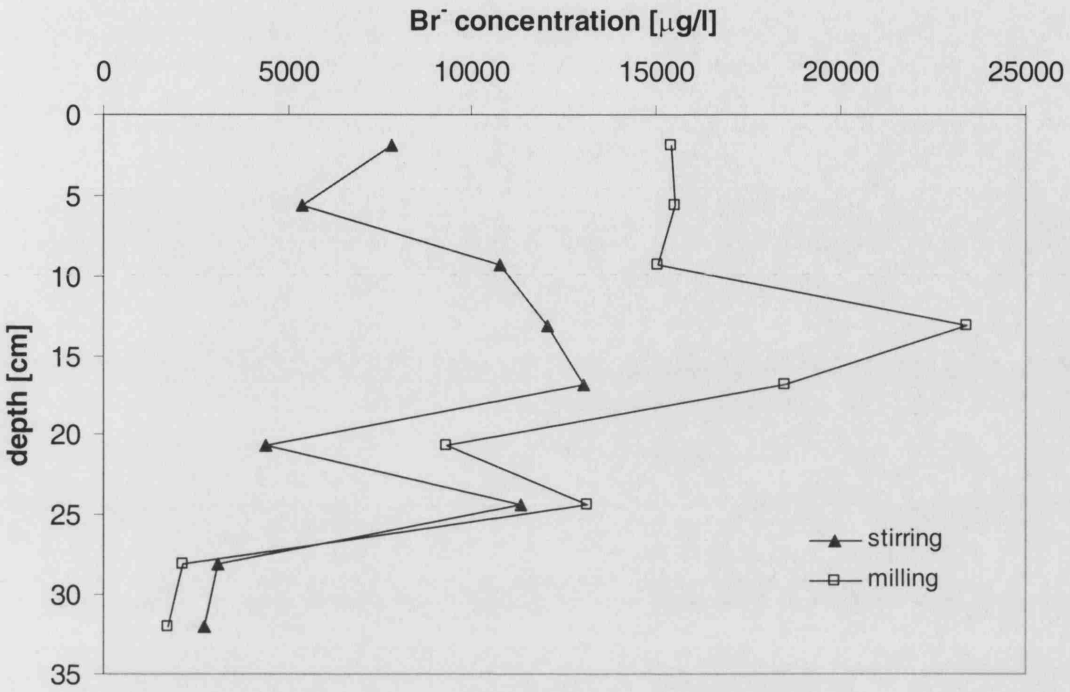

Figure A-VI-1 Bromide concentrations measured on core profile IP 1, taken at the Fleam Dyke research site on 22 May 2002, after extraction by either stirring in distilled water or by a micronizing mill.

2. Blank test

To examine if the extraction method itself led to bromide contamination of the sample, a test was run using ultra-pure water without the soil sample. In a 100 ml beaker, 50 ml of ultra-pure water was stirred for 15 hours. The water was then transferred to a centrifuge tube and centrifuged for 15 minutes at 1500 rpm. From there the water was filtered over a Whatman n°5 paper filter into a 100 ml flask, and the flask was filled up to volume with ultra-pure water. Analysis of the sample by ion chromatography revealed that the bromide in the sample was below the detection limit (< 1 µg/l).

The same blank test was performed for the micronizing mill. A volume of 25 ml of ultra-pure water was shaken for 20 minutes in the mill and subsequently collected in a

centrifugation tube. Afterwards another 25 ml of ultra-pure water was added to the mill and shaken for 5 minutes. The rinsing water was added to the water in the centrifugation tube and the rinsing procedure was repeated once more. From there the water was centrifuged for 15 minutes at 1500 rpm. Finally the centrifugate was filtered over a Whatman n°5 paper filter into a 100 ml flask, and the flask was filled up to volume with ultra-pure water. Analysis of the sample by ion chromatography yielded a bromide concentration of 1.1 µg/l. This is three to four orders of magnitude lower than the concentrations measured from the soil extracts.

To conclude, blank testing of the extraction method showed that the extraction method itself did not lead to bromide contamination.

3. Testing of the equilibration time

For the extraction of chalk samples by stirring in distilled water, the efficiency of the method depends on the time needed to approach diffusive equilibrium between the chalk fragments and the bulk water solution. This can be expressed by following formula (Barker, 1993):

$$t = \frac{x^2}{2D_A}$$

where t is the time to approach diffusive equilibrium [T], x is the distance of diffusion [L], and D_A is the apparent diffusion coefficient [L^2/T]. For chalk fragments with a maximal dimension of 1 cm, the distance of diffusion to the centre of the block is 0.5 cm. Assuming an apparent diffusion coefficient of 3×10^{-10} m^2/s, the time to approach diffusive equilibrium becomes 12 hours. Hence this should be the minimum equilibrium time that needs to be allowed for bromide extraction from chalk fragments. In the experimental set-up, the chalk samples where therefore left to stir in ultra-pure water for 15 hours.

The influence of the extraction time on the measured bromide concentration in the extract was tested. Sub-samples of the background core R2 were left stirring in ultra-pure water for 20 minutes, 3 hours, 15 hours and 45 hours respectively. All other factors remained constant, the bromide concentrations were then measured by ion chromatography (Figure A-VI-2). There was a tendency for concentrations to be higher for longer extraction times, but the trend was not clear and variability was high. In general, it appeared that the lowest extraction time of 20 minutes was sufficient to allow diffusive equilibrium between the sample and the extract.

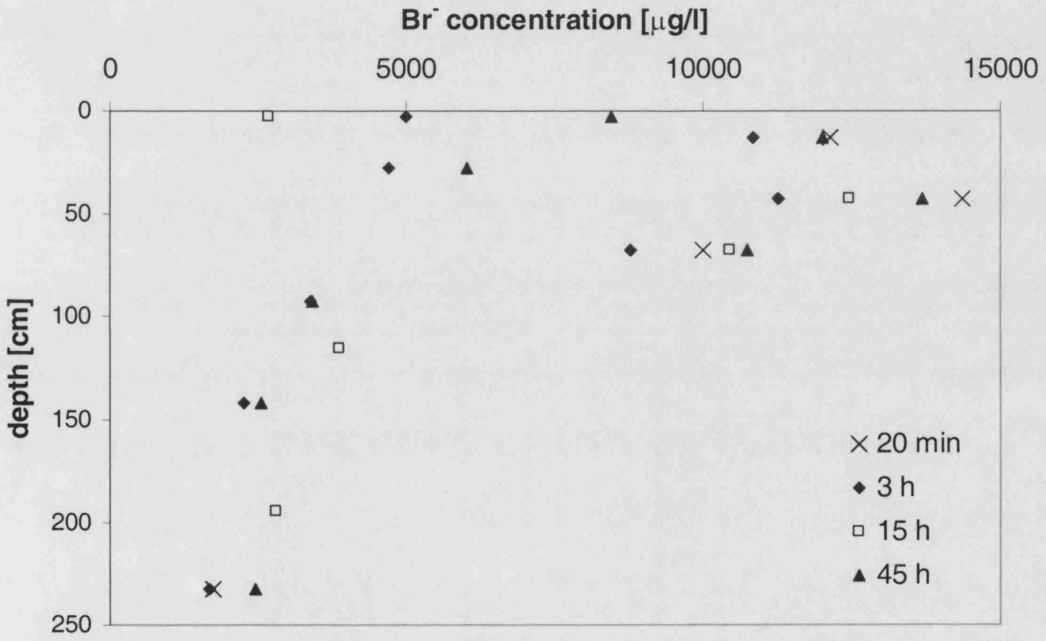

Figure A-VI-2 Bromide concentrations measured on background core profile R2 (taken at the Fleam Dyke research site on 2 July 2002) after extraction by stirring in distilled water, for different equilibration times.

References

Barker, J.A., 1993. Modelling groundwater flow and transport in the Chalk. In: R.A. Downing, M. Price and G.P. Jones (Editors), The hydrogeology of the Chalk of North-West Europe. Clarendon Press, Oxford, pp. 59-66.

Appendix VII Visual Basic code to calculate Penman-Monteith evapotranspiration

```
Option Explicit
Option Base 1
' Calculation of Potential Evapotranspiration (PET) according to
' Penman-Monteith
' Gerd Van den Daele, November 2001
' Coupled to Excel spreadsheet with 3 input worksheets, in the format
' supplied by the British Atmospheric Data Centre (BADC):
' worksheet "dwx", containing nsun
' worksheet "hwx", containing Ta, Twb, Ts, U, Pa
' worksheet "rad", containing St, N
' The programme first converts the data from each input worksheet into
' intermediate variables, and then calculates PET from the intermediate
' variables. Output is displayed in the worksheet "PET".
```

```
Sub Main()

    Const Cp = 1.013          'specific heat of air (kJ/kg/C)

    Dim startdate As Date
    Dim enddate As Date
    Dim num_days As Integer
    Dim LAI As Single         'average Leaf Area Index (-)
    Dim Hc As Single          'average height of crop (m)
    Dim Zu As Single          'height of wind speed measurements (m)
    Dim Ze As Single          'height of humidity measurements (m)
    Dim Ta(5000) As Single    'air temperature (C)
    Dim Twb(5000) As Single   'wet-bulb temperature (C)
    Dim Ts(5000) As Single    'soil temperature (C)
    Dim Pa(5000) As Single    'atmospheric pressure (kPa)
    Dim lambda(5000) As Single      'latent heat of vaporization (MJ/kg)
    Dim gamma(5000) As Single       'psyhrometric constant (kPa/C)
    Dim density(5000) As Single     'air density (kg/m3)
    Dim es(5000) As Single    'sat. vapour pressure at air temp (kPa)
    Dim e(5000) As Single     'prevailing vapour pressure (kPa)
    Dim Delta(5000) As Single       'slope of saturated _
```

```
vapour pressure curve (kPa/C)
Dim U(5000) As Single    'wind speed (m/s)
Dim nsun(5000) As Single 'number of sunshine hours per day (-)
Dim ra(5000) As Single   'aerodynamic resistance (s/m)
Dim G(5000) As Single    'heat conduction in soil (MJ/m2/d)
Dim St(5000) As Single   'tot. incoming shortwave rad. (MJ/m2/d)
Dim N(5000) As Single    'day length (d)
Dim Rn(5000) As Single   'net radiation (MJ/m2/d)
Dim Julianday(5000) As Single    'Julian day number (-)
Dim serialhour(5000) As Single   'serial date (h)
Dim PET(5000) As Single  'Potential Evapotranspiration (mm/d)
Dim cumPET(5000) As Single       'cumulative Potential _
Evapotranspiration (mm/d)

Dim i As Integer

startdate = InputBox("Enter start date as mm/dd/yyyy")
enddate = InputBox("Enter end date as mm/dd/yyyy")
num_days = (enddate - startdate + 1)

LAI = InputBox("Enter Leaf Area Index")
Hc = InputBox("Enter crop height in m")
Zu = InputBox("height of wind speed measurements (m)")
Ze = InputBox("height of humidity measurements (m)")

Worksheets("hwxfile").Select
Call convert_hwxfile(num_days, Ta, Twb, Ts, Pa, lambda, density, _
es, e, Delta, gamma, U, Rn, ra, G, Julianday, serialhour, Hc, _
LAI, Zu, Ze)

Worksheets("dwxfile").Select
Call convert_dwxfile(num_days, nsun)

Worksheets("radtfile").Select
Call convert_radtfile(num_days, St, nsun, N, Julianday, e, Ta, Rn)

'calculate PET (Eq. 7-1)
PET(1) = 0
For i = 2 To num_days
    PET(i) = (Delta(i) * (Rn(i) - G(i)) + 86.4 * density(i) * Cp _
    * (es(i) - e(i)) / ra(i)) / (lambda(i) * (Delta(i) + gamma(i) _
    * (1 + (200 / LAI) / ra(i))))
    If PET(i) < 0 Then
```

```
            PET(i) = 0
        End If
    Next i

    'calculate cumPET
    cumPET(1) = PET(1)
    For i = 2 To num_days
        cumPET(i) = cumPET(i - 1) + PET(i)
    Next i

    With Worksheets("PET")

        For i = 1 To num_days
           .Cells(i + 1, 1).Value = serialhour(i)
           .Cells(i + 1, 2).Value = PET(i)
           .Cells(i + 1, 3).Value = cumPET(i)
        Next i

    End With

End Sub
```

```
Sub convert_hwxfile(num_days As Integer, Ta() As Single, _
Twb() As Single, Ts() As Single, Pa() As Single, lambda() As Single, _
density() As Single, es() As Single, e() As Single, _
Delta() As Single, gamma() As Single, U() As Single, Rn() As Single, _
ra() As Single, G() As Single, Julianday() As Single, _
serialhour() As Single, Hc As Single, LAI As Single, Zu As Single, _
Ze As Single)


    Dim k As Integer

    With Worksheets("hwxfile")

        .Cells(1, 58).Value = "crop height (m)"
        .Cells(2, 58).Value = Hc
        .Cells(1, 59).Value = "LAI"
        .Cells(2, 59).Value = LAI
        .Cells(1, 60).Value = "zu (m)"
        .Cells(2, 60).Value = Zu
        .Cells(1, 61).Value = "ze (m)"
```

```
.Cells(2, 61).Value = Ze

'define variables
For k = 1 To num_days
    Ta(k) = .Cells(k + 1, 34).Value
    Twb(k) = .Cells(k + 1, 36).Value
    Ts(k) = .Cells(k + 1, 38).Value
    U(k) = .Cells(k + 1, 9).Value
    Pa(k) = .Cells(k + 1, 20).Value
Next k

'calculate lambda, es, e, delta, density, ra, G, gamma
.Cells(1, 45).Value = "lambda (MJ/kg)"
.Cells(1, 46).Value = "es (kPa)"
.Cells(1, 47).Value = "e (kPa)"
.Cells(1, 48).Value = "Delta (kPa/C)"
.Cells(1, 50).Value = "density (kg/m3)"
.Cells(1, 51).Value = "ra (s/m)"
.Cells(1, 52).Value = "G(MJ/m2/d)"
.Cells(1, 53).Value = "gamma(kPa/C)"
.Cells(1, 55).Value = "serial hour (h)"

For k = 1 To num_days
    lambda(k) = 2.501 - 0.002361 * Ta(k)
    .Cells(k + 1, 45).Value = lambda(k)
    es(k) = (10 ^ ((7.5 * Ta(k) / (Ta(k) + 237.3)) + 2.7858)) _
    / 1000
    .Cells(k + 1, 46).Value = es(k)
    e(k) = (10 ^ (((7.5 * Twb(k) / (Twb(k) + 237.3)) _
    + 2.7858)) / 1000) - 0.000661 * Pa(k) * (Ta(k) - Twb(k)) _
    * (1 + 0.00115 * Twb(k))
    .Cells(k + 1, 47).Value = e(k)
    Delta(k) = 4098 * es(k) / (237.3 + Ta(k)) ^ 2
    .Cells(k + 1, 48).Value = Delta(k)
    density(k) = 3.486 * Pa(k) / (275 + Ta(k))
    .Cells(k + 1, 50).Value = density(k)
    gamma(k) = 0.0016286 * Pa(k) / lambda(k)
    .Cells(k + 1, 53).Value = gamma(k)
    If U(k) = 0 Then
        ra(k) = 9999999
        .Cells(k + 1, 51).Value = ra(k)
    Else
        .Cells(k + 1, 51).FormulaR1C1 = _
```

```
                "=LN((R2C60-0.67*R2C58) / (0.123*R2C58))" _
                * LN((R2C61-0.67*R2C58)/(0.0123*R2C58)) _
                / ((0.41 ^ 2) * RC[-42])"
                ra(k) = .Cells(k + 1, 51).Value
            End If
        Next k

        G(1) = 0
        For k = 2 To num_days
            G(k) = 0.38 * (Ts(k) - Ts(k - 1))
            .Cells(k + 1, 52).Value = G(k)
        Next k


        'calculate Julian day number and serial hour
        Range(Cells(2, 55), Cells(num_days + 1, 55)).Select
        Selection.NumberFormat = "0.00"
        For k = 1 To num_days
            Julianday(k) = .Cells(k + 1, 7).Value
            .Cells(k + 1, 55).FormulaR1C1 = "=(RC[-13]-R2C42)*24"
            serialhour(k) = .Cells(k + 1, 55).Value
        Next k

    End With

End Sub
```

```
Sub convert_dwxfile(num_days As Integer, nsun() As Single)

    Dim l As Integer

    With Worksheets("dwxfile")

        'remove unnecessary rows and define variables
        For l = 1 To num_days
            .Range(Cells(l + 1, 1), Cells(l + 1, 18)).Select
            Selection.Delete Shift:=xlUp
            nsun(l) = .Cells(l + 1, 9).Value
        Next l

    End With
```

```
End Sub
```

```
Sub convert_radtfile(num_days As Integer, St() As Single, _
nsun() As Single, N() As Single, Julianday() As Single, e() As Single, _
Ta() As Single, Rn() As Single)

    Const rho = 0.000000004903  'Stefan-Boltzmann constant (MJ/m2/K4/d)
    Const alpha = 0.23  'albedo
    Dim m As Integer

    'calculate Rn
    Worksheets("radtfile").Cells(1, 12).Value = "Rn (MJ/m2/d)"
    For m = 1 To num_days
        St(m) = Worksheets("radtfile").Cells(m + 1, 9).Value
        N(m) = Worksheets("radtfile").Cells(m + 1, 13).Value
        Worksheets("radtfile").Cells(m + 1, 12).Formula = ((1 - alpha) _
        * St(m)) - ((0.9 * nsun(m) / N(m)) + 0.1) * (0.34 - 0.14 * _
        Sqr(e(m))) * rho * (Ta(m) + 273.15) ^ 4
        Rn(m) = Worksheets("radtfile").Cells(m + 1, 12).Value
    Next m

End Sub
```